

**REAL-TIME CONTROL OF RESERVOIR SYSTEMS BASED ON THE
SYNTHESIZED RUNOFF MODEL OF
SURFACE FLOW AND SUBSURFACE FLOW**

**By
Shengping Zhang**

February, 1988

**REAL-TIME CONTROL OF RESERVOIR SYSTEMS BASED ON THE
SYNTHESIZED RUNOFF MODEL OF
SURFACE FLOW AND SUBSURFACE FLOW**

**By
Shengping Zhang**

February, 1988

ACKNOWLEDGEMENTS

My graduate studies at Kyoto University were a deeply rewarding experience. I would particularly like to express my gratitude to Professor Takuma Takasao for introducing me to the field of Hydrology. His guidance and continuous encouragement have made it possible to complete this study. I would also like to acknowledge the guidance and valuable advice of Professor Shuichi Ikebuchi and Professor Yasuo Ishihara.

I would like to thank Dr. Michiharu Shiiba for his enlightening discussions during the whole course of this study and his helpful comments on my research.

I am also grateful to Dr. Toshiharu Kojiri, Mr. Kaoru Takara, Mr. Eiichi Nakakita, and Mr. Tomoharu Hori for their helpful studies and their constructive discussions.

To my friends at the Takasao's Lab, I extend my greetings. Their presence made my efforts easier.

Special thanks are due to Professor Xue Yu-Qun of Nanking University, China, for giving me the chance to come to Kyoto University and perform this study.

Miss Qi Jie patiently and excellently typed this thesis and was perhaps as happy as I was when the thesis was finished. To her and to my mother Ji Qiu-Hong, my father Zhang Chun-Hong and my younger sister Zhang Ling, I gratefully dedicate this work. Their true concern and unselfish feelings have always pulled me through difficult times.

CONTENTS

ACKNOWLEDGEMENTS

| | |
|---|----|
| Chapter 1. Introduction..... | 1 |
| 1.1 General Remarks..... | 1 |
| 1.2 Development of Runoff Model..... | 3 |
| 1.3 System Approach to Solving Water Resources Problems..... | 10 |
| 1.4 Thesis' Framework and Outline..... | 15 |
| | |
| Chapter 2. A Synthesized Runoff Model of Surface Flow and Subsurface Flow..... | 17 |
| | |
| 2.1 Mathematical Model..... | 17 |
| 2.1.1 Region of Flow..... | 17 |
| 2.1.2 Equation of Saturated-Unsaturated Subsurface Flow..... | 19 |
| 2.1.2.1 Pressure Head..... | 19 |
| 2.1.2.2 Continuity Equation for Saturated- Unsaturated Flow..... | 20 |
| 2.1.2.3 Equation of Motion for Saturated- Unsaturated Flow..... | 22 |
| 2.1.2.4 Soil Parameters..... | 26 |
| 2.1.2.5 Initial Conditions..... | 29 |
| 2.1.2.6 Boundary Conditions..... | 30 |
| 2.1.3 Equation of Overland Flow..... | 33 |
| 2.1.3.1 Equation of Continuity..... | 33 |
| 2.1.3.2 Equation of Motion..... | 35 |
| 2.1.3.3 Boundary Conditions and Initial Conditions for Overland Flow..... | 38 |
| 2.1.3.4 Linearization of the Equations of Overland Flow..... | 39 |
| 2.2 Solution of the Mathematical Model as a | |

| | |
|---|-----|
| Simultaneous System..... | 41 |
| 2.2.1 Galerkin Finite Element Method..... | 41 |
| 2.2.1.1 Finite Element Method..... | 41 |
| 2.2.1.2 Galerkin's Method..... | 43 |
| 2.2.2 Solution of Steady State Flow Problem..... | 45 |
| 2.2.2.1 Finite Element Mesh..... | 46 |
| 2.2.2.2 Basis Functions..... | 48 |
| 2.2.2.3 Formulating the Matrix Equation for Steady State Flow Problem by Linear Triangular Elements..... | 58 |
| 2.2.2.4 Formulating the Matrix Equation for Steady State Flow Problem by Curved- Sided Triangular Elements..... | 64 |
| 2.2.2.5 Incorporating the Dirichlet Boundary Conditions and Solving the Global Matrix Equation..... | 65 |
| 2.2.2.6 Possibility of Approximating the Land Surface by a Series of Straight-Line Elements..... | 66 |
| 2.2.3 Solution of the Transient Flow Problem..... | 78 |
| 2.2.3.1 Formulation of Matrix Equation..... | 78 |
| 2.2.3.2 Integration Over Time..... | 81 |
| 2.3 Application to Hillslope Systems..... | 83 |
| 2.3.1 Input Data for the Coupled Model..... | 83 |
| 2.3.2 Saturated Hydraulic Conductivity and Roughness..... | 96 |
| 2.3.3 Moisture Characteristic Curve..... | 111 |
| 2.3.4 Specific Storage..... | 112 |
| 2.3.5 Rainfall Pattern..... | 118 |
| 2.3.6 Antecedent Precipitation..... | 118 |
| 2.4 Simulation Analysis of Hillslope Runoff Processes..... | 123 |
| 2.4.1 Distribution of Moisture Content..... | 123 |
| 2.4.1.1 Changing Moisture Profile..... | 123 |
| 2.4.1.2 Redistribution of Soil Moisture..... | 128 |
| 2.4.2 Velocity Distributions of Overland Flow and Subsurface Flow..... | 137 |
| 2.4.2.1 Equations of Motion..... | 137 |
| 2.4.2.2 Distribution of Velocity in Time and Space..... | 137 |

| | | |
|------------|--|-----|
| 2.4.3 | Water Table Level and Seepage Point..... | 141 |
| 2.4.3.1 | Water Table of Subsurface Flow..... | 141 |
| 2.4.3.2 | Free Water Surface of Overland Flow..... | 156 |
| 2.4.3.3 | Seepage Point..... | 156 |
| 2.4.4 | Interaction of Overland Flow with Subsurface Flow..... | 164 |
| 2.4.5 | Hillslope Runoff Processes..... | 166 |
| 2.5 | Summary and Conclusions..... | 173 |
| | | |
| Chapter 3. | Lumping of the Synthesized Runoff Model..... | 175 |
| | | |
| 3.1 | Introduction..... | 175 |
| 3.2 | Formulation of the Lumped Runoff Model..... | 177 |
| 3.2.1 | Lumped Model..... | 177 |
| 3.2.1.1 | Region of Flow..... | 177 |
| 3.2.1.2 | Equations of Continuity..... | 179 |
| 3.3 | Derivation of the Storage-Discharge Expression..... | 187 |
| 3.3.1 | Subsurface Runoff Discharge..... | 187 |
| 3.3.2 | Intensity of Lateral Flow..... | 188 |
| 3.3.3 | Overland Runoff Discharge..... | 193 |
| 3.3.4 | Stability of Model Parameters..... | 197 |
| 3.4 | Analysis of the Lumped model..... | 201 |
| 3.4.1 | Analyses of Lumped Runoff Model..... | 201 |
| 3.4.2 | Comparison between the SSSR Model and the Lumped Runoff Model..... | 201 |
| 3.5 | Summary and Conclusions..... | 209 |
| | | |
| Chapter 4. | Real-Time Control of Multireservoir Systems..... | 210 |
| 4.1 | Introduction and Overview..... | 210 |
| 4.2 | Statistical Second-Order Approximation..... | 219 |
| 4.2.1 | Theory of Statistical Second-Order Approximation..... | 219 |
| 4.2.2 | Relationships between the Expectation of Stochastic Function and Statistical Second-Order Approximation..... | 224 |

| | |
|---|-----|
| 4.3 Modeling of Multireservoir Systems..... | 228 |
| 4.3.1 General Characteristics of a Reservoir System..... | 228 |
| 4.3.2 System Model Development..... | 231 |
| 4.3.3 Modeling of the System's Objectives..... | 238 |
| 4.4 Operation Problem of Multireservoir Systems..... | 246 |
| 4.5 Solution of Operation Problem by the Open-Loop Feedback Controller..... | 257 |
| 4.5.1 Open-Loop Feedback Controller..... | 257 |
| 4.5.2 Solution of the Unconstrained Reservoir Optimization Problem..... | 260 |
| 4.5.2.1 The Unconstrained Reservoir Optimization Problem..... | 260 |
| 4.5.2.2 Newton's Method..... | 264 |
| 4.5.3 Solution of the Problem with Control Constraints..... | 274 |
| 4.5.3.1 The Reservoir Optimization Problem with Control Constraints..... | 274 |
| 4.5.3.2 Constrained Minimization Methods..... | 274 |
| 4.5.4 Solution of the Operation Problem with Both Control and State Constraints..... | 286 |
| 4.5.4.1 The Reservoir Optimization Problem with Both Control and State Constraints | 286 |
| 4.5.4.2 A Penalty Function Method..... | 291 |
| 4.5.5 Completing the OLPC Procedure..... | 295 |
| 4.5.5.1 Observation Information..... | 295 |
| 4.5.5.2 Statistically Approximated Second-Order Filter..... | 296 |

| | |
|---|-----|
| Chapter 5. Simulation Analysis on Real-Time Control of Multireservoir Systems..... | 299 |
| 5.1 Introduction..... | 299 |
| 5.2 Efficency of the Statistical Second-Order Approximation..... | 300 |
| 5.3 A Two-Reservoir Case Study..... | 304 |
| 5.4 Summary..... | 313 |

| | |
|--|-----|
| Chapter 6. Summary of Results and Conclusions..... | 314 |
| 6.1 Summary of Results..... | 314 |
| 6.2 Areas for Future Work..... | 319 |
| | |
| REFERENCES..... | 320 |
| | |
| Appendix A. Equation of Motion for Saturated-Unsaturated Flow..... | 326 |
| | |
| Appendix B. The Transformation of Cartesian Coordinate System to a Natural Coordinate System..... | 329 |
| | |
| Appendix C. Numerical Integration..... | 336 |
| | |
| Appendix D. Coefficients of the Lumping Runoff Model..... | 338 |

Chapter 1

INTRODUCTION

1.1. General Remarks

This work presents a synthesized runoff model of surface flow and subsurface flow for hillslope system, and on the basis of it a powerful approach for real-time operation of reservoir systems is proposed.

In recent past decades, with the industrialization developing over the world, the social environments have greatly changed so that the requirements for the supply of water resources have increased sharply and water pollution has become quite serious. Consequently the shortage of fresh water has become a great problem. For example, in China, according to a preliminary estimation the total amount of water resources will be 2700 billion cubic meters, but the water quantity per capita is only 2700 cubic meters, which is far less than the average of 10930 cubic meters per capita through the world. Moreover, the distribution of water resources is uneven; water resources are deficient in the north. In the Hai-Luan River and Liao River basins, water supply for industrial and agricultural production is by far insufficient and water shortage is so acute that at times people's daily life in the cities is affected. Water deficiency can also be felt in Beijing, Tianjing and many cities in Shanxi, Hebei and

Liaoning provinces as well as in the industrial bases. It is clear that water deficiency in the not-so-distant future will become even more acute and will be a major factor constraining the development of local economy in North China.

In order to guarantee an adequate supply for both national economic development and people's needs, water resources are to be developed in a comprehensive manner through overall planning and with good management, so that optimum results of disaster control and consequential benefits may be achieved at the least possible cost. This thesis will deal with the technical problem concerned. When formulating a development plan of water resources or a management program for existing projects, one of the most important needs is a method to accurately estimate the runoff from hillslope system. In this thesis the runoff processes will be explained from both physical and hydrological points of view, and one approach for real-time control of water resources systems will be presented.

1.2. Development of Runoff Model

Modern hydrology dates from the 1930s with the work of Horton(1933) and Sherman(1932). Horton first outlined in full the classical model of hillslope hydrology in terms of his infiltration theory of runoff. Central to his analysis of runoff was the view that the soil surface acts as a sieve capable of separating rainfall into two basic components, surface runoff and subsurface runoff. Horton's two assumptions that the excess of rainfall intensity over infiltration capacity is the sole source of runoff quick enough to produce the stream hydrograph peak and that all infiltration would pass into groundwater and was the sole source of the baseflow part of the hydrograph fitted very well with Sherman's unit hydrograph theory of basin runoff.

Although the hydrological models of Horton and Sherman proved to be so historically complementary ,they were fundamentally different in character. Sherman employed sweeping assumptions to develop a " black-box " approach to the prediction of storm runoff output from a watershed as the result of storm input. Horton belonged to the traditional " white-box " school of hydrology.

For making the runoff process clear, white-box models are indispensable. In the following pages a summary of white-box hillslope runoff models will be presented.

Figure 1.1 shows the physical setting of a hillslope feeding a stream channel. There may be surface flow(including overland flow) across the land surface and interflow(or subsurface flow) in the soil layers including saturated flow and unsaturated flow. A so-called white-box model is a mathematical model which uses the time- and space-dependent rainfall as inputs, and then outputs (a) the outflow

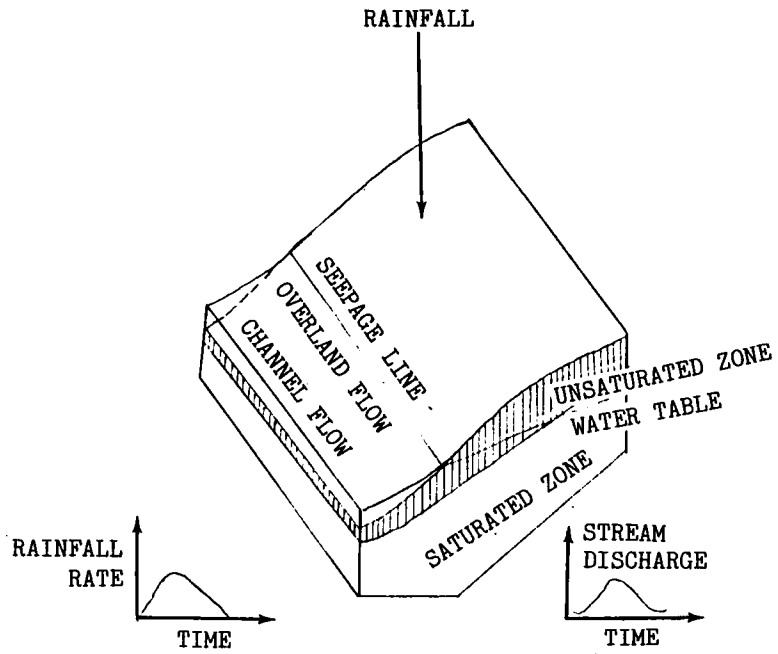


Figure 1.1 The mechanisms of delivery of rainfall to a stream channel from a hillslope.

hydrograph, (b) the time- and space-configurations of such internal variables as the pressure head, water-table height, soil moisture content, seepage-face height, depth and velocity of streamflow and overland flow, and infiltration(or return flow) intensity.

What can be immediately recognized is that a mathematical runoff model in the general form is made up of a set of three component models, one for overland flow, one for subsurface flow and one for channel flow. The near-surface saturated stormflow and unsaturated stormflow are generally classified as subsurface flow. The groundwater flow forms the baseflow of hydrograph, and has fewer contributions for the short-time runoff than the near-surface saturated flow. Moreover, the groundwater flow generally does not fluctuate very widely according to rainfall intensity. For these reasons, it is usually neglected from the short-time runoff models. The three component mathematical models of hillslope hydrology can be summarized as follows:

- (1) Transient, saturated-unsaturated, subsurface flow in a two-dimensional cross-section with heterogeneous, anisotropic media; boundary conditions that allow time- and space-dependent arrival of rainfall on the upper surface and outflow to the stream and overland system through a transient seepage face.
- (2) One-dimensional, transient, channel flow with boundary conditions that allow time- and space-dependent arrival of lateral inflow.
- (3) One-dimensional treatment of the sheetflow representation of transient overland flow; boundary conditions that allow time- and space-dependent arrival of rainfall, infiltration to the

subsurface system or inflow from the subsurface system, and outflow to the stream.

Solutions are available for each of these component systems. Saturated flow is a classical field of geohydrology and hydrogeology. The equation of motion of saturated flow is expressed as Darcy's law. The main solutions were analytical methods until the 1950s. However, in recent decades, the development of computers has made complex problems which cannot be solved with analytical methods capable of being solved with numerical techniques. The biggest remaining problem is that there is seldom enough data of the hydrogeological parameters available at field sites to provide the necessary input to the physically-based models.

Since Darcy's law for saturated flow was extended to unsaturated flow by Richards(1933), unsaturated flow can be treated with the same model and same solving technique as saturated flow. But, the infiltration of rainfall is a pending problem. Hydrologists have tried to explicate what role the infiltration plays, and scientists of agriculture and soil mechanics to explain the mechanism of motion of water in the unsaturated zone. Much of this research was based on the work of Horton and Philip. Satisfactory results have not yet been found.

Flow in stream channels can be analyzed with the classical methodology of open-channel hydraulics. The standard text is Chow(1959). Regan(1966), Strelkoff(1969), and Freeze(1972a) made great contributions to the development of the equations of flow and numerical techniques.

Sueishi(1955) assumed that overland flow can be treated as sheetflow, and first made use of a form of the kinematic approximation of the shallow water equations. Ishihara and Takasao(1959) solved

analytically the kinematic wave model of overland flow with the boundary conditions that allow time-dependent arrival of lateral inflow. Based on the result, they explained the primary characteristics of the overland runoff of rainfall.

However, as shown later by Ishihara and Takasao(1963) themselves, in the hillslope soil near land surface usually there is a high-conductivity layer(termed the A-layer by Takasao), where so-called interflow exists. This interflow sometimes returns to the overland flow system. With Ishihara and Takasao's interflow theory, it has been proven that the interaction of overland flow and interflow has strong influence on the runoff process of hillslope. Furthermore, Takasao, Ikebuchi and Shiiba(1977) proposed a coupled model of overland flow and interflow. Recently, Takasao and Shiiba(1981) have extended the kinematic wave model to consider the effect of hillslope geometry.

In fact, recent research has led one step further. Models of each of these components have been presented which have boundary conditions that are compatible with the adjoining component model. In this way, two or more of these models can be coupled even though they have not been fully integrated. A decision has thus been forced on us by the state of the art. We will have to be satisfied with coupled component boundary problems rather than a single fully-integrated analysis. Takasao et al.'s model mentioned previously is, in fact, a coupled model of overland flow and interflow. Regrettably, unsaturated flow is not included in the model. According to Sloan and Moore (1984) unsaturated flow generally has powerful influence on the runoff process of hillslope. Many of hydrogeologists have tried to couple the saturated and unsaturated flows. Freeze(1971), Neuman(1973) and Akai, Ohnishi and Nishizaki(1977) coupled the models of saturated and unsaturated flows to form a synthesized subsurface model. The

treatment of the water table is satisfactory but the treatment of seepage face is not, because the effect of overland flow is not taken into consideration.

Smith and Woolhiser(1971a, 1971b) coupled an overland flow model in the form of a kinematic cascade to a subsurface flow model in the sense that they determine infiltration from the plane at any point with a one-dimensional, vertical, saturated-unsaturated flow calculation. The mathematical model consisted of the simultaneous solution of the kinematic equation of overland flow and the one-dimensional form of the subsurface flow equation. Similarly to Neuman et al.'s model, in Smith and Woolhiser's model infiltration was calculated on the basis of Darcy's law; the hydraulic effect of overland flow(which was described by the kinematic wave model) on the subsurface system was completely neglected.

Ishihara and Takasao(1959), Wooding(1965a,1965b,1966), Harbaugh and Chow(1967), Chen and Chow(1968) and Kibler and Woolhiser(1970) have created watershed models for upstream catchment areas that couple models of overland flow to models of channel flow. With this approach the shallow water equations, or their kinematic approximation, are first applied to the overland flow phase with rainfall as the lateral inflow, and then to the channel flow phase with overland flow as the lateral flow. In all these watershed models, coupling exists only between the surface flow components. Subsurface flow is either ignored or specified as a simple external function representing loss by infiltration.

Freeze(1972b) has coupled the saturated-unsaturated subsurface flow model with the channel flow model. In the coupled model overland flow is not included.

For the purpose of analyzing comprehensively the hillslope hydrological processes a completely integrated model of overland flow, subsurface flow and channel flow is necessary. In this thesis the saturated-unsaturated subsurface flow model will be coupled with the overland flow model to form a synthesized hillslope model. On the basis of the resulting model the control problem of reservoir systems will be examined.

1.3. The System Approach to Solving Water Resources Problems

In recent decades, in the area of water resources management two new developments are becoming increasingly more important. These are the application of systems analysis techniques to improve the planning and decision-making processes, and the need for interdisciplinary teamwork during such analyses. Systems analysis has provided a new dimension to man's analytical capabilities, and improvements in computer technologies have significantly improved man's computational abilities. These two development, in combinations, now enable planners to develop new and effective management strategies for a resource like water.

In general a system is an arbitrarily isolated combination of elements(abstract and arbitrary subdivisions) of the real world. Usually the elements correspond to physical components of the real world, as illustrated in Figure 1.2 for a river basin. In this case the components are rivers, dams, sources of water, users of water, etc. The mathematical representation of the system is termed the model of the system. The systems approach represents an attempt to find answers to questions that are posed regarding complex assemblies of physical systems with interaction between the subsystems. Systems analysis may be defined as an analytical study that helps the decision maker to identify and select a preferred course of action among several feasible alternatives. It is a logical and systematic approach wherein assumptions, objectives, and criteria are clearly defined and specified. It can significantly aid a decision maker to arrive at better decisions by broadening his information base, by providing a better understanding of the system and the interlinkages of the various subsystems, by predicting the consequences of several

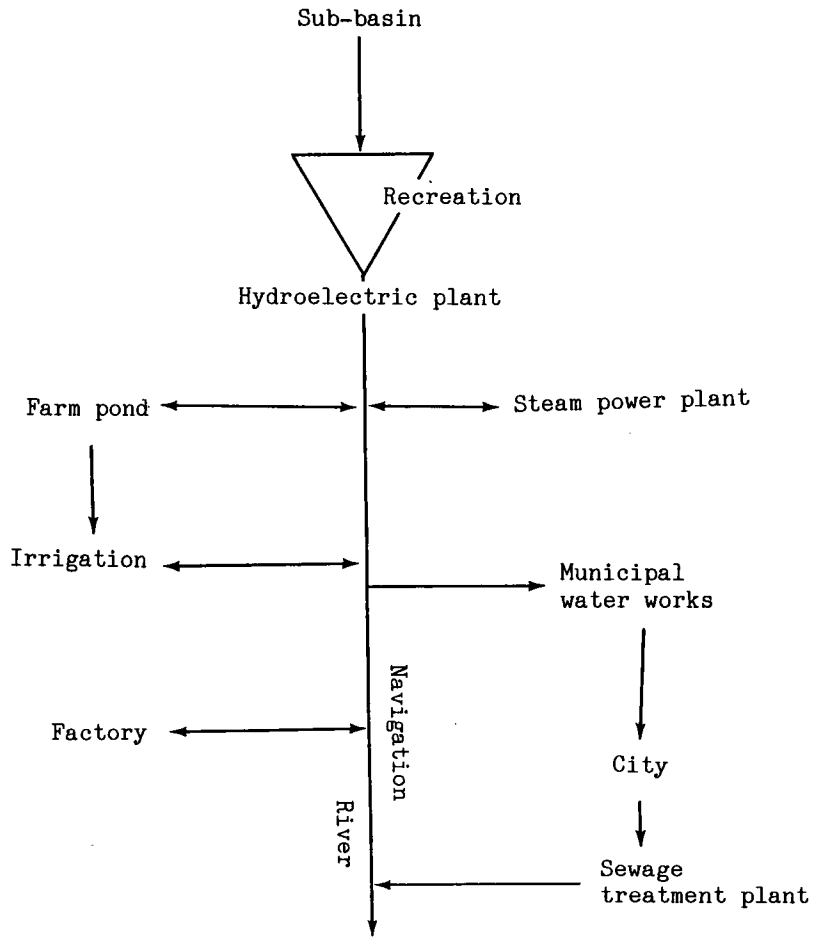


Figure 1.2 Physical components of a river basin that form a system.

alternative courses of action, or by selecting a suitable course of action that will accomplish a prescribed result. Systems analysis has added a totally new dimension to the science of policy-planning and decision-making.

When we relate the concepts of systems analysis to the problems of water resources management, there are two major areas of application: (1) the planning and (2) the operation of water resources systems. Planning for the unified development of a river basin consists of the collection of a data base followed by a series of decisions, e.g., whether and when to build each dam and canal, where to locate new towns and industries, how to operate the reservoirs and so forth. Planning is concerned with selecting from all possible alternatives that particular set of actions which will best accomplish the overall objectives of the policy planner.

Operation of a water resources system, on the other hand, is concerned with what decisions are necessary to best accomplish the objectives of an existing system. While the operation of an existing water resources system may be considered disjointly from the planning functions, the planning for expansion of existing system definitely must encompass the hypothesized future operation of the system. In general, operation is concerned with the optimization of an existing system, whereas planning attempts to formulate an optimal system by possible additions of elements to the existing system. In this work, we only deal with the operation problem of an existing system.

Water resources systems are large-scale projects generating a variety of influential outputs. Water supply for municipal, industrial, or agricultural use, flood protection, energy generation, navigation, water quality improvement and recreation are some of the many benefits these systems offer to the societies living within their

influence range. To fulfil these objectives, a water resources system must successfully manage the water volumes provided by the uncertain natural processes. This is where the element of risk originates and often becomes the cause of costly operational failures.

As defined earlier, operation of a water resources system is concerned with the optimization of the system. Various mathematical optimization models of water resources systems have been suggested (see Chapter 4). Although some of these models perform satisfactorily in the particular applications for which they are developed, a methodology able to handle the operational problem of water resources systems in its full complexity is still lacking. As a result, in practise the majority of water resources systems are operated by heuristic rules derived by computer-aided simulation and engineering intuition.

Optimization of uncertain dynamic systems is the subject of optimal stochastic control theory. A stochastic control study is generally completed in two steps:

(1) system model development: This is the phase where a model able to adequately reproduce the system's behavior is identified. The identification process requires intuitive understanding of the laws governing the system dynamics and can take advantage of input-output data records to properly adjust certain model parameters. A system model, of course, incorporates many simplifying assumptions to make the model manageable. One must be wary that the models developed do not become so simple that they no longer reflect the real physical system, or so rigid and mechanical that they cannot include the social benefits and costs.

(2) stochastic controller design: Based on the identified model and specified performance criteria which must correctly reflect the

system's objectives, an optimization algorithm(controller) is designed to guide the system in successful operation.

This study's developments will proceed along these lines.

1.4 Framework and Outline

This thesis contains two parts: development of hillslope runoff model and real-time operational management of multireservoir systems in their general form. The organization is indicated by the following outline.

In Chapter 2 a synthesized hillslope runoff model will be developed and applied to hillslope systems. The mathematical model consists of the simultaneous solution of the equation of two-dimensional saturated-unsaturated subsurface flow and the sheetflow equation of overland flow. The intention is to take into consideration the hydraulic interaction of overland flow with subsurface flow in a runoff model. The mathematical model is solved by the Galerkin Finite Element Method. This chapter also contains simulation analyses of influence of the various hydrological parameters on runoff characteristics and hillslope hydrologic processes.

In Chapter 3, based on the comprehensive understanding of hillslope runoff processes obtained in Chapter 2, the synthesized runoff model is lumped to form a lumped parameter runoff model for practical purposes.

Chapter 4 discusses the real-time control problem of multireservoir systems. The system model will first be developed in its general form. From the system model, the mathematically treatable operation problem will be derived and then the development of a suitable control algorithm will follow.

Chapter 5 is a verification and test of the control method's reliability, computational efficiency, and potential in real-time decision making.

Chapter 6 concludes the study and identifies further research directions.

Chapter 2

A SYNTHESIZED RUNOFF MODEL OF SURFACE FLOW AND SUBSURFACE FLOW

2.1. Mathematical Model

2.1.1. Region of Flow

The two-dimensional vertical cross-section ABCDEFGHA shown in Figure 2.1 is chosen as the region of flow. We will assume this section to be in a plane parallel to the delivery direction of water toward a stream. The stream bounds the section at ABC and flows roughly perpendicular to it. The region of flow is bounded along AH by the table of overland flow, and along HG by the land surface. The basal boundary is a geological one separating the permeable near-surface soils from the less-permeable underlying soils or rocks. In some cases this boundary may occur where the developed A-layer of soil profile blends into the parent material; in other cases it may separate unconsolidated geological deposits from bedrock. If the permeability contrast across boundary is large enough(say 2 - 3 orders of magnitude or more), we are justified in taking the boundary as impermeable and disregarding the very small contributions to the flow system that occur below it. The right-hand boundary GF is in the plane separating our region of flow from the adjacent hillslope that feeds the adjacent tributary stream. The configuration of the flow

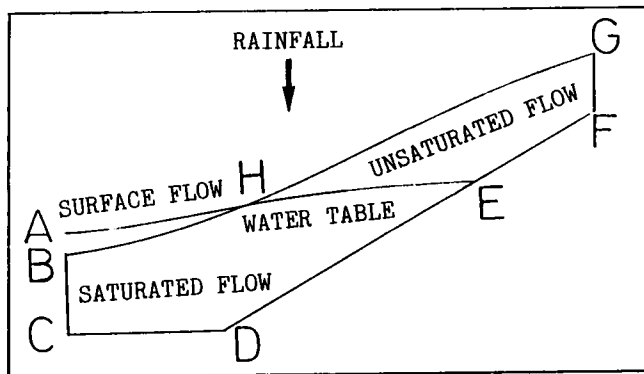


Figure 2.1 Region of flow.

system decrees that there is no flow across this plane and in our two-dimensional section it becomes an imaginary impermeable boundary.

The region of flow consists of three sub-regions: region of overland flow ABHA, region of saturated subsurface flow BCDEHB, and region of unsaturated subsurface flow HEFGH. The boundaries may be highly irregular, and the region may harbour a complex heterogeneous and anisotropic configuration of soil layers and geological formations.

2.1.2. Equation of Saturated-Unsaturated Subsurface Flow

The equation of saturated-unsaturated subsurface flow is developed on the basis of the equation of continuity for transient flow through a saturated-unsaturated porous medium, and is put into its usual form with the aid of Darcy's law.

2.1.2.1 Pressure Head

In the field of soil physics the energy is usually used as state variable. When the fluid is assumed to be homogeneous, a potential function Φ may be introduced such that:

$$\Phi = gZ + \int_{p_0}^p \frac{1}{\rho(p)} dp + \frac{1}{2}v^2 \quad (2.1)$$

where g is gravitational acceleration, Z elevation above some reference datum, p fluid pressure, p_0 reference pressure. If we consider the reference pressure p_0 to be zero, then fluid pressure p is the pressure above atmospheric. ρ is fluid density and a function of fluid pressure p , v is fluid velocity. Generally the kinetic energy

of the fluid through a porous medium is assumed to be too small to be considered by virtue of the low velocities encountered in subsurface flow. Between the fluid pressure p and pressure head h the following relation holds true:

$$dp = g\rho(p)dh \quad (2.2)$$

Combination of (2.1) and (2.2) yields

$$\Phi = gZ + \int_0^h g\rho dh = g(Z + h) \quad (2.3)$$

The hydraulic head H is defined as

$$H = \Phi/g = Z + h \quad (2.4)$$

In the case of saturated-unsaturated flow, the pressure head h is generally selected as a state variable. The soil water in the saturated zone is at a pressure greater than atmospheric, so its pressure head is positive. The soil water in the unsaturated zone is at a pressure lower than atmospheric, so its pressure head is negative(a subpressure commonly known as tension or suction). The pressure head at a free-water surface is zero, thus the pressure head is continuous over the entire region of subsurface flow.

2.1.2.2 Continuity Equation for Saturated-Unsaturated Flow

The equation of continuity is a statement of the conservation of mass during fluid flow through an elemental volume of porous media. It states that the net rate of fluid mass flow into any elemental control volume within the porous media must equal the time rate of change of fluid mass storage within the element. Referring to the elemental volume shown in Figure 2.2, the equation of continuity can be written as follows(Hillel,1971):

$$\frac{\partial}{\partial x}(\rho v_x) + \frac{\partial}{\partial y}(\rho v_y) + \frac{\partial}{\partial z}(\rho v_z) = - \frac{\partial}{\partial t}(\rho\omega) \quad (2.5)$$

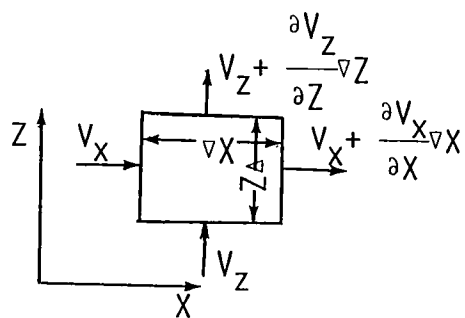


Figure 2.2 Continuity relationship in elemental volume of porous media.

For the two-dimensional flow problem to be considered in this study, Eq.(2.5) becomes:

$$\frac{\partial}{\partial x}(\rho v_x) + \frac{\partial}{\partial z}(\rho v_z) = - \frac{\partial}{\partial t}(\rho\omega) \quad (2.6)$$

where ρ : density of water[M/L³]

$\mathbf{v}=(v_x, v_y, v_z)$: velocity of fluid flow[L/T]

ω : moisture content of soil[decimal fraction]

x, y, z : coordinate directions[L]

t : time[T]

2.1.2.3 Equation of Motion for Saturatd-Unsaturated Flow

For saturated flow, the velocity is given by a simplified form of the momentum balance equation known as Darcy's law

$$\begin{Bmatrix} v_x \\ v_z \end{Bmatrix} = -K \begin{Bmatrix} \frac{\partial H}{\partial x} \\ \frac{\partial H}{\partial z} \end{Bmatrix} = -K \text{ grad}H \quad (2.7)$$

where K : hydraulic conductivity of soil[L/T]

H : hydraulic head defined by Eq.(2.4)[L]

grad : gradient operator

In this case K is constant in space and time.

For saturated flow in an anisotropic porous medium, Darcy's law takes the following form(see Appendix A):

$$\begin{Bmatrix} v_x \\ v_z \end{Bmatrix} = - \begin{bmatrix} K_{xx} & K_{xz} \\ K_{zx} & K_{zz} \end{bmatrix} \begin{Bmatrix} \frac{\partial H}{\partial x} \\ \frac{\partial H}{\partial z} \end{Bmatrix} = -K \text{ grad}H \quad (2.8)$$

where K : hydraulic conductivity tensor

$$K_{xx} = \bar{K}_\zeta \cos^2 \alpha + \bar{K}_\eta \sin^2 \alpha$$

$$K_{zz} = \bar{K}_\zeta \sin^2 \alpha + \bar{K}_\eta \cos^2 \alpha$$

$$K_{xz} = K_{zx} = (\bar{K}_\zeta - \bar{K}_\eta) \sin\alpha \cos\alpha$$

$\bar{K}_\zeta, \bar{K}_\eta$: hydraulic conductivities in the principal directions[L/T]

α : angle of the principal directions relative to the coordinate axes

For saturated flow in a heterogeneous and anisotropic medium, K_{ij} ($i, j = x, z$) becomes a function of space due to the spatial heterogeneity, that is, $K_{ij} = K_{ij}(F) = K_{ij}(x, z)$, where F denotes a specific geologic formation or soil type.

Darcy's law, though originally conceived for saturated flow only, was extended by Richards(1933) to unsaturated flow with the provision that the conductivity is a function of the pressure head h(see Figure 2.3). Since the pressure head changes with time, k is also a function of time. For unsaturated flow in a heterogeneous, anisotropic medium, Darcy's law can then be written as

$$\begin{Bmatrix} v_x \\ v_z \end{Bmatrix} = -K(x, z, h) \text{ grad}H \quad (2.9)$$

Inserting Eq.(2.9) into Eq.(2.6) yields

$$\sum_{i=1}^2 \sum_{j=1}^2 \frac{\partial}{\partial x_i} (\rho K_{ij} - \frac{\partial H}{\partial x_j}) = M_c \frac{\partial H}{\partial t} \quad (2.10)$$

where $(x_1, x_2) = (x, z)$

$$(K_{11}, K_{12}, K_{21}, K_{22}) = (K_{xx}, K_{xz}, K_{zx}, K_{zz}),$$

M_c : fluid mass capacity[M/L⁴]

The fluid mass capacity is defined as follows

$$M_c = \frac{d}{dh}(\rho\omega) = \frac{d}{dh}(\rho n S_r) \quad (2.11)$$

where n: porosity of soil[decimal fraction]

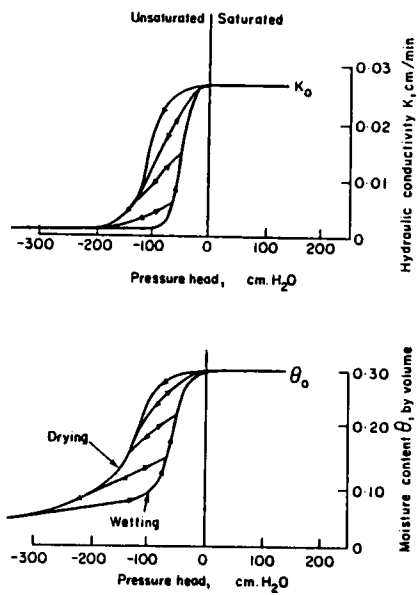


Figure 2.3 Functional relationships between hydraulic conductivity, moisture content and pressure head.

$S_r = \omega/n$: saturation [decimal fraction]

The right-hand side of Eq.(2.11) can be expanded to produce three terms

$$M_c = \rho n \frac{dS_r}{dh} + \rho S_r \frac{dn}{dh} + n S_r \frac{d\rho}{dh} \quad (2.12)$$

The three terms in Eq.(2.12) have very specific and important meanings. They refer respectively to changes in the mass storage within the elemental volume due to (1) changes in the degree of saturation, (2) changes in the porosity, and (3) changes in the fluid density. The first of these effects is limited to the unsaturated zone, and the second to the saturated zone. The changes in the porosity are related to the compressibility of the porous medium, and the changes in the fluid density to the compressibility of the fluid. If water and soil can be considered to be elastic materials. The compressibilities of water and soil can be expressed approximately as follows:

$$\frac{dn}{dh} = \rho g \alpha \quad (2.13)$$

$$\frac{d\rho}{dh} = \rho^2 g \beta \quad (2.14)$$

where α : compressibility of soil

β : compressibility of water

On the other hand, the moisture content ω is a characteristic function of the pressure head. Soil physicists have denoted the slope of this curve, which is also a function of pressure head, as the specific moisture capacity:

$$C = d(nS_r)/dh \quad (2.15)$$

For a heterogeneous medium, $C = C(F,h)$.

Inserting Eqs.(2.12), (2.13), (2.14), and (2.15) into Eq.(2.10) yields

$$\sum_{i=1}^2 \sum_{j=1}^2 \left\{ \rho \frac{\partial}{\partial x_i} (K_{ij} \frac{\partial H}{\partial x_j}) + \frac{\partial \rho}{\partial x_i} K_{ij} \frac{\partial H}{\partial x_j} \right\} = \rho (C + S_r S_s) \frac{\partial h}{\partial t} \quad \text{-----}(2.16)$$

where S_s denotes specific storage and is defined as

$$S_s = \rho g (\alpha + n\beta) \quad (2.17)$$

The second term in the left-hand side of Eq.(2.16) is far smaller than the first term. Thus, it is usually neglected. This approximation reduces Eq.(2.16) to

$$\sum_{i=1}^2 \sum_{j=1}^2 \frac{\partial}{\partial x_i} \left\{ K_{ij} \frac{\partial}{\partial x_j} (h + x_2) \right\} = (C + \frac{\omega}{n} S_s) \frac{\partial h}{\partial t} \quad (2.18)$$

This is the final form of the governing equation for saturated-unsaturated subsurface flow.

2.1.2.4 Soil Parameters

In the unsaturated domain, the hydraulic conductivity K and moisture content are both functions of the pressure head h for any soil type F . The functional relationships are hysteretic in that the curves differ depending on whether the soil is wetting or drying. To illustrate, Figure 2.3 shows the characteristic curves for a naturally-occurring soil known as Del Monte sand (Liakopoulos, 1965). The scanning curves between the main wetting and drying curves provide the necessary data for cases where the soil changes from wetting to drying or vice versa at some intermediate condition of saturation.

The specific moisture capacity C that appears in Eq.(2.18) is simply the slope of the curve $\omega = \omega(h)$. For saturated flow ($h > 0$), the soil parameters are constant, and $K = K^s$ (saturated hydraulic conductivity), $\omega = n$, and $C = 0$.

As pointed out by Freeze(1971), while hysteresis can be important in some applications, it seems likely that the uncertainties as to the exact form of the basic curves for field soils will more than outweigh the secondary influences of hysteresis in hillslope hydrology simulations. It is therefore common to utilize single $K(h)$ and $\omega(h)$ curves to represent the unsaturated hydrologic properties of a soil.

The $K(h)$ and $\omega(h)$ curves are strongly dependent on soil texture. Figure 2.4 shows curves for three hypothetical soil types(Freeze, 1971): (a) a uniform sand, (b) a silty sand, and (c) a silty clay. The uniform sand shows high saturated hydraulic conductivity, a low porosity, a high capacity over a narrow range of pressure heads, and low moisture content at high tension needs. Such a soil would show a sharp gradient in moisture content and permeability across the water table. As a soil becomes less uniform and less permeable(curves b and c), the porosity increases, and the specific storage capacity becomes more uniform. Moisture contents and permeabilities would tend to show more gradual changes in the vicinity of the water table in such soils.

The h_a value shown in Figure 2.5 represents the air-entry pressure head. Over the range $0 \sim h_a$, conditions remain saturated even though the pressure heads are less than atmospheric. This gives rise to the tension-saturated zone above the water table, better known as the capillary fringe.

The characteristic curves can be determined in the laboratory using techniques that are well developed in the soil physics field. Data on naturally-occurring soils abound in the soil physics literature. But the reliability of the data comes in to question.

Clearly, the greater are the changes in hydraulic conductivity (K) and moisture content (ω) due to the changes in pressure head of

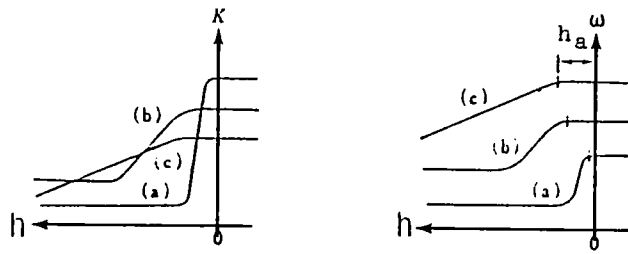


Figure 2.4 Single-valued functional relationships between hydraulic conductivity, moisture content and pressure head for three hypothetical soils (a) Uniform sand, (b) silty sand, (c) silty clay.

unsaturated zone, the stronger is the non-linearity of the governing equation (2.18). Sometimes its solution may be very difficult. In these cases it is common for one to rewrite the pressure head (h) based Eq.(2.18) into the moisture content (ω) based form. The specific storage is generally considered to be constant.

Neuman(1973) assumed that the hydraulic conductivity can be approximately expressed as

$$K = K_r \cdot K^s \quad (2.19)$$

where K^s is the saturated hydraulic conductivity tensor and is only a function of geological formations (F). K_r denotes relative hydraulic conductivity and is a monotone function of moisture content (ω); $K_r = 1$ in the saturated zone, $K_r \leq 1$ in the unsaturated zone.

2.1.2.5 Initial Conditions

The initial conditions for the governing equation (2.18) are the distributions of pressure head over the region of subsurface flow and can be stated as

$$h(x_1, x_2, t) \Big|_{t=0} = h_0(x_1, x_2) \quad (2.20)$$

where $h_0(x_1, x_2)$ is a prescribed function and will not be given arbitrarily. There are two sets of initial conditions that are hydrologically meaningful and mathematically treatable: (1) static conditions, and (2) steady state flow. The first one can be considered a special case of the second one.

Under static initial conditions, it is assumed that there is no flow through the system. The hydraulic head $H(x_1, x_2, 0)$ is constant for

all (x_1, x_2) , and the water table($h = 0$) is horizontal and at an elevation level with the stream surface. Above the water table, there will be an equilibrium configuration of pressure heads and moisture content.

For steady state flow, the time-dependent term is removed from the right-hand side of Eq.(2.18); the steady state equation of flow becomes

$$\sum_{i=1}^2 \sum_{j=1}^2 \frac{\partial}{\partial x_i} \{ K_{ij} \frac{\partial}{\partial x_j} (h + x_2) \} = 0 \quad (2.21)$$

The initial flow regime is determined by solving this reduced flow equation for $h(x_1, x_2)$, given $K(F, h)$ for each soil type and a set of steady state boundary conditions around the region of flow.

2.1.2.6 Boundary Conditions

The boundary conditions can be divided into three types: (1) Dirichlet type(or first-type), (2) Neumann type(or second-type), and (3) mixed type(or third-type). Dirichlet boundary conditions are the value of function h , Neumann boundary conditions the normal derivative of h , and the mixed boundary conditions the combination of the function and the normal derivative on the region of definition. The mixed boundary conditions do not commonly appear in subsurface flow problems.

(1) Neumann Boundary Conditions

Referring to Figure 2.1, along the basal impermeable boundary CDEF and the imaginary vertical impermeable boundary FG

$$\frac{\partial}{\partial \mathbf{n}} (h + x_2) \Big|_{(x_1, x_2) \in \text{CDEFG}} = 0 \quad (2.22)$$

where \mathbf{n} is the outward unit normal direction of the boundaries.

On the land surface BHG

$$\sum_{i=1}^2 \sum_{j=1}^2 K_{ij} \frac{\partial}{\partial x_j} (h+x_2) \cos(\mathbf{n}, \mathbf{x}_i) \Big|_{(x_1, x_2) \in \text{BHG}} = Q(x_1, x_2, t) \quad \text{-----}(2.23)$$

where $Q(x_1, x_2, t)$ is the prescribed flux distribution along the boundary BHG. On the boundary HG we allow a time- and space-dependent rainfall(or evaporation) rate $R(x_1, x_2, t)$ (with dimensions [L/T]), where R positive is a rainfall rate and R negative is an evaporation rate. If we restrict ourselves to rainfall rate less than the saturated hydraulic conductivity of the surface soils, then ponding will not occur on the surface where $h < 0$, and there is no possibility of overland flow. Under these circumstances, all precipitation R becomes infiltration. This fact can be stated as

$$Q(x_1, x_2, t) \Big|_{(x_1, x_2) \in \text{HG}} = R(x_1, x_2, t) \cos \theta \quad , \quad h < 0 \quad (2.24)$$

where θ is the angle of land surface from the horizontal level and is a function of (x_1, x_2) .

Along the saturated land surface BH

$$Q(x_1, x_2, t) \Big|_{(x_1, x_2) \in \text{BH}} = I(x_1, x_2, t) \cos \theta \quad , \quad h \geq 0 \quad (2.25)$$

where I positive is an infiltration rate and I negative is a seepage rate(or return flow flux), I will be treated as another independent variable in addition to the pressure head h . I and h are the solution of simultaneous equations consisting of the subsurface flow equation (2.18) subject to the initial and boundary conditions and the overland flow equation to be derived in the next section.

(2) Dirichlet Boundary Conditions

Along the boundary BC, the hydraulic heads are specified

$$h(x_1, x_2, t) \Big|_{(x_1, x_2) \in BC} = H_D(x_1, x_2, t) - x_2 \equiv h_D(x_1, x_2, t)$$

-----(2.26)

where $H_D(x_1, x_2, t)$ is a prescribed function.

2.1.3 Equation of Overland Flow

Overland flow is assumed to be one-dimensional flow in the S-direction (Figure 2.5) parallel to the X-Z plane of the subsurface cross-section in Figure 2.1. We will also make use of the sheetflow representation of overland flow and form of shallow water equations. The governing equations are derived on the basis of an equation of continuity and the Navier-Stokes equations, and simplified by using the kinematic approximation and the Manning equation.

2.1.3.1 Equation of Continuity

Referring to Figure 2.5, if the fluid is assumed to be homogeneous, incompressible Newtonian fluid, the equation of continuity can be written as

$$\frac{\partial U}{\partial S} + \frac{\partial W}{\partial T} = 0 \quad (2.27)$$

where S and T are the tangent direction and the normal direction of the land surface, respectively, and U and W are the velocity components in S and T directions, respectively. The kinematic boundary conditions at the free-water surface and at the land surface, respectively, can be expressed as follows:

$$\left(\frac{\partial h_s}{\partial t} + U \frac{\partial h_s}{\partial S} - W \right) \Big|_{T=h_s} = R(x_1, x_2, t) \cos \theta \quad (2.28)$$

$$- W \Big|_{T=0} = I(x_1, x_2, t) \cos \theta \quad (2.29)$$

where h_s denotes depth of overland flow in the T-direction and is a function of S. Eq.(2.27) is integrated with respect to T from 0 to h_s using the boundary conditions Eqs.(2.28) and (2.29) and evaluating

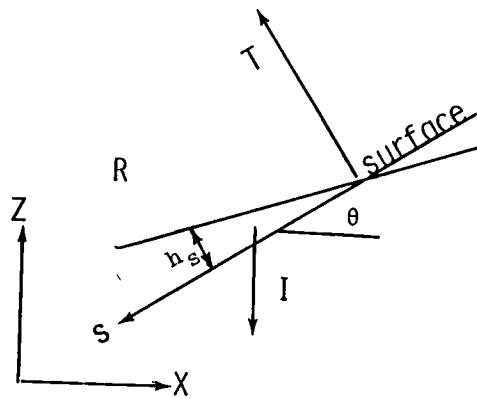


Figure 2.5 The coordinate system for overland flow.

each term by the Leibnitz rule of differentiation under the integral sign, to yield

$$\frac{\partial}{\partial S}(\bar{U}h_s) + \frac{\partial h_s}{\partial t} = (R - I)\cos\theta \quad (2.30)$$

where \bar{U} is average velocity of overland flow in T-direction, and defined as

$$\bar{U} = \frac{1}{h_s} \int_0^{h_s} U \, dT \quad (2.31)$$

2.1.3.2 Equation of Motion

Only S-direction component of the Navier-Stokes equation is necessary due to the assumption that overland flow is one-dimensional flow along the land surface:

$$\frac{\partial U}{\partial t} + U\frac{\partial U}{\partial S} + W\frac{\partial U}{\partial T} = g\sin\theta - \frac{1}{\rho} \frac{\partial p}{\partial T} \quad (2.32)$$

where ρ is the density of water, g gravitational acceleration, and p pressure. The kinematic boundary conditions at the free-water surface and at the land surface, respectively, are given by Eq.(2.28) and Eq.(2.29). The dynamic condition at the free-water surface, neglecting the insignificant surface tension, can be written as

$$p(S,T,t) \Big|_{T=h_s} = 0 \quad (2.33)$$

The dynamic condition at the land surface is expressed as

$$p(S,T,t) \Big|_{T=0} = p_{T_0}(S,t) \quad (2.34)$$

where p_{T_0} is the pressure along the land surface, which depends on the flow conditions. Because a simple relation between the fluid velocity and the changes in pressure has not yet been found, the treatment of

p_{T_0} becomes a problem, In order to avoid this problem, Shiiba(1983)

has assumed that the velocity of overland flow can be expressed as a summation of the velocity of subsurface flow at the land surface and the velocity of overland flow in the case where there is no infiltration or seepage. We shall also make use of this approximation to derive the average velocity of overland flow in the S-direction.

Following the above assumption, even though the continuity equation (2.30) will be used, the pressure at the land surface p_{T_0} depends only on the velocity of overland flow in the case where there is no infiltration or seepage. Under this assumption, we integrate Eq.(2.32) with respect to T from 0 to h_s . Using the Leibnitz rule of differentiation under the integral sign and the corresponding boundary conditions at the free-water and land surfaces yields the following equation:

$$\frac{\partial}{\partial t}(U'h_s) + \frac{\partial}{\partial t}(U'h_s) - RV\cos\theta = gh_s\sin\theta - gh_s\frac{\partial h_s}{\partial S}\cos\theta - \frac{\tau_s}{\rho}$$

-----(2.35)

where V is the mean terminal velocity of rainfall which is assumed vertical, τ_s boundary shear in S-direction. Note that U' represents the average velocity of overland flow in the case where there is no infiltration or seepage.

The mathematical treatment of Eq.(2.35) is very difficult, but many of the problems can be removed if we make use of a simplified analysis based on the kinematic flow model. Kinematic flow occurs on a plane whenever a balance between gravitational and frictional forces is achieved. Under such circumstances, the left-hand side of Eq.(2.35) is too small to be neglected and the equation of motion reduces to

$$\frac{\tau_s}{\rho g} = h_s \sin\theta - h_s \frac{\partial h_s}{\partial S} \cos\theta \quad (2.36)$$

Woolhiser and Liggett(1967) have given the conditions under which the kinematic approximation is valid, and shown that the kinematic approximation is best for a rough, steep slope with low rates of lateral inflow. This approximation is valid on almost all overland flow planes.

The boundary shear τ_s can be defined by a depth-velocity relationship such as the empirical Manning equation. For sheetflow, the Manning equation can be written as:

$$\tau_s = \rho g n_0^2 h_s^{-1/3} |U'| |U'| \quad (2.37)$$

in which n_0 is a resistance parameter known as Manning's friction factor(or roughness) and a dimensionless number. The relation (2.37) was originally proposed for channel flow, but Takasao and Gishimoto(1961) have shown that it is also valid for overland flow. The Manning equation is now widely used for overland flow analyses, though n_0 varies widely with the land surface conditions. Many workers have noted that n_0 is not a true constant but is a function of the depth of flow. In this analysis, however, n_0 is taken as constant for all flow depths and at all times for any point on the hillslope. The value of n_0 is allowed to vary along the length of the hillslope.

Inserting Eq.(2.37) into Eq.(2.36) yields

$$U' = \frac{\alpha}{n_0} \sqrt{|\sin\theta - \frac{\partial h_s}{\partial S} \cos\theta|} h_s^{2/3} \quad (2.38)$$

where $\alpha = 1$ if $(\sin\theta - \frac{\partial h_s}{\partial S} \cos\theta) \geq 0$, $\alpha = -1$ if $(\sin\theta - \frac{\partial h_s}{\partial S} \cos\theta) < 0$. Then following the Shiiba's assumption, the average

velocity of overland flow can be expressed as(for convenience' sake, \bar{U} is written as U below)

$$U = \frac{\alpha}{n_0} \sqrt{|\sin\theta - \frac{\partial h_s}{\partial S} \cos\theta|} h_s^{2/3} + V_g \quad (2.39)$$

where V_g is the velocity of subsurface flow on the land surface. Based on Darcy's law it can be expressed as (Appendix A):

$$V_g = \xi_s \frac{\partial h}{\partial S} + \xi_T \frac{\partial h}{\partial T} + \xi_0 \quad (2.40)$$

where

$$\xi_s = -\frac{1}{n} [K_{11} \cos^2\theta + 2K_{12} \sin\theta \cos\theta + K_{22} \sin^2\theta]$$

$$\xi_T = \frac{1}{n} [(K_{22} - K_{11}) \sin\theta \cos\theta + K_{12} (\cos^2\theta - \sin^2\theta)]$$

$$\xi_0 = \frac{1}{n} [K_{12} \cos\theta + K_{22} \sin\theta]$$

$$K_{12} = K_{21}$$

2.1.3.3 Boundary Conditions and Initial Conditions for Overland Flow

In order to relate overland flow with subsurface flow, we re-write the depth-based equations (2.30) and (2.39) into the pressure-based form. The relation between the flow depth h_s and pressure head h can be expressed as

$$h = h_s \cos^2\theta \quad (2.41)$$

Substitutions of this equation into Eqs.(2.30) and (2.39) reduce the equation of continuity and the equation of motion, respectively, to

$$\frac{\partial}{\partial S}(Uh/\cos^2\theta) + \frac{\partial h}{\partial t}/\cos^2\theta = (R - I)\cos\theta \quad (2.42)$$

$$U = F\left(\frac{\partial h}{\partial S}\right)h^{2/3} + V_g \quad (2.43)$$

where

$$F\left(\frac{\partial h}{\partial S}\right) = \frac{\alpha}{n_0} \sqrt{|\sin\theta - \frac{\partial h}{\partial S}(\frac{1}{\cos\theta})|} (\cos\theta)^{-(4/3)}$$

Now we can write the initial and boundary conditions for overland flow as follows:

Referring to Figure 2.2, at the outlet of overland flow

$$h(S,t) \Big|_{\text{at point B}} = h_D(x_1, x_2, t) \Big|_{(x_1, x_2) = (0, D)} \quad (2.44)$$

where $h_D(x_1, x_2, t)$ is defined by Eq.(2.26).

At the seepage point H, we have

$$h(S,t) \Big|_{S=0} = 0 \quad (2.45)$$

The initial conditions can be stated as

$$h(S,t) \Big|_{t=0} = h_0(x_1, x_2) \Big|_{(x_1, x_2) \in BH} \quad (2.46)$$

2.1.3.4 Linearization of the Equations of Overland Flow

Since Eqs.(2.42) and (2.43) are strongly non-linear with respect to h and $\frac{\partial h}{\partial S}$, their numerical treatments are very difficult and sometimes the solution may diverge. For this reason we shall make use of their quasi-linearized forms for analyses.

U_h can be considered a function of h and $\frac{\partial h}{\partial S}$. If we consider a nominal function $\bar{h} = \bar{h}(S)$ for h , U_h can be approximated as:

$$\begin{aligned} U_h &= U_h \Big|_{-} + \frac{\partial(U_h)}{\partial h} \Big|_{-} * (h - \bar{h}) + \frac{\partial(U_h)}{\partial\left(\frac{\partial h}{\partial S}\right)} \Big|_{-} * \left(\frac{\partial h}{\partial S} - \frac{\partial \bar{h}}{\partial S}\right) \\ &\equiv [A'(S)\frac{\partial h}{\partial S} + B'(S)h + C(S)] + g_T h \frac{\partial h}{\partial T} \end{aligned} \quad (2.47)$$

where $f(\cdot) \Big|_- = f(\cdot) \Big|_{h=\bar{h}, \partial h/\partial S = \partial \bar{h}/\partial S}$

and

$$A'(S) = \bar{h}^{5/3} F'(\frac{\partial \bar{h}}{\partial S}) + g_S \bar{h}$$

$$B'(S) = \frac{5}{3} F(\frac{\partial \bar{h}}{\partial S}) \bar{h}^{2/3} + g_S \frac{\partial \bar{h}}{\partial S} + g_0$$

$$C'(S) = -\frac{2}{3} \bar{h}^{5/3} F(\frac{\partial \bar{h}}{\partial S}) - \bar{h}^{5/3} F'(\frac{\partial \bar{h}}{\partial S}) \frac{\partial \bar{h}}{\partial S} - g_S \bar{h} \frac{\partial \bar{h}}{\partial S}$$

When $F(\frac{\partial \bar{h}}{\partial S}) = 0$, $F'(\frac{\partial \bar{h}}{\partial S})$ becomes infinite. In this case, a enough large number will be chosen by considering the admissible error to approximate it. Then we can put the equation of overland flow into the following final form:

$$\frac{\partial}{\partial S} (A \frac{\partial h}{\partial S} + Bh + C + g_T h \frac{\partial h}{\partial T} / \cos^2 \theta) + \frac{\partial h}{\partial t} / \cos^2 \theta = (R - I) \cos \theta \quad (2.48)$$

where $A = A'(S) / \cos^2 \theta$

$B = B'(S) / \cos^2 \theta$

$C = C'(S) / \cos^2 \theta$

2.2 Solution of the Mathematical Model as a Simultaneous System

In this section we shall solve the hillslope hydrologic model described in the preceding section by the Galerkin Finite Element Method. The steady state flow problem will be first considered to examine the possibility of approximating the land surface curve by a series of straight-line elements, then the transient flow problem is to be solved.

2.2.1 Galerkin Finite Element Method

2.2.1.1 Finite Element Method

The finite element method is a numerical method for solving differential equations by means of " piecewise approximation ". As distinct from the finite difference method, which regards the solution region as an array of grid points, the finite element method envisions the region as being made up of many small interconnected subregions called " finite elements ". Such elements, which generally take simple shapes(e.g. triangular, quadrilateral, and rectangular), are then assembled in various ways to represent a solution domain of arbitrary geometry.

The finite element analysis of a physical problem can be described as follows:

(1) The physical system is subdivided into a series of finite elements that are connected at a discrete number of nodal points, this process is often called " discretization ". Each element is identified by its element number and the lines connecting the nodal points situated on the element boundary. These nodal points serve the purpose

of locating the unknown function, this is, they are the points within the problem domain at which the values of the unknown function are computed. Furthermore, the unknown function within each element is defined in terms of the nodal values by basis or interpolation functions. The unknown function is defined throughout the problem domain in a piecewise fashion over the individual elements.

(2) A matrix expression is developed to relate the nodal variables of each element. The resulting matrix is commonly referred to as an " element matrix ". For a discrete problem, the element matrix relation can often be established via direct physical reasoning. For a continuous problem, the element matrix expression must be obtained via a more general mathematical formulation that normally makes use of either a variational or weighted residual method.

(3) The element matrices are combined or assembled to form a set of algebraic equations that describe the entire global system. The coefficient matrix of the final set of equations is called the " global matrix ". The assembly procedure is performed in such a way that certain compatibility conditions are satisfied at each node shared by different elements.

(4) Prescribed boundary conditions are incorporated into the assembled or global matrix equation.

(5) The resulting set of simultaneous algebraic equations is solved. Here, many different solution algorithms can be employed. Among the widely used algorithms are the Gauss diminution and Choleski decomposition algorithms that take into account the banded and symmetric feature of the coefficient matrix.

The fifth step is the final step if we only want to obtain the nodal values of the unknown function. Additional computation must be

made if other quantities involving derivatives of the function are to be derived from the nodal values.

2.2.1.2 Galerkin's Method

Among the widely used methods for deriving the element matrix equation are the variational method and the weighted residual method. The Galerkin method is a special case of the weighted residual method. The Galerkin method is combined with the finite element technique so frequently that the two have become practically synonymous.

The philosophy behind a variational principle is that a physical quantity, such as the rate of energy dissipation, may be minimized over the problem domain. This rate can be expressed in terms of the potential(head) throughout the domain. If the potential is expressed in terms of its nodal values, the variational principle leads to algebraic equations. Although the variational method provides a convenient approach for deriving the element matrix equation, it is not the only approach available. Frequently we encounter practical problems for which the classical functionals cannot be derived or have not been found(e.g. for non-linear problem). In other words, the variational principle does not exist. For these cases we have to employ a more general approach for formulating the element matrix equations. The weighted residual method is one such approach and has been widely used.

A weighted residual principle is expressed directly in terms of the governing partial differential equation without need to resort to a physical quantity. The residual at each point in the problem domain is a measure of the degree to which the head does not satisfy the governing equation. If a particular weighted average of the residual

is forced to vanish, the nodal heads are obtained as the solution of a system of algebraic equations.

Consider a continuum problem governed by the differential equation

$$L(h) - f = 0 \quad (2.49)$$

in the region D enclosed by Ω , where operator L acts on the unknown function h to generate the known function f . To obtain an approximate solution, the method is applied in three steps. the first step is to approximate the unknown function h by a trial function of the form

$$\bar{h} = \sum_{K=1}^N \alpha_K \phi_K \quad (2.50)$$

where ϕ_K are linearly independent basis functions(also known as coordinate functions and bases) defined over the entire solution domain, and α_K the unknown parameters to be determined subsequently. It is a common practice to select the N basis functions in such a way that all essential(or Dirichlet type) boundary conditions are satisfied.

Because the trial function \bar{h} is only an approximation, it is not likely to satisfy Eq.(2.49) exactly. Substitution of \bar{h} in Eq.(2.49) thus results in an error or residual:

$$\epsilon = L(\bar{h}) - f \neq 0 \quad (2.51)$$

The method of weighted residuals seeks to determine the unknowns α_K in such a way that the error is minimal in some specified sense. This is accomplished by forming a weighted integral of ϵ over the entire solution domain and then setting this integral(weighted residual) to zero. The second step of the procedure thus consists of

selecting N linearly independent " weighting " functions W_n and requiring that

$$\int_D W_n \epsilon \, dD = 0 \quad , \quad n = 1, 2, \dots, N \quad (2.52)$$

Once we specify the functional form of the weighting functions, we can employ Eq.(2.50) to represent \bar{h} and combine this information with Eq.(2.52) to provide a set of simultaneous equations in the N unknowns α_K , $K=1, 2, \dots, N$. The final step is to solve these equations for α_K and hence obtain an approximate representation of the unknown function h via the use of Eq.(2.50). Various classical weighted residual methods can be generated depending on the choice of the weighted functions. The Galerkin method is formulated by selecting the basis function ϕ_K as the weighting functions. Thus the weighted residual equations become

$$\int_D \phi_n \epsilon \, dD = 0 \quad , \quad n = 1, 2, \dots, N \quad (2.53)$$

At this stage, the integral obtained via the Galerkin criterion contains higher-order differentials than the variational functional. This is undesirable because a higher continuity requirement would have to be imposed on the element basis functions(the higher the order of continuity, the narrower our choice of functions becomes). Fortunately, in most cases, we can overcome this difficulty by applying Green's theorem(integration by parts) to the higher-order terms in the integral expression of Eq.(2.53). The order of the integrand is thereby reduced, and this enables us to use interpolating functions with a lower-order inter-element continuity requirement.

2.2.2 Solution of Steady State Flow Problem

In this section, we solve the steady state flow problem. In order to examine the possibility of approximating the land surface curve by a series of straight-line elements, two cases will be used for comparison: the case where all elements are linear triangular elements, and the case where the internal elements(with not more than one node on land surface) are linear triangular elements and all the other elements(surface elements) are curved-sided triangular elements.

2.2.2.1 Finite Element Mesh

The first step of the finite element procedure is to divide the solution domain into a series of finite elements. there are many applicable elements, and it is apparent that the type of element has a great influence upon the degree of accuracy of the solution and the cost of element matrix computation. A question then arises as to which type of element is most appropriate for a particular problem. Unfortunately, there is no clear-cut answer to this question. The optimal element varies generally from problem to problem. The selection of particular elements is very much dependent on the experience and judgment of the analyst. For a two-dimensional problem the most widely used element is a linear triangular element, but it cannot be used directly for our problem described in the preceding section.

The equation of overland flow, Eq.(2.48), contains the partial differentiation with respect to the tangential direction of land surface, $\partial/\partial S$. Because the S-direction is an axis of the curvilinear coordinate system on land surface, its derivative must be continuous. As shown in Figure 2.6, if the linear triangular elements were used,

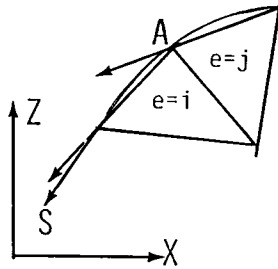


Figure 2.6 The surface curved-sided element

the continuity requirement could not be satisfied. For example, at the point A in Figure 2.6, $\partial/\partial S|_{e=i}$ and $\partial/\partial S|_{e=j}$ would be the differentiations with respect to different directions.

For this reason, it is necessary to approximate land surface by a smooth curve at least with C^1 -continuity. The simplest curve which can satisfy the C^1 -continuity requirement is a quadratic curve. Thus we can use linear triangular elements for internal elements and curved-sided triangular elements with the same quadratic-curved side as the land surface curve for surface elements.

However, it is apparent that the application of two different types of elements to a solution domain must result in complication of the problem and the requirement of more input data and more computation cost. Therefore, we shall examine the possibility of using the simpler linear triangular elements for surface elements, by considering the fact that if the error between the correct solution and the numerical solution is less than the allowed error for a practical purpose, the numerical solution will be referred to as the approximate solution of the problem. In this section we shall solve the steady state flow problem by use of the two different type elements for surface elements respectively and compare the solutions.

2.2.2.2 Basis Functions

Requirements for Basis Functions

The procedures for formulating the element equations via both the variational and weighted residual approaches rely on the assumption that the integral over the entire solution region is equal to the summation of the integrals performed over element subregions. To

ensure that this assumption is valid and that our approximate solution converges to the correct solution as we refine the element mesh, the interpolating(basis or shape) functions must satisfy certain requirements. These requirements are as follows:

(1) At element interfaces, the unknown function h and any of its derivatives up to one order less than the highest derivative appearing in the functional or the weighted residual integral must be continuous. This is called the continuity requirement or the compatibility requirement. Thus, suppose the integrand in the element equation contains up to $(r+1)$ th derivatives of function h . Then at the element interfaces we must have continuity in the r th derivative of h . This is called the C^r -continuity requirement.

(2) The trial function \bar{h} and its derivatives must be able to represent any constant values of h and its derivatives appearing in the functional or the weighted residual integral as, in the limit, the element size is reduced to zero. Thus, suppose the integrand in the element equation contains up to $(r+1)$ th derivatives of function h , then at any of the internal points of the element we must have continuity in the $(r+1)$ th derivative of h . This is known as the completeness requirement.

It is not difficult to derive a C^1 -continuity basis function for linear elements, but the difficulty increases sharply as the order of continuity becomes higher. Fortunately, neither second-order nor higher than second-order derivatives will appear in our problem if we apply Green's theorem to reduce the order of the integrand. Thus, the linear basis functions are appropriate for our problem. In the following we shall derive the linear basis functions for the linear and curved-sided triangular elements, respectively.

Linear Basis Function of the Linear Triangular Element

Consider the typical triangular element e with the nodes numbered in the counterclockwise direction, as shown in Figure 2.7. Following the preceding discussion, the trial function can be represented within this element by the linear polynomial

$$h^e(x, z) = \alpha_1 + \alpha_2 x + \alpha_3 z \quad (2.54)$$

where α_1 , α_2 , and α_3 are constants that need to be determined (note that the symbol e is being used to designate element number). These constants can be determined by setting up three equations which require that the nodal values h_n^e are obtained at the nodal coordinates (x_n, z_n) :

$$\begin{aligned} h_1^e & \quad 1 \quad x_1 \quad z_1 \quad \alpha_1 \\ \{ h_2^e \} & = [1 \quad x_2 \quad z_2] \{ \alpha_2 \} \\ h_3^e & \quad 1 \quad x_3 \quad z_3 \quad \alpha_3 \end{aligned} \quad (2.55)$$

Solving for α_1 , α_2 , and α_3 , and substituting these into Eq.(2.54), we obtain

$$h^e(x, z) = \sum_{n=1}^3 h_n^e \phi_n^e \quad (2.56)$$

in which ϕ_n^e are the element interpolation or basis function and defined as

$$\phi_n^e = \frac{1}{2\Delta_e} (a_n + b_n x + c_n z) \quad , \quad n = 1, 2, 3 \quad (2.57)$$

where $a_1 = x_2 z_3 - x_3 z_2$, $b_1 = z_2 - z_3$, $c_1 = x_3 - x_2$;
 $a_2 = x_3 z_1 - x_1 z_3$, $b_2 = z_3 - z_1$, $c_2 = x_1 - x_3$;
 $a_3 = x_1 z_2 - x_2 z_1$, $b_3 = z_1 - z_2$, $c_3 = x_2 - x_1$;

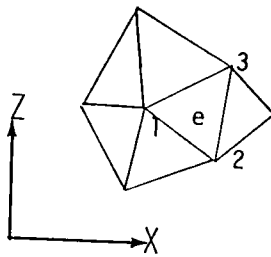


Figure 2.7 A typical triangular element.

and

$$\Delta_e = \frac{1}{2} \begin{vmatrix} 1 & x_1 & z_1 \\ 1 & x_2 & z_2 \\ 1 & x_3 & z_3 \end{vmatrix} = \text{area of the triangular element}$$

Linear Basis Function of the Curved-Sided Triangular Element

In the case of the linear triangular element, the geometry is described by the same degree polynomial as that used in the trial function. In other words, the element geometry and the trial function are expressed in terms of the same basis. Elements using the same basis for both purposes are denoted as isoparametric elements. There are occasions, however, when complex geometry dictates the use of polynomials of higher degree than is required in the trial function. Elements that use higher-degree polynomials to define the geometry than the trial function are called superparametric elements.

As discussed in the preceding section, the linear trial function is sufficient for the requirement of our problem. This means that the curved-sided triangular elements must be treated as superparametric elements.

Referring to Figure 2.8, by dividing the region of subsurface flow, the land surface becomes a series of curves defined over the discrete intervals

$$L_2 = x_1 > x_2 > \dots > x_{M-1} > x_M = L_1 \quad (2.58)$$

where M is the number of the nodes on the saturated surface. Because S is an axis of the curvilinear coordinate system, C^1 -continuity is required. Therefore we approximate it by

$$z_i(x) = z_i(x_i) + \alpha_i(x-x_i) + \beta_i(x-x_i)^2, \quad x_i \leq x \leq x_{i+1}$$

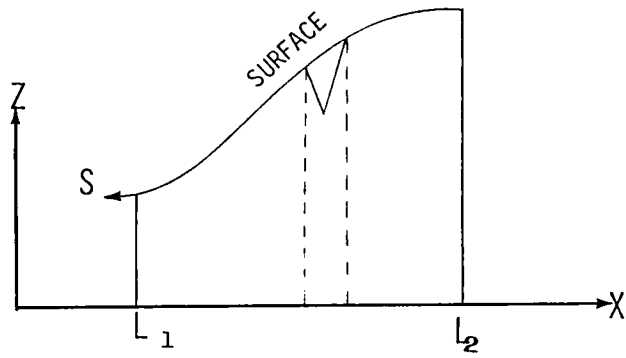


Figure 2.8 The division of land surface.

$$i = 1, 2, \dots, M-1 \quad (2.59)$$

where α_i and β_i are constants. These constants are determined in such a way that the following constraints are satisfied

$$z_i(x_{i+1}) = z_{i+1}(x_{i+1})$$

$$z'_i(x_{i+1}) = z'_{i+1}(x_{i+1})$$

$$i = 1, 2, \dots, M-1 \quad (2.60)$$

Now, we derive the linear basis function for the surface elements. For convenience' sake, a natural coordinate system is used. Referring to Figure 2.9a, the Cartesian coordinate system (x,z) can be transformed into a natural coordinate system (ξ,η) by

$$\xi = PQ/L, \quad \eta = QS/OS \quad (2.61)$$

where L is length of the curved side of the surface triangular element. As shown in Figure 2.9b, the curved-sided triangular element becomes a right-angled triangle in the natural coordinate system (ξ,η) (Appendix B). Thus, the trial function within this element can be represented in the same way as the linear triangular element by the linear polynomial

$$h^e(\xi,\eta) = \alpha_1 + \alpha_2\xi + \alpha_3\eta \quad (2.62)$$

where α_1 , α_2 , and α_3 are constants. These constants are determined by writing

$$\begin{Bmatrix} h_1^e \\ h_2^e \end{Bmatrix} = \begin{bmatrix} 1 & \xi_1 & \eta_1 \\ 1 & \xi_2 & \eta_2 \end{bmatrix} \begin{Bmatrix} \alpha_1 \\ \alpha_2 \end{Bmatrix} \quad (2.63)$$

$$h_3^e \quad 1 \quad \xi_3 \quad \eta_3 \quad \alpha_3$$

note that $(\xi_1,\eta_1)=(0,0)$, $(\xi_2,\eta_2)=(1,0)$, and $(\xi_3,\eta_3)=(0,1)$. Solving for α_1 , α_2 , and α_3 , and substituting these into Eq.(2.62), we obtain

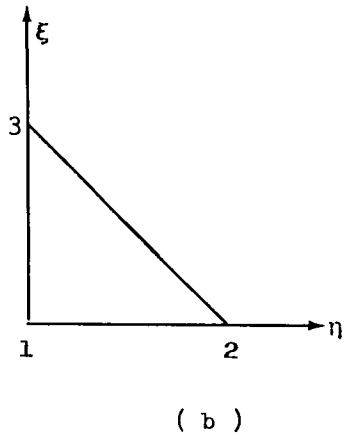
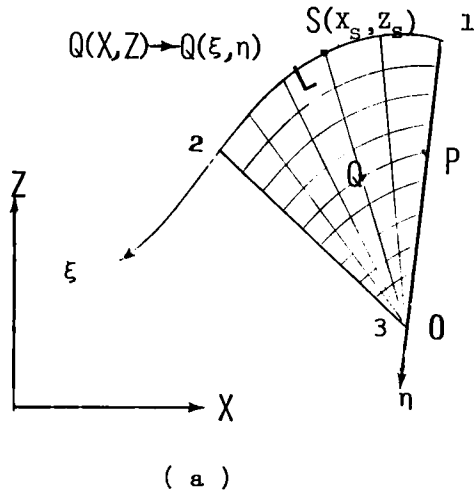


Figure 2.9 The natural coordinate system for surface curved-sided elements.

$$h^e(\xi, \eta) = \sum_{n=1}^3 h_n^e \phi_n^e \quad (2.64)$$

where ϕ_n^e are the basis function of the curved-sided triangular element and defined as

$$\begin{aligned} \phi_1^e &= 1 - \xi - \eta \\ \phi_2^e &= \xi \\ \phi_3^e &= \eta \end{aligned} \quad (2.65)$$

$$0 \leq \xi \leq 1 - \eta, \quad 0 \leq \eta \leq 1$$

Since the trial functions within the linear and the curved-sided triangular elements are both linear polynomials, the compatibility(continuity) requirement is satisfied at the interface of the linear and curved-sided triangular elements.

The relationship between the natural and Cartesian coordinates is derived in Appendix B and reproduced below

$$\begin{aligned} L\xi &= S_i(x_S) (1 - \eta) \\ x &= (1 - \eta)x_S + \eta x_3 \\ z &= (1 - \eta)z_S + \eta z_3 \end{aligned} \quad (2.66)$$

$$z_S = z_1 + \alpha_i(x_S - x_1) + \beta_i(x_S - x_1)^2$$

Jacobian Matrix:

$$J = \frac{\partial(x, z)}{\partial(\xi, \eta)} = \begin{bmatrix} \frac{\partial x}{\partial \xi} & \frac{\partial x}{\partial \eta} \\ \frac{\partial z}{\partial \xi} & \frac{\partial z}{\partial \eta} \end{bmatrix} \quad (2.67)$$

$$\frac{\partial x}{\partial \xi} = L/S'_1(x_S)$$

$$\frac{\partial z}{\partial \xi} = Lr_i(x_S)/S_i'(x_S)$$

$$\frac{\partial x}{\partial \eta} = x_3 - x_S + S_i(x_S)/S_i'(x_S)$$

$$\frac{\partial z}{\partial \eta} = z_3 - z_S + r_i(x_S)S_i(x_S)/S_i'(x_S)$$

$$S_i(x) = \int_{x_1}^x dS \quad , \quad x_1 \leq x \leq x_1$$

$$r_i(x_S) = dz_S / dx_S = \alpha_i + 2\beta_i(x_S - x_1) \quad (2.68)$$

The derivatives of the basis function can be calculated by

$$\frac{\partial \phi_i^e}{\partial x} = \frac{1}{|J|} \begin{vmatrix} \frac{\partial \phi_i^e}{\partial \xi} & \frac{\partial z}{\partial \xi} \\ \frac{\partial \phi_i^e}{\partial \eta} & \frac{\partial z}{\partial \eta} \end{vmatrix}$$

$$i = 1, 2, 3 \quad (2.69)$$

$$\frac{\partial \phi_i^e}{\partial z} = \frac{1}{|J|} \begin{vmatrix} \frac{\partial x}{\partial \xi} & \frac{\partial \phi_i^e}{\partial \xi} \\ \frac{\partial x}{\partial \eta} & \frac{\partial \phi_i^e}{\partial \eta} \end{vmatrix}$$

2.2.2.3 Formulating the Matrix Equation for Steady State Flow

Problem by Linear Triangular Elements

The region of flow is subdivided into a finite element network that consists of N nodes and M elements.

We define the basis function in the region of flow as

$$\phi_K = \begin{cases} \phi_k^e & , \text{ if the element } e \text{ contains node } K. \\ 0 & , \text{ otherwise.} \end{cases} \quad (2.70)$$

where $K=1, 2, \dots, N$, and $e=1, 2, \dots, M$. Note that the subscript K indicates the number of the node in the global coordinate system and the subscript k is the number of node K in the local coordinate system. Thus the trial function in the region of flow can be expressed as(cf. Eq.(2.50), " - " is omitted)

$$h = \sum_{K=1}^N h_K \phi_K \quad (2.71)$$

We first formulate the element matrix equation for subsurface flow. Application of Galerkin's criterion to the governing equation (2.21) yields

$$\int_D \int \sum_{i=1}^2 \sum_{j=1}^2 [K_{ij} \frac{\partial}{\partial x_j} (\sum_{K=1}^N h_K \phi_K + x_2)] \phi_n dx_1 dx_2 = 0$$

$$n=1, 2, \dots, N \quad (2.72)$$

Applying Green's theorem to Eq.(2.72) we obtain

$$\int_D \int \sum_{i=1}^2 \frac{\partial \phi_n}{\partial x_i} [\sum_{j=1}^2 K_{ij} \frac{\partial}{\partial x_j} (\sum_{K=1}^N h_K \phi_K) + K_{i2}] dx_1 dx_2 -$$

$$- \oint_{\Omega} \phi_n \sum_{i=1}^2 [\sum_{j=1}^2 K_{ij} \frac{\partial}{\partial x_j} (\sum_{K=1}^N h_K \phi_K) + K_{i2}] \cos(\mathbf{n}, \mathbf{x}_i) d\Omega = 0$$

$$n=1, 2, \dots, N \quad (2.73)$$

where Ω is the boundary of the region of flow, and \mathbf{n} the outward unit normal direction of Ω .

Let the above two integrals be I_1 and I_2 , respectively. Next, we assume that the saturated hydraulic conductivity is constant within the triangular element and that the relative hydraulic conductivity can be interpolated in the same way as the pressure head, that is,

$$K_r^e = \sum_{l=1}^3 K_l^r \phi_l^e \quad (2.74)$$

in which l stands for the corners of the triangular element. Thus, the integrals I_1 and I_2 can be performed analytically. The procedures are as follows.

Inserting Eq.(2.74) into I_1 , and noting that the integral over the region of flow is equal to the summation of the integrals over all the element subregions, we obtain

$$\begin{aligned} I_1 &= \sum_{e=1}^M I_1^e \\ &= \sum_{e=1}^M \int \int_{De} \sum_{i=1}^2 \frac{\partial \phi_i^e}{\partial x_i} \left[\sum_{j=1}^2 K_{ij}^s \left(\sum_{l=1}^3 K_l^r \phi_l^e \right) \frac{\partial}{\partial x_j} \left(\sum_{K=1}^3 h_K^e \phi_K^e \right) \right] + \\ &\quad + K_{i2}^s \left(\sum_{l=1}^3 K_l^r \phi_l^e \right)] dx_1 dx_2 \\ &= \sum_{e=1}^M \sum_{K=1}^3 h_K^e \frac{\bar{K}^r}{K_4 \Delta} (K_{11}^s b_n b_K + K_{12}^s b_n c_K + K_{21}^s c_n b_K + K_{22}^s c_n c_K) + \\ &\quad + \frac{\bar{K}^r}{2} (K_{12}^s b_n + K_{22}^s c_n) \end{aligned} \quad (2.75)$$

where

$$\bar{K}^r = \frac{1}{3} (K_1^r + K_2^r + K_3^r)$$

Assembling the results of the integrals over the element subregions into the global coefficient matrix at the appropriate locations yields

$$I_1 = \sum_{K=1}^N A_{nK} h_K + F'_n \quad (2.76)$$

Now consider the integral I_2 . Note that

$$\sum_{i=1}^2 \left[\sum_{j=1}^2 K_{ij} \frac{\partial}{\partial x_j} \left(\sum_{K=1}^N h_K \phi_K \right) + K_{i2} \right] \cos(n, x_i)$$

is the flux per unit length along Ω (cf. Eq(2.23)). Along the impermeable boundary the flux is zero, so this term vanishes. When a constant head or Dirichlet boundary is encountered, no equation is generated and consequently, it is unnecessary to evaluate this term. When a Neumann boundary is encountered the flux is specified, and we have to evaluate this term.

Inserting the Eqs.(2.23), (2.24), and (2.25) into I_2 we obtain

$$I_2 = - \int_{GH} \phi_n R \cos \theta dS - \int_{HB} \phi_n I \cos \theta dS \quad (2.77)$$

Because the seepage rate I is an unknown variable, the above integral cannot be evaluated. Later we shall show that it can be removed by treating overland flow and subsurface flow as a simultaneous system. Here we first formulate the matrix equation for overland flow.

As in the case of subsurface flow, applying the Galerkin criterion to the governing equation of steady state overland flow we obtain

$$- \int_{HB} \phi_n I \cos \theta dS = \int_{HB} \frac{\partial}{\partial S} (Uh / \cos \theta) \phi_n dS - \int_{HB} \phi_n R \cos \theta dS \quad (2.78)$$

Let the first integral in the right-hand side be I'. Performing the integration by parts yields

$$I' = Uh/\cos\theta\phi_n \Big|_B^H - \int_{HB} \frac{\partial\phi}{\partial S} (Uh/\cos\theta) dS \quad (2.79)$$

At point H, $h=0$ and $Uh/\cos\theta\phi_n \Big|_H$ vanishes. At point B, which belongs to a Dirichlet boundary, h is specified, no equation is generated and consequently, it is unnecessary to evaluate $Uh/\cos\theta\phi_n \Big|_B$. The second integral in the right-hand side of Eq.(2.79) is easily evaluated if we use the quasi-linearization approximate instead of Uh . The procedures are as follows.

The trial function takes the following simpler form along the land surface(Figure 2.10)

$$\begin{aligned} h^{e_s} &= \phi_1^{e_s} h_1^{e_s} + \phi_2^{e_s} h_2^{e_s} \\ &= (1 - S/L^{e_s}) h_1^{e_s} + S/L^{e_s} h_2^{e_s} \end{aligned} \quad (2.80)$$

where the symbol e_s is being used to designate surface element number.

Inserting Eqs.(2.47) and (2.80) into Eq.(2.79) yields

$$\begin{aligned} -I' &= \sum_{e_s} \frac{\delta}{L^{e_s}} \left\{ \frac{h_2^{e_s} - h_1^{e_s}}{L^{e_s}} \int_{S_1}^{S_2} A dS + \int_{S_1}^{S_2} B h^{e_s} dS + \int_{S_1}^{S_2} C dS + \right. \\ &\quad \left. + g_T/\cos\theta \int_{S_1}^{S_2} \left[\frac{\partial \bar{h}^{e_s}}{\partial T} h^{e_s} + \frac{\partial h^{e_s}}{\partial T} \bar{h}^{e_s} - \frac{\partial \bar{h}^{e_s}}{\partial T} \bar{h}^{e_s} \right] dS \right\} \end{aligned} \quad (2.81)$$

where $\delta = \begin{cases} -1, & \phi_n = \phi_1^{e_s} \\ 1, & \phi_n = \phi_2^{e_s} \end{cases}$

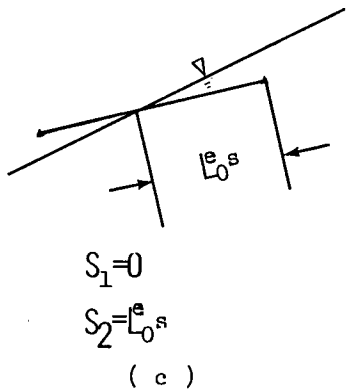
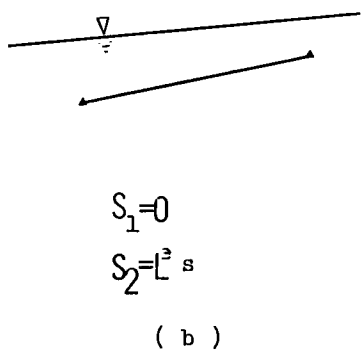
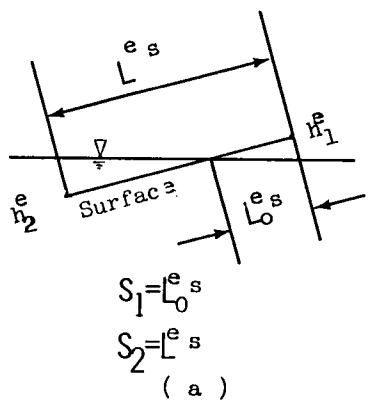


Figure 2.10 The basic function for land surface element.

If the same interpolation function for h is used for \bar{h} , all these integrals can then be performed analytically. Assembling the results into the global matrix at the appropriate locations, I' can be written as

$$I' = - \sum_{K=1}^N F_{nK} h_K - F_n^0 \quad (2.82)$$

Now it can be seen that the seepage rate I is removed by inserting Eq.(2.78), (2.79), and (2.82) into Eq.(2.72). thus, we obtain

$$\begin{aligned} I_2 &= - \int_{GH} \phi_n R \cos \theta dS - \int_{HB} \phi_n R \cos \theta dS + I' \\ &= - \sum_{K=1}^N F_{nK} h_K - F_n \end{aligned} \quad (2.83)$$

where $F_n = F_n^0 + \int_{GH} \phi_n R \cos \theta dS + \int_{HB} \phi_n R \cos \theta dS$

Substitution of I_1 and I_2 into Eq.(2.73) gives

$$\sum_{K=1}^N (A_{nK} - F_{nK}) h_K = F_n - F_n' , n=1,2,\dots,N \quad (2.84)$$

2.2.2.4 Formulating the Matrix Equation for Steady State Flow Problem by Curved-Sided Triangular Elements

The formulating procedures are the same as in the case of linear triangular elements. However, since the integrals over the surface elements here cannot be performed analytically, we have to use some numerical technique. In this study, the Gauss numerical integration method is used. For more information about the Gauss numerical integration method see the Appendix C. For overland flow, the Gauss numerical integration method is applied after transforming the integrals in the curvilinear coordinate system into their counterparts in the natural coordinate system by the relationship expression $S = L \xi$ (see Eq.(2.65), at the land surface $\eta = 0$). Thus, a global matrix equation with the same form as in the case where all elements are linear triangular elements can be obtained.

2.2.2.5 Incorporating the Dirichlet Boundary Conditions
and Solving the Global Matrix Equation

The Neumann type boundary conditions have been considered through the formulation process. What remains to be incorporated is the Dirichlet type boundary conditions. For convenience' sake, we rewrite Eq(2.84) into the following matrix form

$$\begin{matrix} [A] \{h\} = \{F\} \\ N \cdot N \quad N \cdot 1 \quad N \cdot 1 \end{matrix} \quad (2.85)$$

The incorporating procedure is as follows.

If h_n is specified, we set $F_n = h_n$, $F_i =: F_i - A_{in} h_n$ for all $i \neq n$, and $A_{nn} = 1$, $A_{ni} = A_{in} = 0$ for all $i \neq n$. This procedure is repeated for each specified head h .

Once the boundary conditions have been incorporated, the algebraic equations are solved by the Gauss-Siedel method. Because the problem is nonlinear, an iterative process is necessary. The iteration procedure is repeated until the difference between successive iterations is within a specified error α , i.e.

$$\text{Max}\{ |h_n^{(i)} - h_n^{(i+1)}|, n = 1, 2, \dots, N \} < \alpha \quad (2.86)$$

where the superscript (i) indicates the number of iterations. In this study we have set $\alpha = 0.001(m)$. During the iterative cycle, each h is updated by

$$h_n^{(i)} = \epsilon h_n^{(i)} + (1 - \epsilon) h_n^{(i-1)}, \quad 0 < \epsilon \leq 1 \quad (2.87)$$

Each nominal head \bar{h} is used for $h^{(0)}$.

2.2.2.6 Possibility of Approximating the Land Surface by a
Series of Straight-Line Elements

In order to examine the possibility of approximating the land surface by a series of straight-line elements, we simulated nine cases that are generated from three types of land surface curves and three kinds of flow conditions.

The three kinds of flow conditions are shown in Table 2.1 and Figure 2.11. The soils are assumed to be isotropic and homogeneous. The three types of land surface curves are as follows

$$\begin{aligned}
 S_1: \quad & z=1.6641112*10^{-3}x^2-0.031116821x+2.0, & 0 \leq x \leq 50.078 \\
 & z=2.4792419*10^{-4}x^2+0.011072280x-1.5551522, & 50.078 \leq x \leq 100 \\
 S_2: \quad & z=1.6185489*10^{-3}x^2-0.028835152x+2.0, & 0 \leq x \leq 68.139 \\
 & z=-1.634232*10^{-3}x^2+0.414447324x-13.102412, & 68.139 \leq x \leq 100 \\
 S_3: \quad & z=1.1960000*10^{-3}x^2 & +2.0, & 0 \leq x \leq 68.139 \\
 & z=-7.348626*10^{-4}x^2+0.263134000x-6.9648406, & 68.139 \leq x \leq 100
 \end{aligned}$$

It is easy to show that the three curves have C^1 -continuity at any point. The maximum curvatures are, respectively,

$$\begin{aligned}
 C(S_1) &= 1.498708544 * 10^{-3} (m^{-1}) \\
 C(S_2) &= 2.009461473 * 10^{-3} (m^{-1}) \\
 C(S_3) &= 2.392000000 * 10^{-3} (m^{-1})
 \end{aligned}$$

The three types of region of flow with the different land surface curves are shown in Figure 2.12. Each of them is divided into 342 elements with 232 nodes. Consequently, each land surface is divided into 57 linear or curved elements.

Table 2.1 Soil parameters and Dirichlet boundary condition

| Case | K M/Hr | N $M^{-1/3}S$ | I M/Hr | H M |
|--------|-----------|------------------|-----------|--------|
| Case 1 | 0.6 | 0.15 | 0.001 | 2.5 |
| Case 2 | 0.7 | 0.1 | 0.005 | 2.5 |
| Case 3 | 1.5 | 0.1 | 0.010 | 2.5 |

K :Saturated hydraulic conductivity
 N :Roughness
 I :Rainfall intensity
 H :Water level at outlet

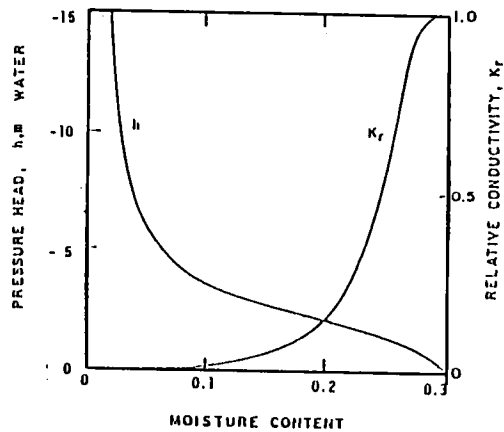


Figure 2.11 Moisture characteristic curve

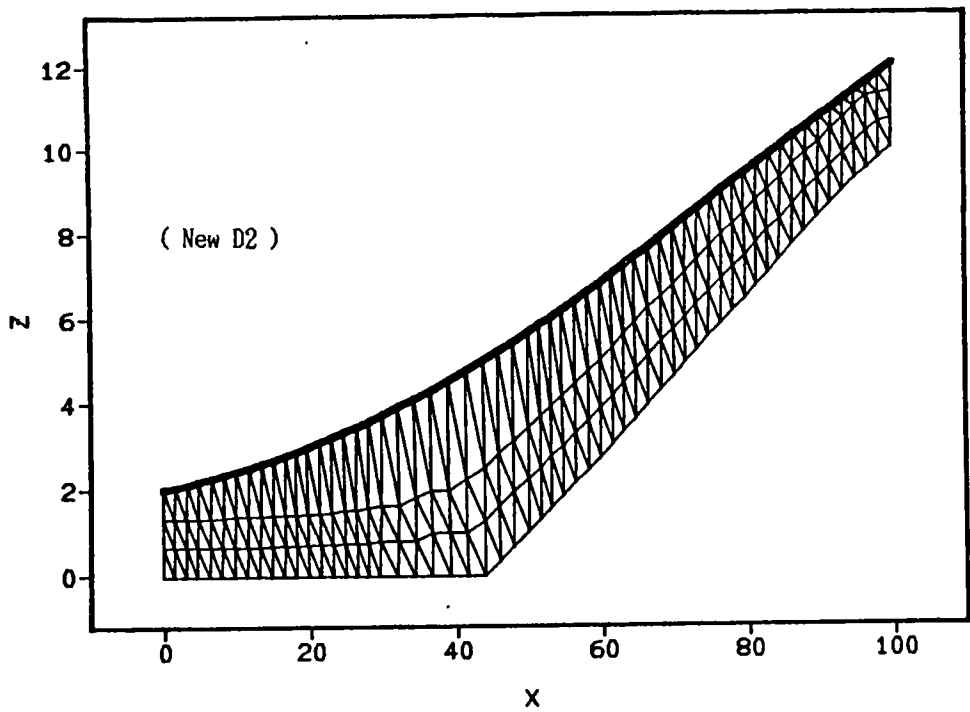
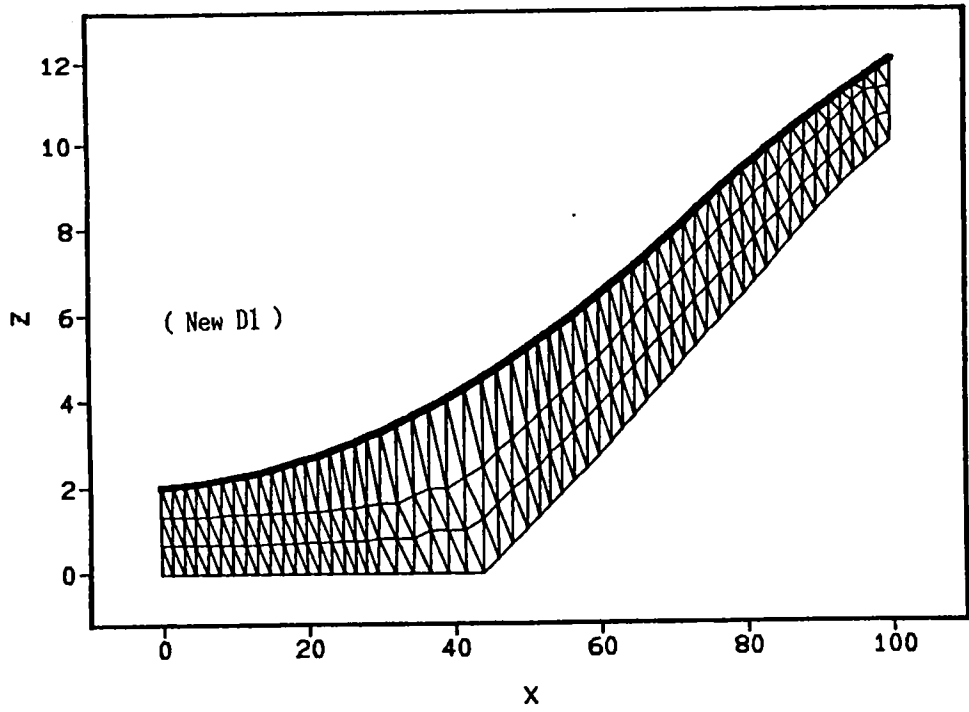


Figure 2.12a Element partition data

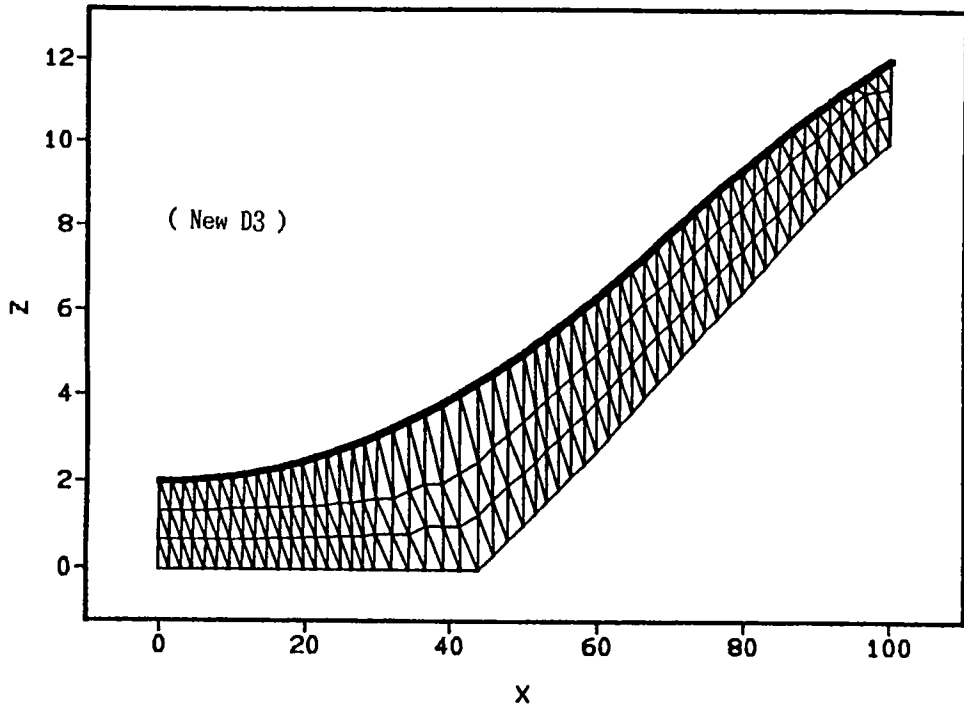


Figure 2.12b Element partition data

Combining the three types of land surface curves with the three kinds of flow conditions, we generated nine cases as shown in Table 2.2. For the each case, two kinds of simulation have been made: in the first case the surface elements are treated as linear triangular elements, and the second as curved-sided triangular elements. The results of simulations are shown in Figures 2.13, 2.14, and 2.15. Figures 2.13 and 2.14 show that both pressure heads and discharges resulting from the two kinds of simulation agree very well with each other. The maximum differences of pressure heads and discharges between the two kinds of simulation for each case are given in Table 2.3, and the relations between the differences and the maximum curvature of land surface curve are shown in Fig.2.15. Although the differences show a tendency to increase with curvature, the difference of heads is less than the allowed error 0.001m of numerical analysis, and the relative error of discharge(ratio of the difference of discharge to discharge) is less than 1% for all of the nine cases.

The above simulation results show that it is possible to use the linear triangular elements for surface elements if land surface can be approximately expressed by such a quadratic curve as applied for the simulation. In the following we shall formulate the matrix equation by applying linear triangular elements to all elements for the transient flow problem.

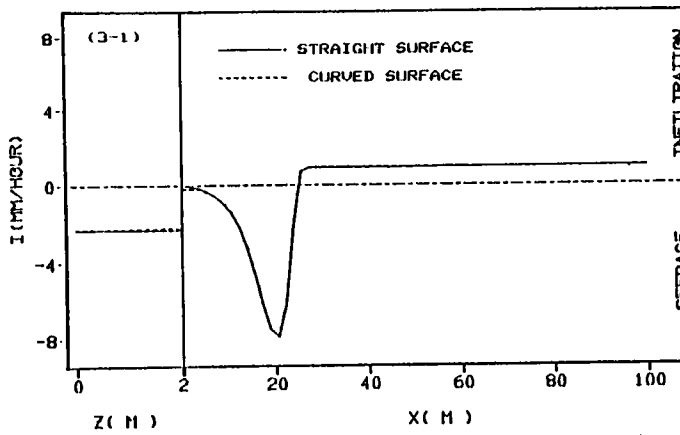
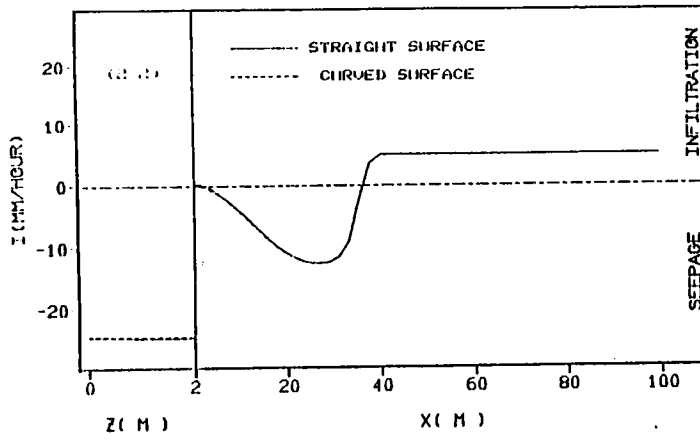
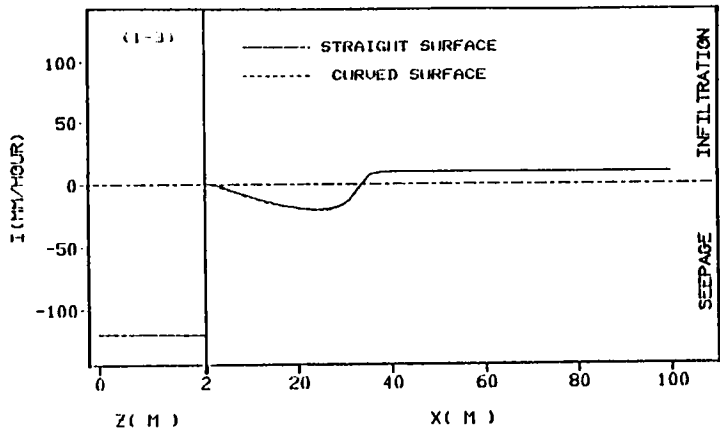


Figure 2.13 Infiltration and seepage intensity on surface

Table 2.2 Simulation case conditions

| | | | | |
|---|---|---|---|-------------------------|
| 1 | - | 1 | = | (New D1) * (Case 1) |
| 1 | - | 2 | = | (New D1) * (Case 2) |
| 1 | - | 3 | = | (New D1) * (Case 3) |
| 2 | - | 1 | = | (New D2) * (Case 1) |
| 2 | - | 2 | = | (New D2) * (Case 2) |
| 2 | - | 3 | = | (New D2) * (Case 3) |
| 3 | - | 1 | = | (New D3) * (Case 1) |
| 3 | - | 2 | = | (New D3) * (Case 2) |
| 3 | - | 3 | = | (New D3) * (Case 3) |

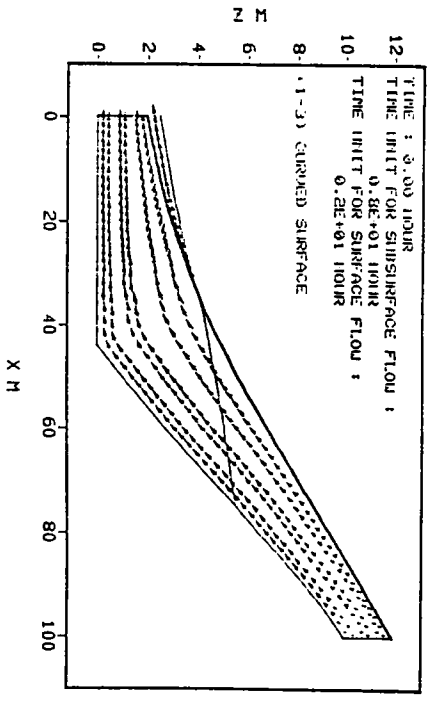
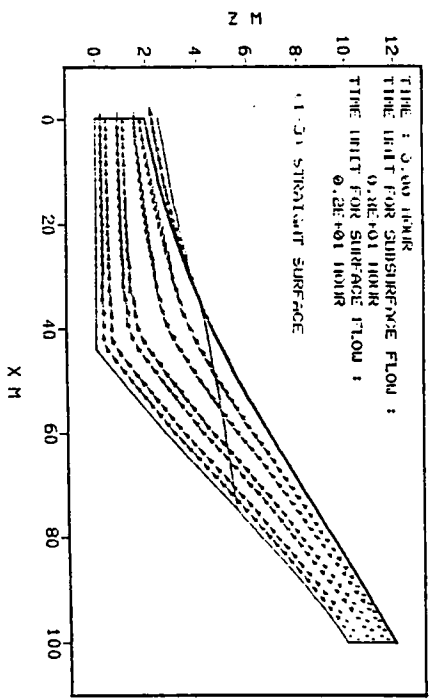
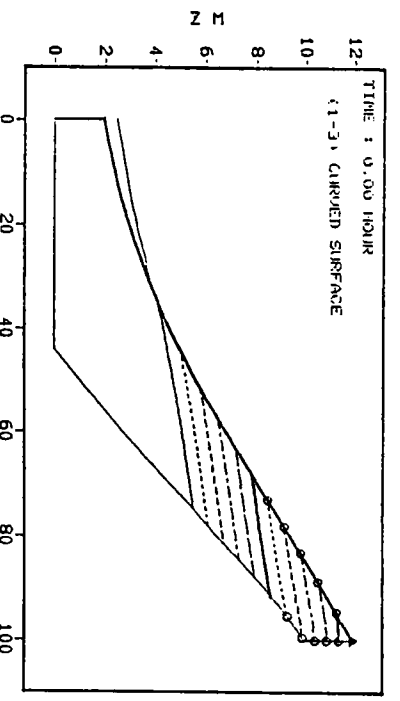
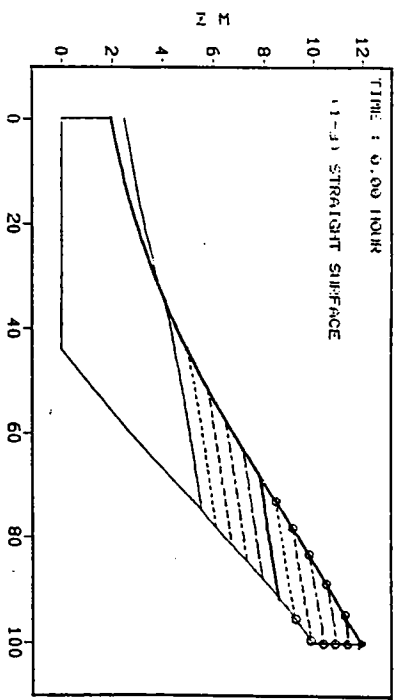


Figure 2.14a The isoplethic curves of pressure head and the velocity vectors

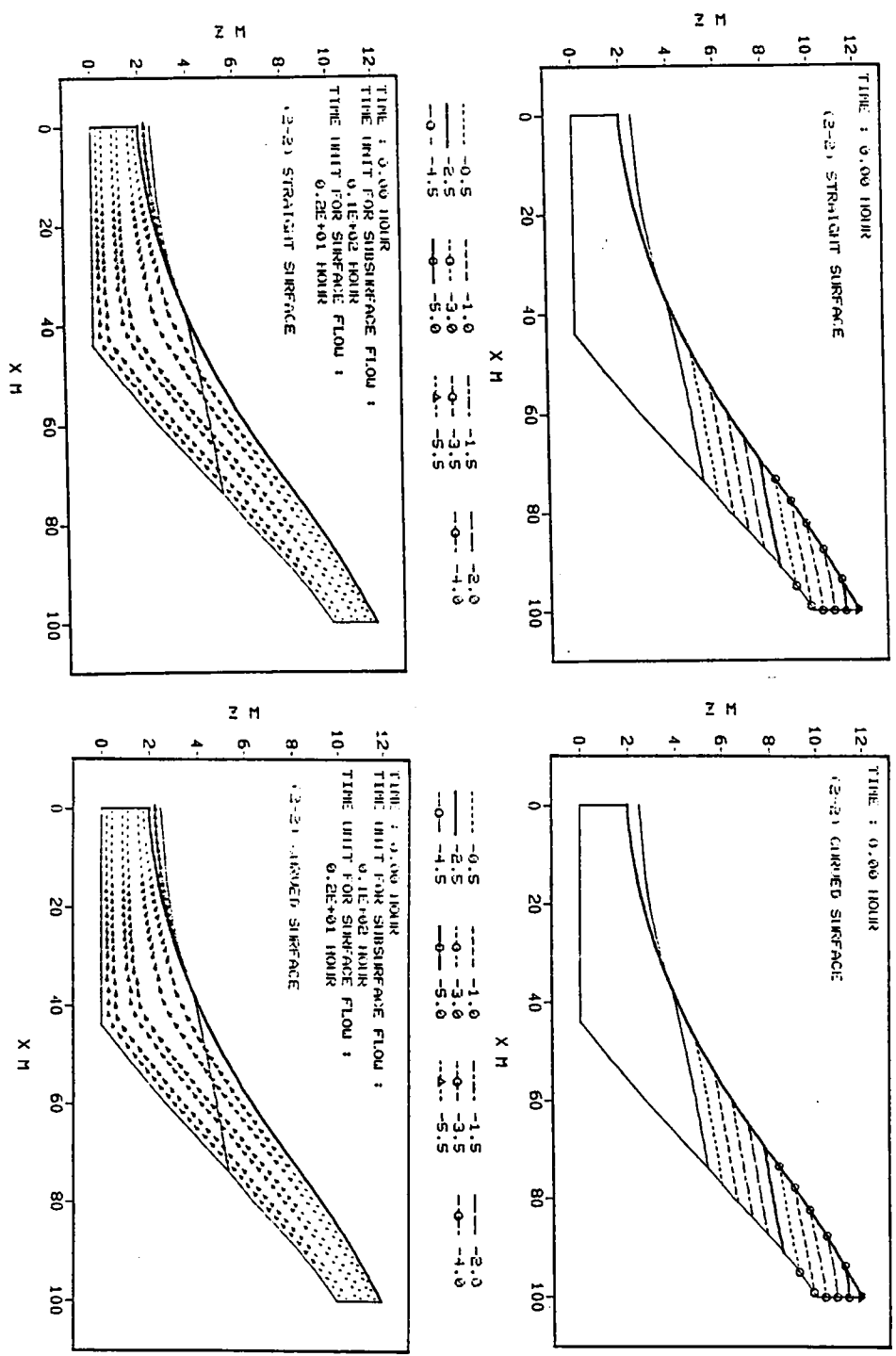


Figure 2.14b The isoplethic curves of pressure head and the velocity vectors

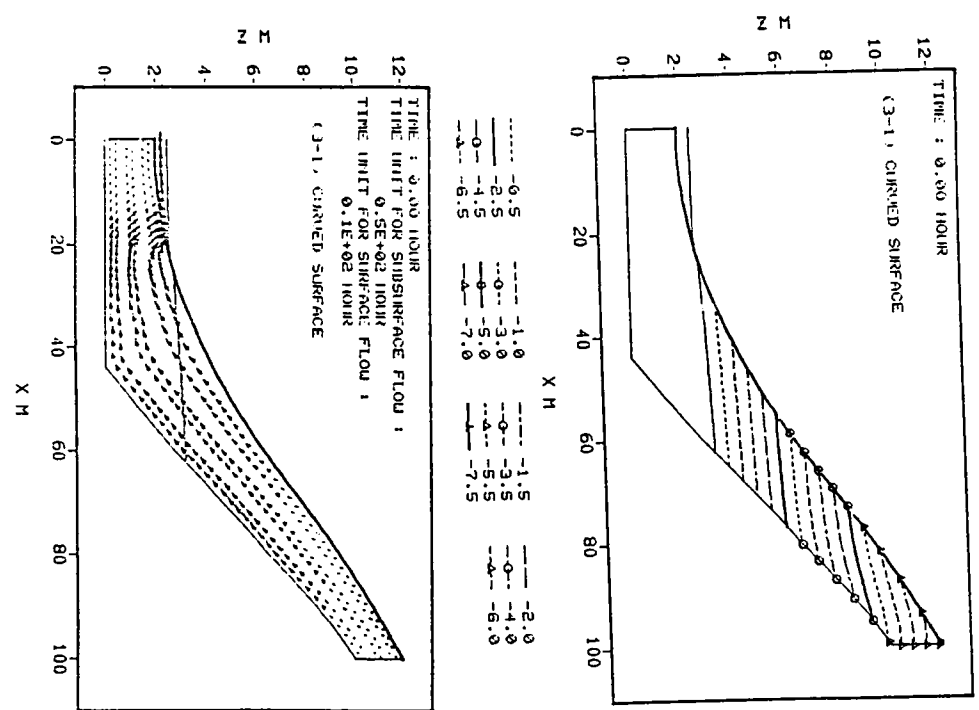
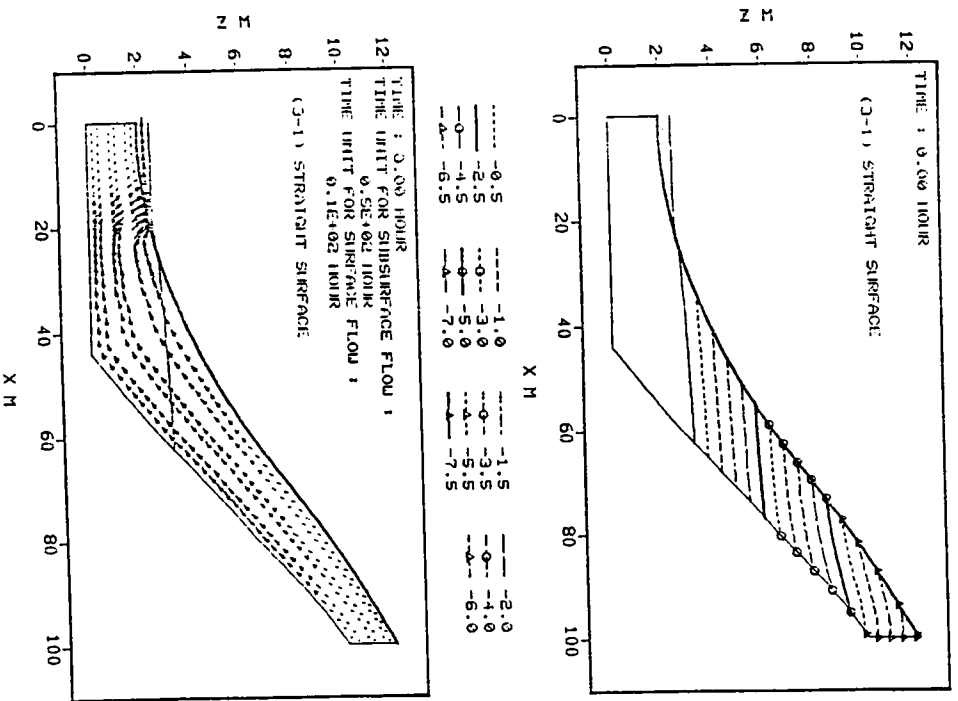


Figure 2.14c The isoplethic curves of pressure head and the velocity vectors

Table 2.3 Pressure head error and flow quantity error

| | Pressure Head Error (M) | Flow Quantity Error (M/HOUR) |
|-------|----------------------------|---------------------------------|
| 1 - 1 | 0.501632690 E-03 | 0.150179956 E-03 |
| 1 - 2 | 0.587463379 E-03 | 0.174729852 E-03 |
| 1 - 3 | 0.697135925 E-03 | 0.187259982 E-03 |
| 2 - 1 | 0.476837158 E-03 | 0.174477696 E-03 |
| 2 - 2 | 0.569343567 E-03 | 0.256568193 E-03 |
| 2 - 3 | 0.608444214 E-03 | 0.319520012 E-03 |
| 3 - 1 | 0.425338745 E-03 | 0.372299924 E-03 |
| 3 - 2 | 0.638961792 E-03 | 0.540561974 E-03 |
| 3 - 3 | 0.707626343 E-03 | 0.721156597 E-03 |

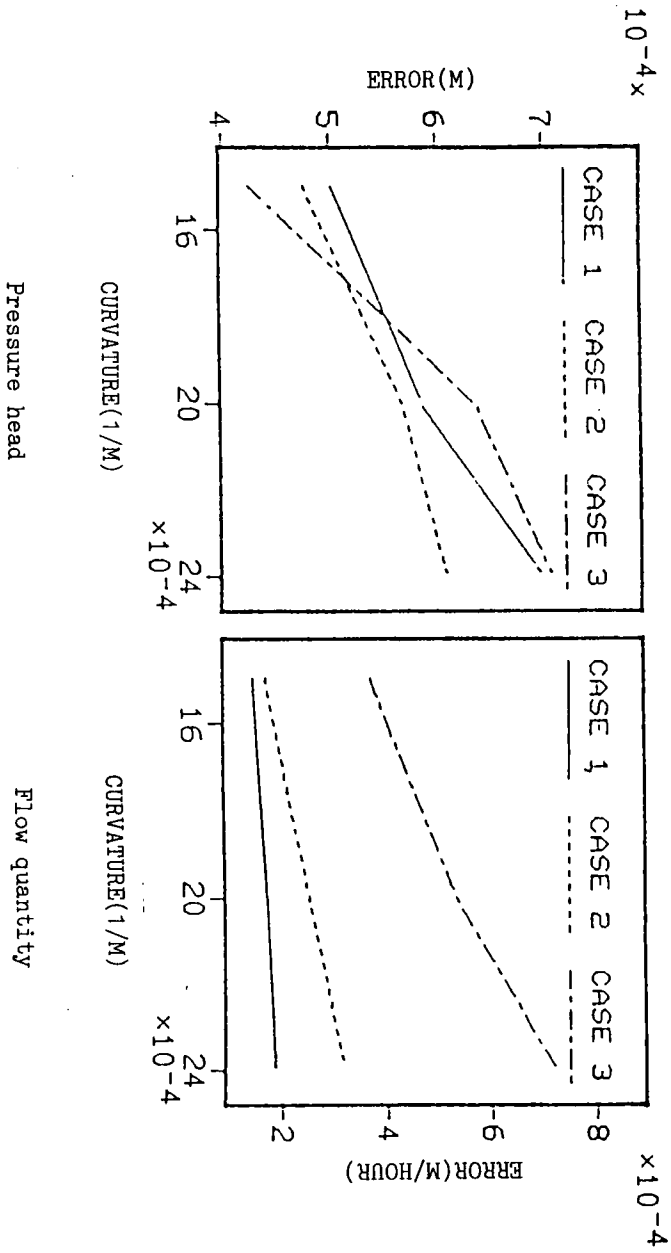


Figure 2.15 The relations between the curvature of land surface and pressure head error as well as flow quantity error

2.2.3 Solution of the Transient Flow Problem

2.2.3.1 Formulation of Matrix Equation

The difference between the transient flow problem and the steady state flow problem arises from the existence of the time derivative in the governing equation. Therefore, the matrix equation of the transient flow problem can be obtained by adding the term corresponding to the time derivative into the matrix equation of the steady state flow problem. The procedures are as follows.

As in the case of steady state flow, applying Galerkin's criterion to the governing equation (2.18) of transient subsurface flow, we obtain:

$$\int_D \int \sum_{i=1}^2 \sum_{j=1}^2 \left[K_{ij} \frac{\partial}{\partial x_j} \left(\sum_{K=1}^N h_K \phi_K + x_2 \right) \right] \phi_n dx_1 dx_2 -$$

$$- \int_D \int \left(C + \frac{\omega}{n} S_s \right) \frac{\partial}{\partial t} \left(\sum_{K=1}^N h_K \phi_K \right) \phi_n dx_1 dx_2 = 0$$

$$n=1, 2, \dots, N \quad (2.88)$$

In the preceding section we have shown that the first integral can be performed analytically by applying Green's theorem. Now we consider the second integral. Let this integral be I_3 .

Since the Galerkin method applies only at a given instant of time, the time derivative, $\partial h / \partial t$, must be determined independent of the orthogonalization process. Experience indicates that for the numerical method to converge in the case of unsaturated flow, $\partial h / \partial t$ must not be replaced by $\partial h^e / \partial t$. A much more stable solution is obtained by defining the nodal values of the time derivatives, $\partial h_n / \partial t$, as weighted averages of $\partial h / \partial t$ over the entire flow region:

$$\frac{\partial h_n}{\partial t} \equiv \int_D \int (C + \frac{\omega}{n} S_s) \frac{\partial h_n}{\partial t} \phi_n dx_1 dx_2 / \int_D \int (C + \frac{\omega}{n} S_s) \phi_n dx_1 dx_2 \quad (2.89)$$

In addition, it is assumed that the porosity(n), and the specific storage(S_s), are constant within each element, while the specific moisture capacity(C), and the moisture content(ω), vary linearly according to

$$C^e = \sum_{l=1}^3 C_l \phi_l^e \quad (2.90a)$$

$$\omega^e = \sum_{l=1}^3 \omega_l \phi_l^e \quad (2.90b)$$

in which l stands for the corners of the triangle.

By using Eqs.(2.89) and (2.90) the integral I_3 can be performed analytically

$$I_3 = - \sum_{e=1}^M \sum_{K=1}^3 \frac{\partial h_K^e}{\partial t} \frac{\Delta}{12} \sum_{K=1}^3 \tau_{ln} (C_l + S_s^e \omega_l / n^e)$$

$$\equiv \sum_{K=1}^N R_{nk} \frac{\partial h_K}{\partial t} \quad (2.91)$$

where $\tau_{ln} = 2$ for $l = n$, $\tau_{ln} = 1$ for $l \neq n$.

$$R_{nk} = 0 \text{ for } n \neq K.$$

On the other hand, applying the Galerkin criterion to the governing equation (2.42) of overland flow, we obtain

$$- \int_{HB} \phi_n I \cos \theta dS =$$

$$\int_{HB} \frac{\partial}{\partial S} (U_h / \cos \theta) \phi_n dS - \int_{HB} \phi_n R \cos \theta dS + \int_{HB} \frac{\partial h}{\partial t} (1 / \cos \theta) \phi_n dS \quad (2.92)$$

If we apply an approximation similar to Eq.(2.89) for $\partial h_n / \partial t$, the third integral in the right-hand side Of Eq.(2.92) can be easily evaluated.

$$\int_{HB} \frac{\partial h}{\partial t} (1/\cos\theta) \phi_n dS = \frac{\partial h_n}{\partial t} \int_{HB} \phi_n / \cos\theta dS$$

$$\equiv \sum_{K=1}^N T_{nk} \frac{\partial h_K}{\partial t} \quad (2.93)$$

where $T_{nK} = 0$ for $K \neq n$.

Combining Eqs.(2.88), (2.76), (2.77), (2.92), and (2.93) we obtain a set of quasilinear first-order differential equations:

$$\sum_{K=1}^N [(A_{nK} - F_{nK}) h_K + (R_{nK} - T_{nK}) \frac{\partial h_K}{\partial t}] = F_n - F'_n$$

$$n=1,2,\dots,N \quad (2.94)$$

2.2.3.2 Integration Over Time

For convenience, we rewrite Eq.(2.94) as

$$[D]\{h\} + [G]\left\{\frac{\partial h}{\partial t}\right\} = \{E\} \quad (2.95)$$

To integrate Eq.(2.95), the time domain is discretized into a sequence of finite intervals, Δt^T , where T represents time-step number, and the time derivatives of h_n are replaced by finite differences. Experience indicates that for this problem good results can be obtained by employing the time-centered scheme.

$$[D^{T+1/2}] \left\{ \frac{h^{T+1} + h^T}{2} \right\} + [G^{T+1/2}] \left\{ \frac{h^{T+1} - h^T}{\Delta t^T} \right\} = \{E^{T+1/2}\} \quad (2.96)$$

where $t = t_t$, $\Delta t^T = t_{T+1} - t_T$. In order to evaluate the coefficient matrices, one must know the values of h at $t = t_T + \Delta t^T / 2$. At the beginning of each time step, these values are predicted by linear extrapolation from previously calculated values according to

$$h_n^{T+1/2} = h_n^T + \Delta t^T (h_n^T - h_n^{T-1}) / \Delta t^{T-1/2} \quad (2.97)$$

After incorporating the Dirichlet boundary conditions, the resulting set of simultaneous linear algebraic equations is solved by the Gauss-Siedel algorithm for the value of h_n^{T+1} at all nodes. Due to the nonlinear nature of Eq.(2.95) these results must be improved by an iterative process. At each iteration, the most recent values of h_n^{T+1} are used to obtain improved estimates of $h_n^{T+1/2}$ from

$$h_n^{T+1/2(i+1)} = \epsilon h_n^{T+1/2(i)} + \frac{1}{2}(1 - \epsilon)(h_n^T + h_n^{T+1}), \quad 0 < \epsilon \leq 1 \quad (2.98)$$

where supercript (i) indicates the number of iterations. After reevaluating the coefficient matrices, the equations are again solved for the improved values of h_n^{T+1} . The iterative procedure continues as long as necessary to achieve a satisfactory degree of convergence.

2.3 The Application to Hillslope Systems

In this section we apply the coupled model of overland flow and subsurface flow proposed in the foregoing sections to hillslope systems and simulate the influences of soil hydraulic properties and rainfall on the runoff characteristics.

2.3.1 Input Data for the Coupled Model

The input data for the coupled model can be classified as four kinds:

- (1) information about the flow region subdivision,
- (2) soil parameters: space-dependent hydraulic conductivity, functional relationships between relative conductivity and pressure head as well as moisture content and pressure head, specific storage and space-dependent Manning's friction factor(roughness),
- (3) boundary conditions: time- and space-dependent distribution of pressure head along the Dirichlet boundaries, time- and space-distribution of flux along the Neumann boundaries,
- (4) allowed error for the iterative procedure,
- (5) time intervals for transient flow case.

25 cases for steady state flow, and 30 cases for transient flow have been simulated. The input data for all of the cases are given in Table 2.4 ~ Table 2.7 and Fig.2.16 ~ Fig.2.21. The following analyses are based on these simulation results.

Before analyzing the simulation results, we define some key words for an understanding of hillslope runoff processes(see Figure 2.1):

Table 2.4 Simulation case conditions(Steady flow)

| K \ N | 3.6 | 11.4 | 36. | 114. | 360. |
|-------|-------|-------|-------|-------|-------|
| 1. | 1 - 1 | 2 - 1 | 3 - 1 | 4 - 1 | 5 - 1 |
| 3.16 | 1 - 2 | 2 - 2 | 3 - 2 | 4 - 2 | 5 - 2 |
| 10. | 1 - 3 | 2 - 3 | 3 - 3 | 4 - 3 | 5 - 3 |
| 31.6 | 1 - 4 | 2 - 4 | 3 - 4 | 4 - 4 | 5 - 4 |
| 100. | 1 - 5 | 2 - 5 | 3 - 5 | 4 - 5 | 5 - 5 |

N : Roughness($M^{-1/3}Sec$)

K : Saturated hydraulic conductivity(M/Hr)

Table 2.5a Simulation case conditions(Transient flow)

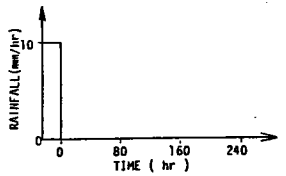
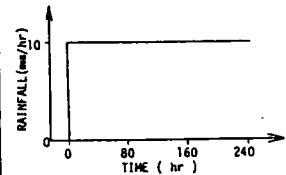
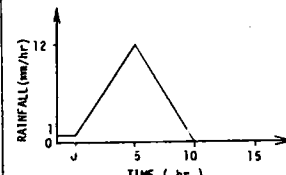
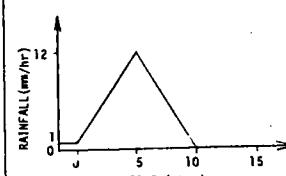
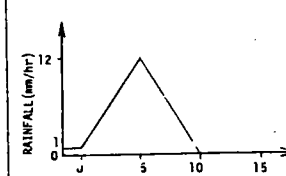
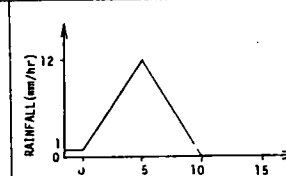
| Case | Region of flow | Time Step | K | N | M | S | Rainfall pattern |
|------|----------------|-----------|------|--------|--------|--------|--|
| | | | M/Hr | M-1/2S | | 1/M | |
| 1 | New D1 | Type T0 | 3. | 360. | Type A | 0.0001 |  |
| 2 | New D1 | Type T0 | 3.16 | 114. | Type A | 0.0001 |  |
| 3 | New D1 | Type T1 | 1. | 36. | Type A | 0.0001 |  |
| 4 | New D1 | Type T1 | 100. | 36. | Type A | 0.0001 |  |
| 5 | New D1 | Type T1 | 1. | 360. | Type A | 0.0001 |  |
| 6 | New D1 | Type T1 | 100. | 360. | Type A | 0.0001 |  |

Table 2.5b Simulation case conditions(Transient flow)

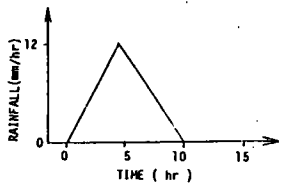
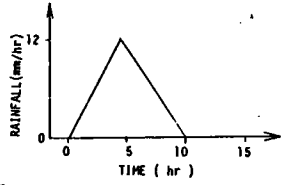
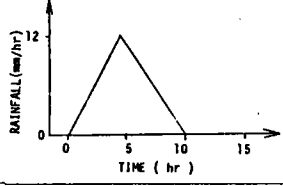
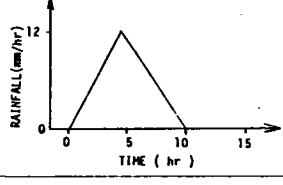
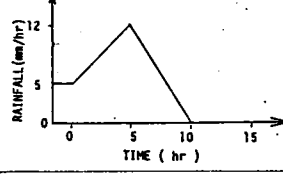
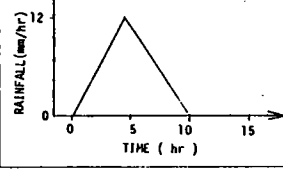
| | | | | | | | |
|----|-----------|------------|------|------|--------|--------|--|
| 7 | New D1 | Type T1 | 1. | 36. | Type B | 0.0001 |  |
| 8 | New D1 | Type T1 | 1. | 360. | Type B | 0.0001 |  |
| 9 | New D1 | Type T1 | 50. | 360. | Type B | 0.0001 |  |
| 10 | New D1 | Type T1 | 50. | 360. | Type C | 0.0001 |  |
| 11 | New D1 | Type T1 | 100. | 360. | Type A | 0.0001 |  |
| 12 | New D1 | Type T1 | 50. | 360. | Type B | 0.001 |  |

Table 2.5c Simulation case conditions(Transient flow)

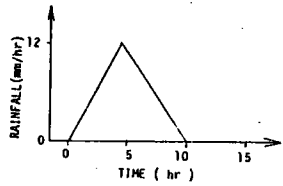
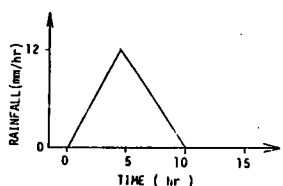
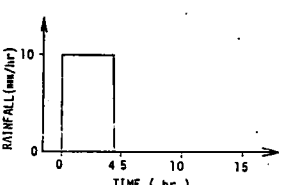
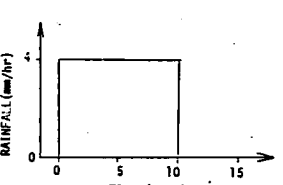
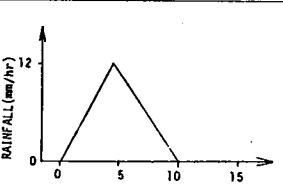
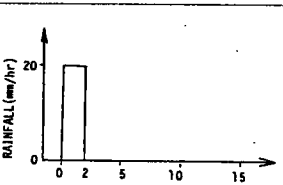
| | | | | | | | |
|----|-----------|------------|-----|------|--------|--------|--|
| 13 | New D1 | Type T1 | 50. | 360. | Type D | 0.0001 |  |
| 14 | New D1 | Type T1 | 20. | 360. | Type C | 0.0001 |  |
| 15 | New D1 | Type T1 | 50. | 360. | Type C | 0.0001 |  |
| 16 | New D1 | Type T1 | 50. | 360. | Type C | 0.0001 |  |
| 17 | New D1 | Type T1 | 50. | 360. | Type E | 0.0001 |  |
| 18 | New D1 | Type T1 | 50. | 360. | Type C | 0.0001 |  |

Table 2.5d Simulation case conditions(Transient flow)

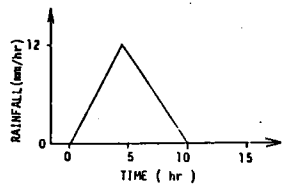
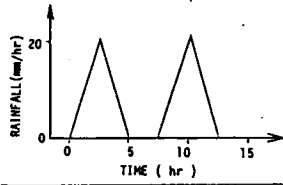
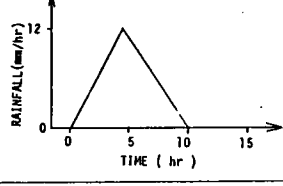
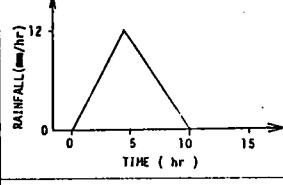
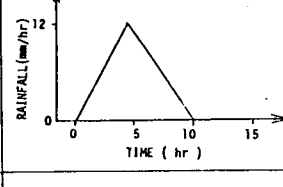
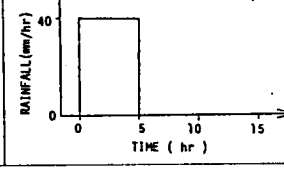
| | | | | | | | |
|----|-----------|------------|---------------------------|--------------------|--------|--------|--|
| 19 | New D1 | Type T1 | $K_x = 50.$ $K_y = 1.$ | 360. | Type C | 0.0001 |  |
| 20 | New D1 | Type T1 | 50. | 360. | Type C | 0.0001 |  |
| 21 | New D1 | Type T2 | 50. | 360. | Type E | 0.0001 |  |
| 22 | New D1 | Type T1 | $K_x = 1.$ $K_y = 50.$ | 360. | Type C | 0.0001 |  |
| 23 | New D1 | Type T1 | 50. | 360. | Type C | 0.0001 |  |
| 24 | New D1 | Type T1 | 50. | 1.08×10^4 | Type C | 0.0001 |  |

Table 2.5e Simulation case conditions(Transient flow)

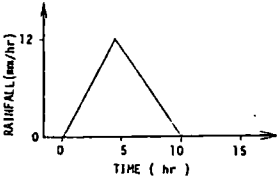
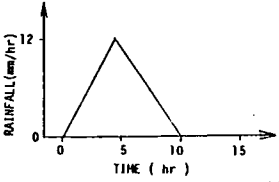
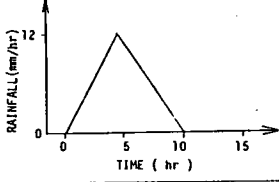
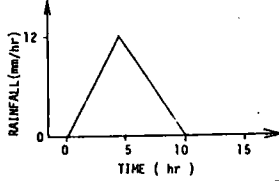
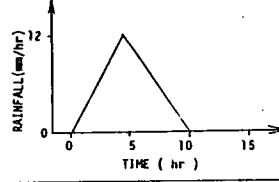
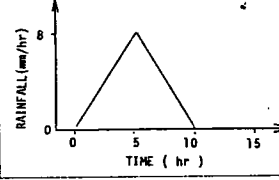
| | | | | | | | |
|----|-------------------|------------|-----------------------------------|------|--------|--------|--|
| 25 | New D1 | Type T1 | 50. | 360. | Type C | 0.0001 |  |
| 26 | New D4 | Type T1 | $K_1 K_4 = 1.$ $K_2 K_3 = 50.$ | 360. | Type C | 0.0001 |  |
| 27 | New D5 | Type T1 | $K_1 K_2 = 50.$ | 360. | Type C | 0.0001 |  |
| 28 | New D1 | Type T1 | $K_1 K_4 = 50.$ $K_2 K_3 = 1.$ | 360. | Type C | 0.0001 |  |
| 29 | New D1 *0.5 | Type T1 | 50. | 360. | Type C | 0.0001 |  |
| 30 | New D1 | Type T1 | 50. | 360. | Type C | 0.0001 |  |

Table 2.6 Numbers of Nodes and Elements

| | N_1 | N_2 | N_3 | N_4 |
|-----------|-------|-------|-------|-------|
| New D1-D3 | 232 | 342 | 58 | 4 |
| New D4 | 255 | 400 | 51 | 5 |
| New D5 | 304 | 450 | 76 | 4 |

N_1 :number of nodes

N_2 :number of elements

N_3 :number of surface nodes

N_4 :number of outlet nodes

Table 2.7a Time Step for transient flow
(CASE3-CASE20, CASE22-CASE30)

| Time (From , To) | Time Step (Hour) |
|--------------------|------------------|
| 0.000 0.100 | 0.050 |
| 0.100 0.500 | 0.100 |
| 0.500 0.750 | 0.125 |
| 0.750 1.000 | 0.250 |
| 1.000 15.000 | 0.500 |

Table 2.7b Time Step for transient flow
(CASE21)

| Time (From , To) | | Time Step (Hour) |
|--------------------|--------|------------------|
| 0.000 | 0.100 | 0.050 |
| 0.100 | 0.500 | 0.100 |
| 0.500 | 0.750 | 0.125 |
| 0.750 | 15.000 | 0.250 |

Table 2.7c Time Step for transient flow
(CASE1, CASE2)

| Time (From , To) | | Time Step (Hour) |
|--------------------|---------|------------------|
| 0.000 | 0.100 | 0.050 |
| 0.100 | 0.500 | 0.100 |
| 0.500 | 0.750 | 0.125 |
| 0.750 | 1.000 | 0.250 |
| 1.000 | 2.000 | 1.000 |
| 2.000 | 10.000 | 2.000 |
| 10.000 | 240.000 | 10.000 |

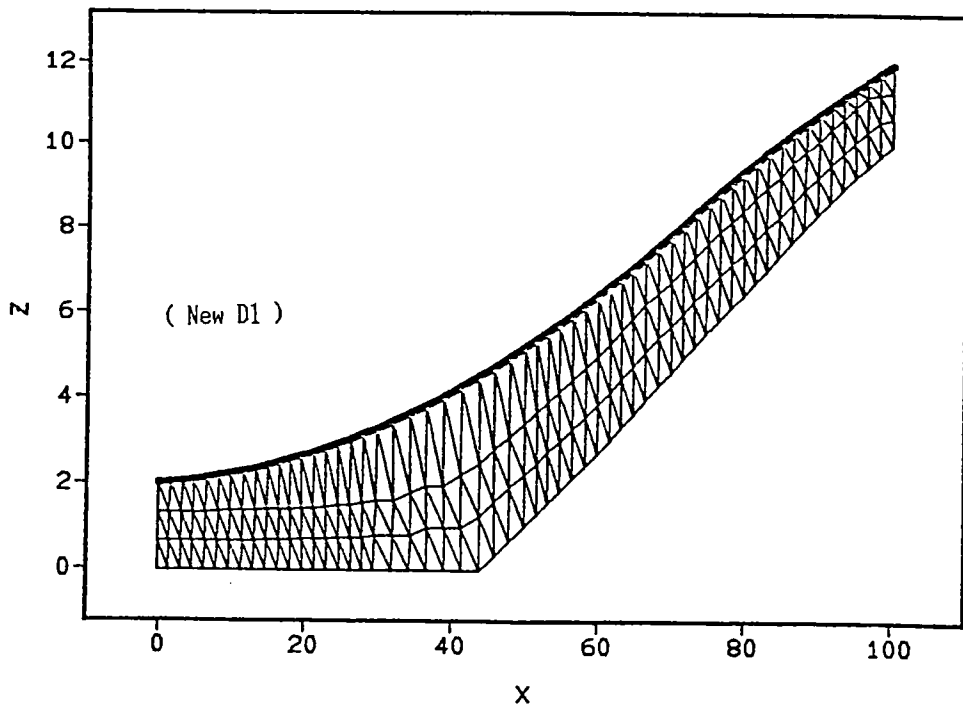


Figure 2.16 Element Partition Data

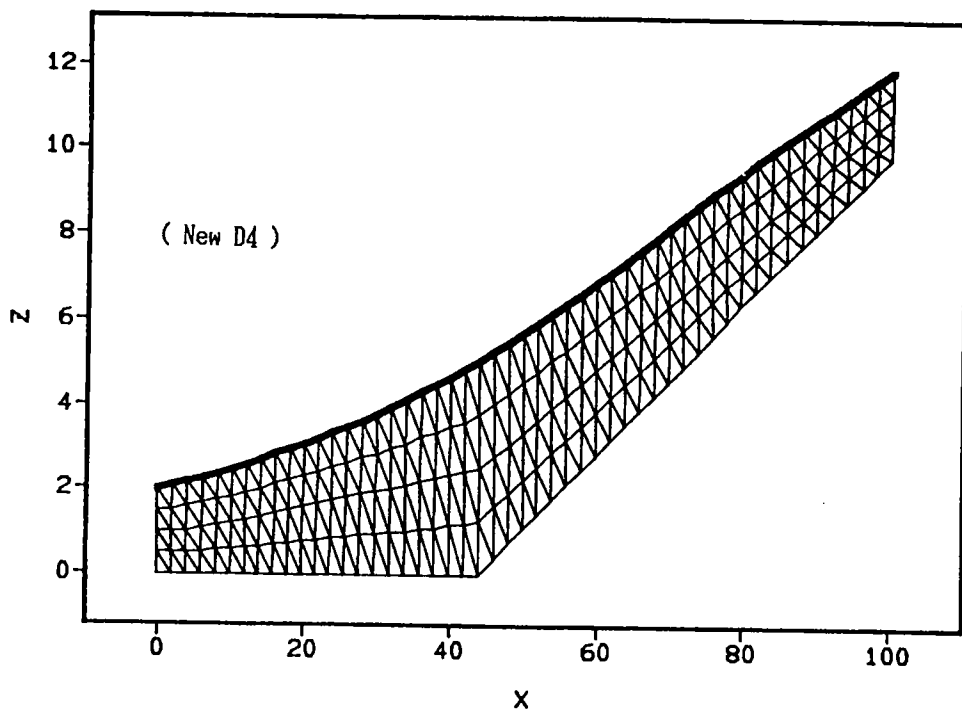


Figure 2.17 Element Partition Data

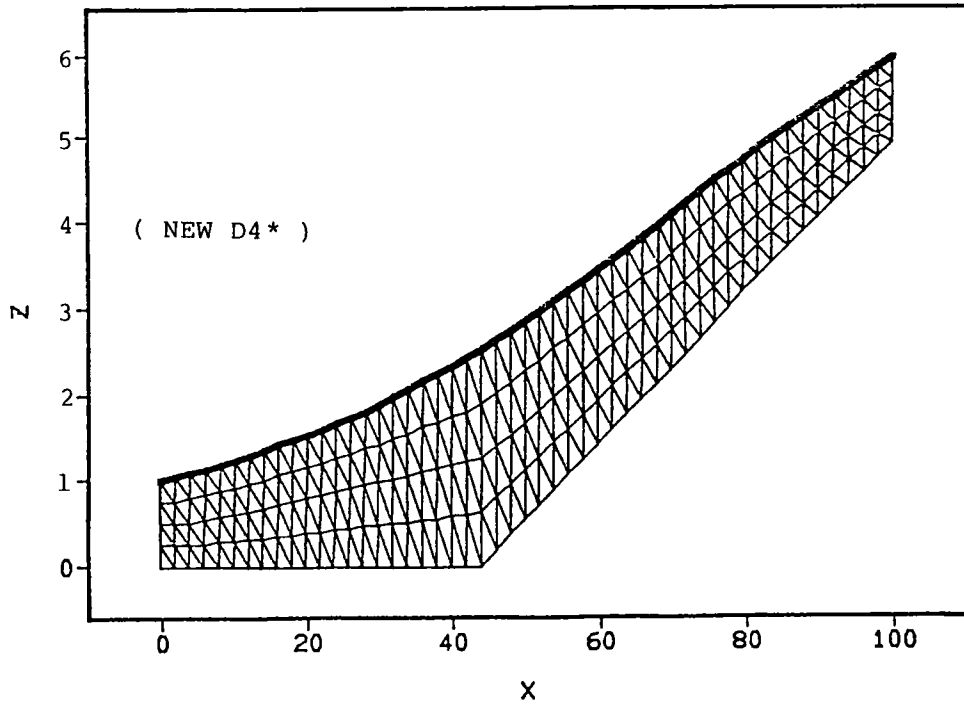


Figure 2.18 Element Partition Data

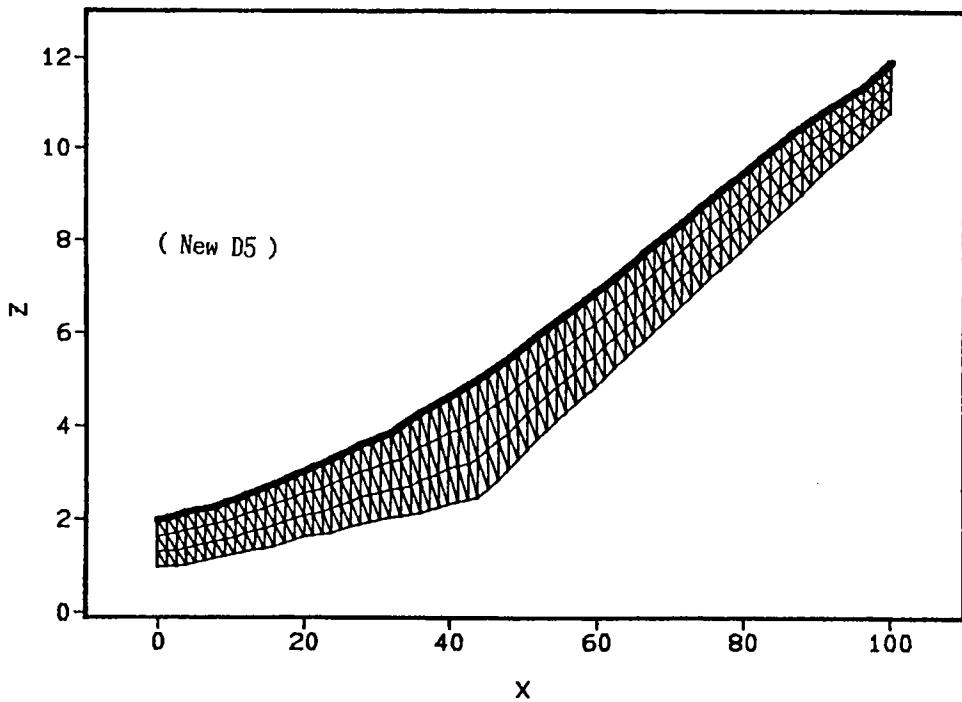
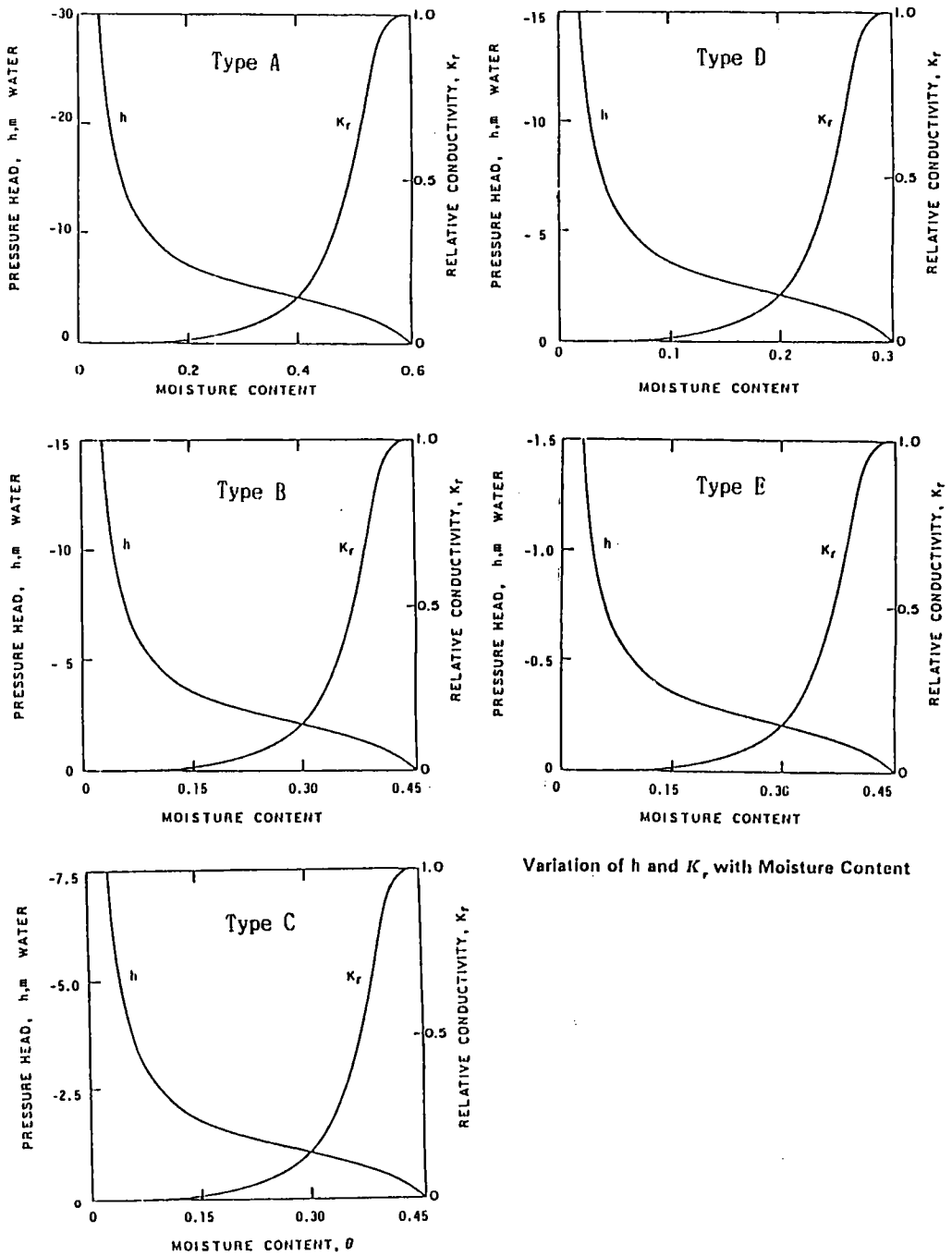


Figure 2.19 Element Partition Data



Variation of h and K_r with Moisture Content

Figure 2.20 Moisture characteristic curve

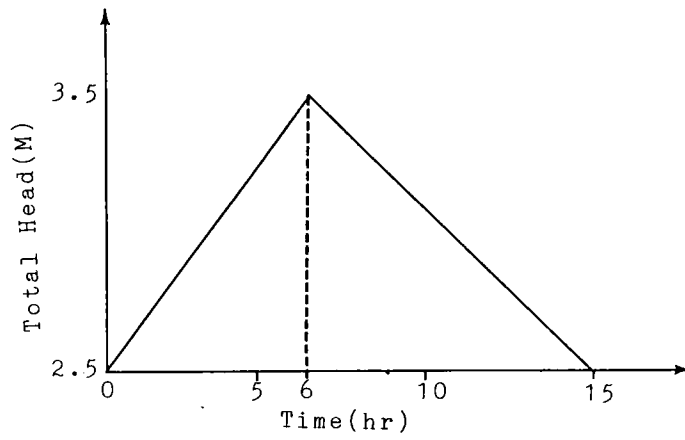


Figure 2.21 The Changing Dirichlet Condition

Overland flow is the flow of water over the land surface BH toward a stream channel which originates from rain and return flow. Return flow is the infiltrated water which returns to the land surface BH after flowing in the soil horizon. Overland runoff discharge indicates the outflow from AB, and Subsurface runoff discharge the outflow from BC. Total runoff discharge is defined as the summation of overland and subsurface runoff discharges.

2.3.2 Saturated Hydraulic Conductivity and Roughness

Saturated hydraulic conductivity is one of the most important parameters that are considered to have great influence on subsurface runoff, which, in turn, has great influence on the total runoff. Roughness is the parameter which immediately governs overland flow. Since we considered the hydraulic interaction of overland flow with subsurface flow when deriving the governing equations, the runoff characteristics are considered to be determined by all the combinations of the parameters. In the following, by applying the coupled model to hillslope systems the influences of saturated hydraulic conductivity and roughness on runoff are examined for steady state flow and transient flow, respectively.

Fig.2.22 shows the relationships between runoff and saturated hydraulic conductivity as well as roughness of hillslope land surface in the case where rain of constant intensity, 8mm/hour, falls upon the hillslope. When the roughness is relatively small, the ratio of overland runoff to subsurface runoff does not vary widely as the saturated hydraulic conductivity changes, and the overland runoff accounts for a very great part of the total runoff. If the roughness becomes larger, the subsurface runoff increases sharply as the

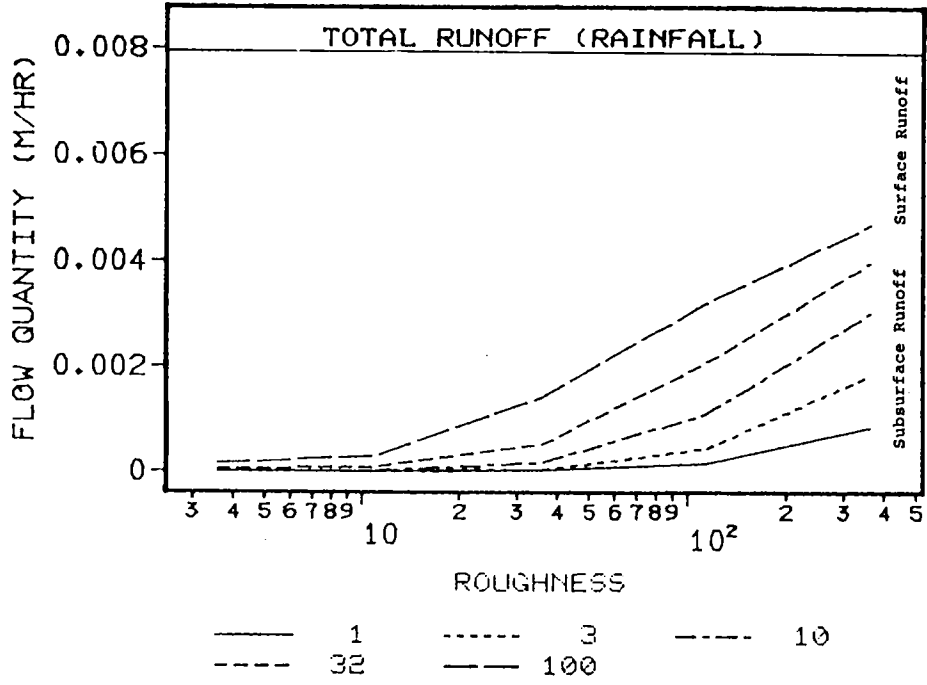


Figure 2.22 The runoff discharges change with the saturated conductivity and roughness

saturated hydraulic conductivity increases. this can be explained as follows:

The resistance of soil to subsurface flow decreases as the hydraulic conductivity becomes greater. Therefore, if the roughness is small, the water infiltrates into the soil of the upper hillslope, where the pressure head is lower than in the lower hillslope, does not flow in the soil of the lower hillslope but returns to the land surface which has low resistance to the flow. In the case of large roughness, the return flow is restrained and as a result the subsurface flow increases.

Figure 2.23 shows the hydrographs in the cases where the saturated hydraulic conductivity ranges from 1 m/hour(CASE3,CASE5,CASE8) to 100 m/hour(CASE4, CASE6,CASE9) and the roughness from $0.01 \text{ m}^{-1/3} \text{ hour}$ (CASE3, CASE4) to $0.1 \text{ m}^{-1/3} \text{ hour}$ (CASE5,CASE6,CASE8,CASE9). In the cases where the saturated hydraulic conductivity is 1 m/hour, the subsurface runoff discharge is nearly zero, while the saturated hydraulic conductivity becomes 100 m/hour, the subsurface runoff discharges increase so that the total runoff discharges of CASE4,CASE6 and CASE9 exceed those of CASE3,CASE5 and CASE8, respectively. However, the increase of CASE4 in the overland flow is more considerable than those of CASE6 and CASE9. This results from the difference of roughness between CASE4 and CASE6 or CASE9, In CASE6 and CASE9 the return flows are restrained by the large roughness.

Now let us look at the peak-time of the hydrograph. Since overland flow is generally faster than subsurface flow, the difference between the ratios of overland runoff or subsurface runoff to total runoff naturally results in a difference in the peak-time of the

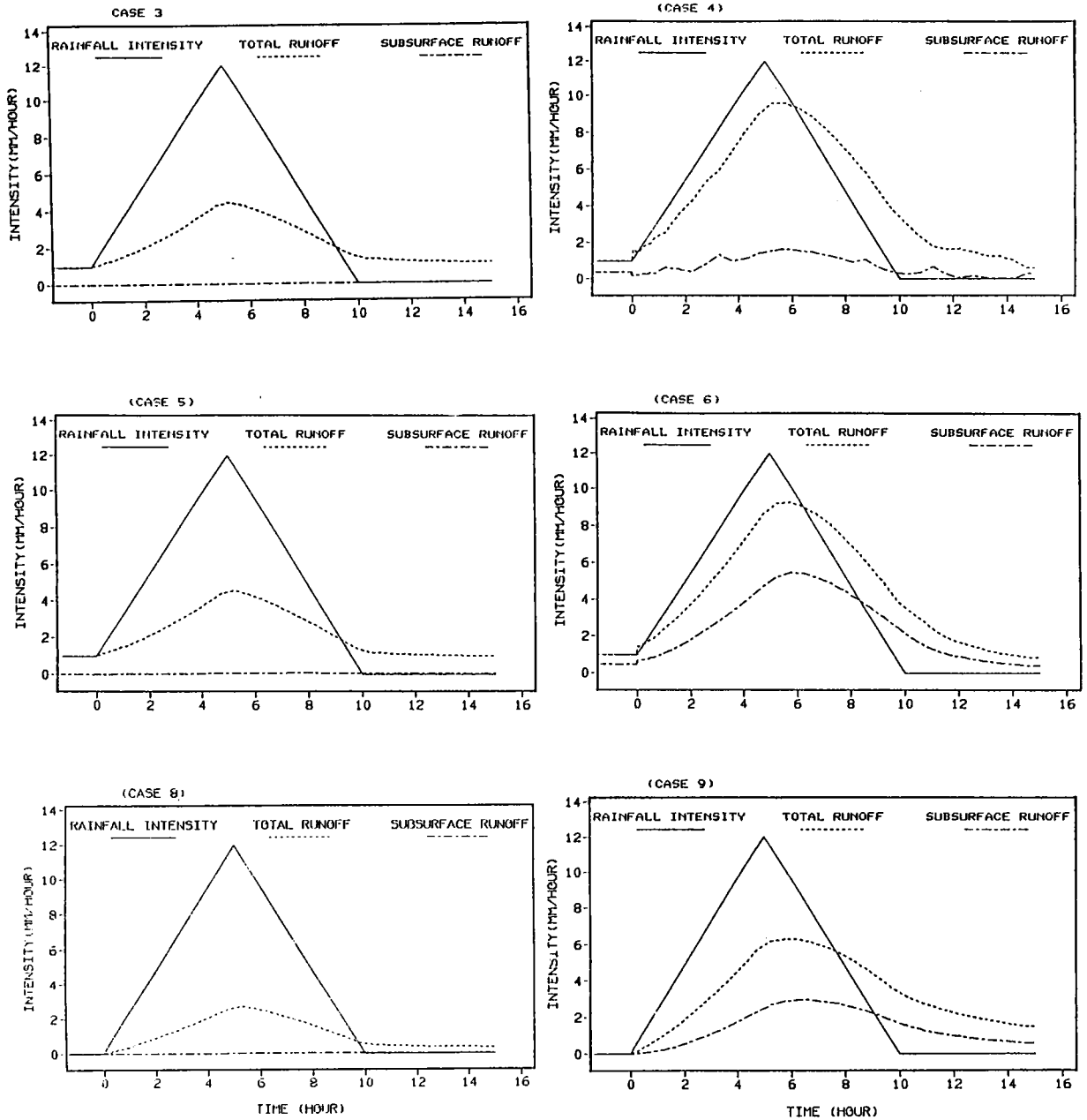


Figure 2.23 Hydrograph (CASE3.4.5.6.8.9)

hydrograph. The lag-times of the peak in CASE3, CASE5(with an initial precipitation, 1mm/hour) and CASE8(without any initial precipitation) to the peak of precipitation are about 20 min., 20 min., and 38 min., respectively. However, when the saturated hydraulic conductivity is 100 m/hour, the lag-times increase to 45 min., 45 min., and 58 min.

Ishihara and Takasao(1963) have pointed out that there is usually a highly permeable soil layer(known as the A-layer) in the hillslope. The most important hydraulic characteristics of the A-layer are its anisotropy and heterogeneity. The first has been simulated by CASE10, CASE19 and CASE22, and the results are shown in Figure 2.24 and Figure 2.25. We have also simulated the heterogeneity by considering a two-layer region of flow(Figure 2.28), and the results are shown in Figure 2.26, Figure 2.27 and Figure 2.29.

Figure 2.30 shows the maximum velocity of overland flow for CASE4, CASE5, CASE7 and CASE8, where all of the parameters other than roughness are held constant for all cases. The velocity distributions are shown in Figure 2.31. It can be seen that when the saturated hydraulic conductivity is low return flow is promoted and the influence of roughness on the runoff is little. This is also indicated by the change in water table(Figure 2.32). When the saturated hydraulic conductivity is so great that the subsurface flow velocity has the same order to overland flow, return flow(and consequentially overland flow) becomes sensitive to the change in roughness. The distribution of the total runoff among the overland runoff and subsurface runoff for steady state flow(Figure 2.33) can be explained in the same way.

Based on the above simulation results, the influences of saturated hydraulic conductivity and roughness on the runoff characteristics can be summarized as follows:

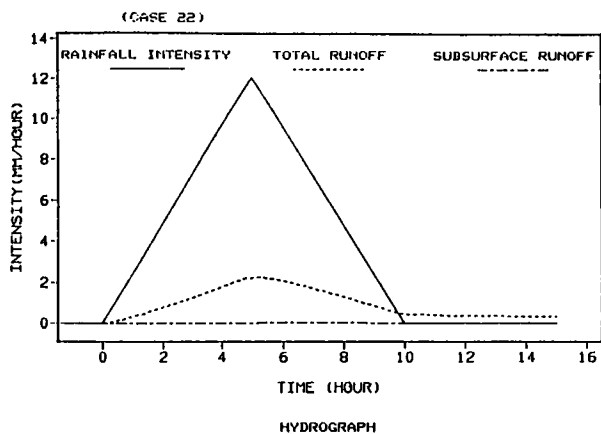
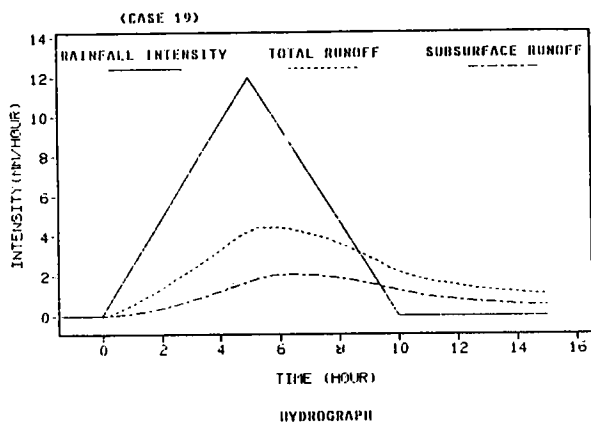
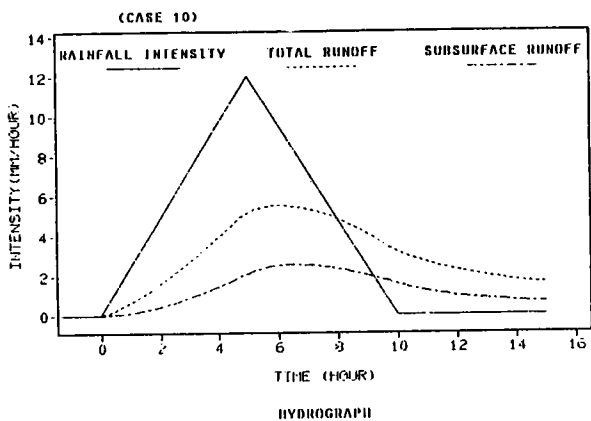


Figure 2.24 Hydrograph (CASE10.19.22)

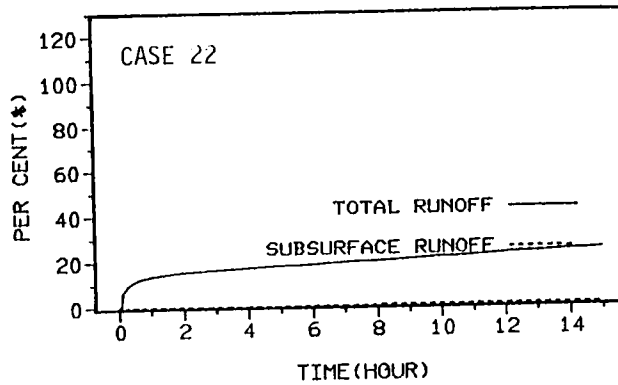
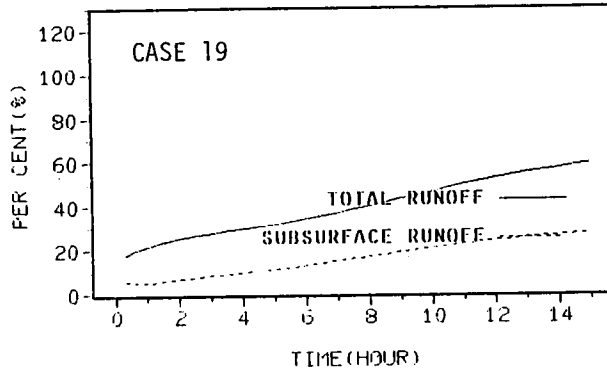
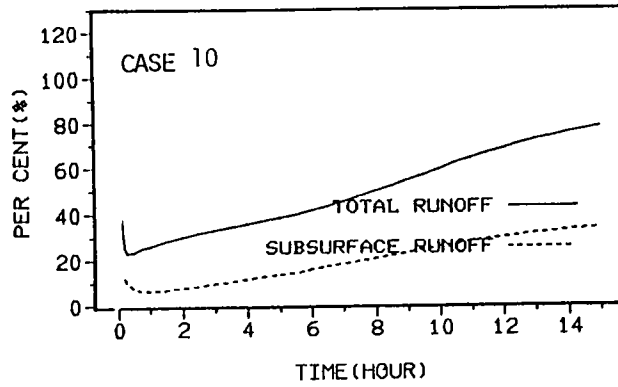


Figure 2.25 The comparison between the precipitation and runoff discharge(CASE10.19.22)

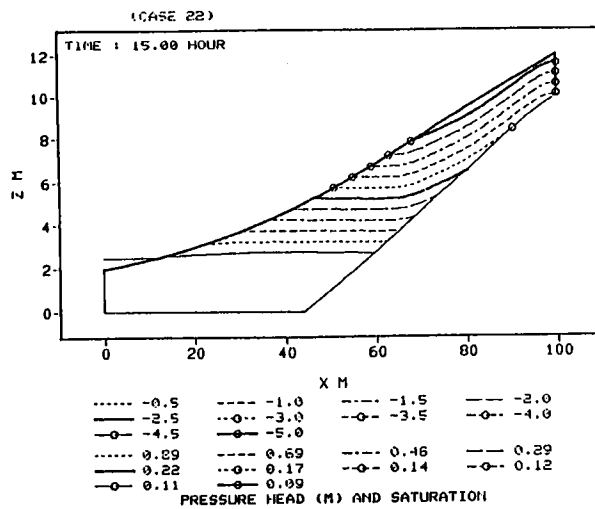
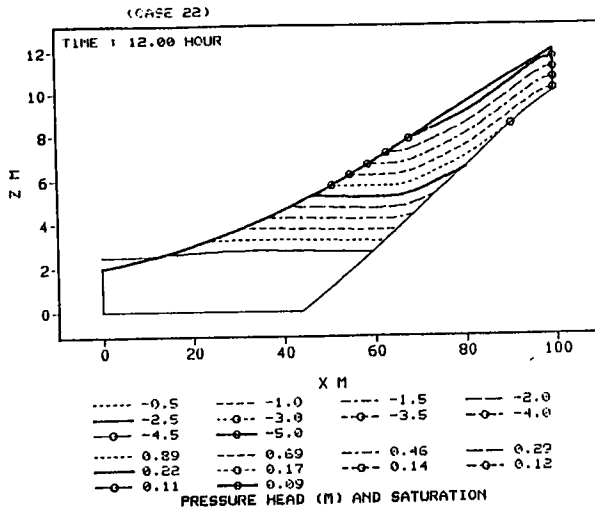
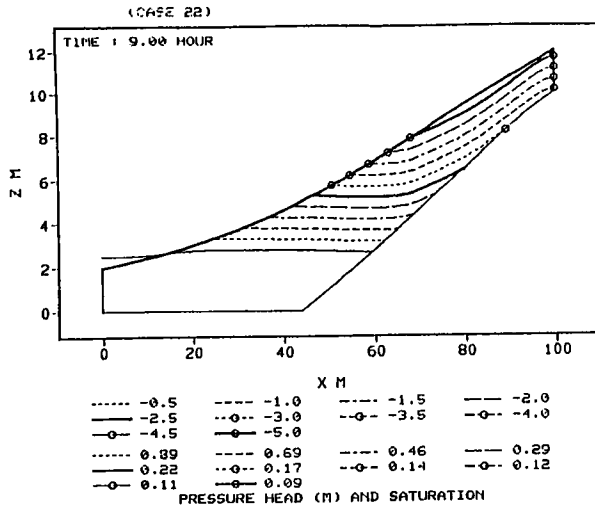


Figure 2.26 The moving isoplethic curve of pressure head(CASE22)

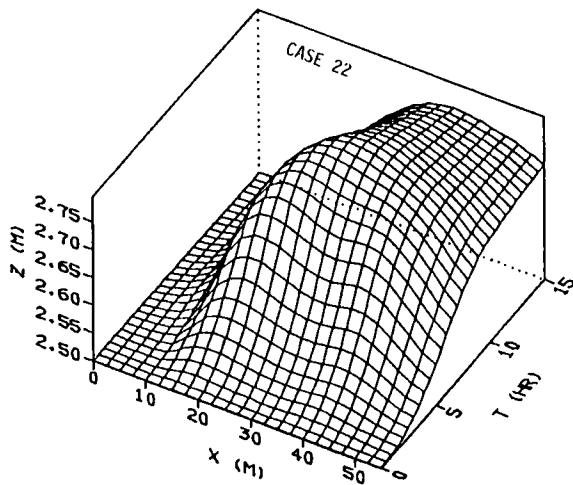
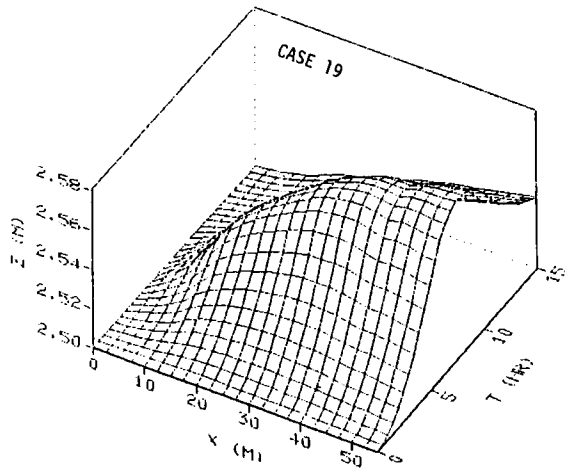
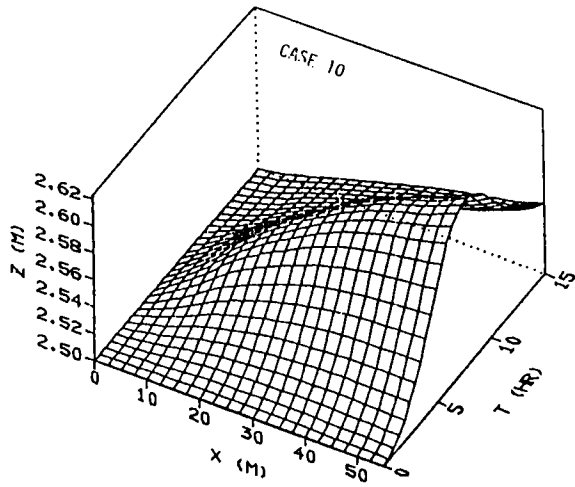


Figure 2.27 The water table changes with time and distance (CASE10.19.22)

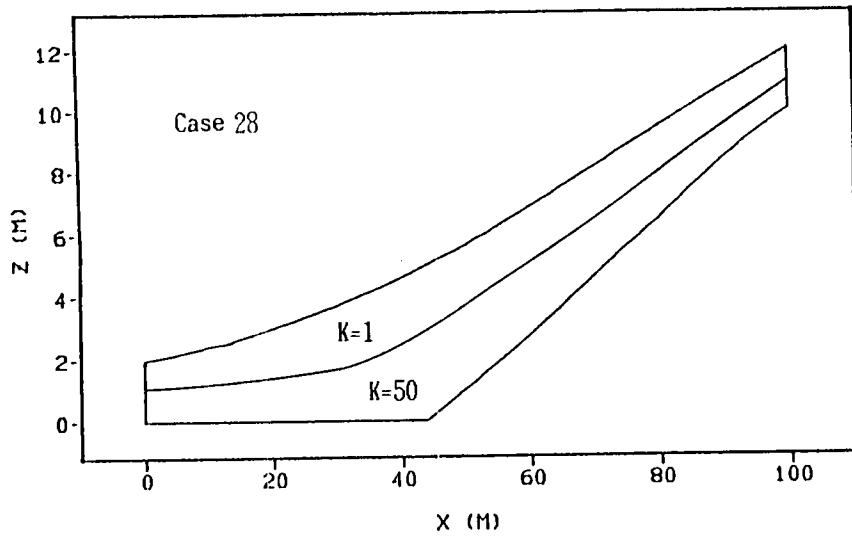
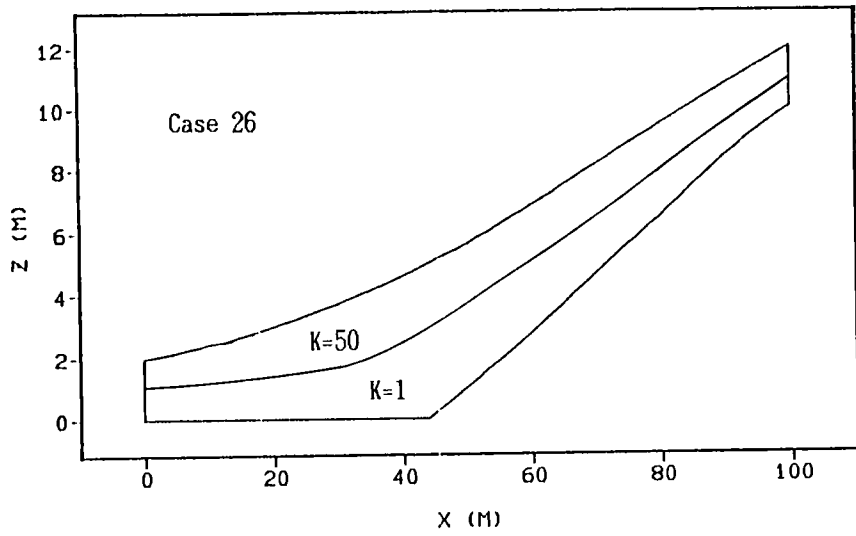


Figure 2.28 Two-layer region of flow

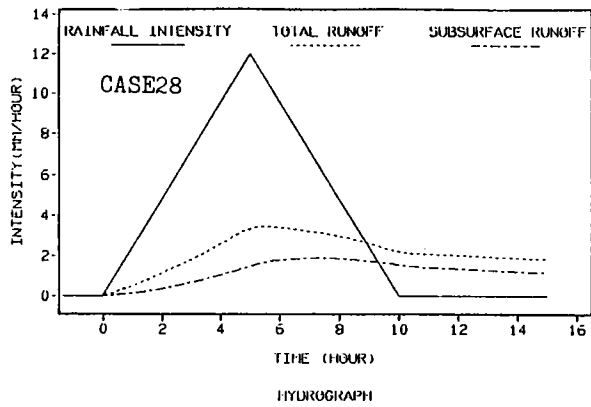
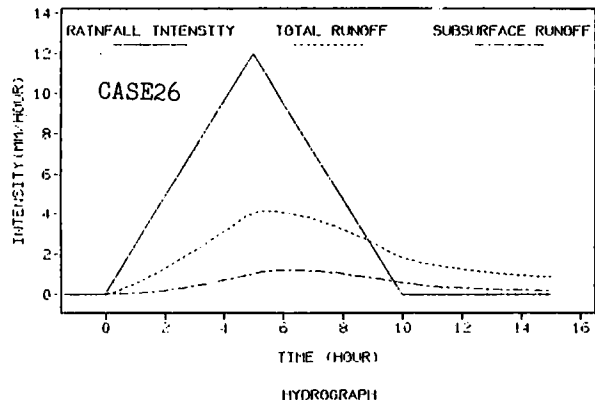


Figure 2.29 Hydrograph(CASE26.28)

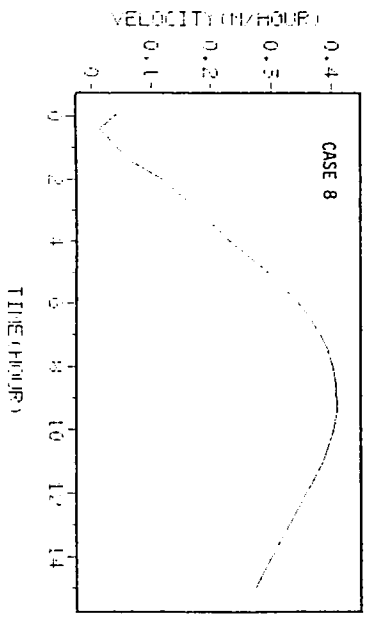
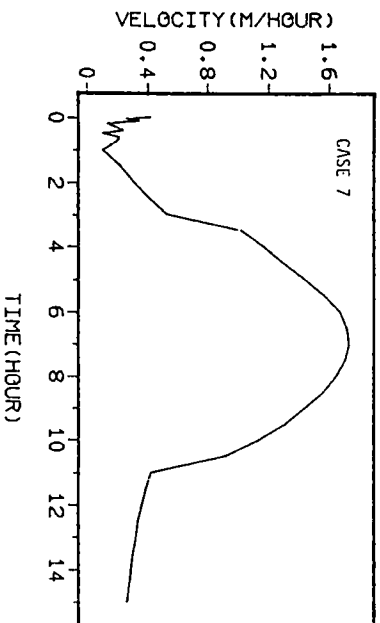
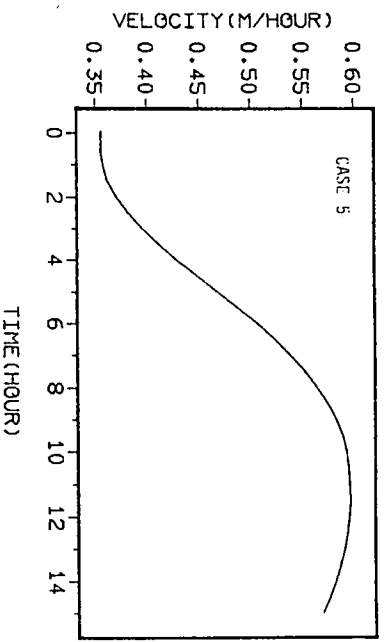
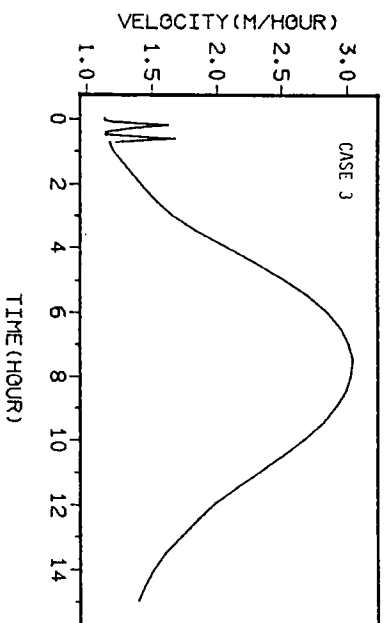


Figure 2.30 The maximum velocity of surface flow(CASE3.5.7.8)

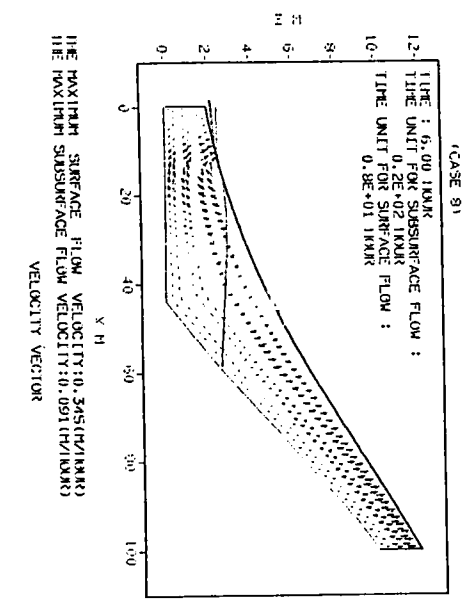
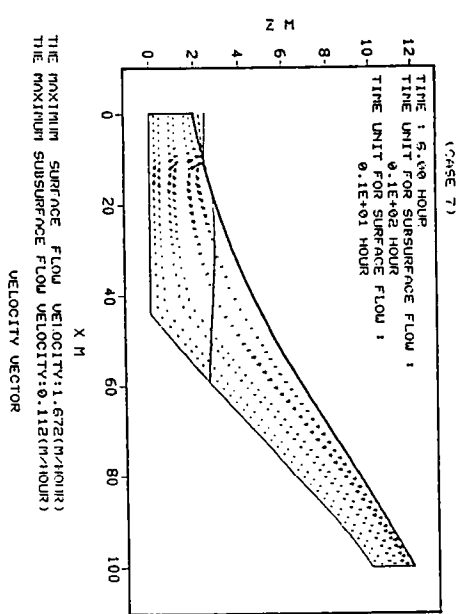
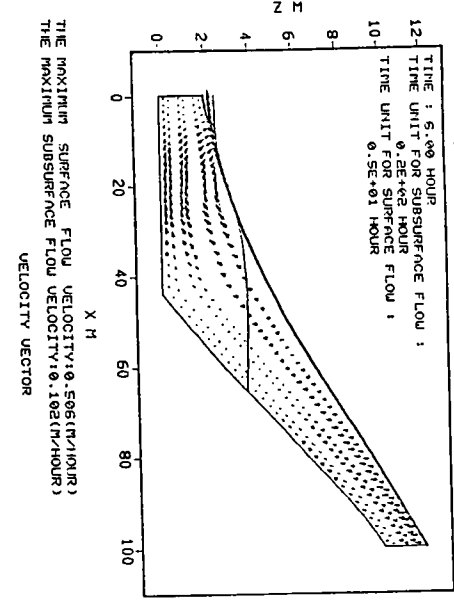
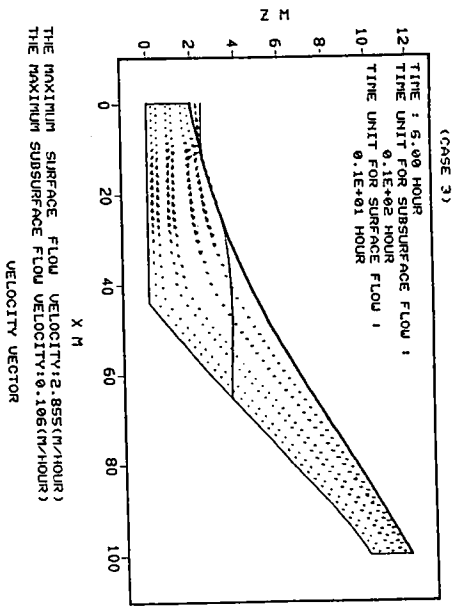


Figure 2.31 Velocity vector (CASE3,5,7,8)

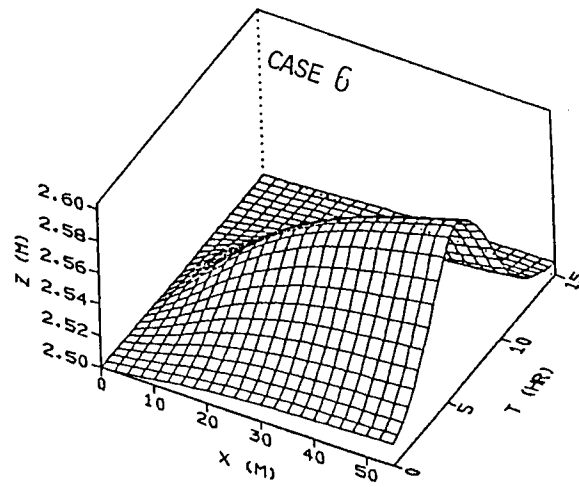
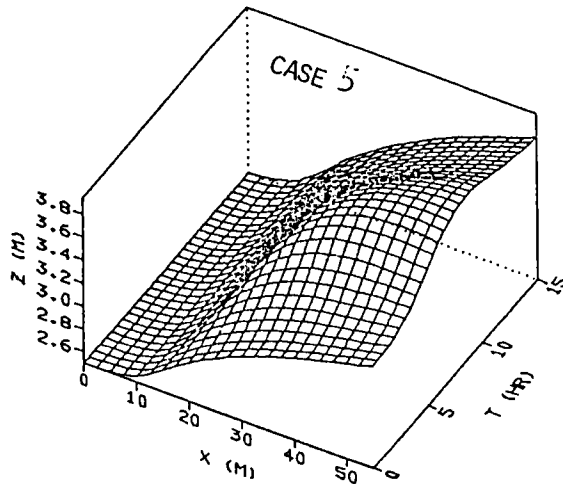


Figure 2.32 The water table changes with time and distance(CASE5.6)

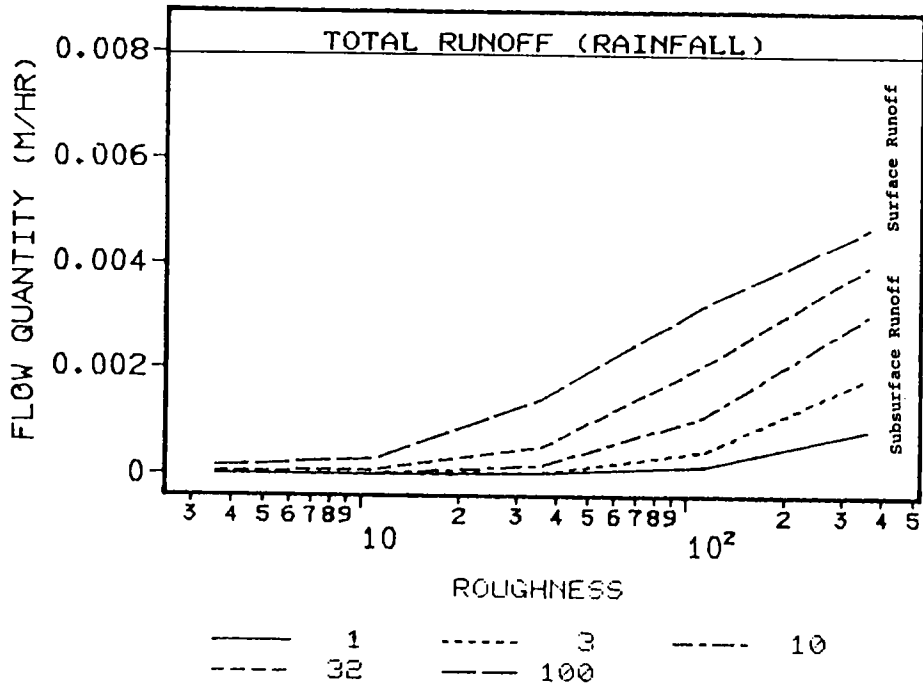


Figure 2.33 The runoff discharges change with the saturated conductivity and roughness

1) In the case of steady state flow, the greater the saturated hydraulic conductivity is, the higher is the ratio of overland runoff to total runoff.

2) In the case of transient flow, the short-time runoff discharges of both overland flow and subsurface flow increase as the saturated hydraulic conductivity becomes greater.

3) As the roughness becomes larger, the subsurface runoff increases and the overland runoff decreases. As a result the total runoff generally decreases.

4) In the case of flow in an anisotropic porous medium, a greater vertical component of the saturated hydraulic conductivity generally quickens drainage, and a greater horizontal component results in an increase in storage.

5) In the case of a two-layer hillslope, the thinner the upper layer with a greater saturated hydraulic conductivity, the better the return flow develops and the more the overland runoff discharge.

2.3.3 Moisture Characteristic Curve

The moisture characteristic curve is said to produce strong influence on runoff process by controlling the storage capacity of soil. Figure 2.34 shows the hydrographs of CASE9 and CASE10, which have different moisture content at the same pressure head(CASE9 is higher than CASE10). Although the initial conditions are the same static flow, CASE9 has a higher storage than CASE10. The difference in the initial storage results in the difference in the peak discharge(CASE9 is 6.5 mm/hour, while CASE10 is only 5.5 mm/hour) and the difference in the lag-time(1 hour and 40 min. respectively).

Since CASE9 has a higher storage capacity than CASE10, the declining slope of the hydrograph of CASE9 is not so gentle as that of CASE10. As a result the ratio of total runoff to total precipitation in the two cases is the same 80% at a point in time five hours after cessation of the rainfall(Figure 2.35).

Figure 2.36 shows the hydrographs of CASE9 and CASE13, in which the porosities are 0.45 and 0.3, respectively. Since CASE9 has a higher moisture content than CASE13 at a given pressure head, the water table rises more quickly in CASE9(Figure 2.37). This also causes the difference in maximum velocity between the two cases(Figure 2.38) and the difference in discharge(five hours after the rain has stopped, the ratios of discharge to precipitation in CASE9 and CASE13 are 80% and 95%, respectively).

The above simulation results can be summarized as follows:

1) When all of the other conditions are the same, the lower the storage capacity is, the gentler are both the increasing and the declining slopes of the hydrograph.

2) The higher the porosity is, the slower is the drainage.

2.3.4 Specific Storage

Specific storage is a parameter which accounts for the elastic nature of water and soil. Figure 2.39 shows the simulation results of two cases with different specific storage. There is little difference between the two hydrographs. This may be because a) the soil layer considered is very thin, and b) the range in which the pressure head varies is narrow. For these reasons, when considering the near-surface, short-time runoff, we can in general ignore the influence of specific storage.

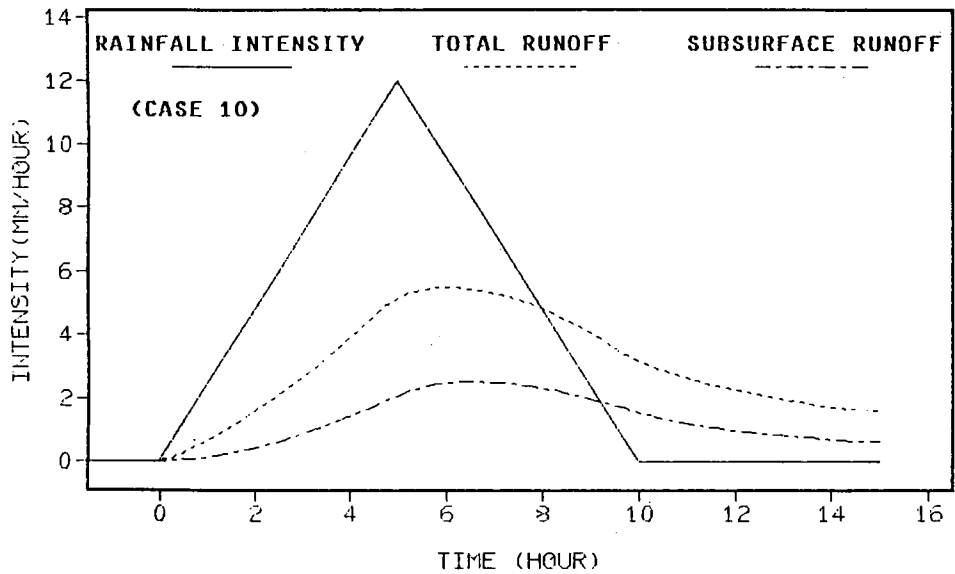
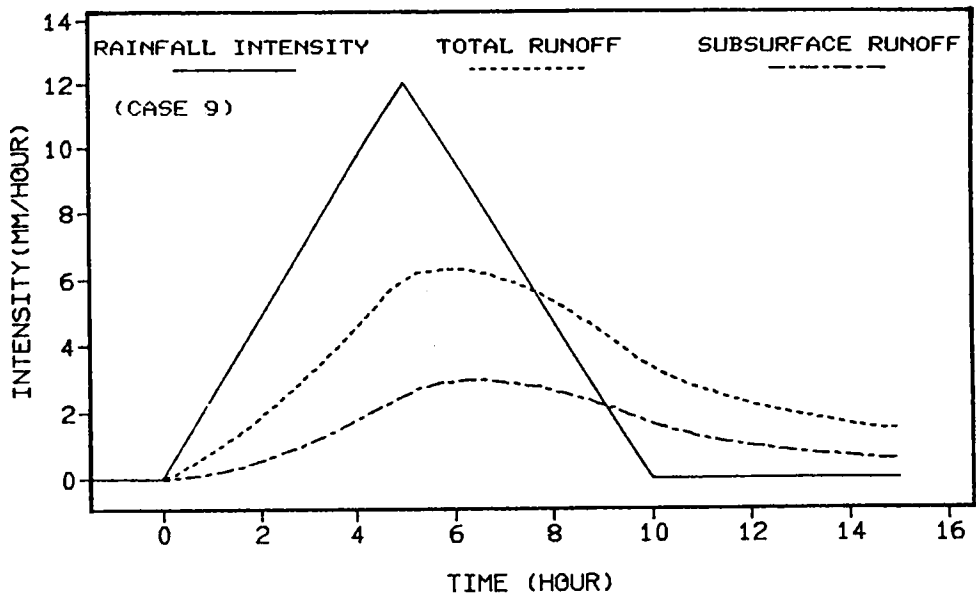


Figure 2.34 Hydrograph(CASE9.10)

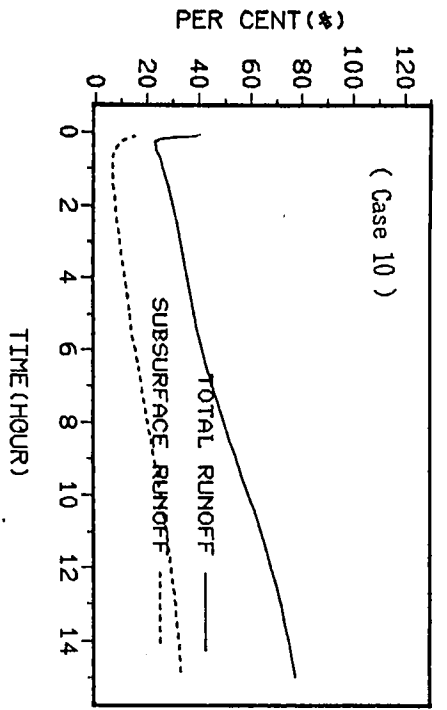
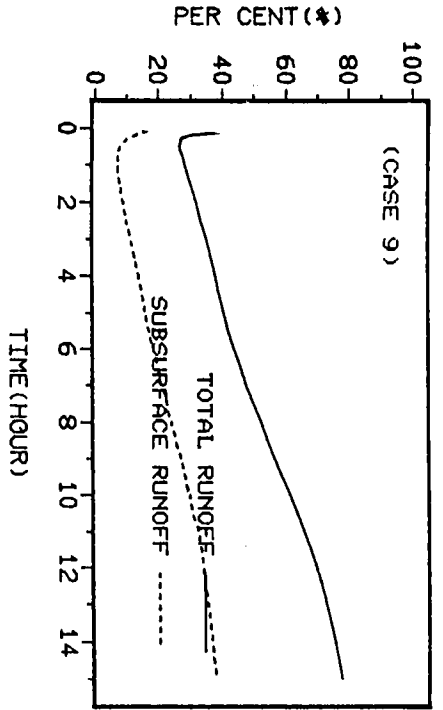


Figure 2.35 The changing ratio of runoff to precipitation with time

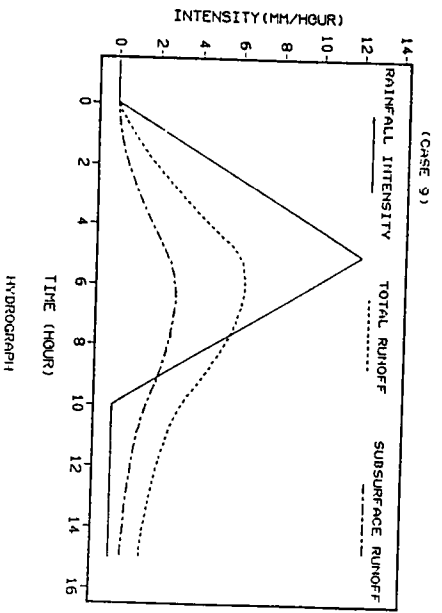
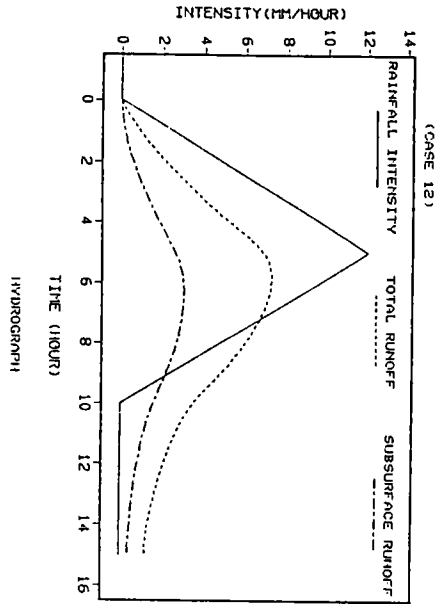


Figure 2.39 Hydrograph(CASE9,12)

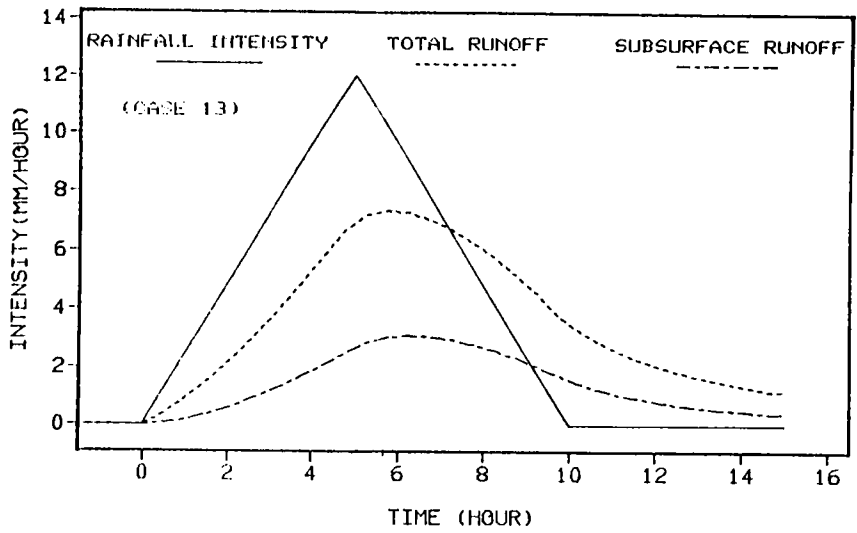
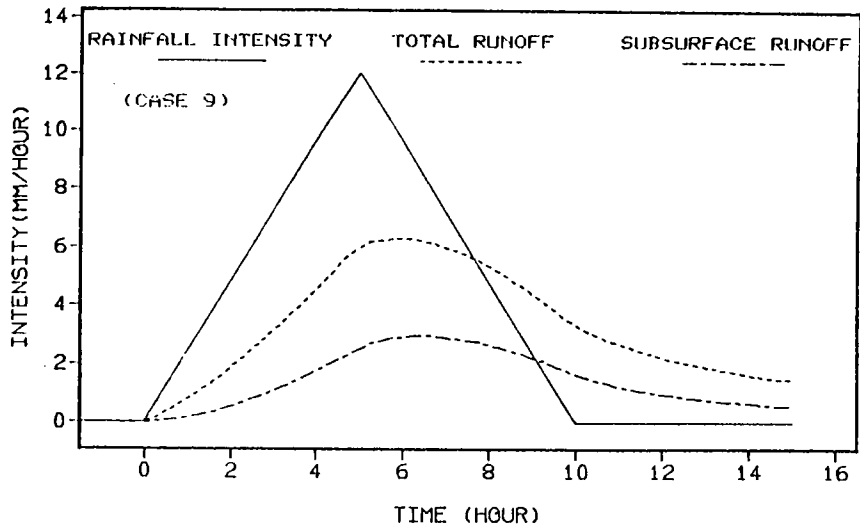


Figure 2.36 Hydrograph(CASE9.13)

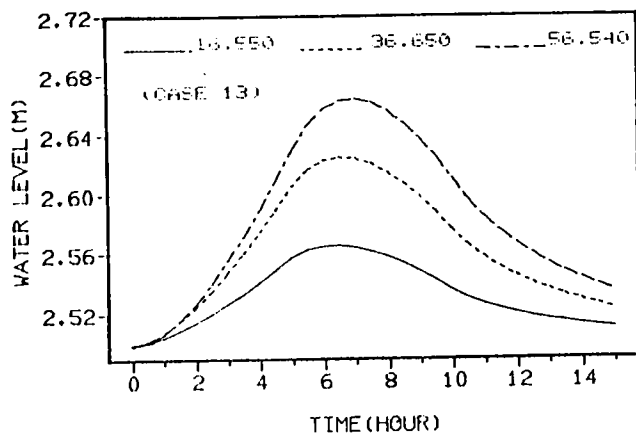
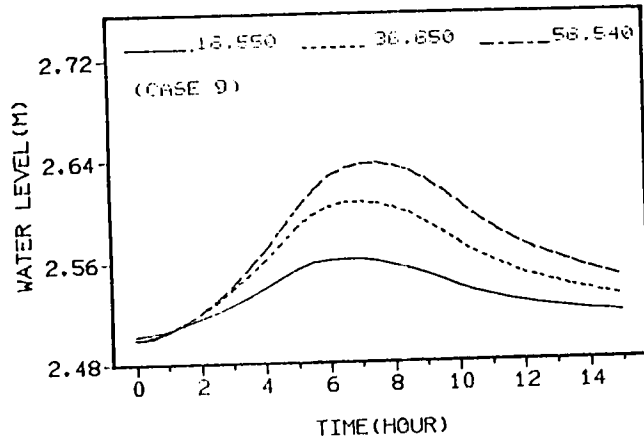
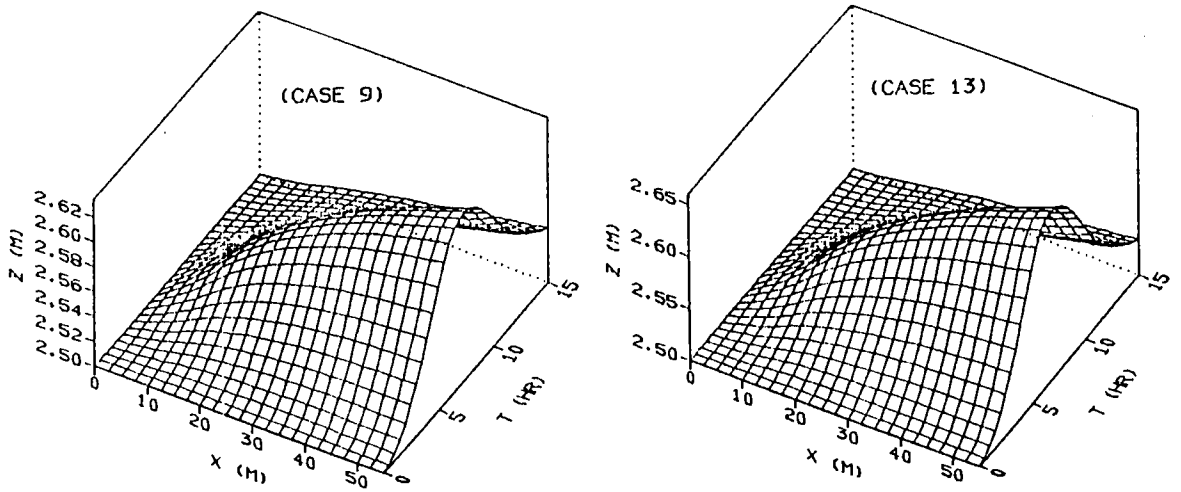
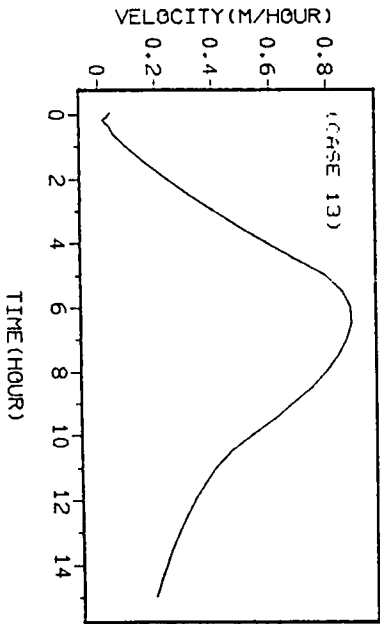
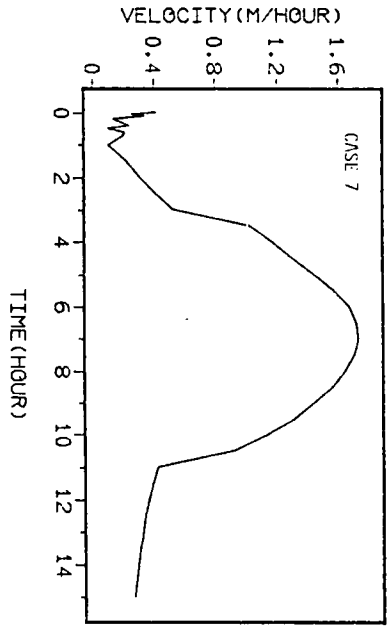
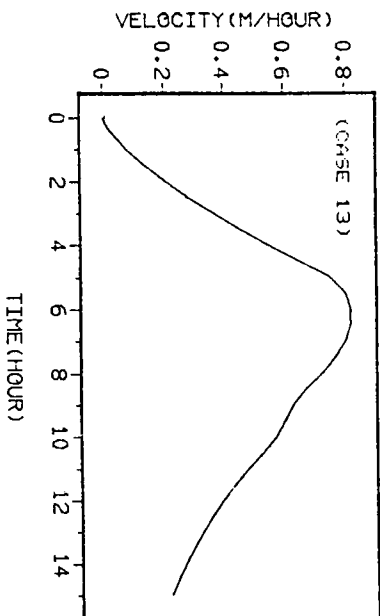
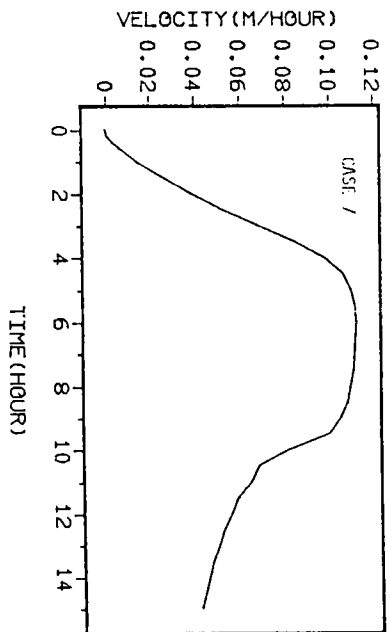


Figure 2.37 The water table changes with time and distance



The Maximum Velocity of Surface Flow



The Maximum Velocity of Subsurface Flow

Figure 2.38 The maximum velocity(CASE7,13)

2.3.5 Rainfall Pattern

We have simulated the influences of concentration and dispersion of rainfall in time on runoff by considering simple rectangular rainfalls with different intensity and duration.

CASE15, CASE16 and CASE18 have the same total precipitation, 40 mm/hour, but the intensity and duration are 10 mm/hour, 4 hours; 4 mm/hour, 10 hours; and 20 mm/hour, 2 hours; respectively. Figure 2.40 shows the hydrographs, the shapes of which are all similar. However, the rising heights of seepage point are 0.034m, 0.019m and 0.050, respectively(Figure 2.41). These values show a tendency to increase as rainfall concentrates. This tendency can also be seen from the ratio of total discharge to precipitation(Figure 2.42 and Table 2.8). Based on the simulation results we come to the conclusion that the drainage becomes quicker as the rainfall concentrates.

2.3.6 Antecedent Precipitation

Figure 2.43 shows the hydrograph for the case in which the rainfall has two peaks. The difference between the corresponding two peaks of the hydrograph can be explained by the difference of the antecedent saturation situation. The second peak is higher and gentler than the first one. This means that the higher the degree of saturation of soil, the quicker will be the drainage.

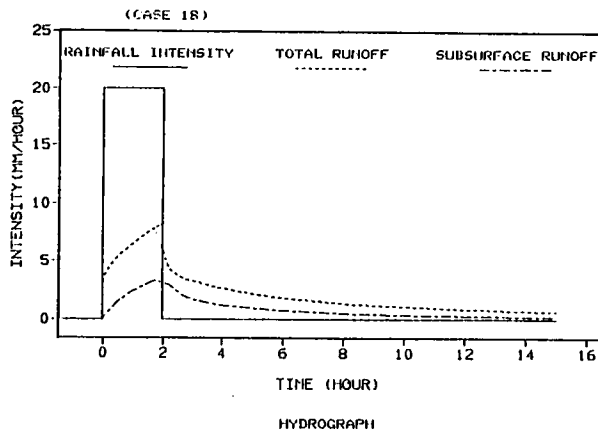
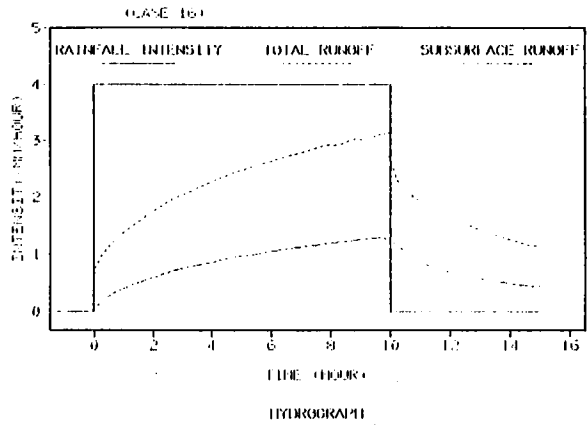
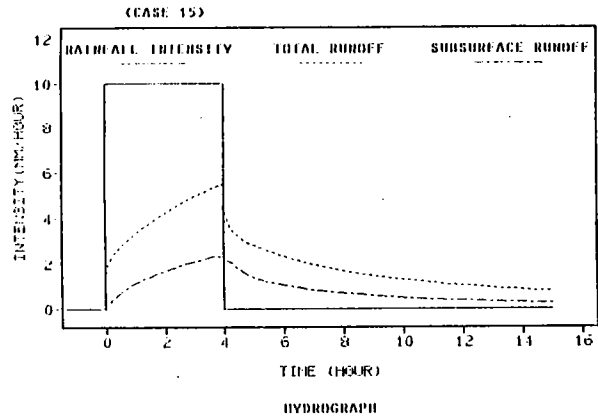
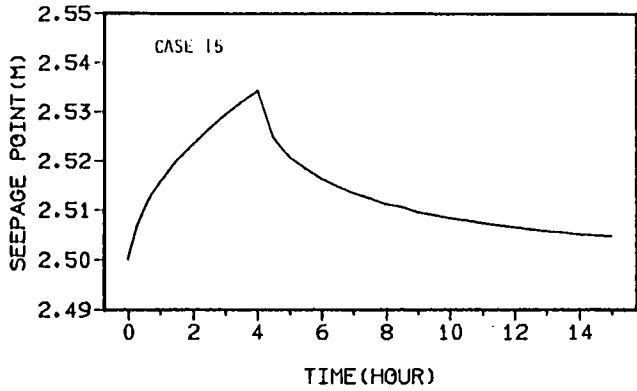
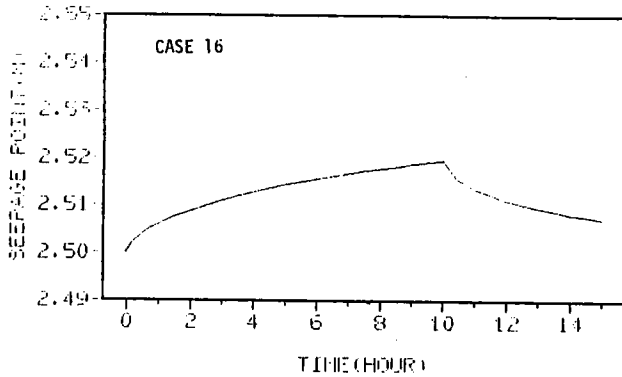


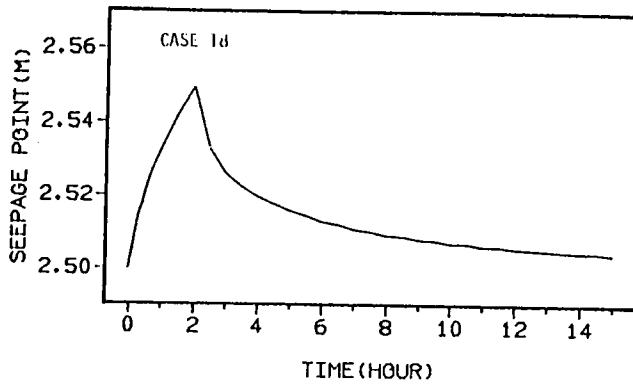
Figure 2.40 Hydrograph(CASE15.16.18)



THE MOVING SEEPAGE POINT

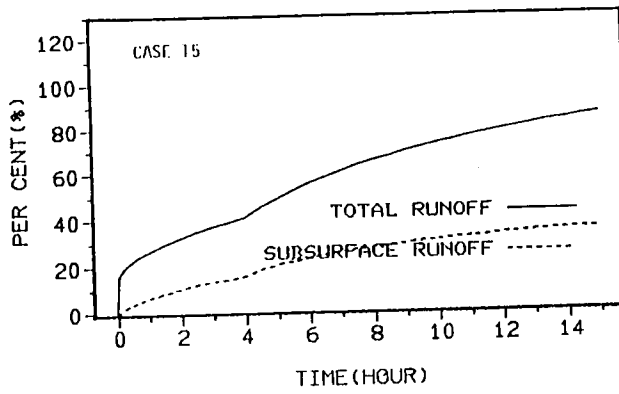


THE MOVING SEEPAGE POINT

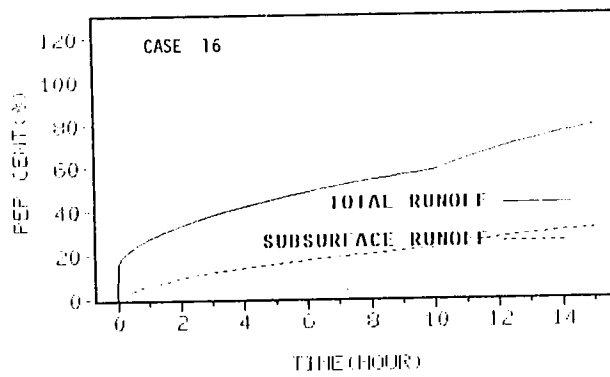


THE MOVING SEEPAGE POINT

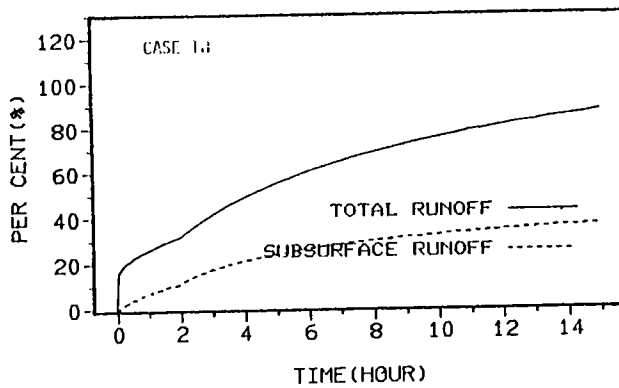
Figure 2.41 The moving seepage point



THE COMPARISON BETWEEN THE RAINFALL AND RUNOFF



THE COMPARISON BETWEEN THE RAINFALL AND RUNOFF



THE COMPARISON BETWEEN THE RAINFALL AND RUNOFF

Figure 2.42 The changing ratio of runoff to precipitation with time

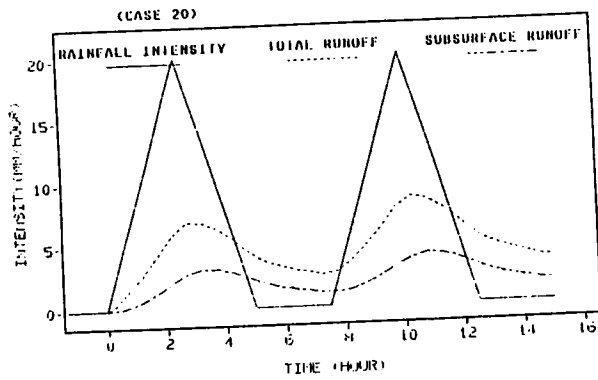


Figure 2.43 Hydrograph(CASE20)

Table 2.8 The ratio of runoff discharge to precipitation

| | A (%) | B (%) | C (%) |
|---------|-------|-------|-------|
| Case 18 | 86 | 49 | 37 |
| Case 15 | 83 | 49 | 34 |
| Case 16 | 77 | 47 | 30 |

A :ratio of total discharge to total precipitation
 B :ratio of total surface discharge to total precipitation
 C :ratio of total subsurface discharge to total precipitation

2.4 Simulation Analysis of Hillslope Runoff Processes

In the preceding section, the synthesized runoff model has been applied to hillslope system, and the influences of the main factors which govern the runoff process have been examined by considering the runoff process as a " black box " transforming rainfall into discharge. It is apparent that the analysis was made from a macro point of view. In this section we shall analyze the runoff process from a micro point of view. We will try to make clear the mechanism of the infiltration and runoff process by examining the interior variables such as moisture content, velocity of flow, interaction of overland flow with subsurface flow and movements of water table and seepage point.

2.4.1 Distribution of Moisture Content

2.4.1.1 Changing Moisture Profile

Figure 2.44 shows the moisture profile of CASE2 in which the flow changes from static state to steady state due to a constant rainfall, 10 mm/hour. The characteristics of the moisture profile can be summarized as follows.

1) As the rainfall starts, the unsaturated zone is rapidly saturated by the infiltrated water. This process continues from the lower slope towards the upper slope and from the base of the region of flow towards the land surface. With the passage of time, the rising speed of the water table becomes gradually slower at the lower slope, but at the upper slope the rising continues until a steady state is achieved(Figure 2.45 and Figure 2.46).

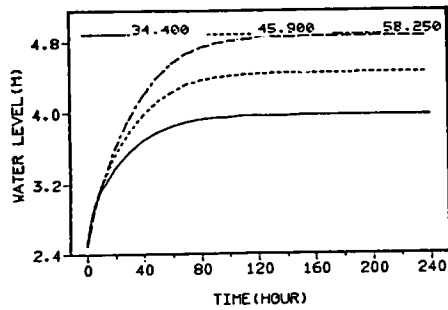
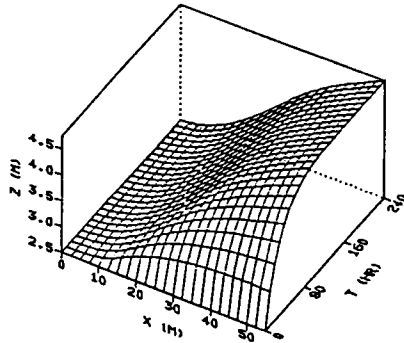
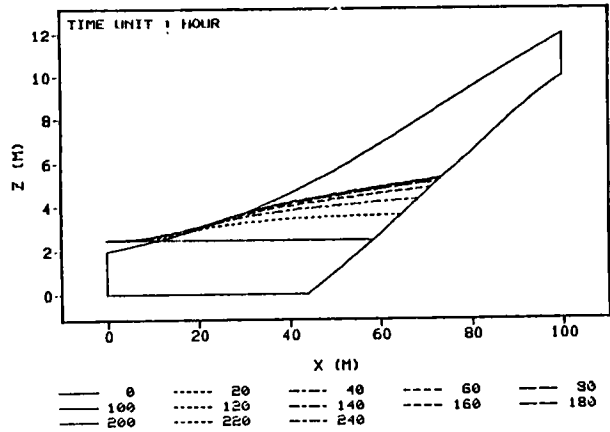


Figure 2.45 The moving water table with time(CASE2)

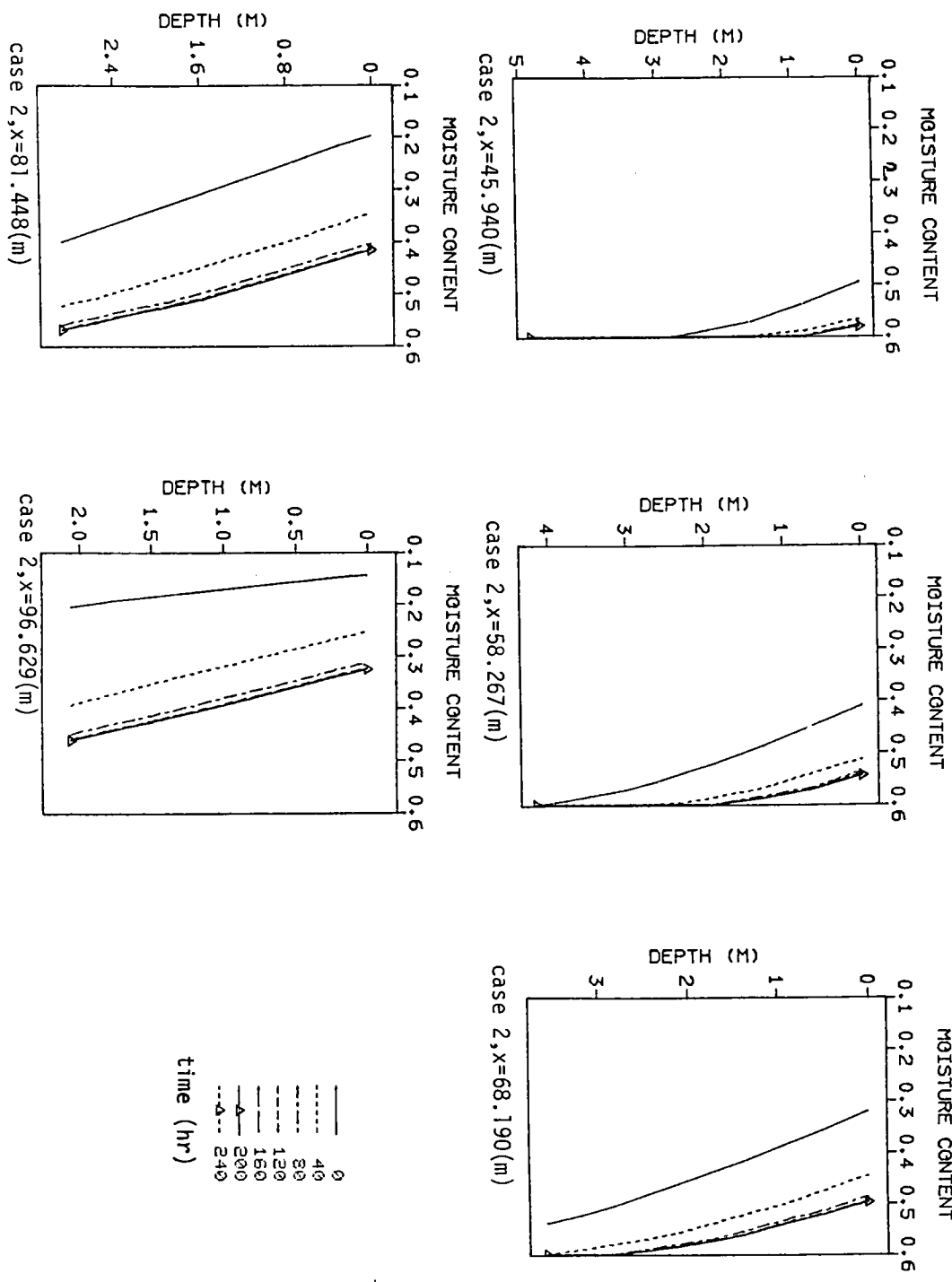


Figure 2.44 The changing moisture content profile(CASE2)

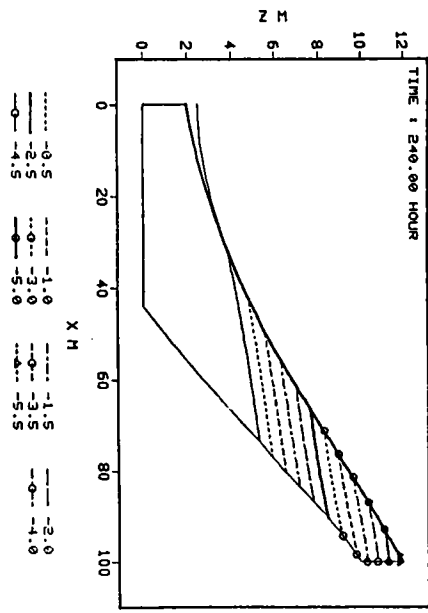
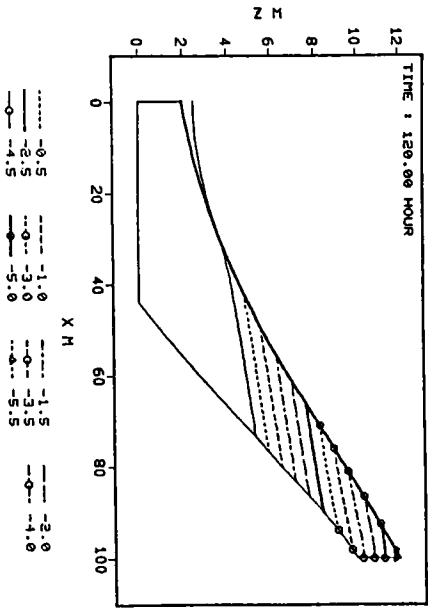
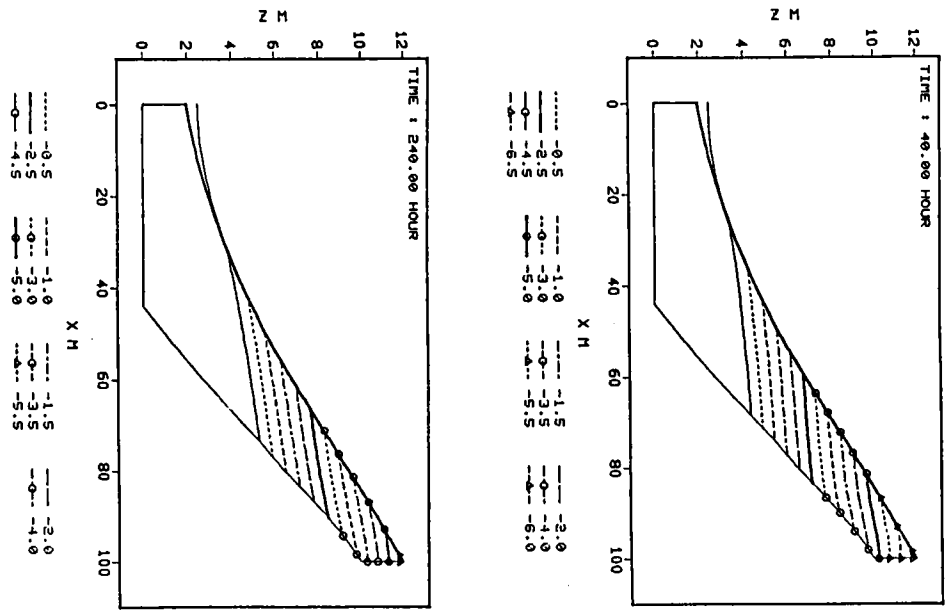
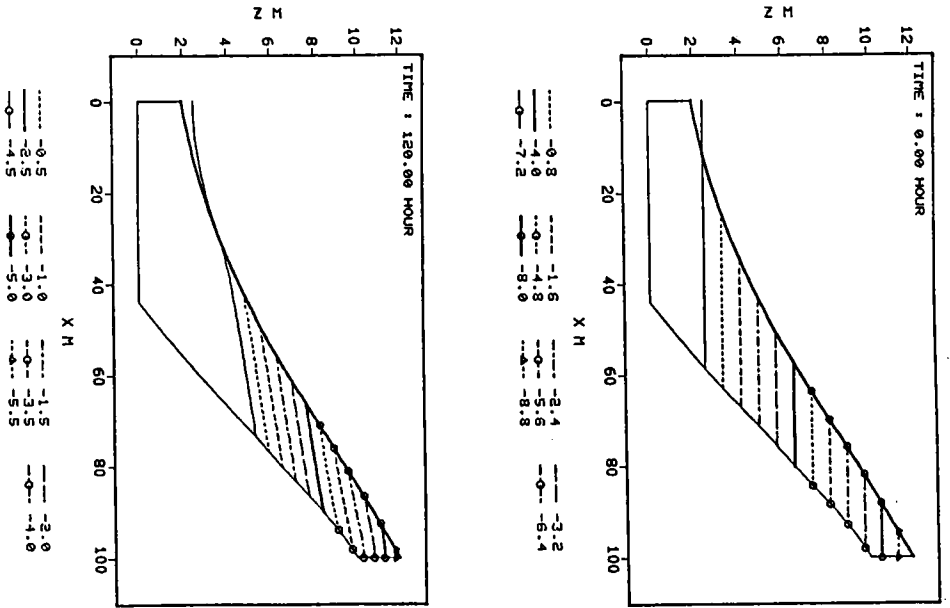


Figure 2.46a The changing isoplethic curve of pressure head(CASE2)

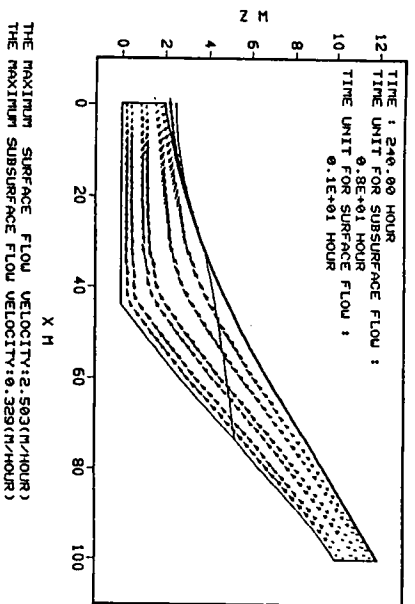
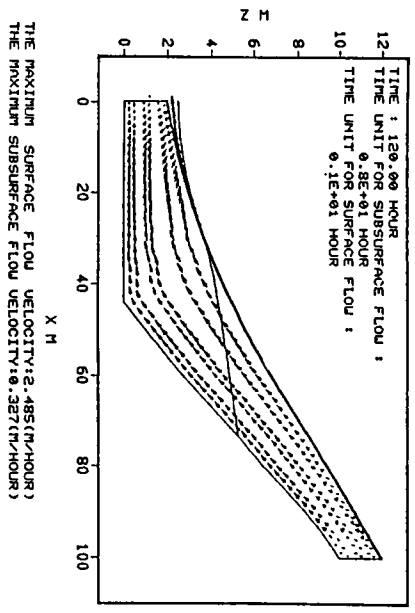
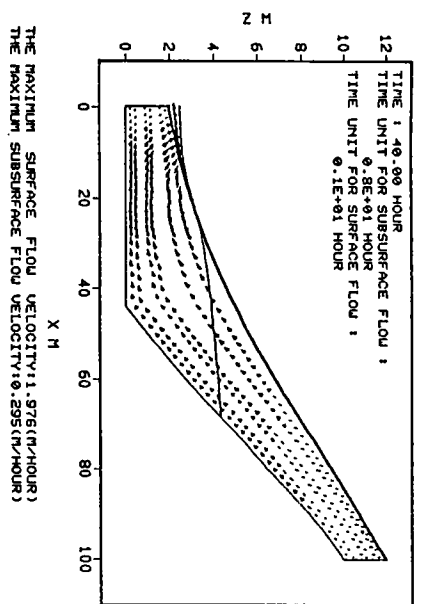
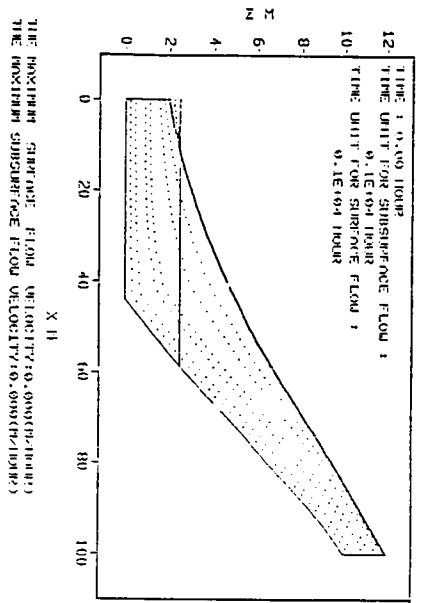


Figure 2.46b The changing velocity distribution with time(CASD2)

2) At the lower slope, since the antecedent moisture content is higher, the range of variation of moisture content is not so wide as at the upper slope.

3) At the lower slope, the range variation is wider around the water table than nearby the land surface, while at the upper slope, the range nearby the land surface is wider than around the water table. This is because the right-hand vertical boundary GF(Figure 2.1) is an impermeable boundary and there is no lateral flow across GF into the region of flow.

The changing water tables and moisture profiles of CASE8 and CASE9 are shown in Figure 2.47 and Figure 2.48. Since CASE8 has a greater hydraulic conductivity, the infiltrated water does not remain in the unsaturated zone, but returns to the land surface or flows down the slope and consequently, the ranges of both the changing of moisture content and the rising of water table in CASE8 are not so wide as in CASE9. The influence of hydraulic conductivity on the distribution of moisture content can also be seen in CASE26 or CASE28, in which the soils are heterogeneous(Figure 2.49).

Figure 2.50 contains the moisture profiles for CASE7 and CASE8 in which the roughness assumes different values. It can be seen that there is little difference between the two cases. This may be because the influence of roughness on subsurface flow system is indirect.

Figure 2.51 shows the moisture profile of CASE9 and CASE10 which have different moisture characteristic curves. These profiles are very similar except that the distributions of antecedent moisture content are different. This similarity is due to the high conductivity in both cases.

2.4.1.2 Redistribution of Soil Moisture

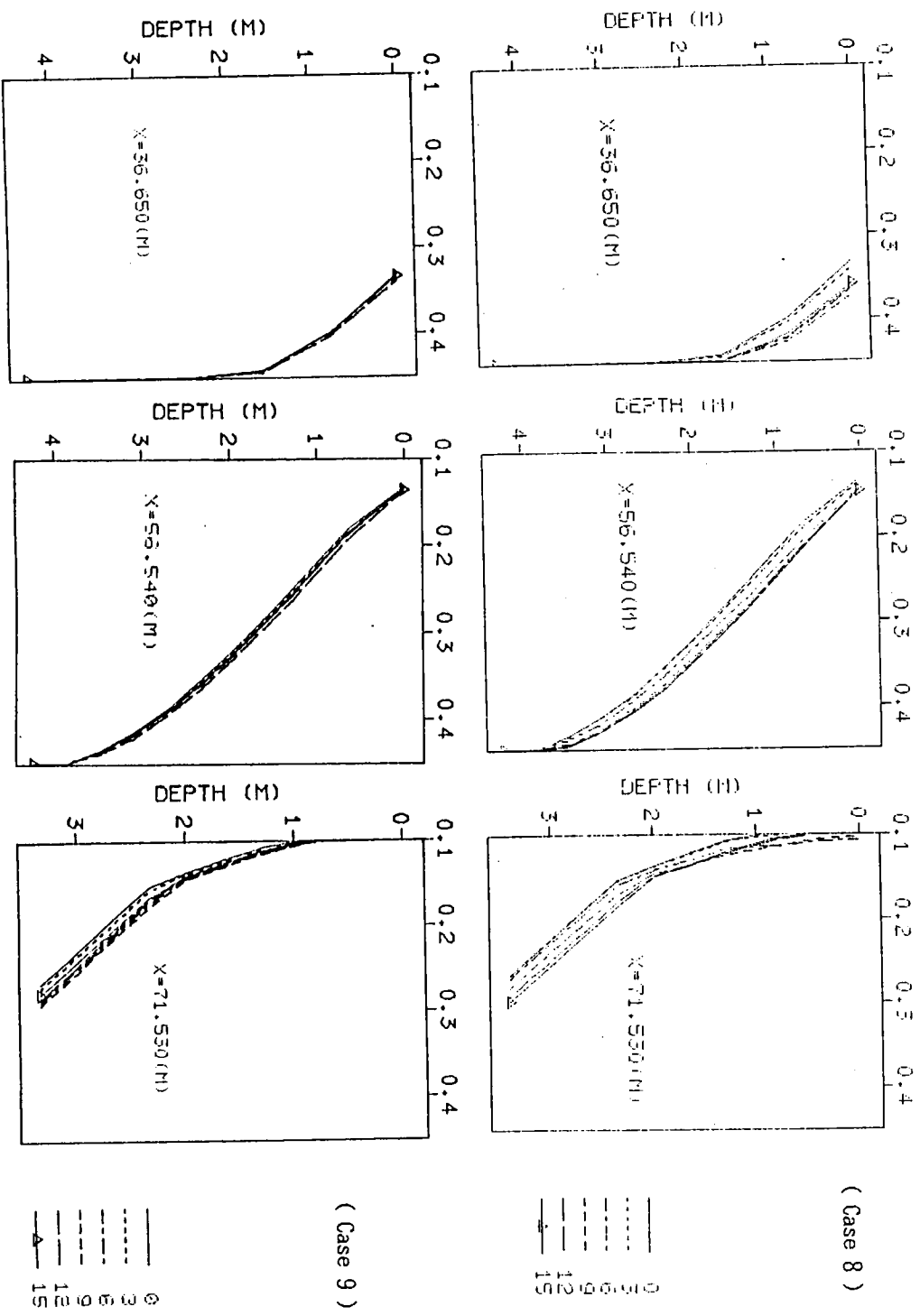


Figure 2.47 The changing moisture content profile with time and depth

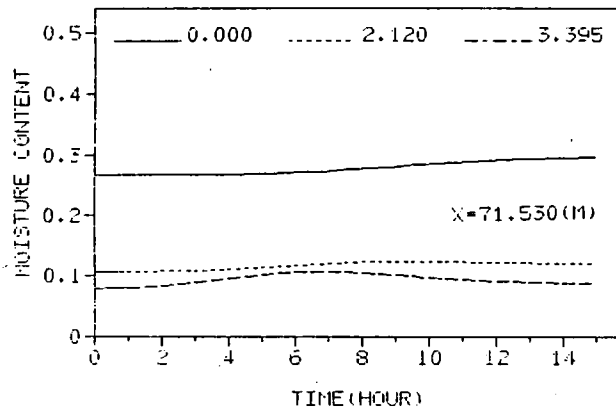
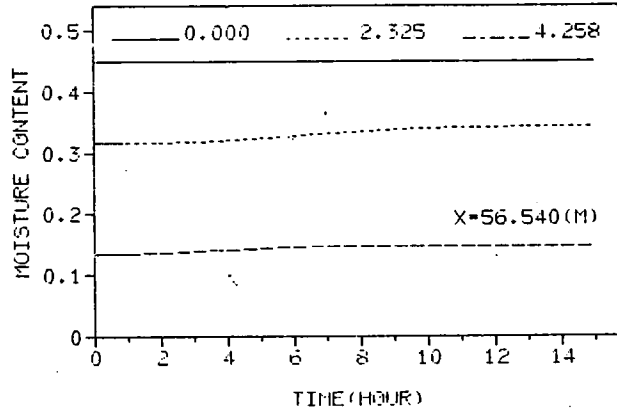
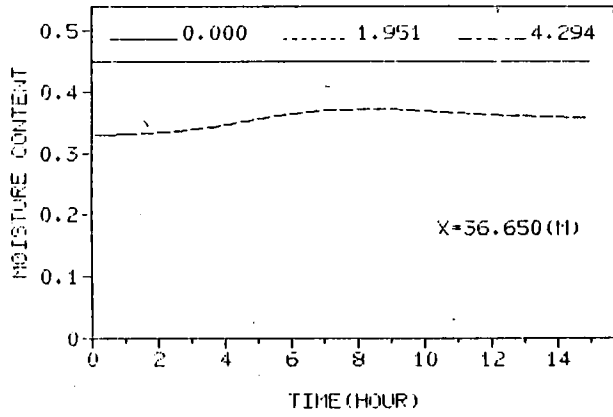


Figure 2.48 The moving water table(CASE8)

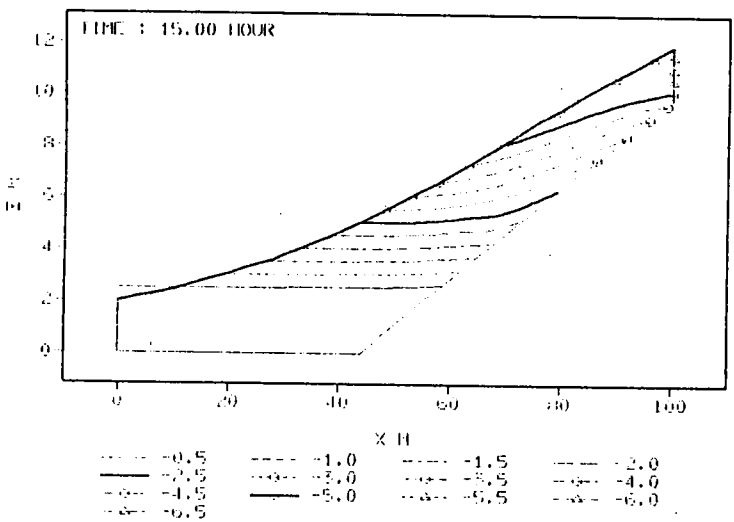
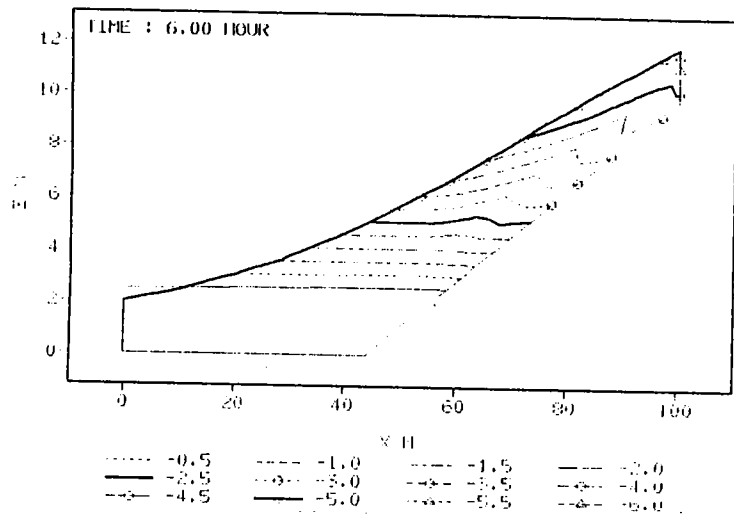
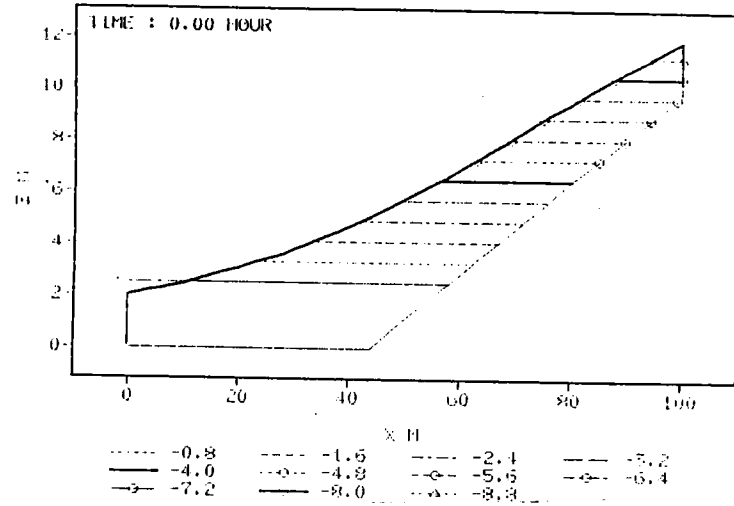


Figure 2.49 The changing isoplethic curve of pressure head(CASE26)

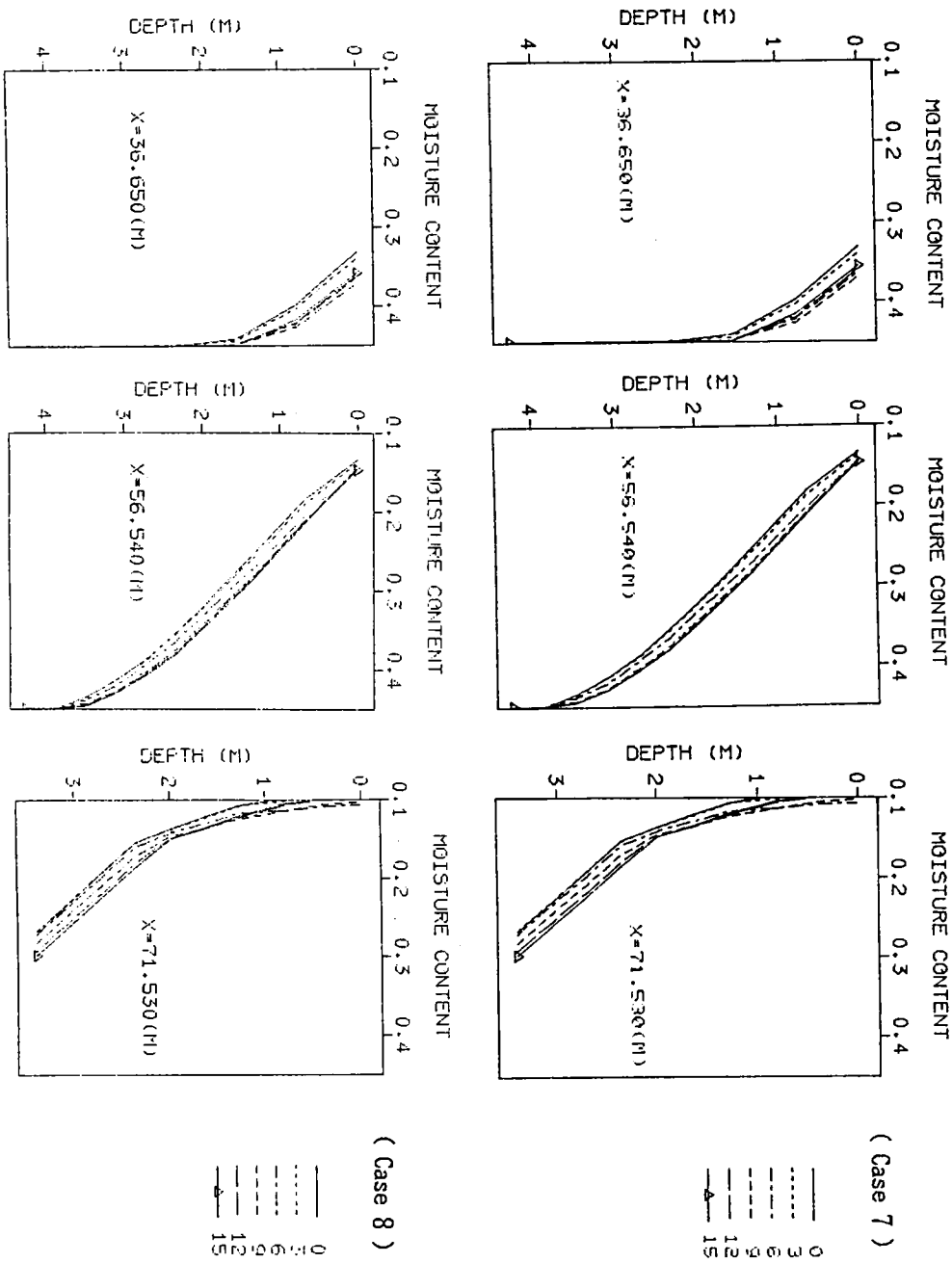


Figure 2.50 The changing moisture content profile with time and depth

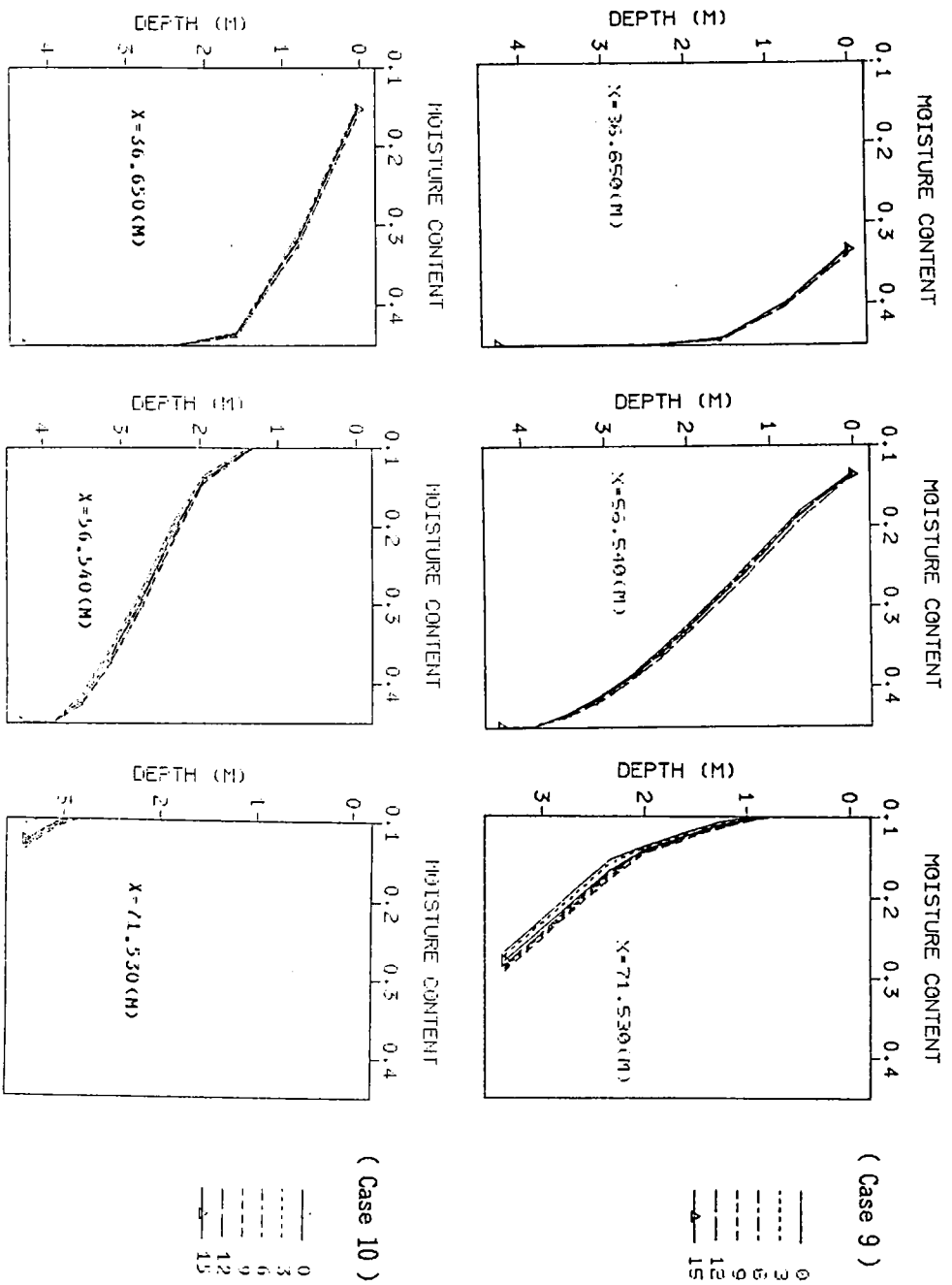


Figure 2.51 The changing moisture content profile with time and depth

Most of the researchers on the infiltration problem have primarily focused their attention on the evaluation of basic theory. By examining a vertical soil column, the nature of the response and the theoretical moisture profile have been made clear. However, relatively little has been published on the redistribution of soil moisture on a natural hillslope.

Hewlett and Hibbert(1963) have shown that while the upper part of the slope rapidly de-saturates and asymptotically approaches its equilibrium value, the lower part soon develops a remarkably stable moisture content value approximating saturation. Figure 2.52 contains the moisture profile of CASE1 in which the initial condition is a steady state flow with a rainfall intensity of 10 mm/hour. This case reproduces the redistribution process of soil moisture when the flow changes from steady state to static state. The changing pressure head within the process is shown in Figure 2.53. The simulation results reveal the following:

- 1) Drainage is quickest at the land surface and at the lower part of slope, and becomes progressively slower towards the water table and the upper part of slope. The moisture content value is thus stable in the vicinity of the water table for a long time after drainage. This is supported by the lateral flow from the upper slope.

- 2) Drainage becomes slower as time passes. The drainage can be divided into two processes, the first is transient and the second is near a steady state.

- 3) Finally the slope will drain towards values determined by the moisture characteristic curve of the soil.

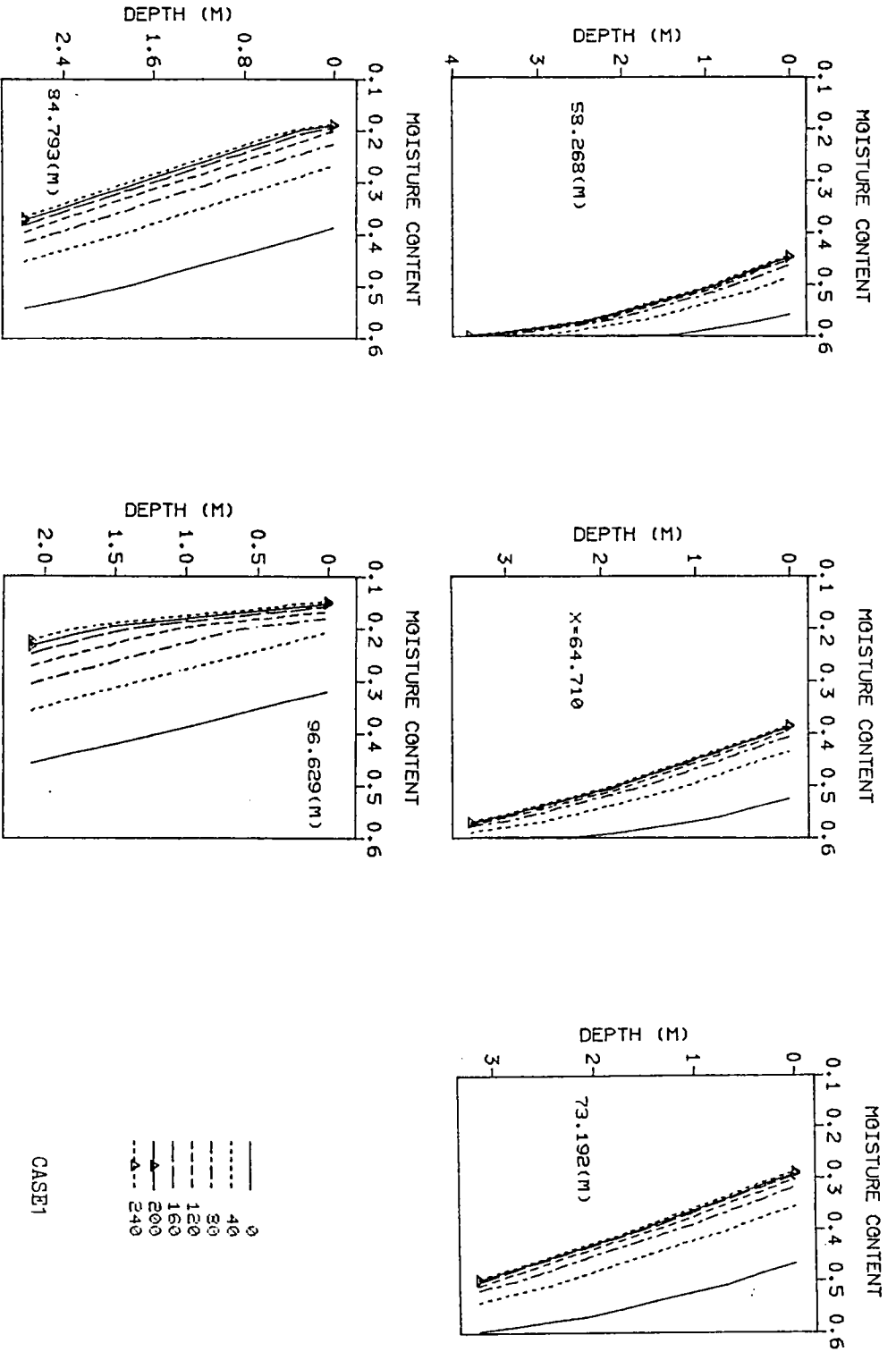


Figure 2.52 The changing moisture content profile with time and depth

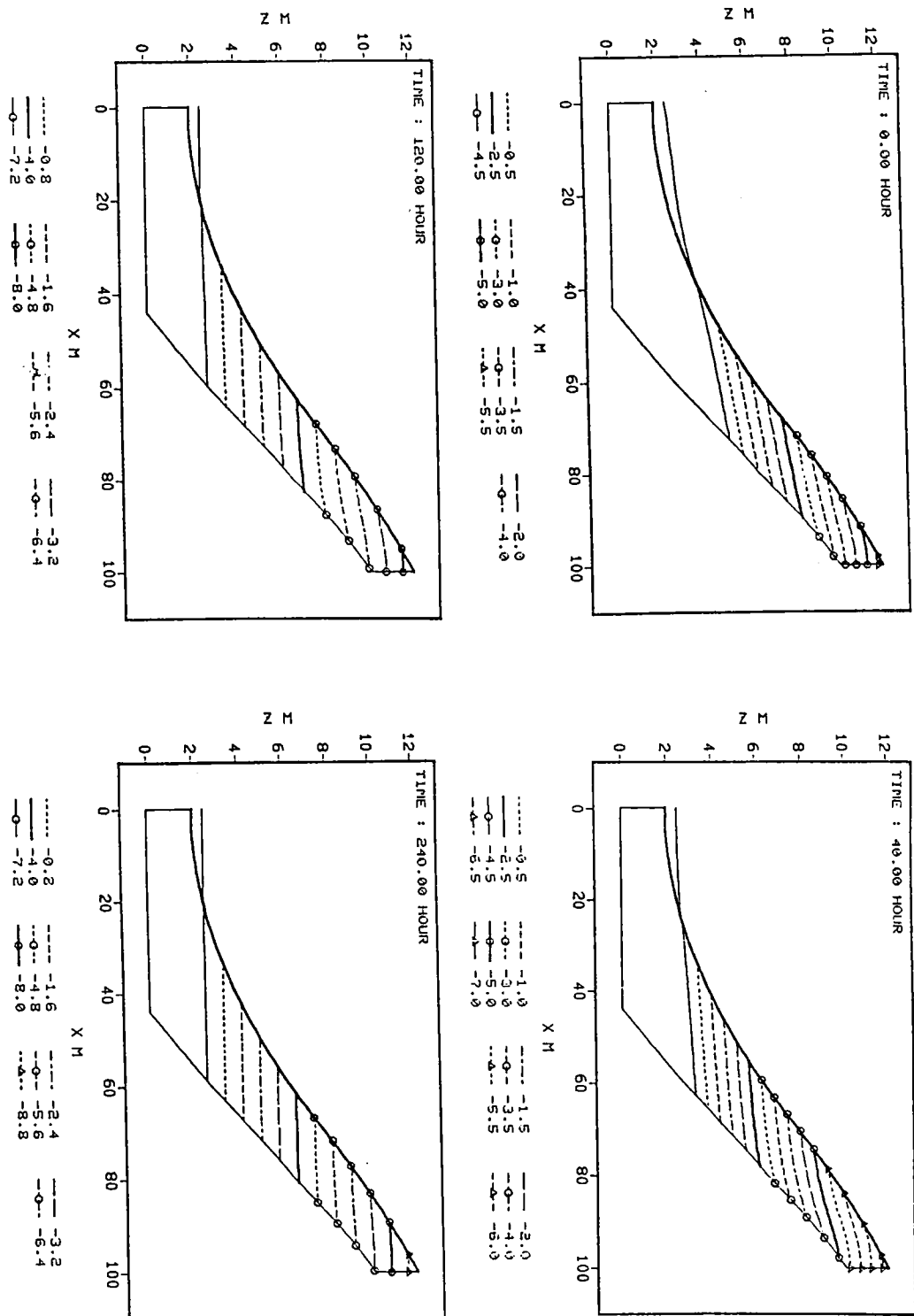


Figure 2.53 The changing isoplethic curve of pressure head(CASE1)

2.4.2 Velocity Distributions of Overland Flow and Subsurface Flow

2.4.2.1 Equations of Motion

As mentioned in Section 2.1, Darcy's law is used for saturated and unsaturated flows with the provision that the conductivity is a function of the pressure head. For overland flow, we have assumed that the kinematic approximation and the Manning equation are valid, and that the velocity of overland flow can be expressed as a summation of the velocity of subsurface flow on the land surface and the velocity of overland flow when there is no infiltration or seepage. According to Shiiba(1983), if we consider only the overland flow, the velocity becomes zero as the depth of flow approaches zero. On the other hand, if the overland flow and subsurface flow are treated as a continuous system, the velocity of overland flow must be equal to the velocity of subsurface flow on the land surface. In this study this requirement has been satisfied by taking into consideration the momentum balance along the land surface.

2.4.2.2 Distribution of Velocity in Time and Space

Figure 2.54 shows the distribution of velocity in space at different times. Since the initial condition is static state the velocities before the beginning of rainfall are zero. The characteristics of the velocity distribution can be summarized as follows:

- 1) At the beginning of the rainfall, overland flow and unsaturated subsurface flow occur rapidly due to the direct

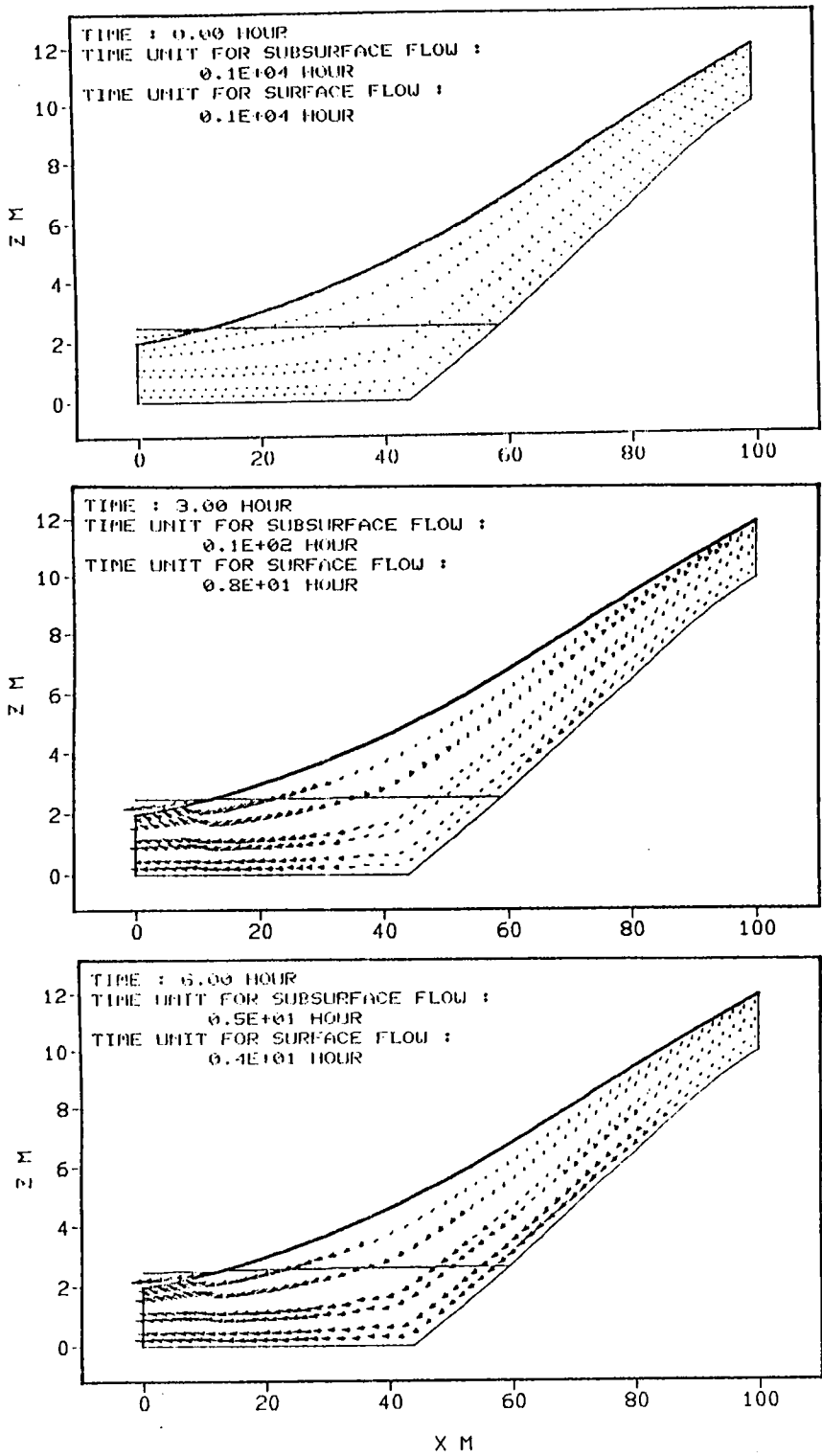


Figure 2.54a The changing velocity distribution with time(CASE12)

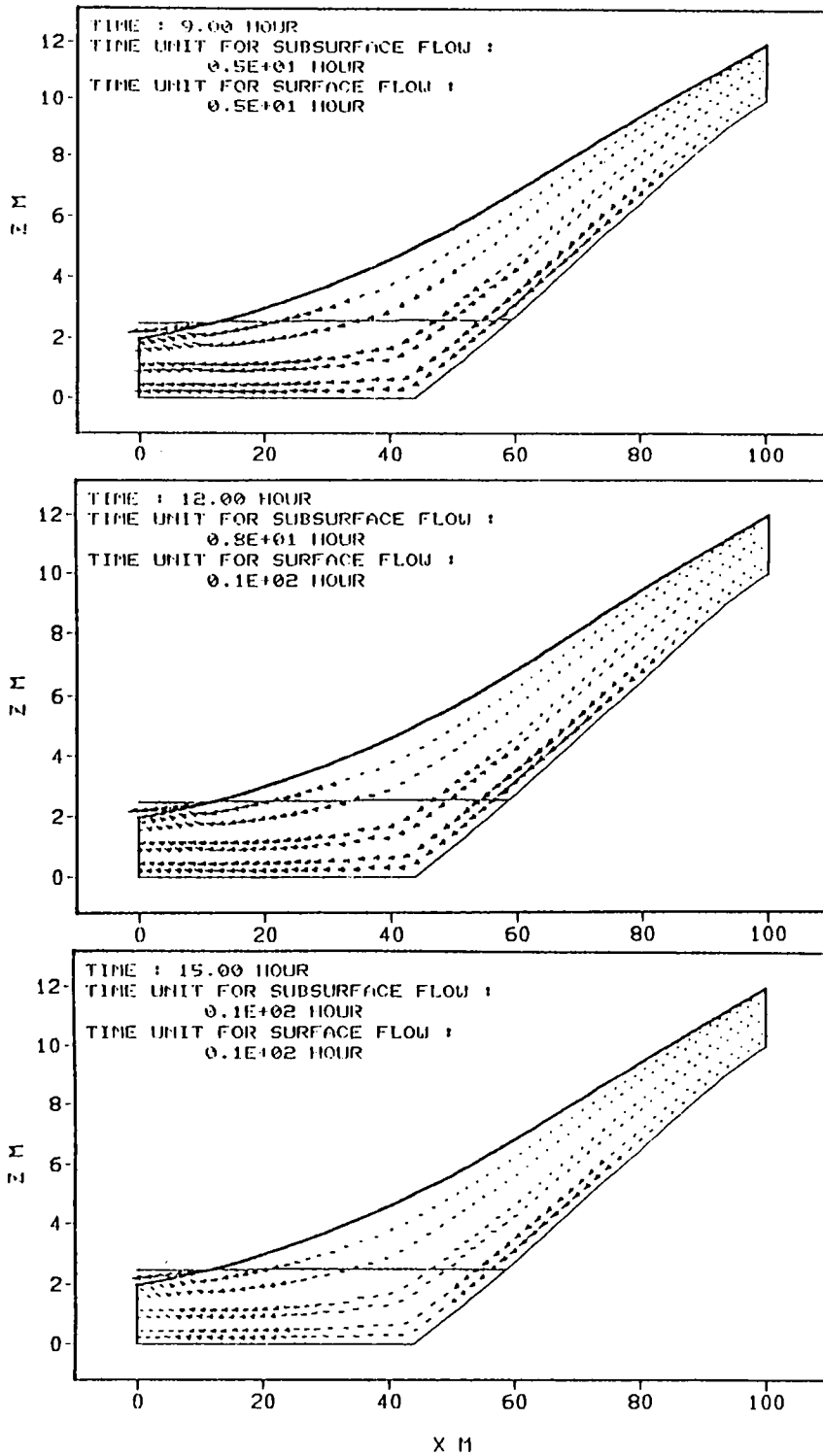


Figure 2.54b The changing velocity distribution with time(CASE12)

precipitation onto the saturated land surface and the infiltrated water, respectively.

2) Since the antecedent moisture content is very low in the vicinity of the land surface, the unsaturated hydraulic conductivity is low, the infiltrated water therefore cannot flow quickly towards the base of slope, and a zone with a sharp gradient in moisture content(and hence in pressure head) occurs. It is very similar to the so-called " wetting front " in the generation mechanism. If the conductivity is very low and the rain is very strong, the land surface may be saturated and Horton overland flow may occur.

3) The vertical component of the velocity of subsurface flow is greatest at the top of the upper slope and becomes smaller towards the base and the lower part of the slope, while the horizontal component is smallest at the top of the upper slope and becomes greater towards the base and the lower slope. This is because the base boundary and the right-hand vertical boundary are impermeable. The infiltrated water accumulates on the base boundary and then forms lateral flow, which develops increasingly with flow towards the lower slope.

4) The maximum velocity of subsurface flow occurs at the seepage face, across which a part of subsurface flow returns to the land surface with a smaller resistance to flow.

5) Once the rainfall stops, the velocity of subsurface flow decreases rapidly from the top of slope towards the base and from the upper part of slope towards the lower part. Relatively to subsurface flow, the velocity of overland flow decreases gently. This is because the return flow accounts for a far greater part of overland flow than the direct precipitation on the saturated land surface.

The distribution of velocity affected by various factors and the above characteristics may not always been seen. For example, in

CASE11, since there is antecedent precipitation, the lateral flow develops very well. Therefore the maximum velocity does not occur at the seepage face, but on the impermeable base boundary(Figure 2.55). Another exception is CASE8. Since the saturated hydraulic conductivity is extremely low, the lateral flow does not develop(Figure 2.56), the infiltrated water raises the water table so that the water table shows a " domelike " shape and water flows locally up the slope(Figure 2.57).

Figure 2.58 shows the maximum velocities of CASE12 and Figure 2.59 the corresponding hydrograph. The peak times for the maximum velocities of the overland and subsurface flows coincide. They lag about 1 hour behind the peak of precipitation and 15 min. behind the peak of hydrograph. From these it can be surmised that the return flow plays a very important part in runoff processes.

Figure 2.60 shows the distribution of velocity in space in the case of heterogeneous soil(CASE26 and CASE28). It can be seen that the lateral flow is restrained within the layer with a lower hydraulic conductivity.

2.4.3 Water Table Level and Seepage Point

2.4.3.1 Water Table of Subsurface Flow

The water table is the zero-pressure surface which separates the saturated zone from the unsaturated zone. In the classical approaches the water table is considered to be a moving material boundary and is usually referred to as a free surface. The rate of advance of the zero pressure surface is strongly affected by antecedent moisture

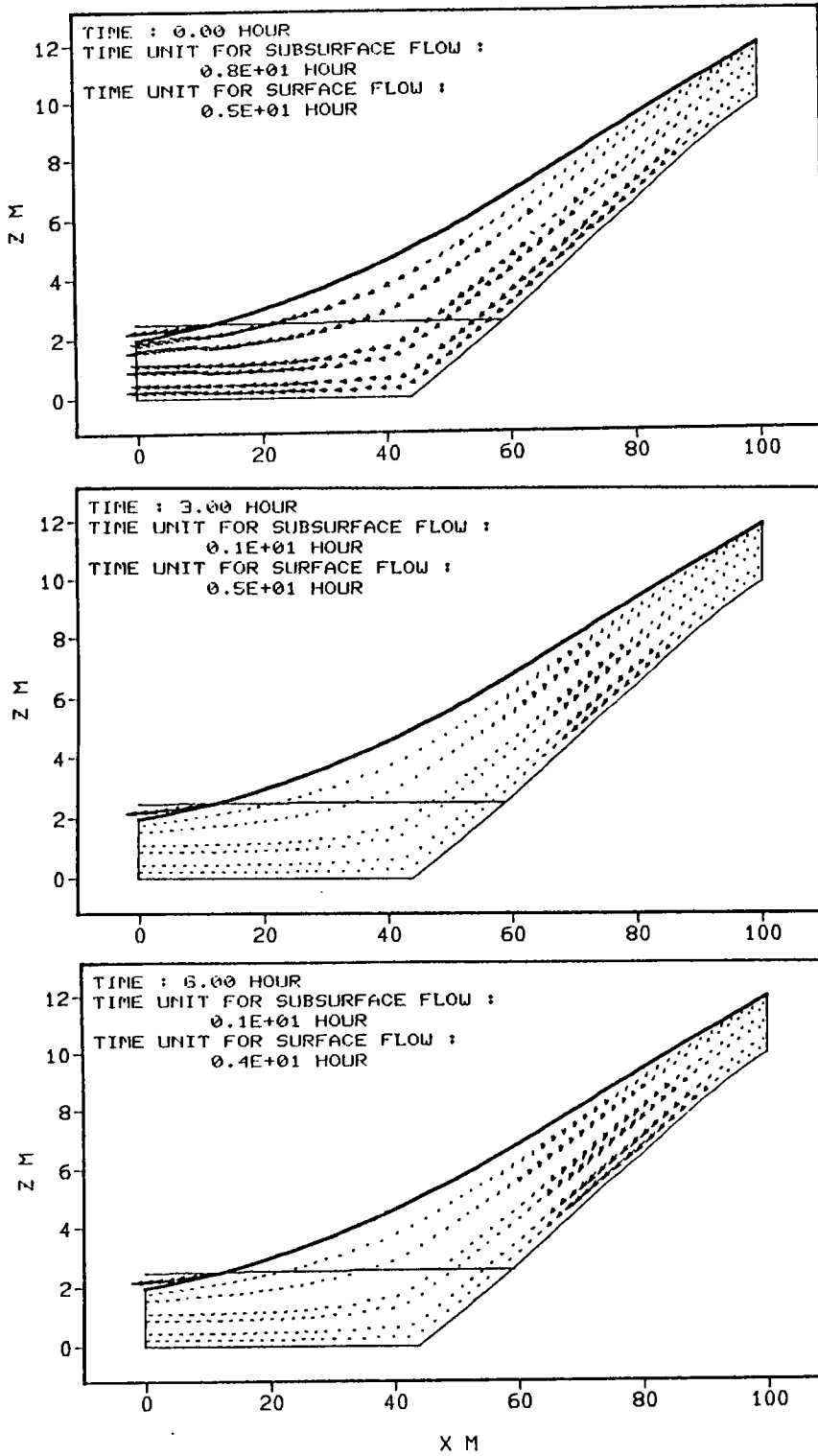


Figure 2.55a The changing velocity distribution with time(CASE11)

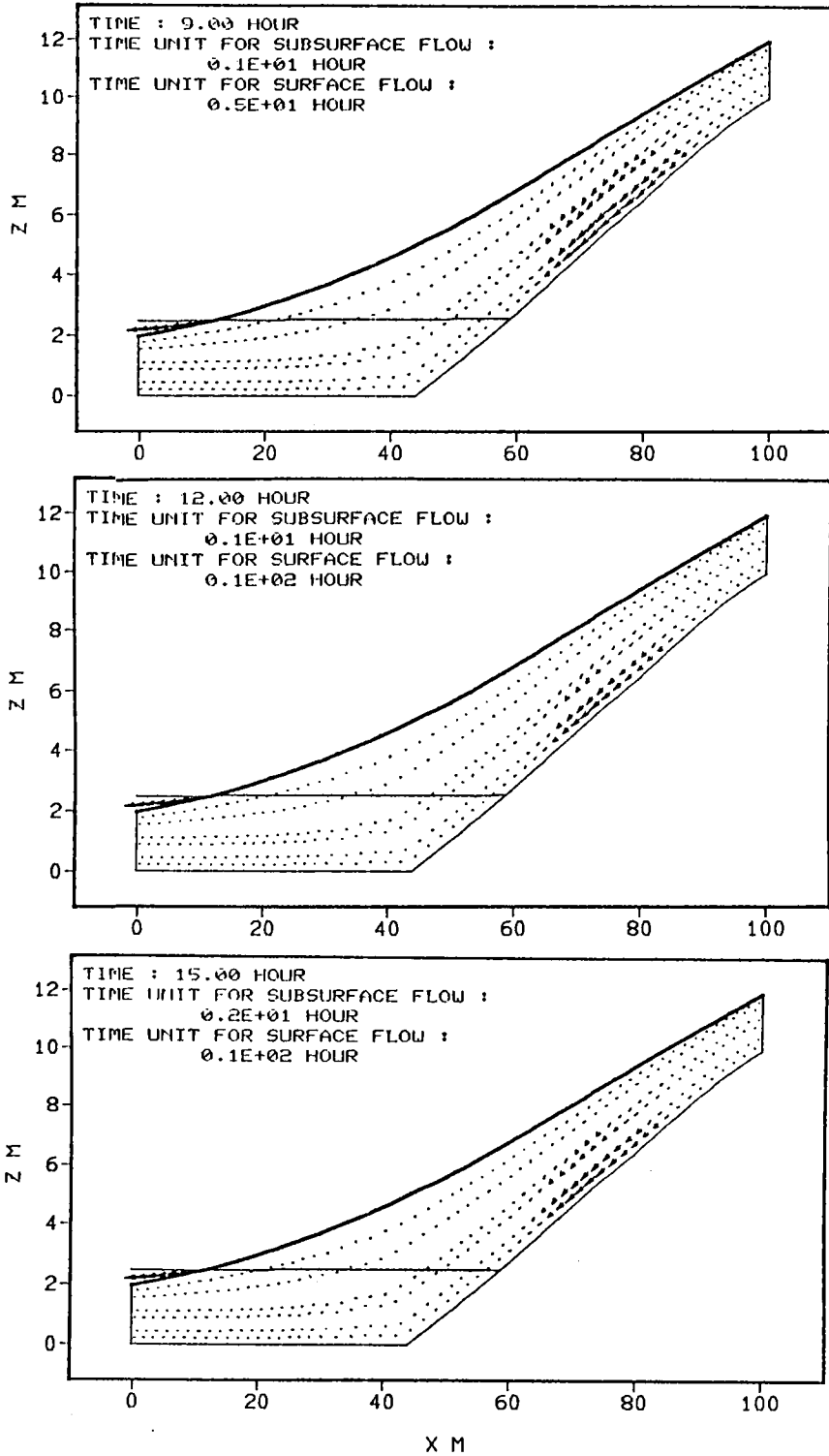
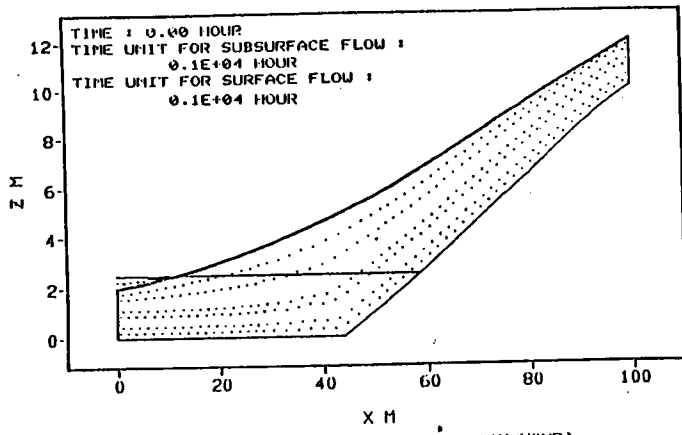
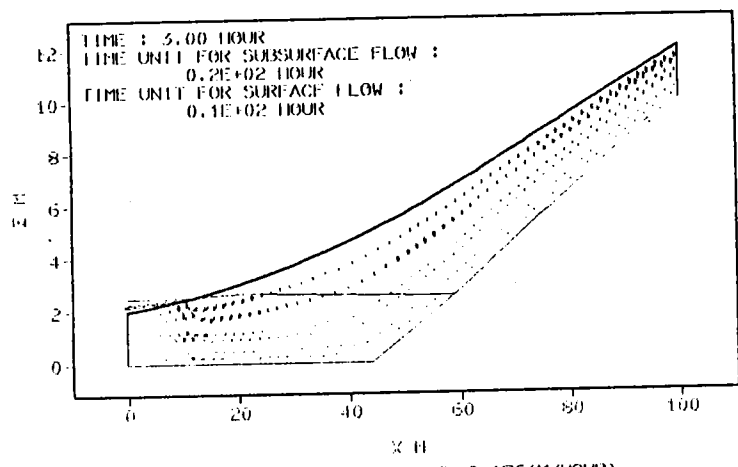


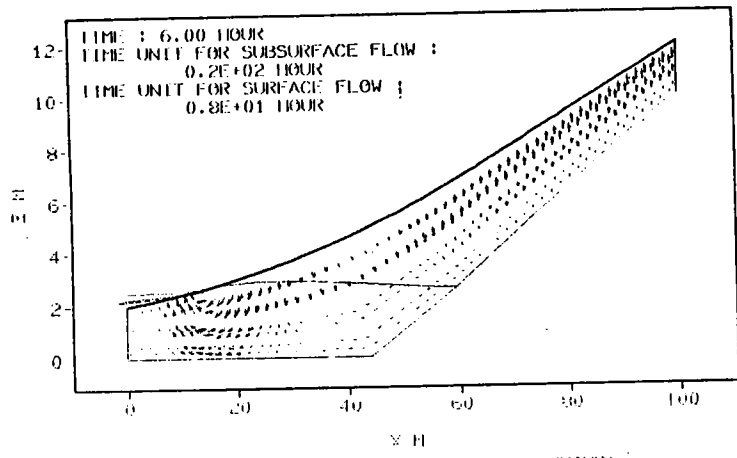
Figure 2.55b The changing velocity distribution with time(CASE11)



THE MAXIMUM SURFACE FLOW VELOCITY:0.000(M/HOUR)
 THE MAXIMUM SUBSURFACE FLOW VELOCITY:0.000(M/HOUR)

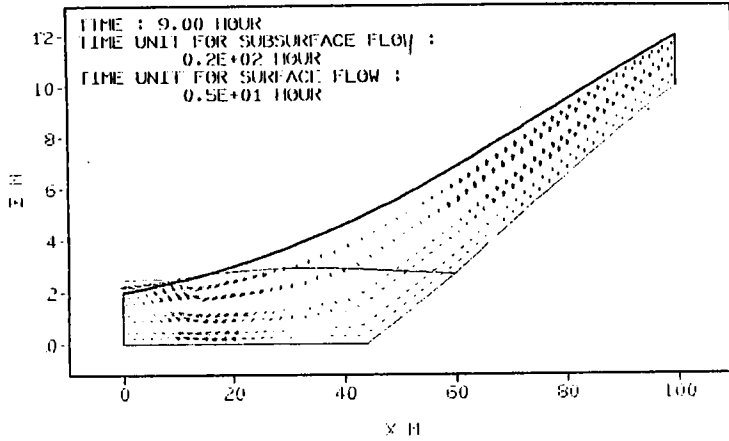


THE MAXIMUM SURFACE FLOW VELOCITY:0.176(M/HOUR)
 THE MAXIMUM SUBSURFACE FLOW VELOCITY:0.055(M/HOUR)

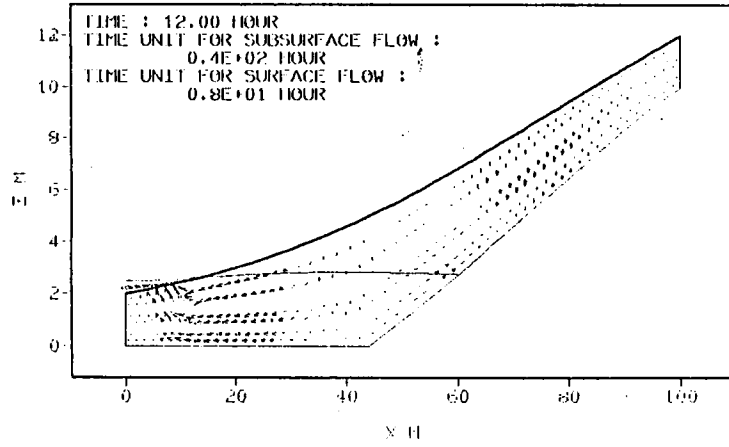


THE MAXIMUM SURFACE FLOW VELOCITY:0.345(M/HOUR)
 THE MAXIMUM SUBSURFACE FLOW VELOCITY:0.091(M/HOUR)

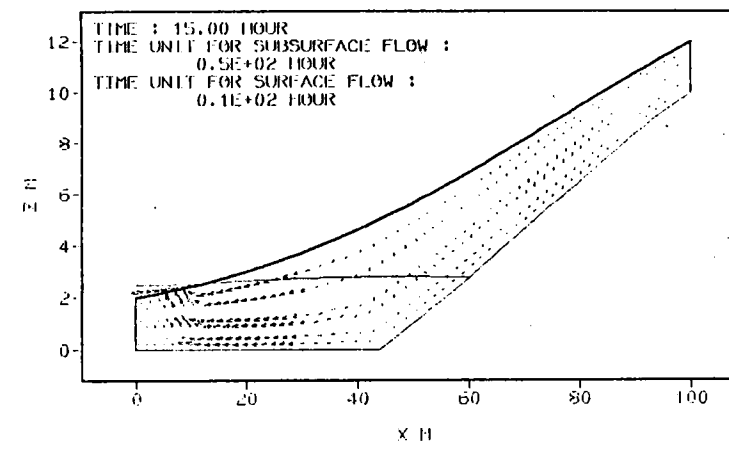
Figure 2.56a The changing velocity distribution with time(CASE8)



THE MAXIMUM SURFACE FLOW VELOCITY:0.407(M/HOUR)
 THE MAXIMUM SUBSURFACE FLOW VELOCITY:0.074(M/HOUR)



THE MAXIMUM SURFACE FLOW VELOCITY:0.558(M/HOUR)
 THE MAXIMUM SUBSURFACE FLOW VELOCITY:0.049(M/HOUR)



THE MAXIMUM SURFACE FLOW VELOCITY:0.274(M/HOUR)
 THE MAXIMUM SUBSURFACE FLOW VELOCITY:0.055(M/HOUR)

Figure 2.56b The changing velocity distribution with time(CASE8)

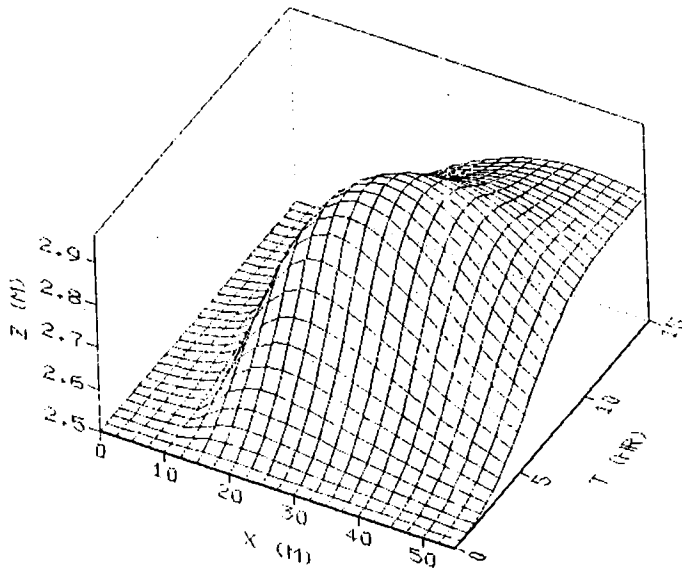


Figure 2.57 The water table changes with time and distance(CASE8).

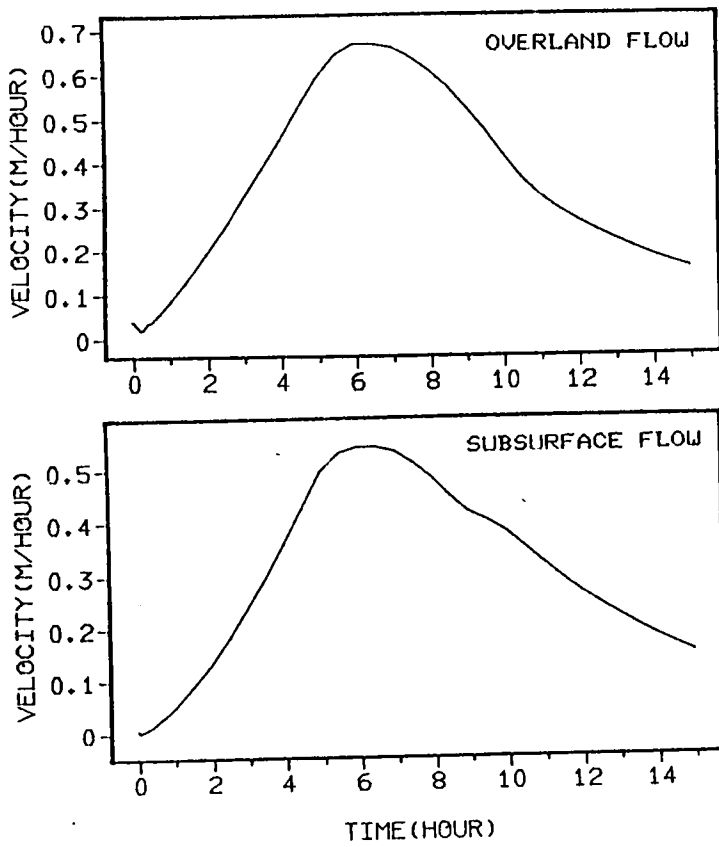


Figure 2.58 The changing maximum velocity(CASE12)

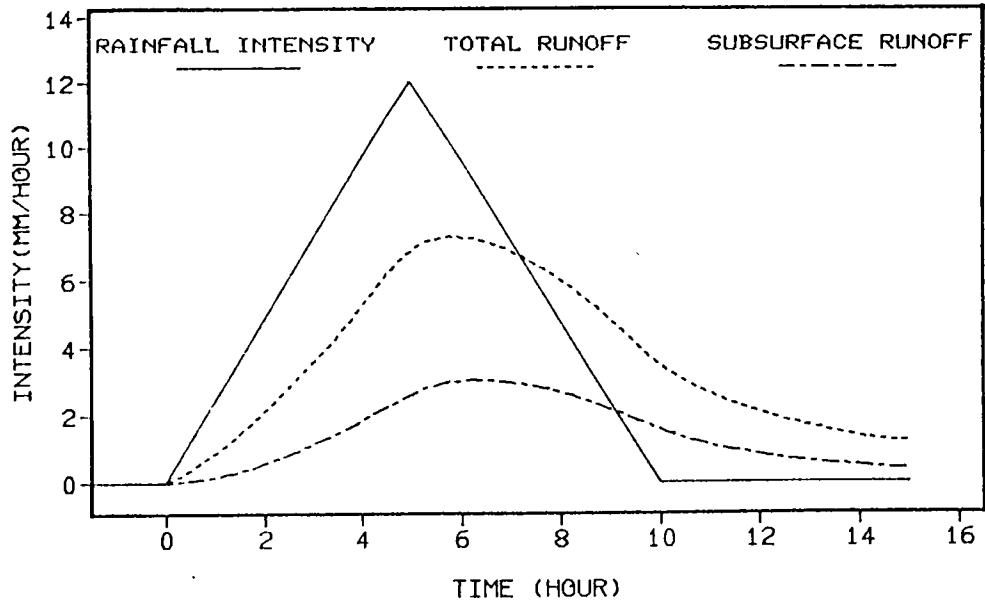
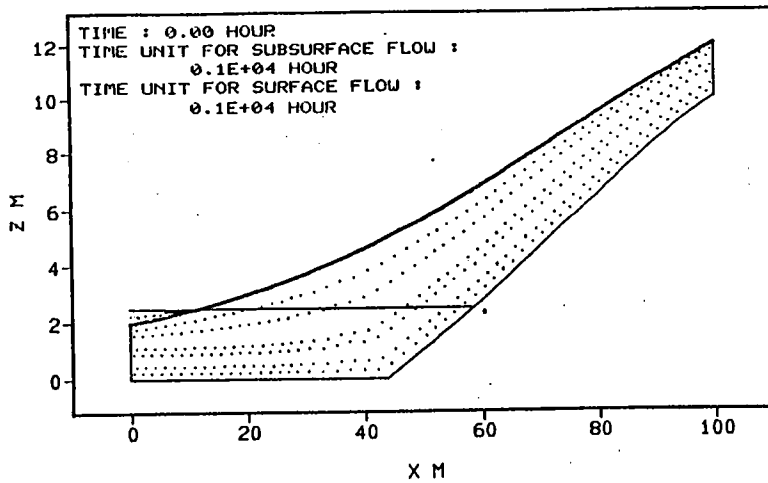
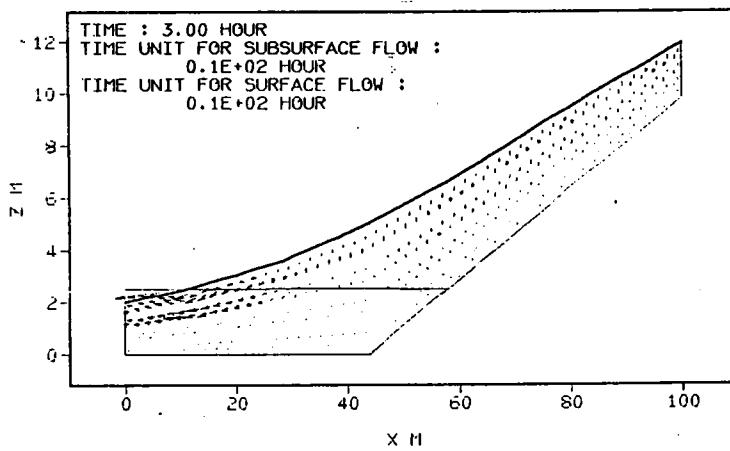


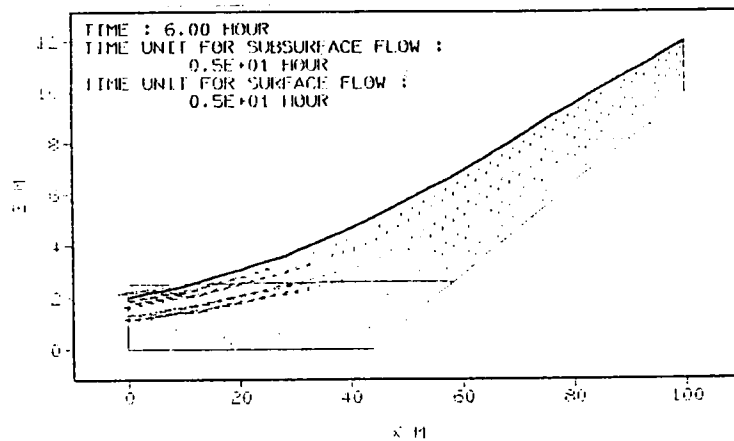
Figure 2.59 Hydrograph(CASE12)



THE MAXIMUM SURFACE FLOW VELOCITY:0.000(M/HOUR)
 THE MAXIMUM SUBSURFACE FLOW VELOCITY:0.000(M/HOUR)



THE MAXIMUM SURFACE FLOW VELOCITY:0.274(M/HOUR)
 THE MAXIMUM SUBSURFACE FLOW VELOCITY:0.224(M/HOUR)



THE MAXIMUM SURFACE FLOW VELOCITY:0.583(M/HOUR)
 THE MAXIMUM SUBSURFACE FLOW VELOCITY:0.490(M/HOUR)

Figure 2.60a The changing velocity distribution with time(CASE26)

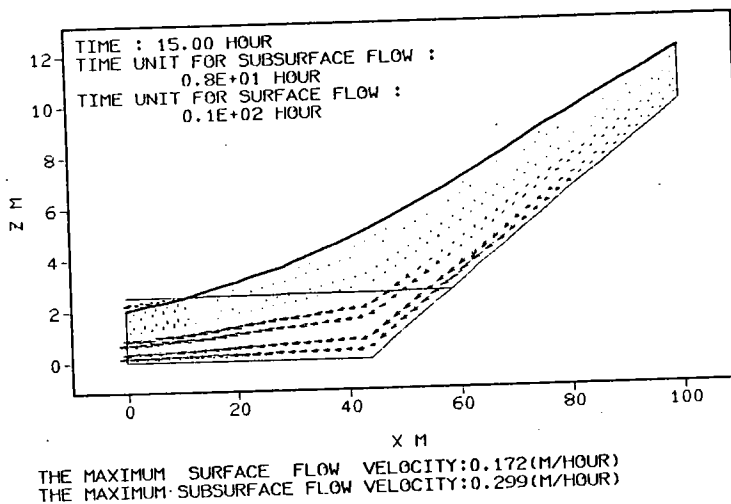
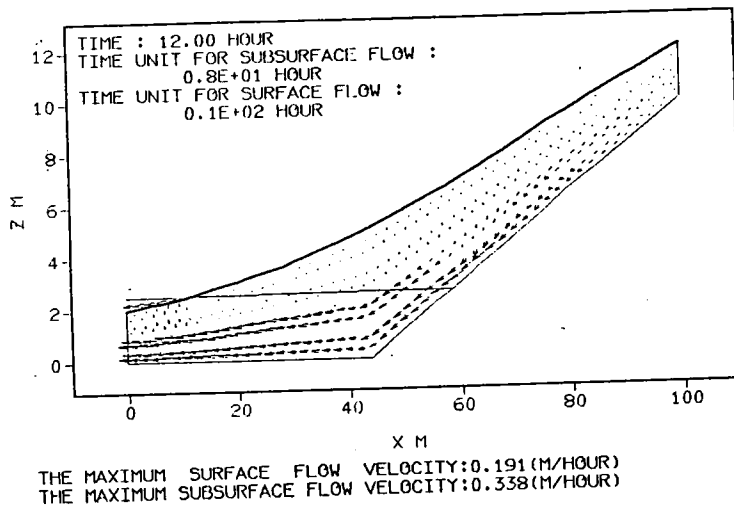
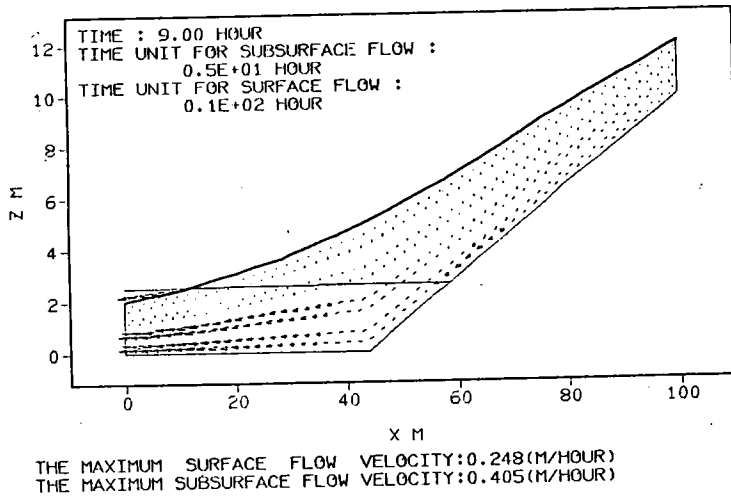
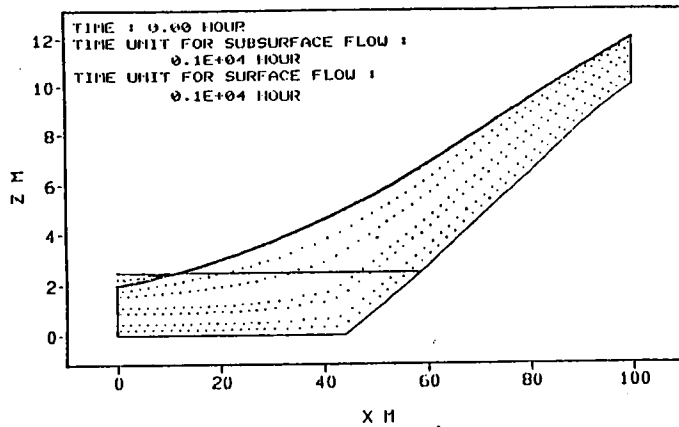
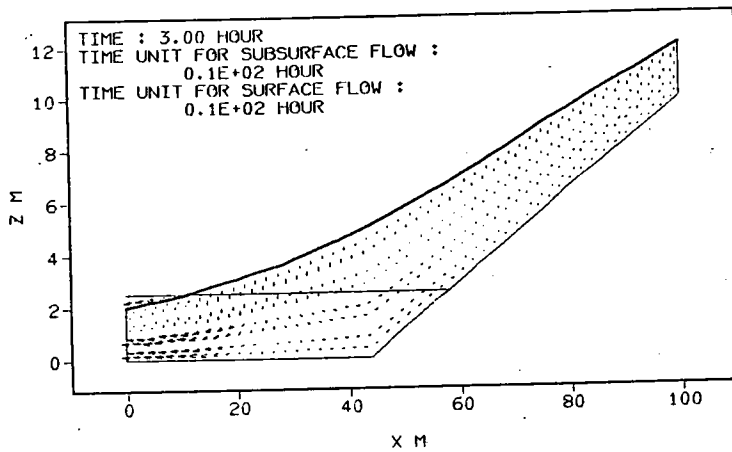


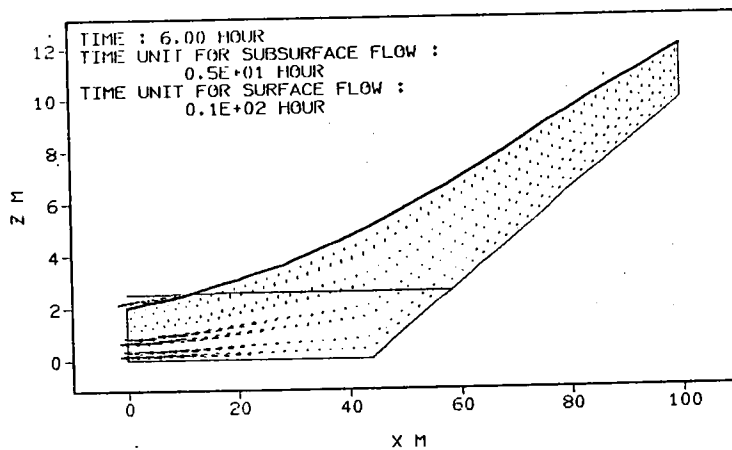
Figure 2.60b The changing velocity distribution with time(CASE28)



THE MAXIMUM SURFACE FLOW VELOCITY:0.000(M/HOUR)
 THE MAXIMUM SUBSURFACE FLOW VELOCITY:0.000(M/HOUR)

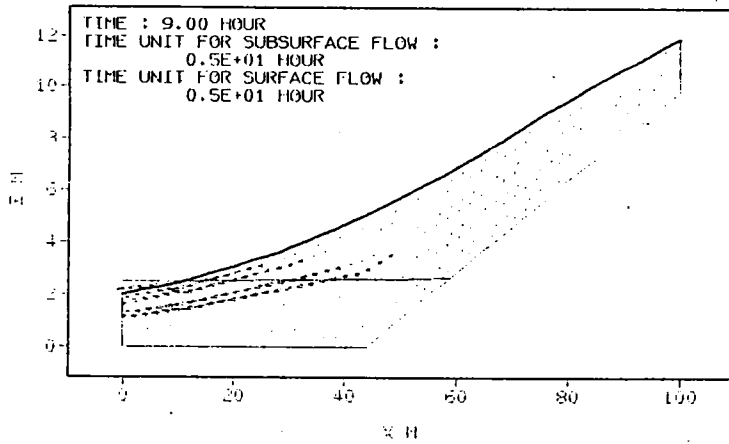


THE MAXIMUM SURFACE FLOW VELOCITY:0.147(M/HOUR)
 THE MAXIMUM SUBSURFACE FLOW VELOCITY:0.155(M/HOUR)

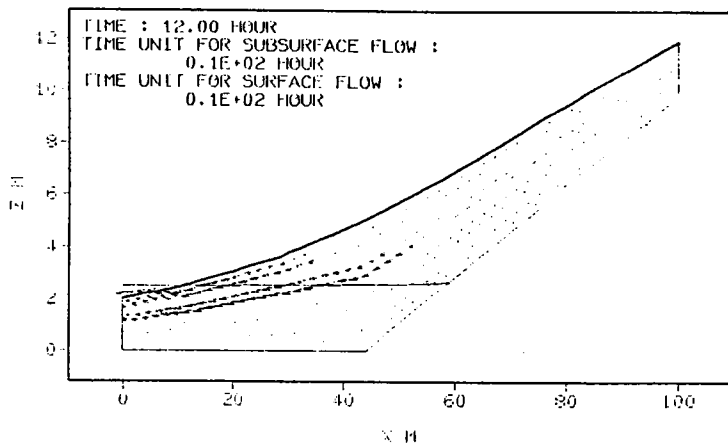


THE MAXIMUM SURFACE FLOW VELOCITY:0.274(M/HOUR)
 THE MAXIMUM SUBSURFACE FLOW VELOCITY:0.408(M/HOUR)

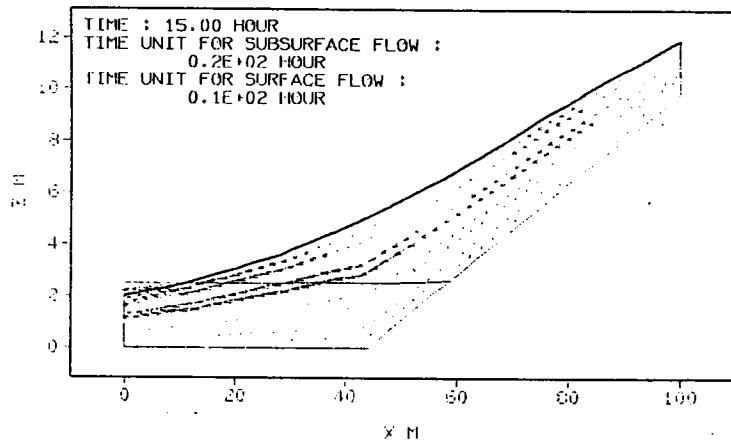
Figure 2.60c The changing velocity distribution with time(CASE28)



THE MAXIMUM SURFACE FLOW VELOCITY:0.471(M/HOUR)
 THE MAXIMUM SUBSURFACE FLOW VELOCITY:0.388(M/HOUR)



THE MAXIMUM SURFACE FLOW VELOCITY:0.267(M/HOUR)
 THE MAXIMUM SUBSURFACE FLOW VELOCITY:0.216(M/HOUR)



THE MAXIMUM SURFACE FLOW VELOCITY:0.188(M/HOUR)
 THE MAXIMUM SUBSURFACE FLOW VELOCITY:0.146(M/HOUR)

Figure 2.60d The changing velocity distribution with time(CASE26)

conditions in the unsaturated zone and therefore this rate cannot always be correctly predicted with the free surface approach.

Figure 2.61 shows the advance of the water table in various flow conditions. The main factors which affect the rate of advance of the water table are as follows:

1) saturated hydraulic conductivity

Comparing CASE3 with CASE4(the saturated hydraulic conductivities are 1 m/hour and 100 m/hour, respectively), we find that the maximum rising of CASE3 in the elevation above the reference datum is 7.1 times as great as one of CASE4 and in the elevation above the downslope water level 15 times. In addition, the water table of CASE3 declines far more gently than that of CASE4. The same tendency exists in CASE5 and CASE6.

Figure 2.62 shows the time at which the water table reaches the maximum elevation. It can be seen that in CASE9 the water table reaches the maximum elevation at the same time at different distances. However, in CASE8, in which the hydraulic conductivity is only 1/50 of that in CASE9, there is a great time-lag at the lower part of slope and at the upper part. This is because the lateral flow is restrained by the lower conductivity. For this reason the water table shows a " domed shape "(Figure 2.61).

In the case of heterogeneous and anisotropic media, the shape of the water table becomes more complex. For example, in CASE26 or CASE28 the water table shows a very " unnatural " shape.

2) moisture characteristic curve

The water table in CASE9 and CASE10 have similar shapes, although the moisture characteristic curves differ. On the other hand, by comparing CASE9 with CASE13, it can be seen that the lower the porosity of the soil is, the greater is the rise of the water table.

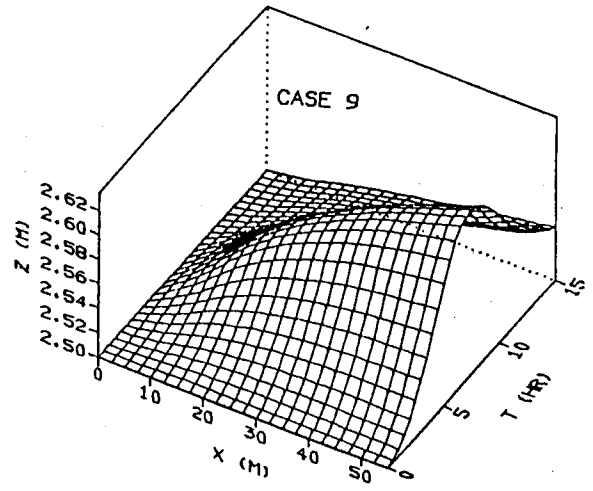
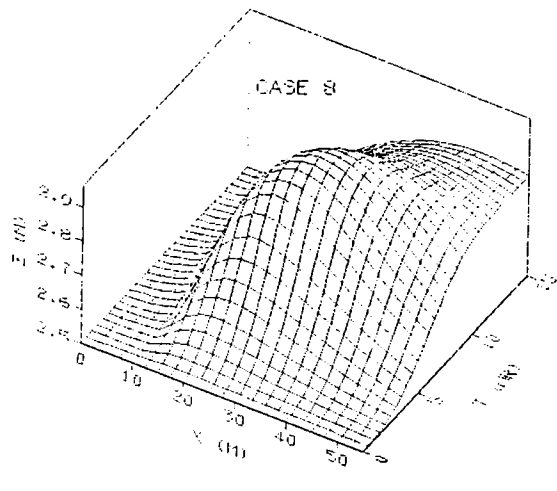
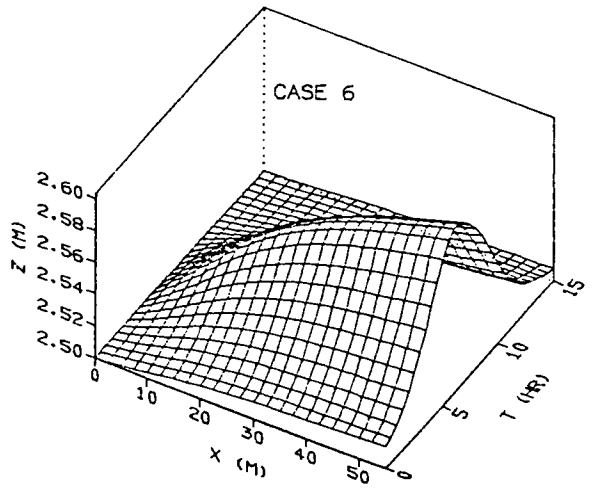
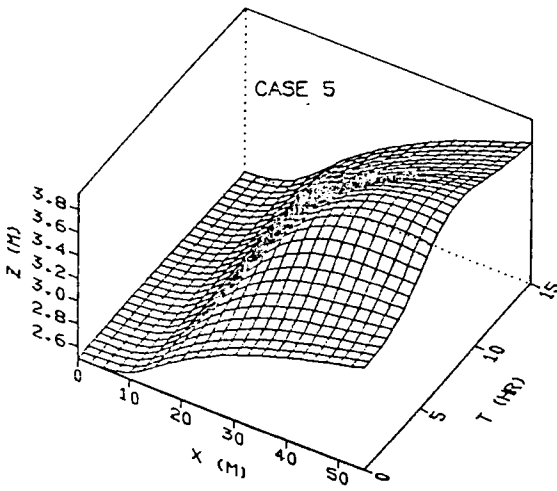
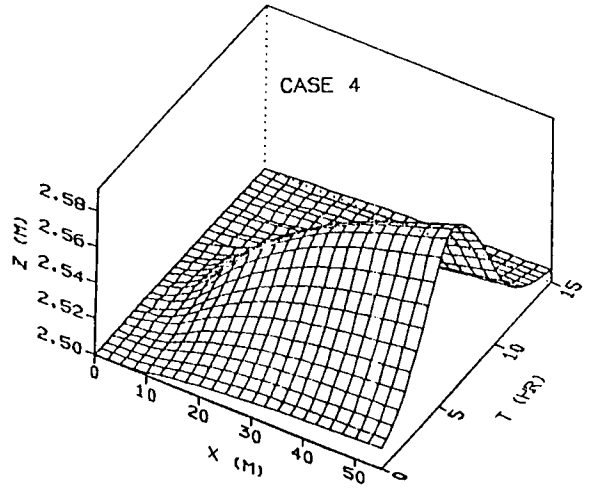
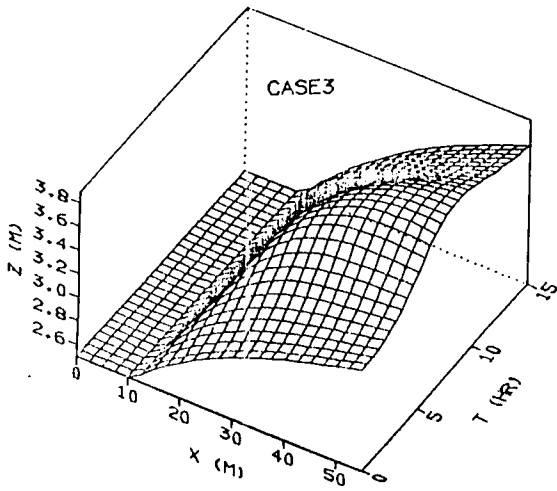


Figure 2.61a The water table changes with time and distance

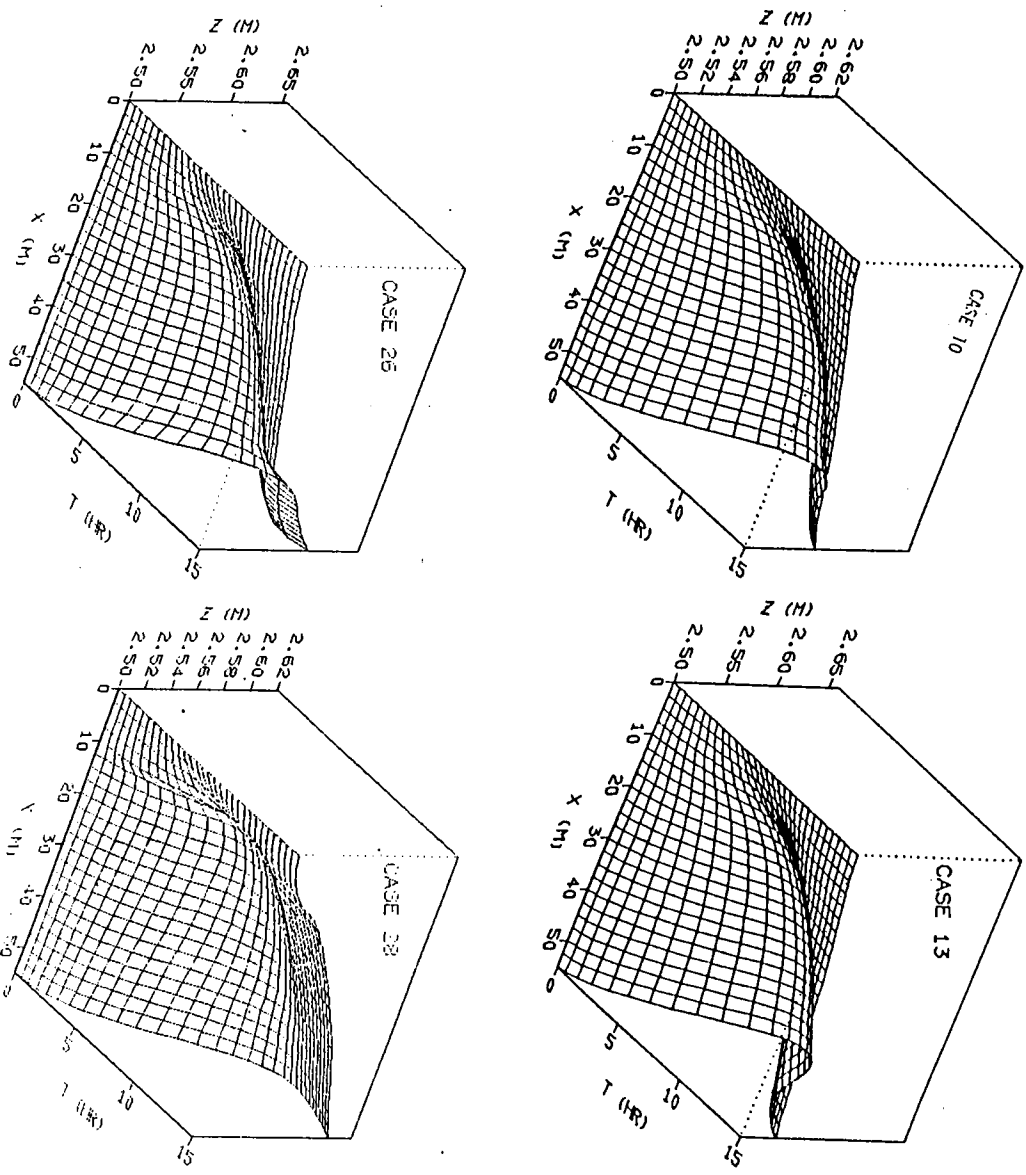


Figure 2.61b The water table changes with time and distance

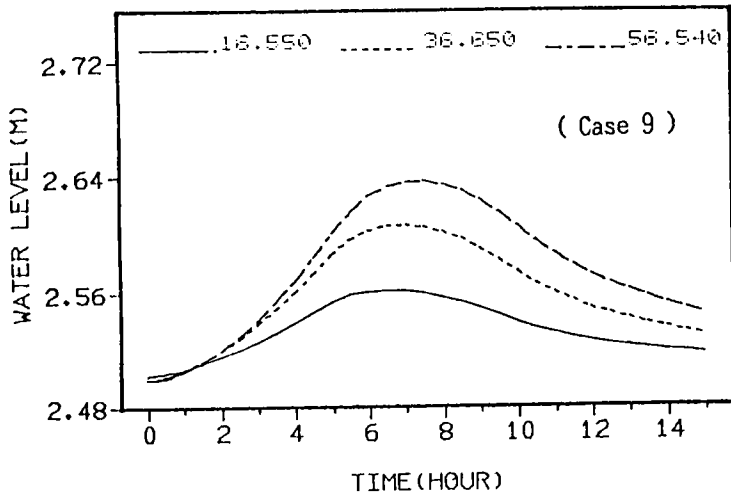
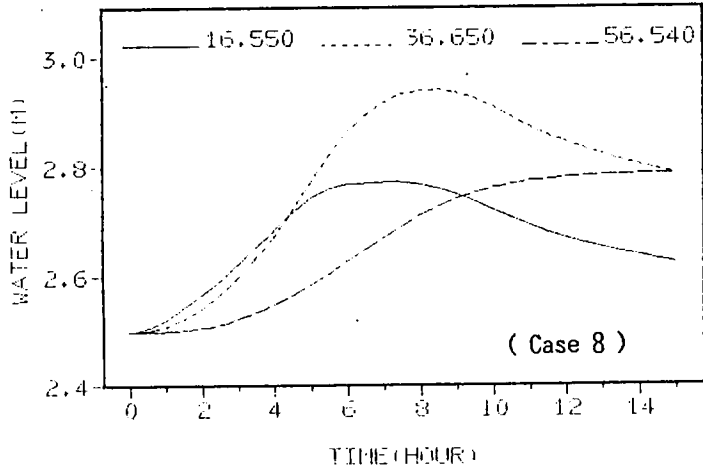


Figure 2.62 The water table changes with time and distance

2.4.3.2 Free Water Surface of Overland Flow

One of the most important parameters which determine the shape of the free water surface of overland flow is roughness. Figure 2.63 shows the different shapes for steady flow. When roughness is large, the free water surface rises along the land surface. As roughness becomes less, the water surface approaches the horizontal level. This is because the less the roughness is, the quicker is the overland flow.

The hydraulic conductivity affects the shape of the free water surface by changing the amount of return flow. In general, the greater the conductivity is, the greater is the rise of the free water surface(Figure 2.64 and Figure 2.65).

2.4.3.3 Seepage Point

The seepage point is the intersection point of the land surface with the free water surface of overland flow(and hence water table of subsurface flow). The elevation of the seepage point is a measure of the degree of development of overland flow.

Figure 2.66 and Figure 2.67 show the relationship between the rising elevation of the seepage point and hydraulic conductivity as well as roughness for steady and transient flows, respectively. The characteristics can be simply summarized as follows.

- 1) The lower the hydraulic conductivity is, the quicker is the rising rate of the seepage point.

- 2) The larger the roughness is, the slower is the declining rate of the seepage point.

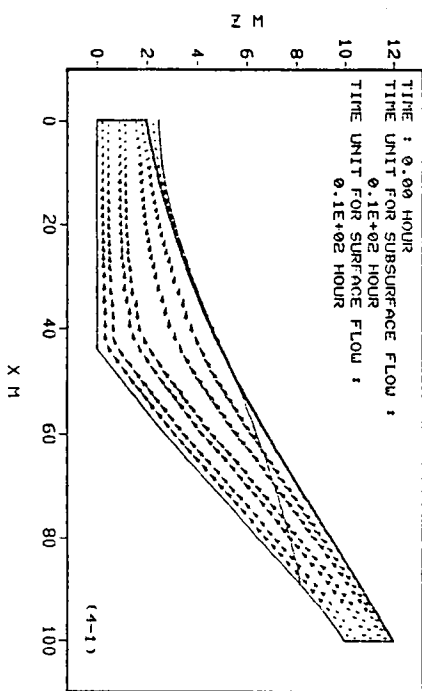
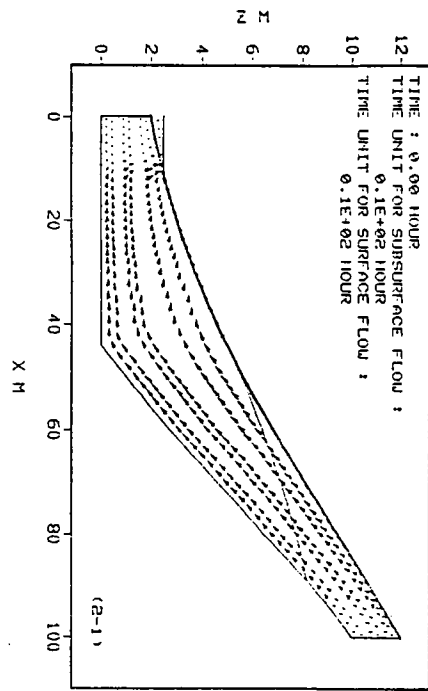
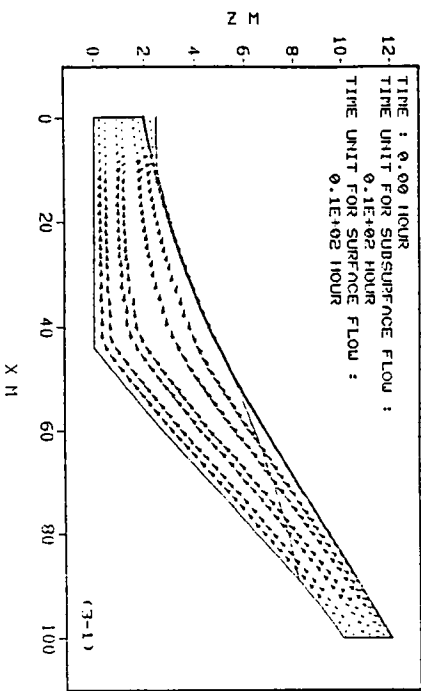
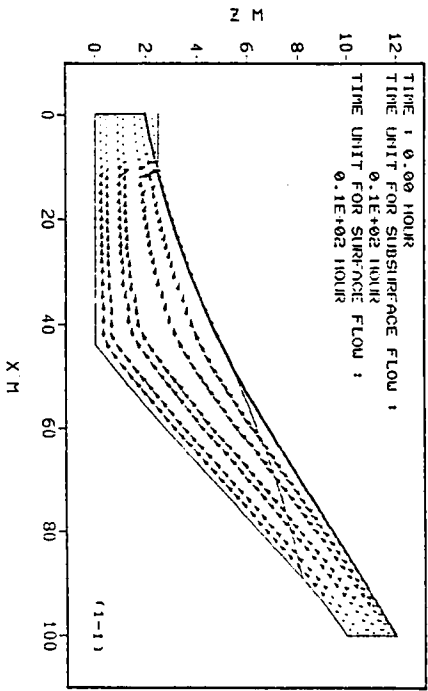


Figure 2.63a The velocity distribution of steady flow

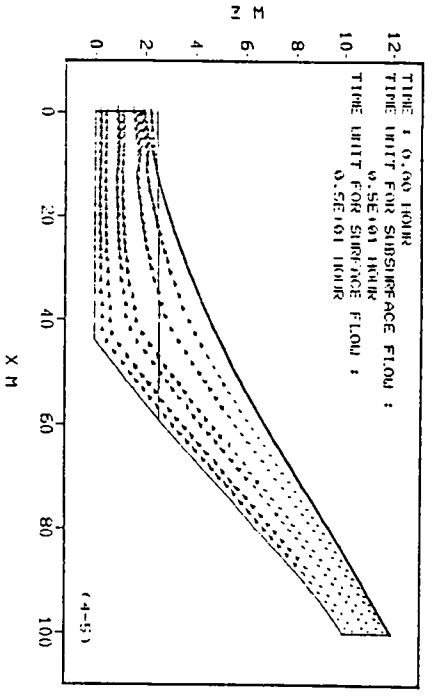
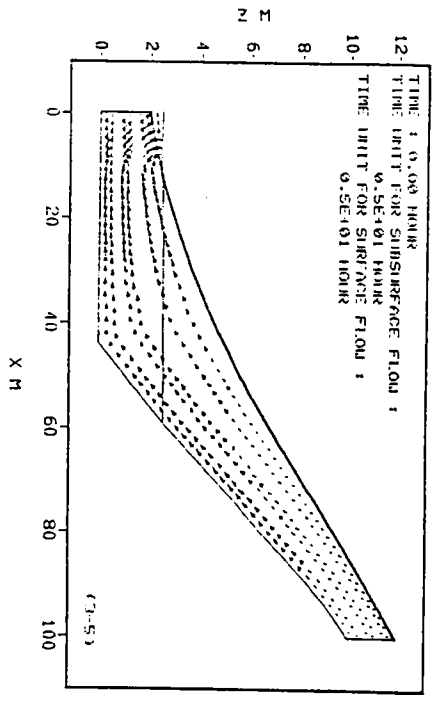
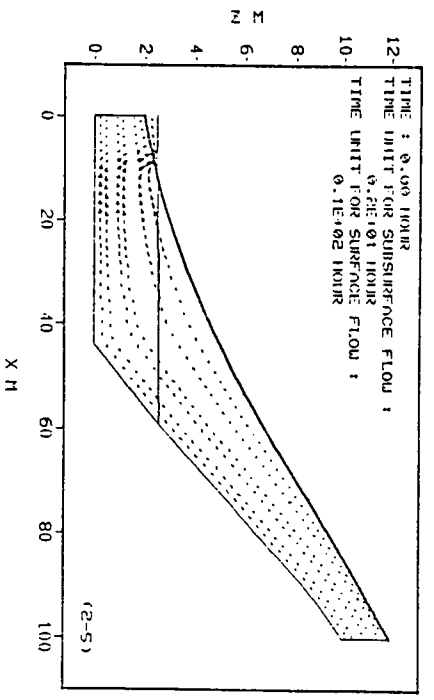
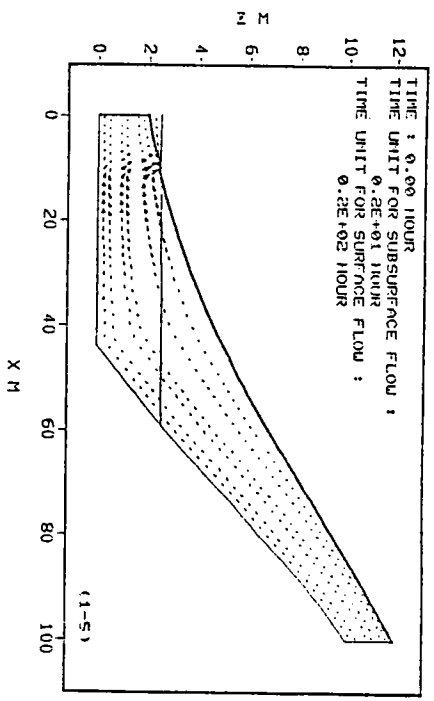


Figure 2.63b The velocity distribution of steady flow

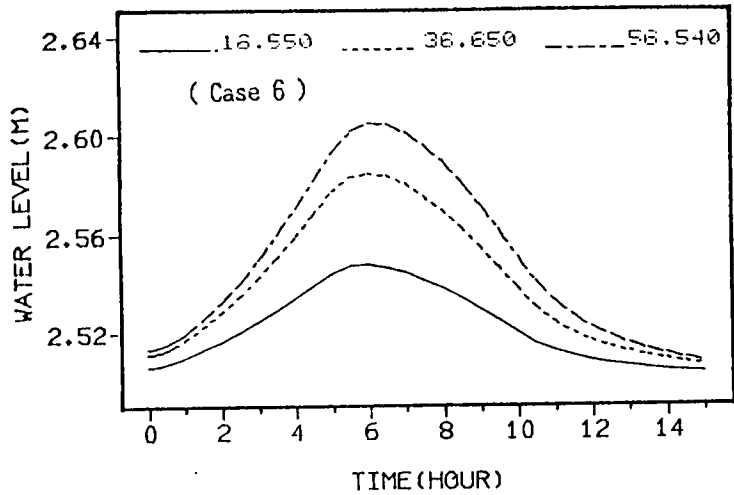
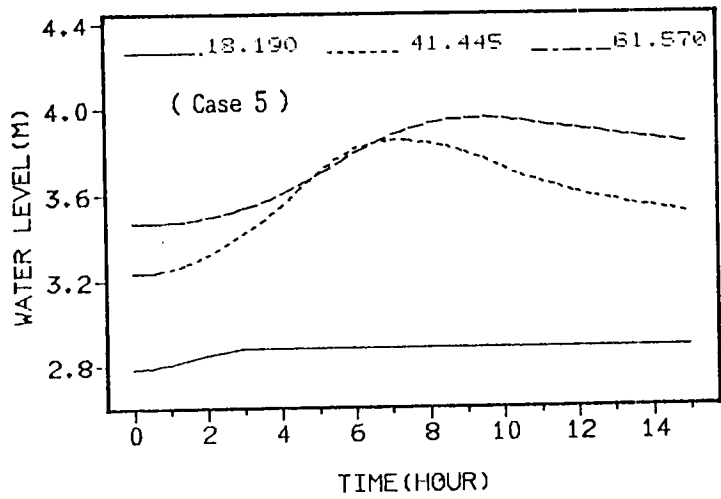


Figure 2.64 The water table changes with time and distance

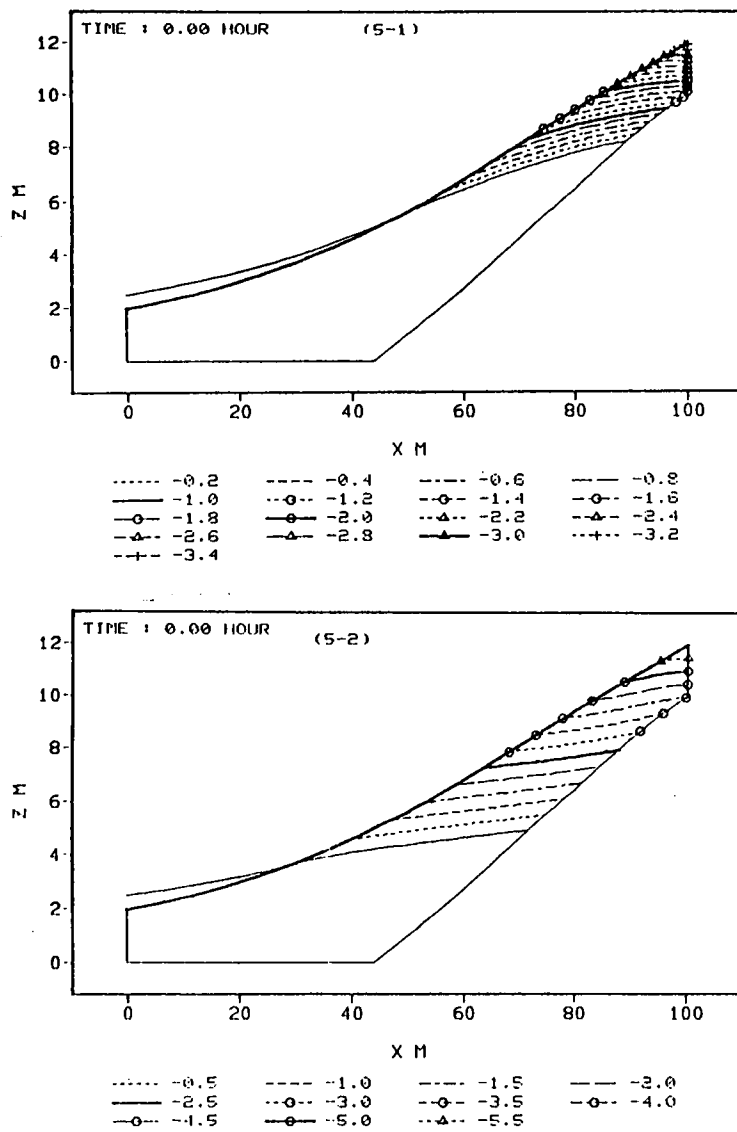


Figure 2.65a The isoplethic curve of pressure head of steady flow

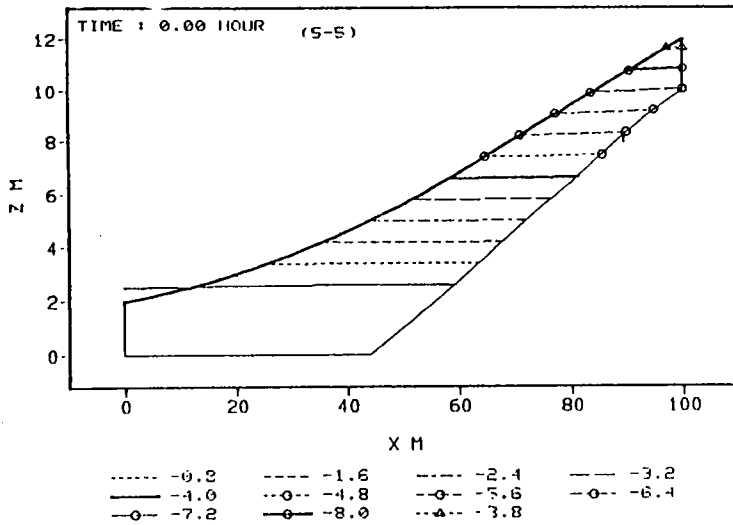
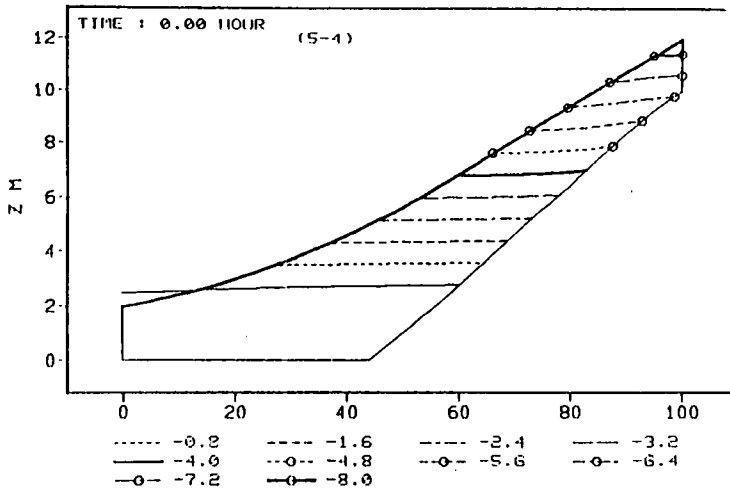
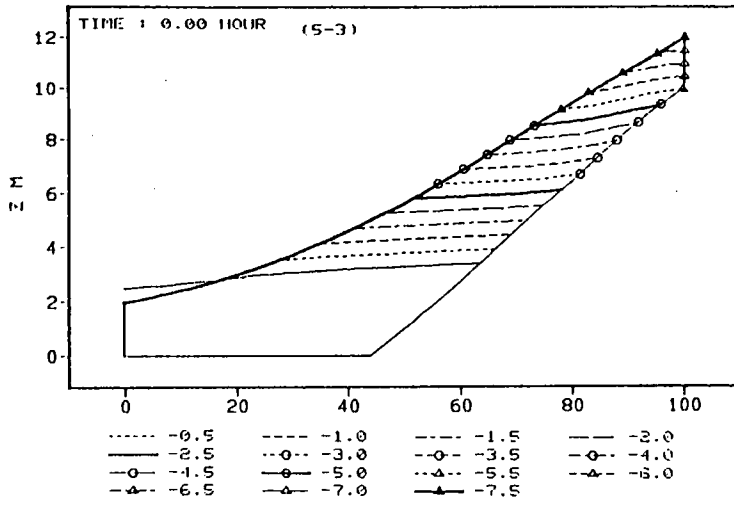


Figure 2.65b The isoplethic curve of pressure head of steady flow

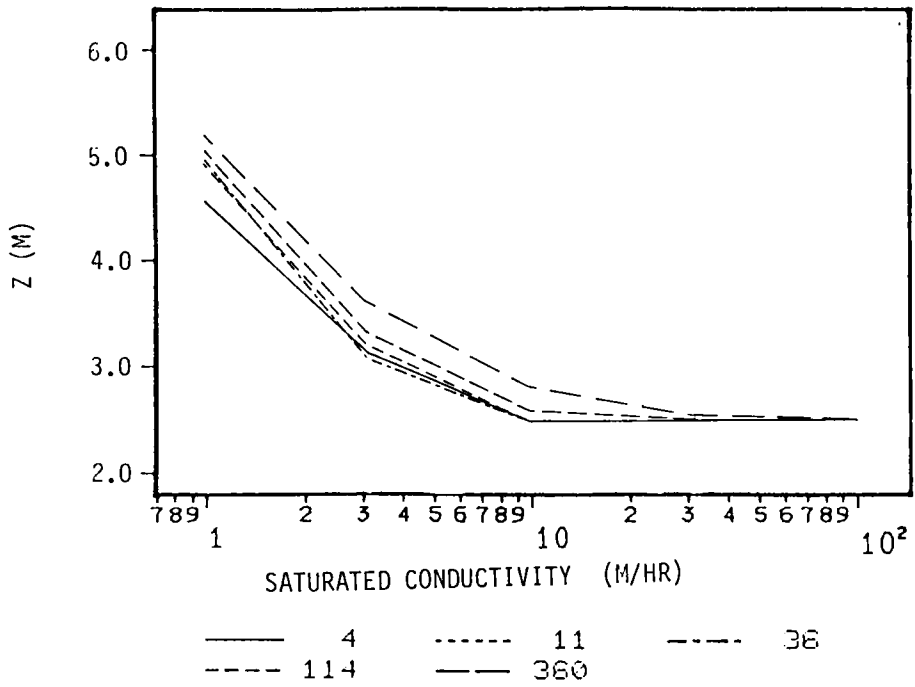


Figure 2.66 The relation between seepage point elevation and saturated conductivity as well as roughness in the case of steady flow

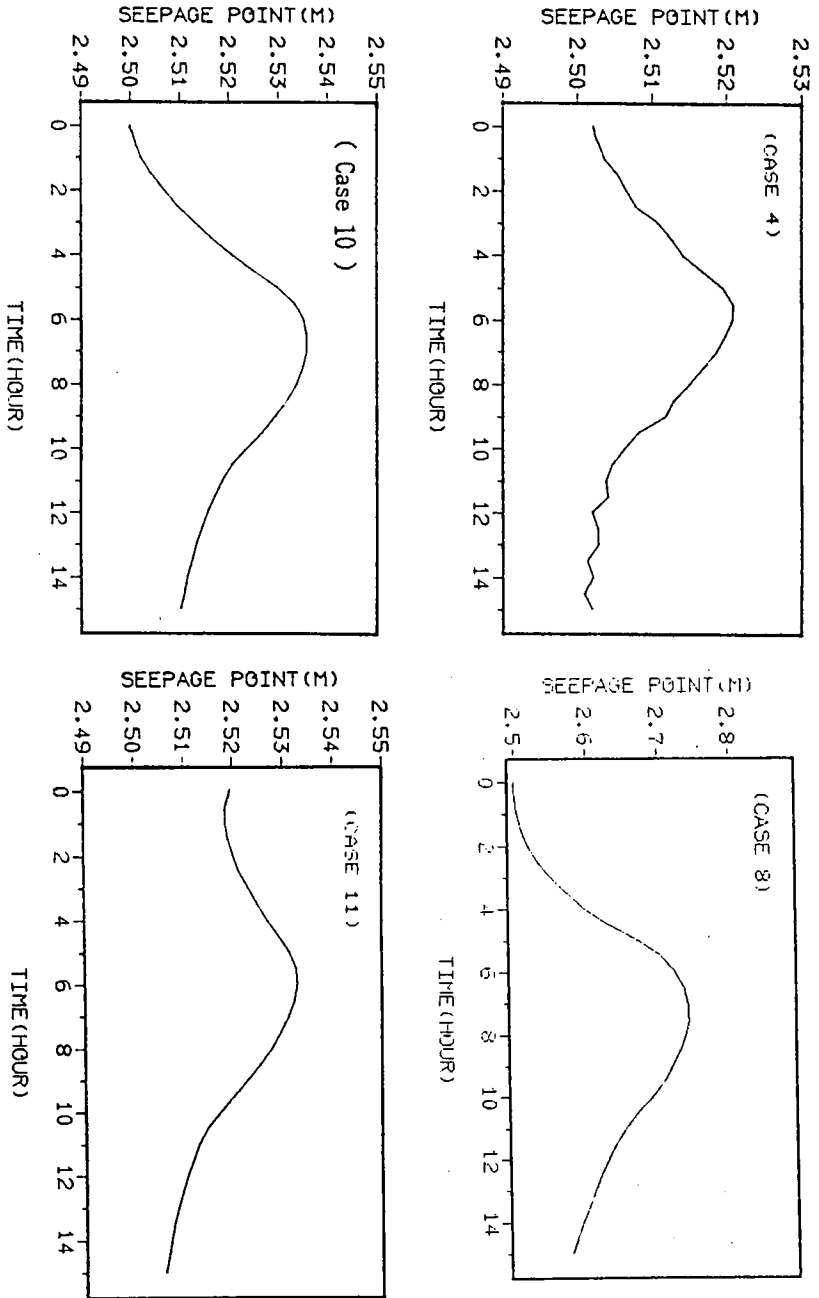


Figure 2.67 The moving seepage point

3) The time when the seepage point reaches its maximum elevation is later than the peak time of the hydrograph. This may be because of the time-lag between the peaks of the hydrograph and the return flow.

2.4.4 Interaction of Overland Flow with Subsurface Flow

It has been recognized that overland flow and subsurface flow interact with one another in hillslope hydrologic processes. However, in most runoff models the interaction has been completely neglected or only conceptually taken into consideration. The classical approaches for simulating the interaction may be classified into two kinds: 1) infiltration is represented by means of some simple expressions(e.g., Horton's infiltration-capacity equation) and then the analyses of overland flow and subsurface flow are separately carried out; 2) one of the governing equations of overland flow and subsurface flow is solved to give the infiltration rate which then is used for the input data to the remained equation(Smith and Woolhiser, 1971a, 1971b). In these approaches, the hydraulic relationship between overland flow and subsurface flow(the balance of momentum) cannot be reflected in runoff models. In addition, as one can see in the preceding sections, the return flow plays a very great part in hillslope hydrologic processes. However, in the classical approaches the interaction is limited to infiltration, and return flow cannot be satisfactorily accounted for.

Figure 2.68 shows the ratios of return flow to overland and total discharges. It is apparent that the curves can be classified into two types according to whether or not there is antecedent precipitation. In the case with an antecedent precipitation(CASE3 - CASE6), the

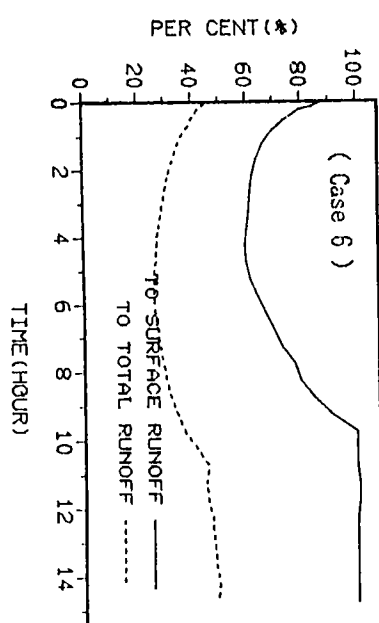
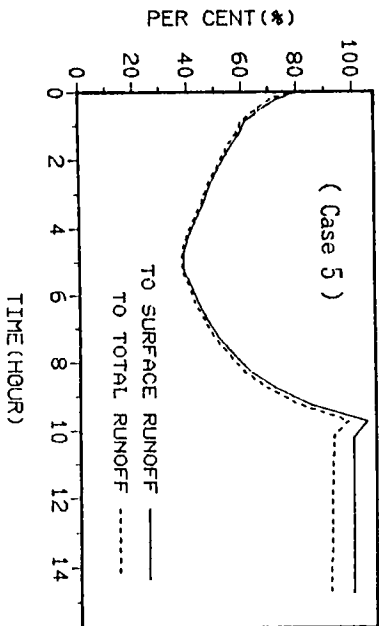
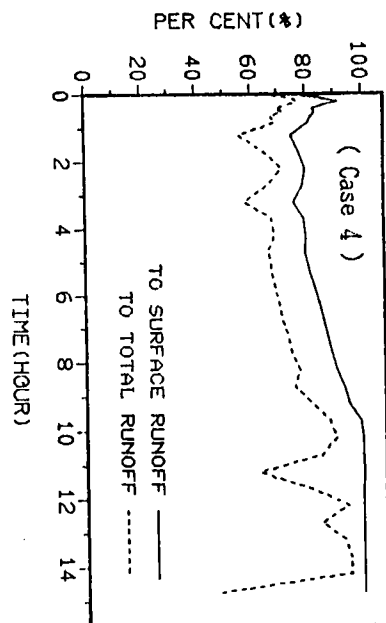
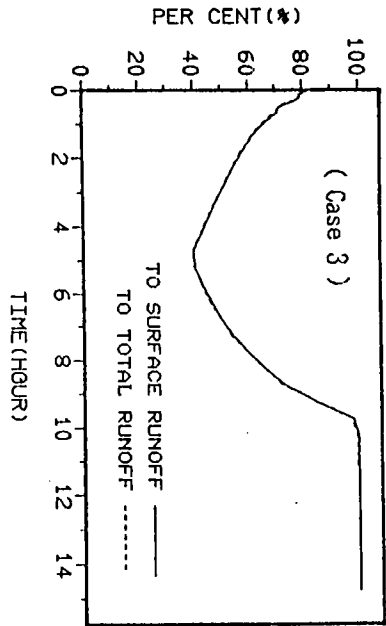


Figure 2.68 The return flow in comparison to surface and total runoff discharges

curve assumes a downward convex semi-circular shape; and the lowest point occurs around the peak of rainfall. In the case without any antecedent precipitation, the curve is stair-shaped.

Figure 2.69 shows the distribution of the intensity of return flow along the saturated land surface for steady state flow. When the roughness is very small, the return flow accumulates at the seepage point and at the intersection point of the horizontal level with the land surface. As the roughness becomes larger, the accumulation at the intersection point of the horizontal level with the land surface vanishes and the distribution becomes uniform along the seepage face.

Figure 2.70 shows the distribution of the intensity of return flow for transient flow. It agrees with the results of steady state flow. However, CASE5 and CASE8 present an interesting feature of the interaction of overland flow with subsurface flow: the infiltration occurs nearby the seepage point immediately after the rainfall stops. This may be because the roughness in CASE8 or CASE5 is very large and the overland flow drains slower than the subsurface flow.

2.4.5 Hillslope Runoff Processes

In the preceding sections, we have examined hillslope runoff processes from various angles. In this section we shall try to summarize all of the results.

Ishihara and Takasao(1962) described the texture of the near-surface soil of hillslopes as follows:

•••Though the characteristics of structure of surface soil layer differs in each basin they may be classified into two regions,

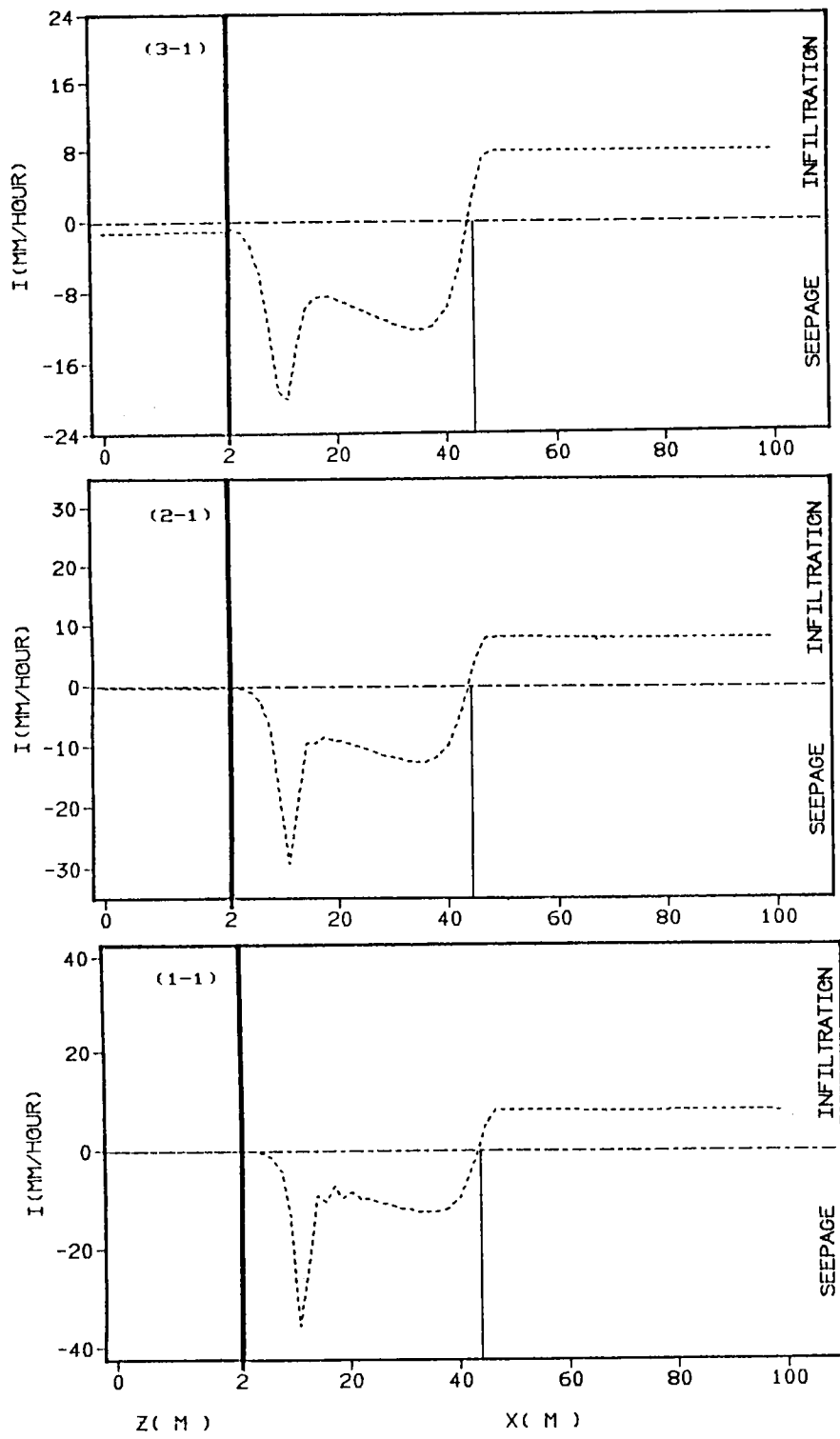


Figure 2.69a Infiltration intensity and seepage point in the case of steady flow

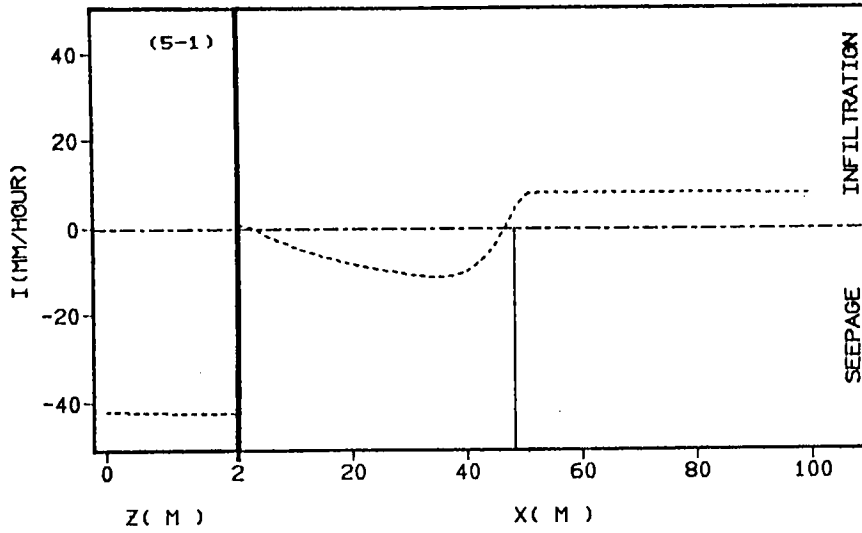
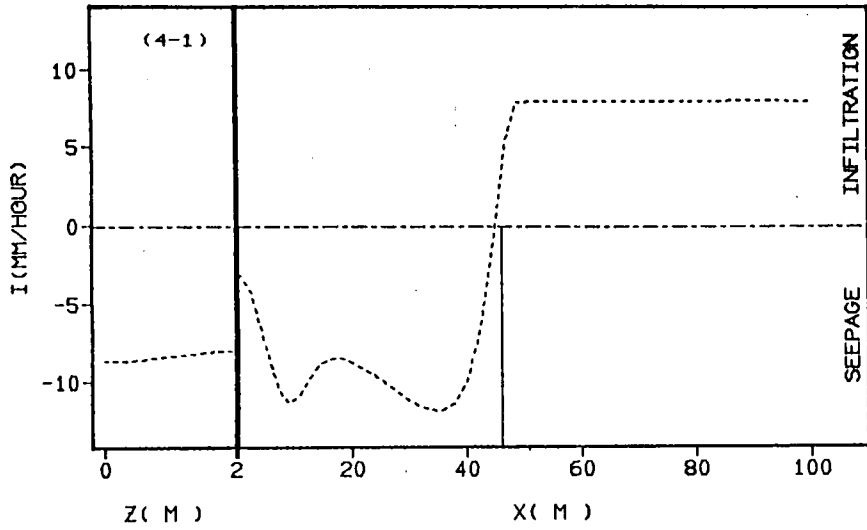


Figure 2.69b Infiltration intensity and seepage point in the case of steady flow

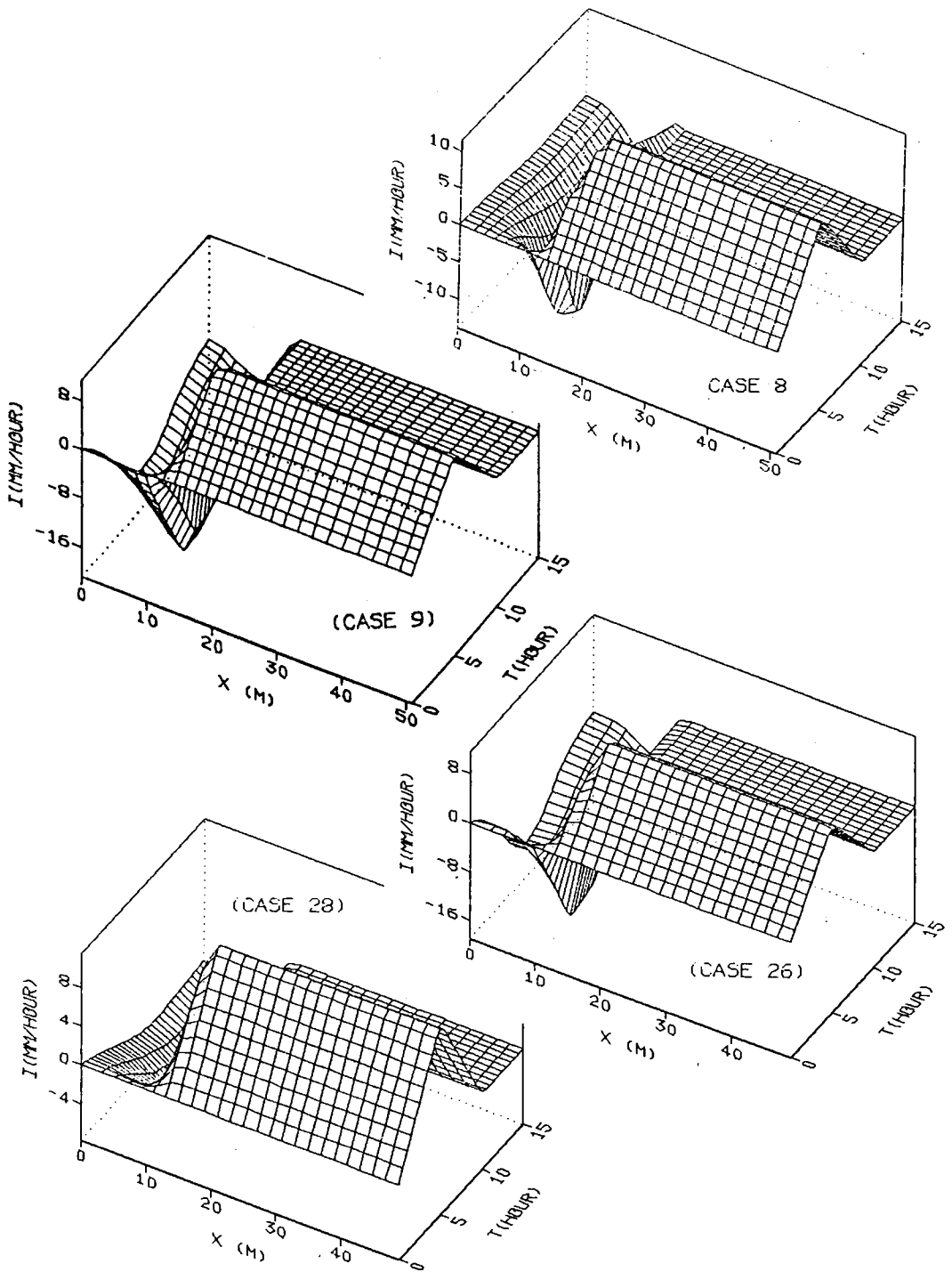


Figure 2.70a Infiltration or return flow intensity along land surface

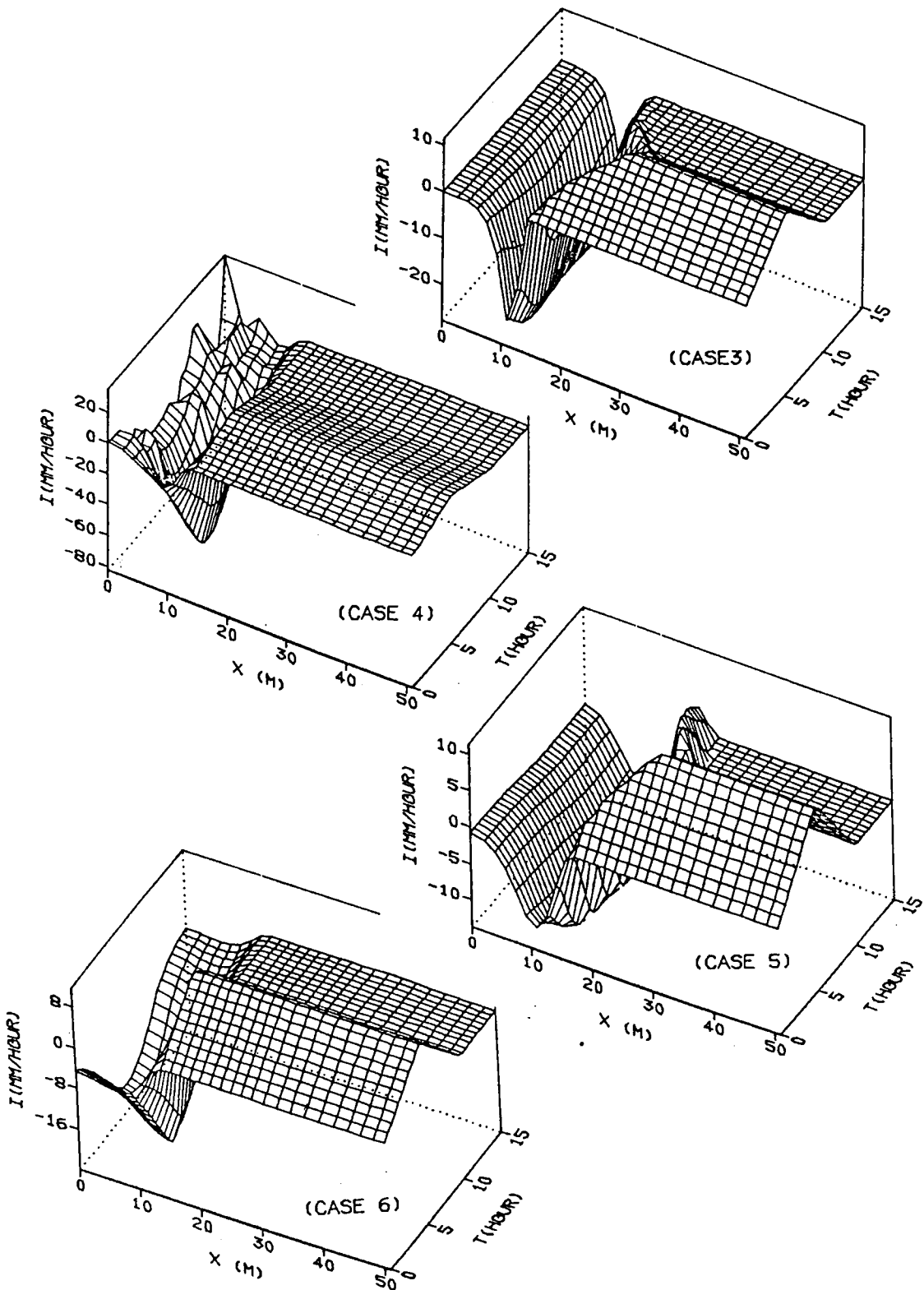


Figure 2.70b Infiltration or return flow intensity along land surface

vegetable covered and barren, for practical hydrologic problems. The former is normally characterized by the surface soil layer which is several tens centimeters in depth and consists of organic matters. Water in such a layer has a tendency to flow laterally as gravity water, for the porosity of soils in the layer is high....

Ishihara and Takasao termed this layer the A-layer. On the hillslopes where the A-layer exists, the infiltration capacity is generally high because of the open soil structure. Under these conditions, rainfall intensities generally do not exceed infiltration capacities and Horton overland flow does not occur. At the beginning of rainfall, water infiltrates into soil. Since the antecedent moisture content is very low near land surface, the unsaturated hydraulic conductivity is low. Infiltrated water therefore cannot flow quickly towards the base of slope. It may become part of the soil's field moisture, or may respond to gravity and flow downward. As the rainfall continues, infiltrated water begins to accumulate on the impermeable base boundary and then flows down the slope responding to gravity. This flow is termed lateral flow(sometimes interflow or throughflow). Lateral flow is recharged by continuous rainfall and develops increasingly. Water travelling as lateral flow raises the water table(and hence the seepage point). Since the land surface has a smaller resistance to flow than do porous media, a part of the lateral flow may return to the land surface and is known as return flow. The remaining water stays in the soil until it discharges as subsurface runoff into a stream channel. Return flow and direct precipitation upon the saturated land surface become overland flow and discharge as overland runoff into a stream channel. After the rain stops, the upper part of

slope rapidly de-saturates and asymptotically approaches its equilibrium value. The lower part soon develops a remarkably stable moisture content value approximating saturation. It is supported by the lateral flow from the upper slope over a long time. Finally the slope will drain towards the moisture profile determined by the moisture characteristic curve of soil.

The distribution of total runoff among overland runoff and subsurface runoff is determined by hydraulic conductivity, roughness, the moisture characteristic curve and antecedent moisture content.

2.5 Summary and Conclusions

In this chapter, we presented a synthesized runoff model of overland flow and subsurface flow for analyzing comprehensively hillslope hydrologic processes. The mathematical model consists of saturated-unsaturated subsurface flow and sheetflow equations. The equation of saturated-unsaturated subsurface flow is developed on the basis of the equation of continuity for transient flow through a porous medium and is put into the pressure head based form with the aid of Darcy's law. Overland flow is assumed to be one-dimensional sheetflow. The governing equation is derived from the equation of continuity and Navier-Stokes equations, and is simplified by using the kinematic approximation and the Manning equation. Since the equation of overland flow is strongly non-linear, and sometimes the solution may diverge, its quasi-linearized form is used. In the synthesized runoff model, not only the conservation of mass but also the balance of momentum are reflected. This implies that the interaction of overland flow with subsurface flow is complete from a hydraulic point of view.

The mathematical model has been solved by the Galerkin Finite Element Method. Because the overland flow and subsurface flow have been treated as a simultaneous system, not only pressure head but also intensity of return flow are determined as independent variables. Sequentially, hydrograph, moisture profile, saturation, water table level, elevation of seepage point, depth of overland flow and velocity distribution are calculated using pressure head.

We call the model developed here Synthesized Surface and Subsurface Runoff model(SSSR model).

From the simulation results, we come to the following conclusions:

1) The synthesized runoff model is very powerful for analyzing hillslope runoff processes and the interaction of overland flow with subsurface flow. It is also effective for forecasting runoff by using the predicted precipitation as input data.

2) Among all of the parameters, saturated hydraulic conductivity, roughness and the moisture characteristic curve have the greatest influence on runoff.

3) On a hillslope where the A-layer of the soil profile develops very well, rainfall intensities generally do not exceed infiltration capacities and Horton overland flow does not occur.

4) Return flow plays an important part in the interaction of overland flow with subsurface flow.

Chapter 3

LUMPING OF THE SYNTHESIZED RUNOFF MODEL

3.1 Introduction

In Chapter 2, we presented a synthesized runoff model and showed that it is very powerful for analyzing hillslope runoff processes, especially for analyzing the interaction of overland flow with subsurface flow. However, since it is a typical distributive(conceptual) model(Clarke, 1973), to fully define the model we need to know:

- 1) the spatial and temporal distribution of boundary conditions around the boundaries of the region,
- 2) the spatial distribution of the initial condition,
- 3) the spatial distribution of the hydraulic or geohydraulic parameters that control the flow.

The boundary conditions and initial condition are normally presupposed from historical records. In this case, even if the temporal distribution can be known, the spatial distribution is very difficult to obtain.

The physically-based approach requires complete spatial specification of the saturated and unsaturated hydrogeological parameters and surface roughness characteristics. Even when the distribution of these parameters is relatively even through space, there is seldom enough data available at field sites to provide the

necessary input to hillslope hydrologic models. When the hydrologic or hydrogeologic patterns are highly heterogeneous, as is usually the case, the data problem is intensified even further.

In addition, the numerical treatment of the distributive model has a great computational requirement. Sometimes its application may be limited by the inadequacy of computer capacity.

For these reasons, it is necessary to develop a simpler model for practical purposes. In this chapter, we shall try to lump the synthesized runoff model without losing its characteristics. In the lumped model, overland flow, saturated subsurface flow and unsaturated subsurface flow will be treated as a simultaneous system, and the relationships between the three subsystem will be derived from the simulation results obtained with the synthesized model.

3.2 Formulation of Lumped Runoff Model

In this section, based on the understanding of hillslope hydrologic processes in Chapter 2, we develop the continuity equations for the three subsystems: overland flow, saturated subsurface flow and unsaturated subsurface flow.

3.2.1 Lumped Model

3.2.1.1 Region of Flow

The two-dimensional vertical cross-section ABCDEFGA shown in Figure 3.1 is chosen as the region of flow. It is defined by three parameters, that is, horizontal length of the hillslope, L ; vertical depth, D ; and angle of land surface from horizontal land, θ . We shall assume this section to be in a plane parallel to the delivery direction of water toward a stream. For the same reason as the case of the synthesized runoff model, we take the base boundary CDE and the right-hand side vertical boundary EF as impermeable.

In Chapter 2, we have shown that when the saturated hydraulic conductivity is relatively great, as is usually the case, the free water surface of the overland flow and the water table of the subsurface flow rise so uniformly in space that we can take them as straight lines. Thus, the region of flow can be divided into three subregions: ABGA, BCDGB and DEFGD, which correspond respectively to overland flow, saturated subsurface flow and unsaturated subsurface flow. These subregions are defined by the following three independent variables, H : the depth of the overland flow at the lowest point of

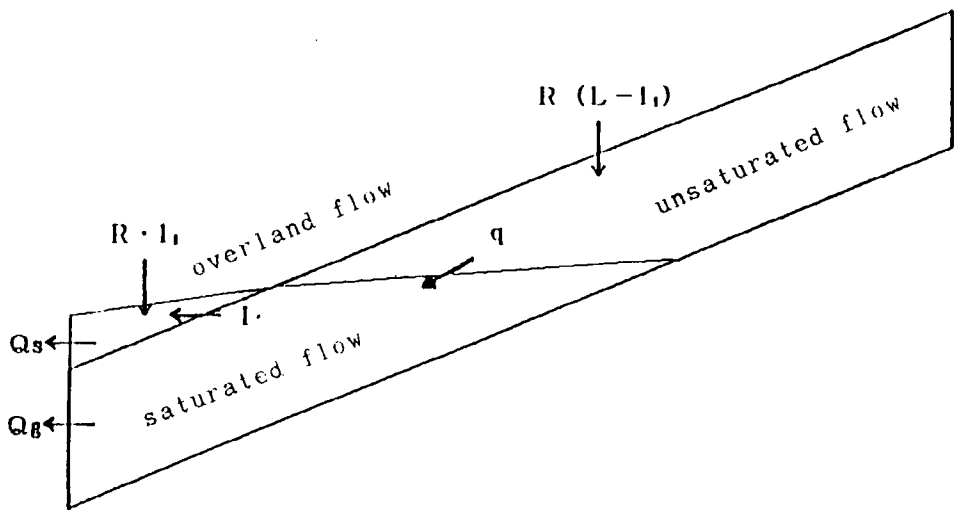
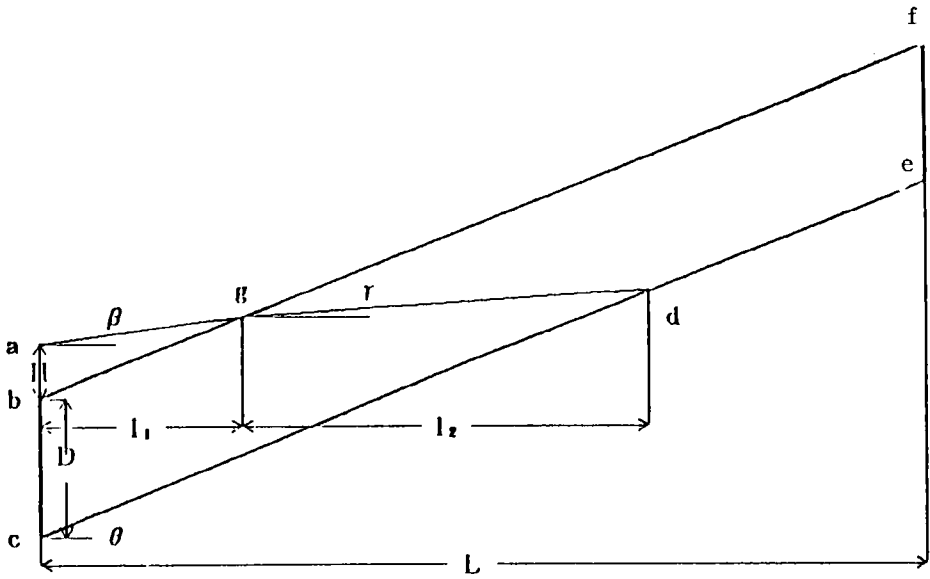


Figure 3.1 The region of flow for the lumped model

slope; β : the angle of the free water surface from horizontal level;
and γ : the angle of the water table from horizontal level.

3.2.1.2 Equations of Continuity

Referring to Figure 3.1, for overland flow the equation of continuity can be written as

$$\frac{dS_s}{dt} = R \cdot l_1 + I + Q_s \quad (3.1)$$

where S_s is storage in the region of overland flow, R intensity of rainfall, l_1 horizontal distance of saturated land surface, I intensity of return flow (or infiltration), Q_s overland runoff discharge, and t time.

For saturated subsurface flow the equation of continuity can be written as

$$\frac{dS_g}{dt} = \xi + q - I - Q_g \quad (3.2)$$

where S_g is storage in the region of saturated subsurface flow, ξ moisture volume in the zone which changes from unsaturated (or saturated) state to saturated (or unsaturated) state as water table rises (or declines), q total amount of lateral flow from unsaturated zone into saturated zone, and Q_g subsurface runoff discharge.

For unsaturated subsurface flow the equation of continuity is expressed as

$$\frac{dS_u}{dt} = R \cdot (L - l_1) - q - \xi \quad (3.3)$$

where S_u is storage in the region of unsaturated subsurface flow.

Each of the terms in Eqs.(3.1) - (3.3) must be expressed by a function of the independent variables (H,β,γ). These functions are derived as follows

Storage in the Region of Overland Flow

Storage in the region of overland flow is equal to the area of the region, that is,

$$S_s = 0.5 H^2 / (\text{tg}\theta - \text{tg}\beta) \quad (3.4)$$

dS_s/dt thus can be calculated from

$$\frac{dS_s}{dt} = H \left[\frac{1}{\text{tg}\theta - \text{tg}\beta} \frac{dH}{dt} + \frac{H}{2(\text{tg}\theta - \text{tg}\beta)^2 \cos^2\beta} \frac{d\beta}{dt} \right] \quad (3.5)$$

Storage in the Region of Saturated Subsurface Flow

Storage in the region of saturated subsurface flow is equal to the product of the area of the region with the porosity of soil, that is,

$$S_g = n D \left[H / (\text{tg}\theta - \text{tg}\beta) + 0.5D / (\text{tg}\theta - \text{tg}\gamma) \right] \quad (3.6)$$

where n is porosity of soil. Therefore, dS_g/dt can be calculated from

$$\begin{aligned} \frac{dS_g}{dt} = n D \left[\frac{1}{\text{tg}\theta - \text{tg}\beta} \frac{dH}{dt} + \frac{H}{(\text{tg}\theta - \text{tg}\beta)^2 \cos^2\beta} \frac{d\beta}{dt} + \right. \\ \left. + \frac{D}{2(\text{tg}\theta - \text{tg}\gamma)^2 \cos^2\gamma} \frac{d\gamma}{dt} \right] \quad (3.7) \end{aligned}$$

Storage in the Region of Unsaturated Subsurface Flow

Suppose the moisture characteristic curve of soil can be expressed approximately by the the following equation(Tani, 1982, see Figure 3.2):

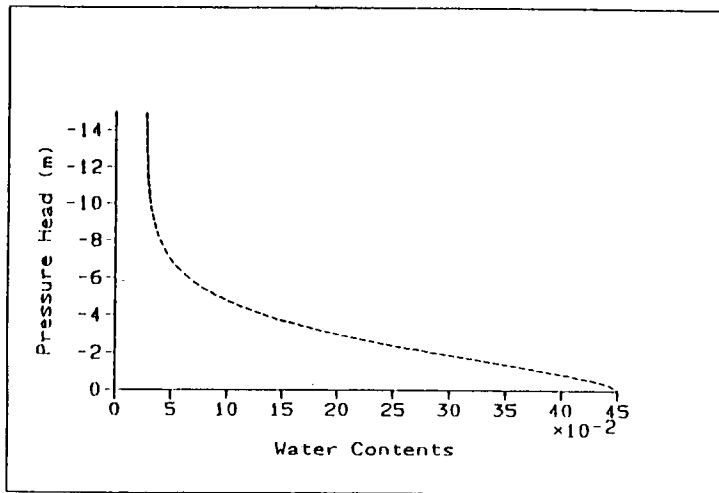


Figure 3.2 The moisture characteristic curve

$$\omega = (n - \omega_0)(1 + h/h_0)\exp(-h/h_0) + \omega_0 \quad (3.8)$$

where ω_0 is the lowest moisture content of the soil, h pressure head, h_0 known parameter. Here, h_0 determines the shape of the moisture characteristic curve. It is easy to prove that h_0 is equal to the pressure head at which the specific moisture capacity(= $d\omega/dh$) reaches its peak. On the other hand, in Chapter 2 we have shown that when the A-layer of the soil profile develops very well(Ishihara and Takasao(1962) have pointed out that this requirement is usually satisfied for almost all natural hillslopes), the contours of the pressure head are approximately parallel to the water table and keep much the same distance from each other. This means that the pressure head is directly proportional to the distance from the water table, z , namely,

$$h = \alpha z \quad (3.9)$$

When the saturated hydraulic conductivity is great and the hillslope is relatively gentle, the proportionality constant α can be approximately taken as -1.0. Under these circumstances, the storage in the region of unsaturated subsurface flow can be obtained as follows.

Inserting Eq.(3.9) and $\alpha = -1.0$ into Eq.(3.8) yields

$$\omega = (n - \omega_0)(1 + z/z_0)\exp(-z/z_0) + \omega_0 \quad (3.10)$$

where $z_0 = -h_0$.

The storage in the region of unsaturated subsurface flow is given by integrating moisture content over the whole region(see Figure 3.1),

$$S_u = \int_{DEFGD} \omega \, dA \quad (3.11)$$

where dA is an elemental control area within the region of unsaturated flow. Inserting Eq.(3.10) into Eq.(3.11) yields

$$S_u = \frac{l_2}{\cos\gamma} [0.5\omega_0(h_1+h_2) + (n-\omega_0)h_0(E_1+E_2+E_3)] \quad (3.12)$$

where

$$E_1 = (x-2)\exp(x) \Big|_0^{\text{ph2}}$$

$$E_2 = \frac{1}{D\cos\gamma} h_1(x-2)\exp(x) \Big|_{\text{ph1}}^{\text{ph2}}$$

$$E_3 = \frac{1}{D\cos\gamma} h_0(x^2-3x+3)\exp(x) \Big|_{\text{ph1}}^{\text{ph2}}$$

$$f(x) \Big|_a^b = f(b) - f(a)$$

$$l_1 = H/(\text{tg}\theta - \text{tg}\beta)$$

$$l_2 = D/(\text{tg}\theta - \text{tg}\gamma)$$

$$h_1 = (L-l_1-l_2)(\text{tg}\theta - \text{tg}\gamma)\cos\gamma$$

$$h_2 = h_1 + D\cos\gamma$$

$$\text{ph1} = -h_1/h_0$$

$$\text{ph2} = -h_2/h_0$$

Consequently, dS_s/dt is calculated as follows.

$$\frac{dS_u}{dt} = \frac{\partial S_u}{\partial H} \cdot \frac{dH}{dt} + \frac{\partial S_u}{\partial \beta} \cdot \frac{d\beta}{dt} + \frac{\partial S_u}{\partial \gamma} \cdot \frac{d\gamma}{dt} \quad (3.13)$$

where

$$\frac{\partial S_u}{\partial H} = \frac{\partial S_u}{\partial h_1} \cdot \frac{\partial h_1}{\partial l_1} \cdot \frac{\partial l_1}{\partial H}$$

$$\frac{\partial S_u}{\partial \beta} = \frac{\partial S_u}{\partial h_1} \cdot \frac{\partial h_1}{\partial l_1} \cdot \frac{\partial l_1}{\partial \beta}$$

$$\frac{\partial S_u}{\partial \gamma} = \frac{\partial S_u}{\partial \gamma'} + \frac{\partial S_u}{\partial \gamma''} + \frac{\partial S_u}{\partial l_2} \cdot \frac{\partial l_2}{\partial \gamma} + \frac{\partial S_u}{\partial h_1} \left[\frac{\partial h_1}{\partial l_2} \cdot \frac{\partial l_2}{\partial \gamma} + \frac{\partial h_1}{\partial \gamma} \right]$$

in which γ' stands for the first γ that occurred explicitly in the right-hand side of Eq.(3.12) and γ'' the second γ .

Total Volume of Moisture in the Changing Zone

Following the definition of ξ , it can be written as

$$\xi(t) = \lim_{\Delta t \rightarrow 0} \frac{\xi'(t, \Delta t)}{\Delta t} \quad (3.14)$$

where Δt is a time interval during which the configuration of the three subregions, (H, β, γ) , changes into $(H+\Delta H, \beta+\Delta \beta, \gamma+\Delta \gamma)$, where $\Delta H = \Delta t \, dH/dt$, $\Delta \beta = \Delta t \, d\beta/dt$, and $\Delta \gamma = \Delta t \, d\gamma/dt$; $\xi'(t, \Delta t)$ is the total volume of moisture in the zone which changes from an unsaturated(or saturated) state to a saturated(or unsaturated) state as the configuration changes from (H, β, γ) into $(H+\Delta H, \beta+\Delta \beta, \gamma+\Delta \gamma)$, and can be calculated by integrating the moisture content over the changing zone.

$$\xi'(t, \Delta t) = \frac{1}{\cos \gamma} [0.5 \omega_0 (h_3 + h_5) + (n - \omega_0) h_0 (F_1 + F_2 + F_3)] \quad (3.15)$$

where

$$F_1 = (x-2) \exp(x) \Big|_0^{\text{ph}5}$$

$$F_2 = \frac{1}{h_4} h_3 (x-2) \exp(x) \Big|_{\text{ph}3}^{\text{ph}5}$$

$$F_3 = \frac{1}{h_4} h_0 (x^2 - 3x + 3) \exp(x) \Big|_{\text{ph}3}^{\text{ph}5}$$

$$h_3 = \cos \gamma \, \Delta t \, dH/dt + (\text{tg} \theta - \text{tg} \gamma) \left[\frac{H + \Delta t \, dH/dt}{\text{tg} \theta - \text{tg}(\beta + \Delta t \, d\beta/dt)} - 1 \right] / \cos \theta$$

$$h_4 = \frac{D \cos \gamma [\text{tg}(\gamma + \Delta t \, d\gamma/dt) - \text{tg} \gamma]}{\text{tg} \theta - \text{tg}(\gamma + \Delta t \, d\gamma/dt)}$$

$$h_5 = h_3 + h_4$$

$$\text{ph}3 = -h_3/h_0$$

$$\text{ph}5 = -h_5/h_0$$

Inserting Eq.(3.15) into Eq.(3.14) and performing the limitation, we obtain

$$\xi = H_{\xi} \frac{dH}{dt} + \beta_{\xi} \frac{d\beta}{dt} + \gamma_{\xi} \frac{d\gamma}{dt} \quad (3.16)$$

where

$$H_{\xi} = n L_g \left[\cos\gamma + \frac{\text{tg}\theta - \text{tg}\gamma}{\cos\gamma(\text{tg}\theta - \text{tg}\beta)} \right]$$

$$\beta_{\xi} = n L_g \frac{H(\text{tg}\theta - \text{tg}\gamma)}{\cos\gamma \cos^2\beta (\text{tg}\theta - \text{tg}\beta)^2}$$

$$\gamma_{\xi} = (0.5n - \omega_0) L_g$$

$$L_g = D / \cos\gamma / (\text{tg}\theta - \text{tg}\gamma)$$

Discharges and Lateral Flow Intensity

The discharges of overland runoff and subsurface runoff and the intensity of lateral flow are both functions of (H, β, γ) , namely,

$$Q_s = Q_s(H, \beta, \gamma)$$

$$Q_g = Q_g(H, \beta, \gamma) \quad (3.17)$$

$$q = q(H, \beta, \gamma)$$

These functions will be derived in the next section from the simulation results with the synthesized runoff model developed in Chapter 2.

Putting the above results together reduces the lumped runoff model to the following form,

$$\begin{bmatrix} a_{11} & a_{12} & a_{13} \\ a_{21} & a_{22} & a_{23} \\ a_{31} & a_{32} & a_{33} \end{bmatrix} \begin{bmatrix} dH/dt \\ d\beta/dt \\ d\gamma/dt \end{bmatrix}^T = \begin{bmatrix} f_1 + I \\ f_2 - I \\ f_3 \end{bmatrix} \quad (3.18)$$

All of the coefficients are given in Appendix D.

Solution of the Lumped Model

As a boundary condition the depth of overland flow at the lowest point of slope is given, that is,

$$H = H(t) \quad (3.19)$$

where $H(t)$ is a prescribed function. Thus, the lumped runoff model can be rewritten as follows,

$$\begin{bmatrix} a_{12}+a_{22} & a_{13}+a_{23} \\ a_{32} & a_{33} \end{bmatrix} \begin{bmatrix} d\beta/dt & d\gamma/dt \end{bmatrix}^T = \begin{Bmatrix} f' \\ f'_3 \end{Bmatrix} \quad (3.20)$$

where $f' = f_1 + f_2 - (a_{11}+a_{21})dH/dt$

$$f'_3 = f_3 - a_{31}dH/dt$$

Solving Eq.(3.20) for $(d\beta/dt \ d\gamma/dt)$ gives

$$d\beta/dt = F_\beta, \quad d\gamma/dt = F_\gamma \quad (3.21)$$

where

$$F_\beta = F_\beta(\beta, \gamma, t) = [f'_3(a_{13}+a_{23}) - f'_3 a_{33}] / A$$

$$F_\gamma = F_\gamma(\beta, \gamma, t) = [f'_3 a_{32} - f'_3(a_{12}+a_{22})] / A$$

$$A = a_{32}(a_{13}+a_{23}) - a_{33}(a_{12}+a_{22})$$

Eq.(2.21) is solved by the Runge-Kutta method.

3.3 Derivation of Discharge Expressions

In Section 2, we have formulated the lumped runoff model on the basis of conservation of mass. However, for making the model soluble, it is necessary to express overland runoff discharge, subsurface runoff discharge, and intensity of lateral flow from unsaturated zone toward saturated zone as functions of (H, β, γ) . In this section, we shall derive the function expressions from the simulation results with the synthesized runoff model described in Chapter 2.

3.3.1 Subsurface Runoff Discharge

A storage function model is considered for subsurface runoff discharge. Following Kimura(1961), the relationship between storage and discharge can be represented by an exponential function, that is,

$$S = K Q_g^P \quad (3.22)$$

where S is water storage, K and P model parameters. Eq.(3.22) also can be written as

$$Q_g = A S^B \quad (3.23)$$

Our purpose is to evaluate the model parameters, A and B , by using the simulation results with the synthesized runoff model. For water storage we consider the following two cases,

$$S = S_g - S_{g0}$$

and

$$S = S_g - S_{g0} + S_u - S_{u0}$$

where S_{g0} is water storage in the region of saturated subsurface flow in static state, and S_{u0} water storage in the region of unsaturated subsurface flow in static state.

Solving the synthesized runoff model, we obtain $Q_{gi}, S_{ui}, S_{gi}, i = 1, 2, \dots, T$. where i indicates discrete time. By means of the regression analysis method, the regression lines can be drawn and the correlation coefficient of Q_g and S as well as the regression estimates of model parameters A and B are obtained. For some examples (Table 3.1), the results are shown in Figure 3.3 and Figure 3.4. It can be seen that there is a high correlation between storage and discharge for both the case $S = S_g - S_{g0}$ and the case $S = S_g - S_{g0} + S_u - S_{u0}$. However, In the first case, the parameters A and B vary widely according to roughness and saturated hydraulic conductivity. This is undesirable for a runoff model. In the following analyses, we shall make use of $S = S_g - S_{g0} + S_u - S_{u0}$.

The relationship between hydraulic conductivity and model parameters is shown in Figure 3.5.

3.3.2 Intensity of Lateral Flow

Similarly to the subsurface runoff discharge, the intensity of lateral flow from the region of unsaturated flow into the region of saturated flow also can be determined from a storage function model. For water storage the following three cases have been tested,

$$S = S_g - S_{g0}$$

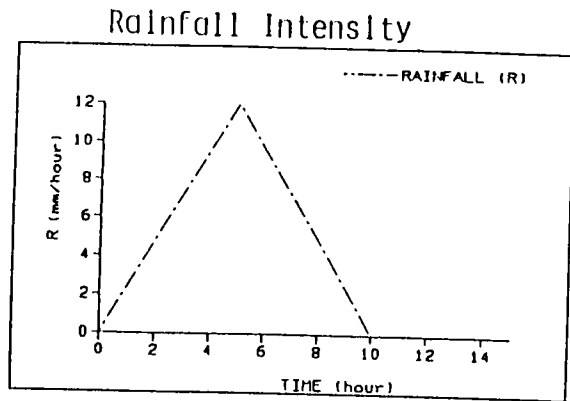
$$S = S_g - S_{g0} + S_u - S_{u0}$$

$$S = S_u - S_{u0}$$

Table 3.1 Simulation case conditions

Fixed Condition

| Model Parameter | | |
|-------------------|---------|------------------|
| L | 100.0 | (m) |
| θ | 0.17453 | (rad) |
| D | 2.0 | (m) |
| H | 0.1 | (m) |
| dH/dt | 0.0 | (m/hr) |
| Soil Parameter | | |
| N | 0.02 | ($m^{-1/3}hr$) |
| Cs | 0.45 | - |
| Wr | 0.027 | - |
| ho | 1.5 | (m) |
| Initial Condition | | |
| β_0 | 0.0 | (rad) |
| γ_0 | 0.00001 | (rad) |



Case Data

| Case | K(m/hr) | A(q) | B(q) | A(Qg) | B(Qg) |
|------|---------|---------|---------|---------|---------|
| 1 | 50. | 0.09965 | 0.60639 | 0.09568 | 0.57934 |
| 2 | 100. | 0.14994 | 0.54486 | 0.14429 | 0.52351 |
| 3 | 250. | 0.26739 | 0.62729 | 0.25880 | 0.59047 |
| 4 | 500. | 0.46417 | 0.78500 | 0.44154 | 0.78246 |

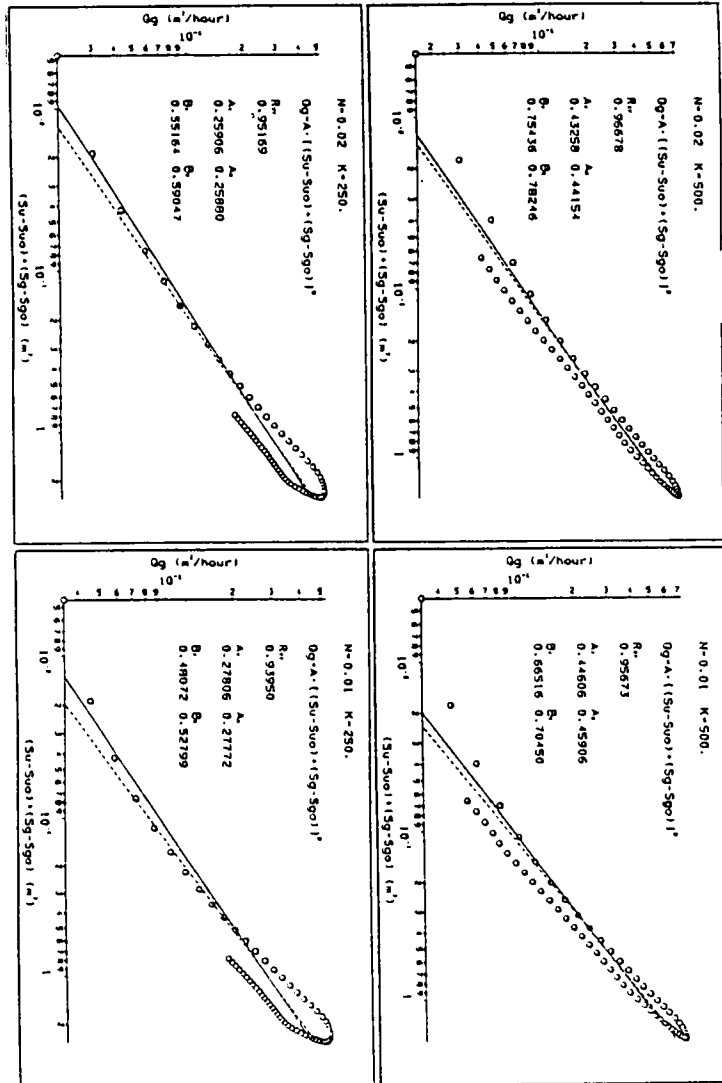


Figure 3.3 The regression line between Q_g and S .

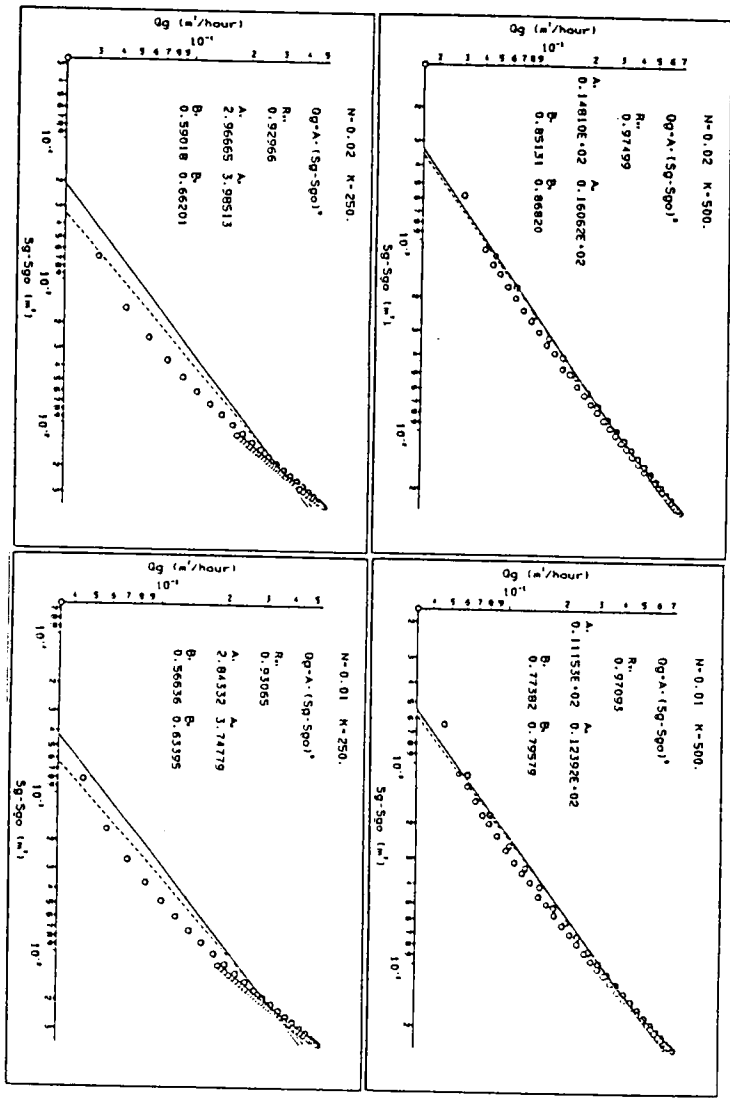


Figure 3.4 The regression line between Q_g and S_g .

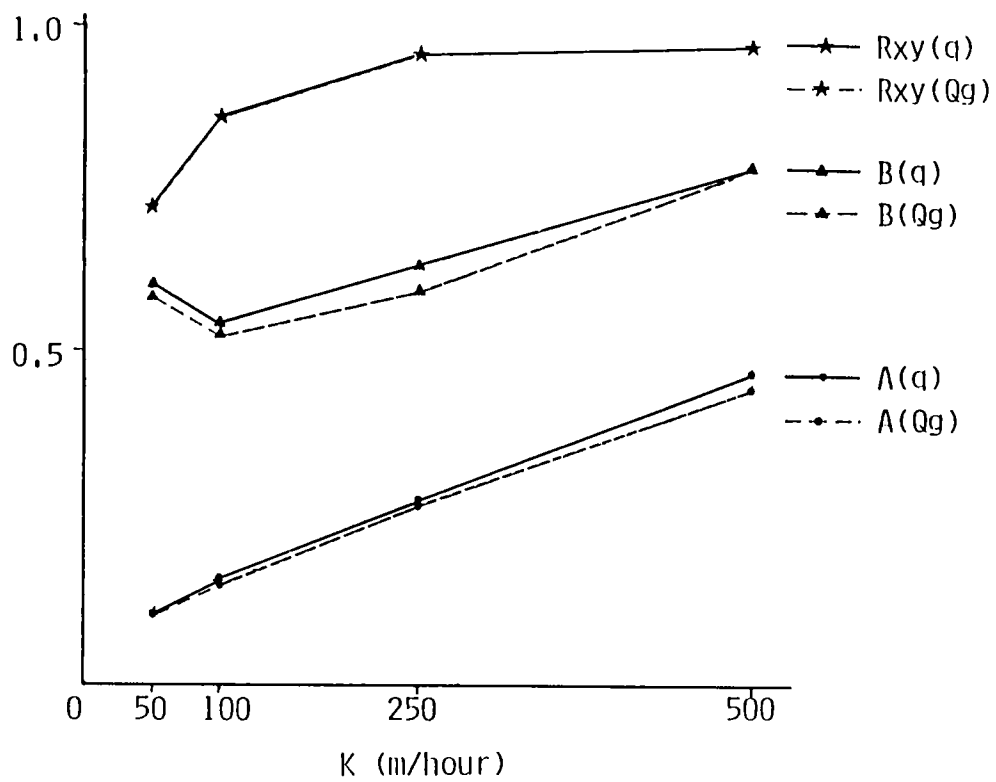


Figure 3.5 The relationships between model parameters and hydraulic conductivity

The results of some examples are shown in Figure 3.6, Figure 3.7, and Figure 3.8. Since the model parameters estimated are lacking in stability, the case $S = S_g - S_{g0}$ is considered to be unsuitable. In the remaining two cases, $S = S_g - S_{g0} + S_u - S_{u0}$ has been selected for our runoff model, since it has a greater correlation coefficient.

3.3.3 Overland Runoff Discharge

In the lumped model, overland flow has been treated as an one-dimensional sheetflow along land surface in the same way as in the synthesized runoff model. Therefore, the velocity of overland flow can be represented by Eq.(2.39), and then the average velocity of overland flow at the lowest point of slope(outlet) can be written as

$$V_s = \frac{\alpha}{n_0} \sqrt{|\sin\theta - dH/dS| \cos\theta} H^{1/3} + V_g \quad (3.24)$$

where n_0 : roughness of land surface,

S : tangent direction of land surface,

$V_g = Q_g/D$: average velocity of subsurface flow at the outlet,

Q_g : subsurface runoff discharge,

$\alpha = 1$ if $\sin\theta - dH/dS / \cos\theta \geq 0$,

$\alpha = -1$ if $\sin\theta - dH/dS / \cos\theta < 0$.

dH/dS can be obtained from the geometrical relationship,

$$\begin{aligned} dH/dS &= H \cos\theta / (l_1 / \cos\theta - H \sin\theta) \\ &= \cos^2\theta (tg\theta - tg\beta) / [1 - \sin\theta \cos\theta (tg\theta - tg\beta)] \end{aligned} \quad (3.25)$$

The overland runoff discharge is the product of the average velocity of overland flow in the tangent direction of land surface and the flow depth in the normal direction, that is,

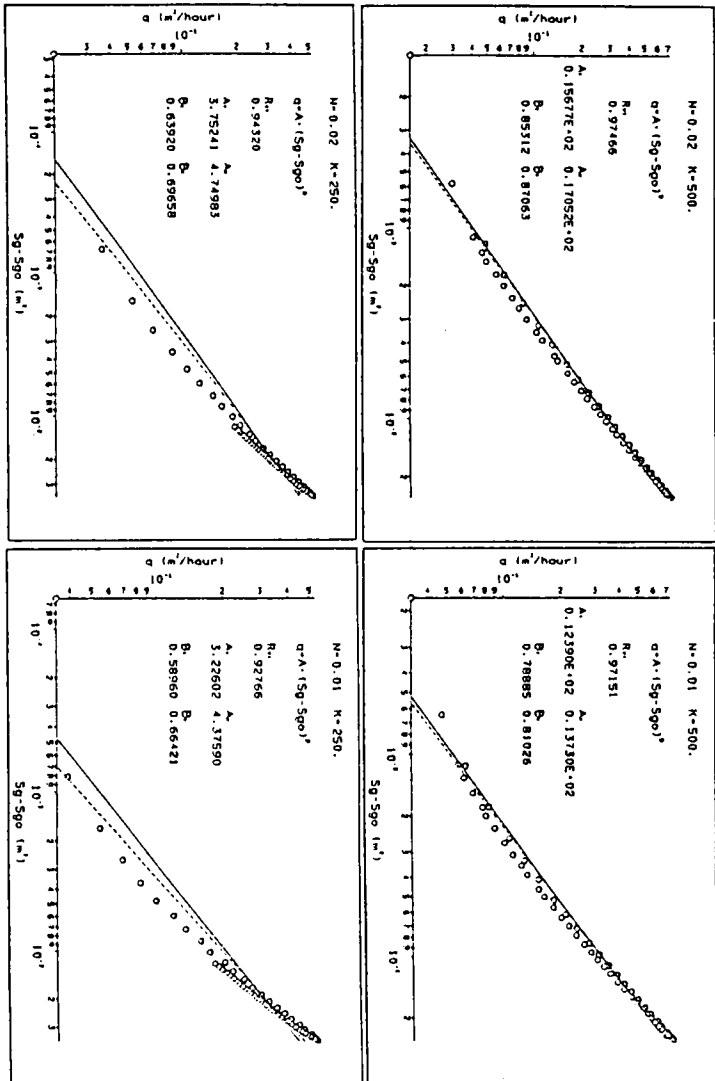


Figure 3.6 The regression line between Q_g and S_g .

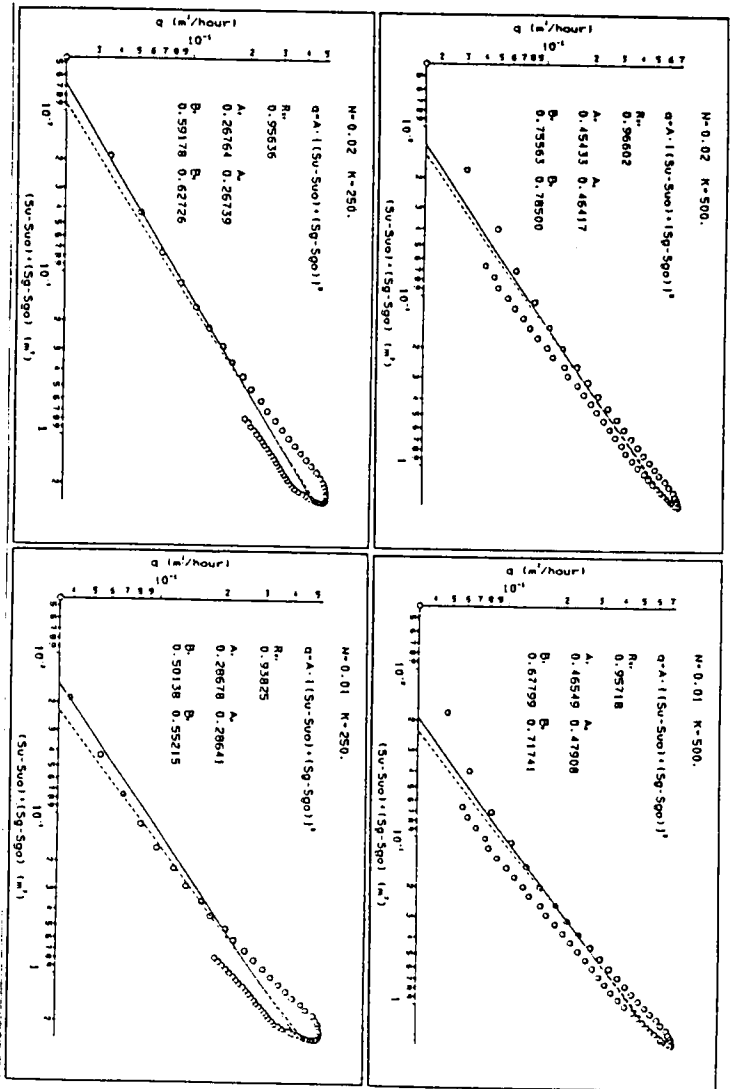


Figure 3.7 The regression line between Q_g and S .

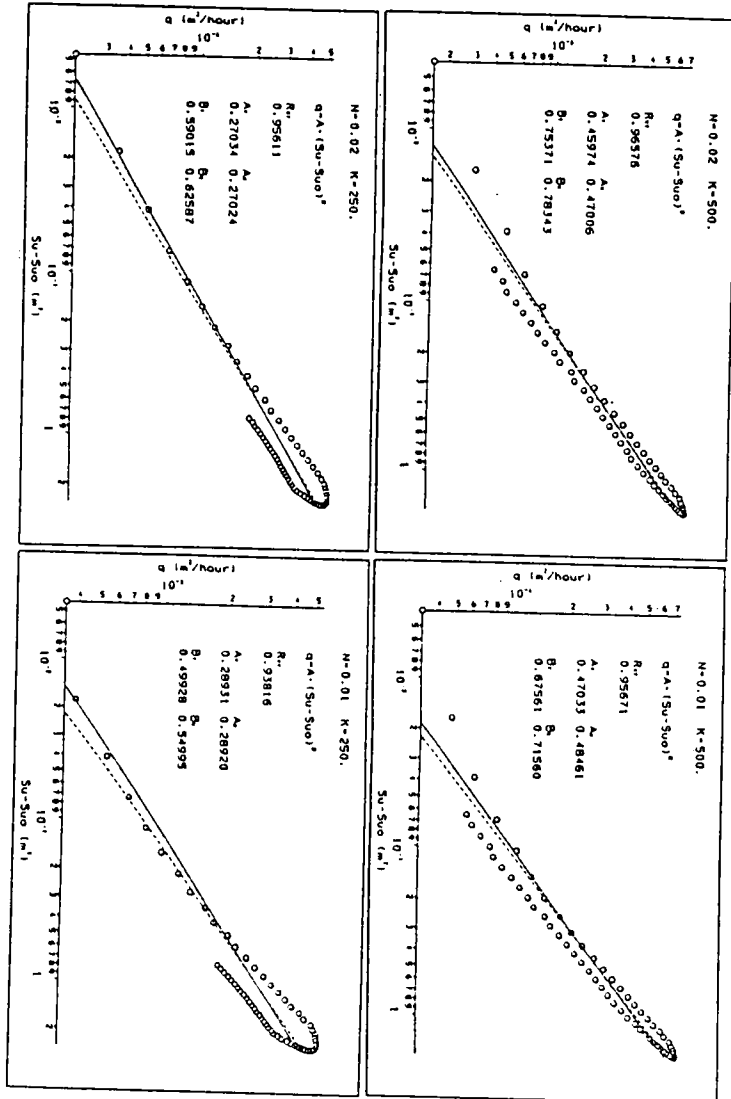


Figure 3.8 The regression line between Q_g and S .

$$Q_s = H V_s \cos\theta \quad (3.26)$$

3.3.4 Stability of Model Parameters

We have shown the procedure for evaluating model parameters. However, it is necessary to check whether or not the parameters determined by the above procedure are suitable for a runoff model. The criterion of suitability can be stated as follows: If the parameters are stable, in other words, if they do not change with rainfall intensity or pattern, they are considered to be suitable for a runoff model.

For triangular rainfall, the relation between model parameters and rainfall intensity is shown in Figure 3.9. It is apparent that the suitability requirement is satisfied. By this result, we are justified in considering the parameters as stable. When rainfall intensity is weak, the parameter values shift slightly from their stable values. This may be due to a greater relative error in the numerical solution.

The relation between the parameters and the rainfall pattern has been examined by comparing rectangular rainfall with triangular rainfall. The regression estimates of the model parameters are given in Figure 3.10 and Figure 3.11. It can be seen that the results of the two rainfall patterns agree very well.

In summary, there is a high correlation between storage and discharge, and the relation can be approximately represented by a storage function model (exponential function). The parameters of the storage function model determined by the regression analysis method are stable.

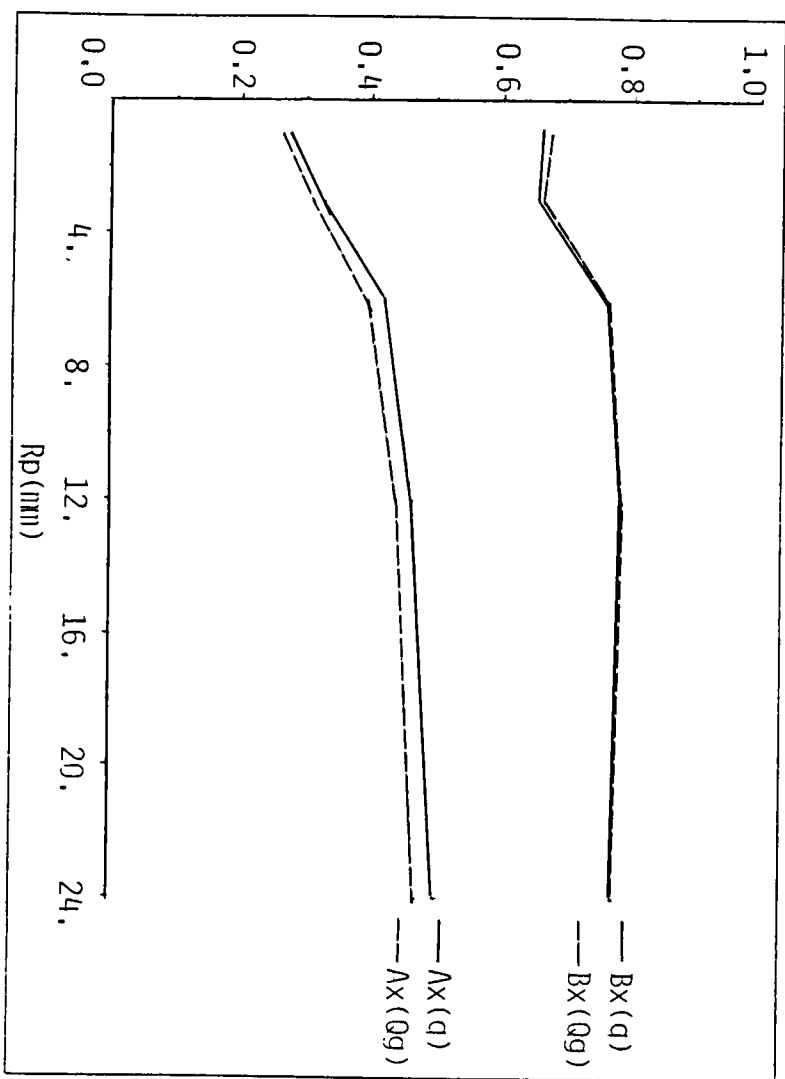


Figure 3.9 The relationship between model parameters and rainfall intensity for triangular rainfall.

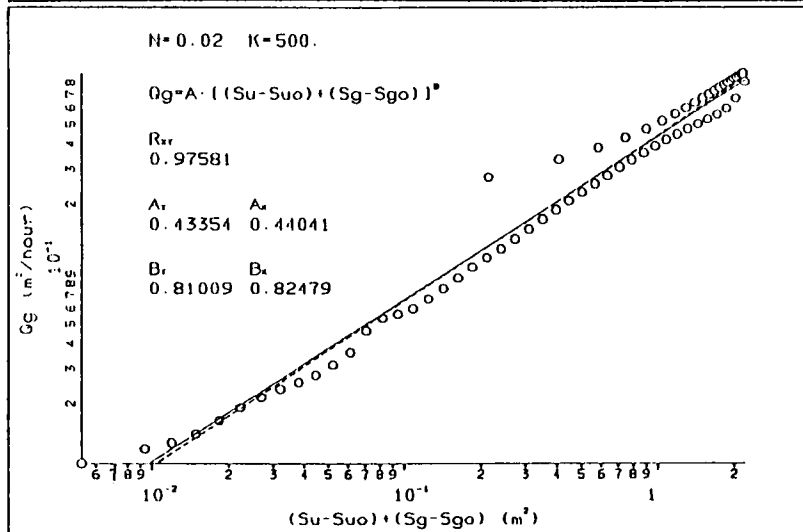
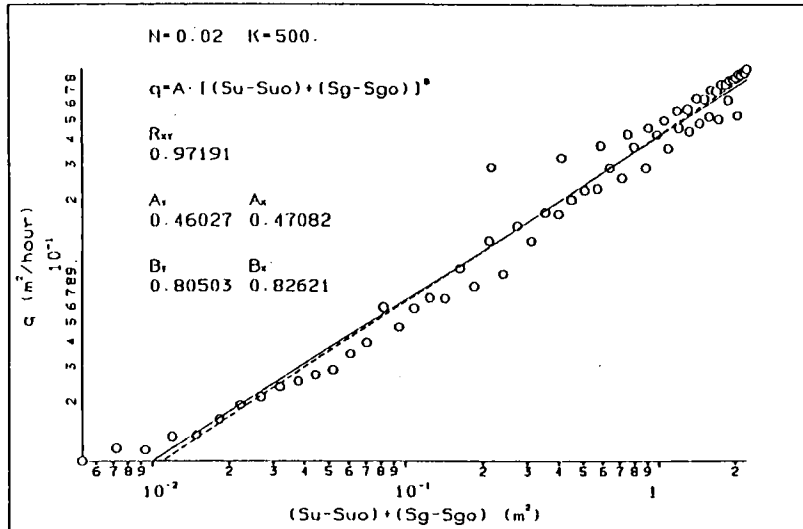


Figure 3.10 The regression line between Q_g and S for rectangular rainfall.

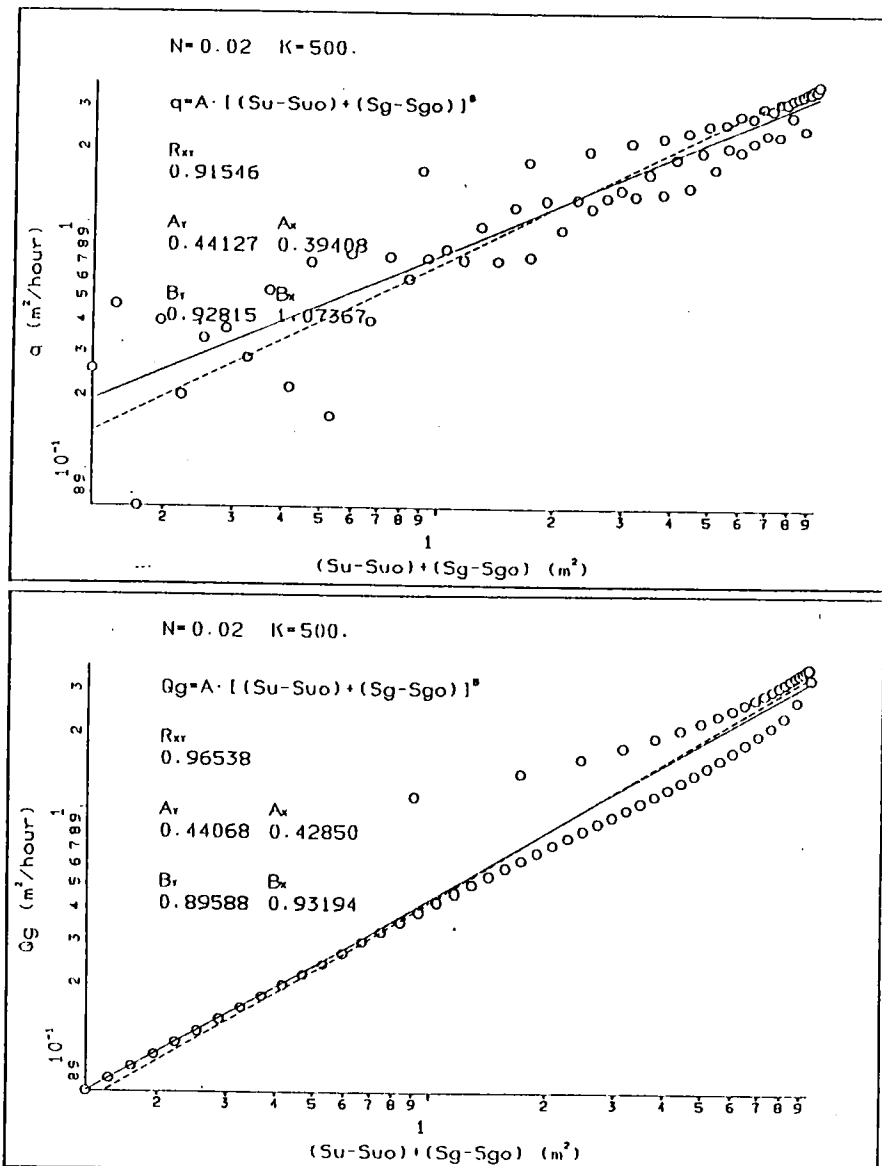


Figure 3.11 The regression line between Q_s and S for rectangular rainfall.

3.4 Analyses of Lumped Runoff Model

In the preceding sections we have formulated the lumped model and derived the discharge-storage expressions. This section is concerned with examining the characteristics of the lumped runoff model.

3.4.1 Approximating Water Surface and Water Table by Straight Lines

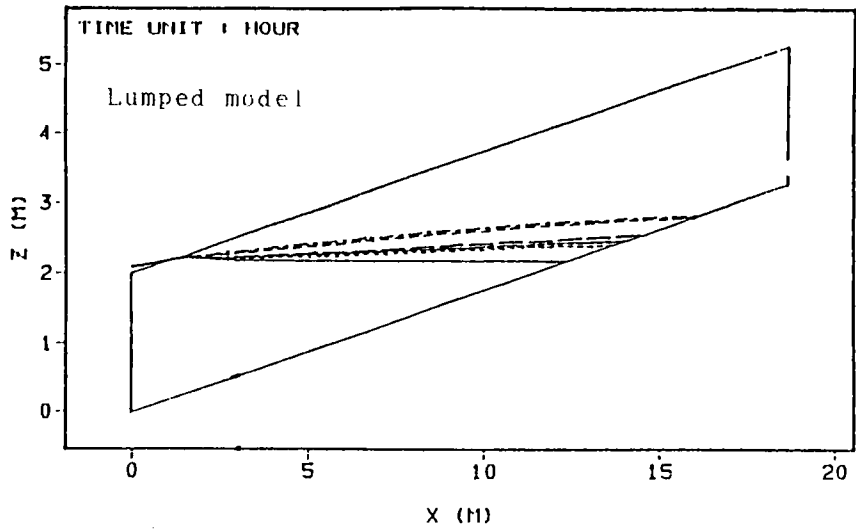
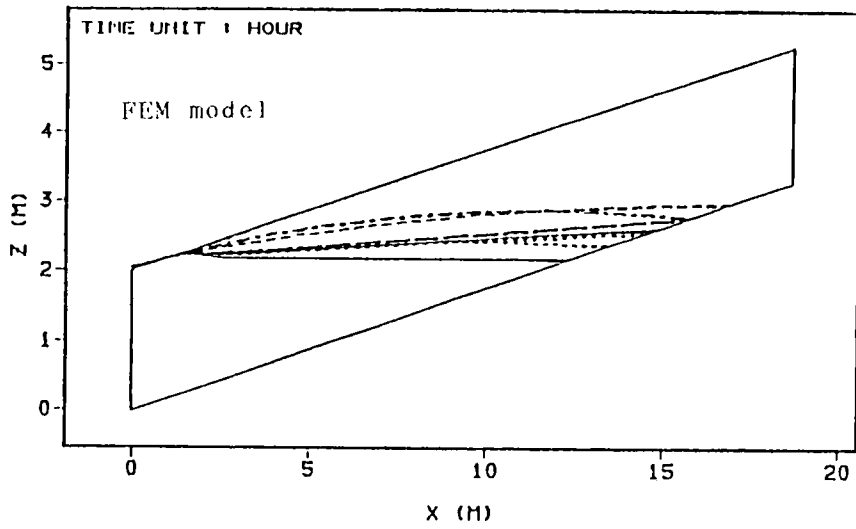
In the lumped model, we have taken the free water surface of overland flow and the water table of subsurface flow as straight lines. However, they are usually curves. Questions thus arise as to whether or not the approximations are appropriate, and how much the approximations affect simulation results.

Figure 3.12 shows the changing water table and water surface obtained by the synthesized runoff model and the lumped runoff model. Although they differ somewhat, the results are, on the whole, in good agreement.

The hydrograph of the same case is shown in Figure 3.13. It can be seen that the hydrograph obtained by the lumped runoff model is in excellent agreement with the results of the synthesized runoff model.

In summary, when the land surface is gentle, and the distributions of saturated hydraulic conductivity and roughness are even, as is usually the case, the agreement between the lumped runoff model and the synthesized runoff model is quite satisfactory. Thus, we can say that the straight line approximation of the water surface and the water table are suitable and acceptable for a runoff model for practical purposes.

3.4.2 Comparison between the SSSR Model and the Lumped Runoff Model



— 0 - - - 3 - - - 5 - - - 8 - - - 10
 — 13 - - - 15

WATER TABLE

Figure 3.12 The changing water table and free water surface.

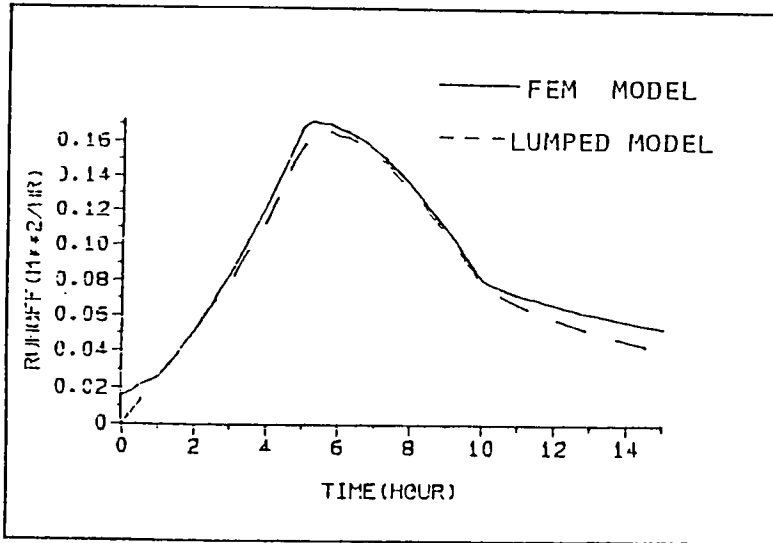


Figure 3.13 The hydrographs obtained by the synthesized runoff model and the lumped runoff model.

We have tested the lumped runoff model under various flow conditions, and the results are shown in Figure 3.14 - 3.16. For comparison the results obtained by the synthesized runoff model are shown together. In general, they are in agreement. However, there are two problems which must be pointed out.

1) The lumped runoff model tends to overestimate the total runoff discharge around the peak of the hydrograph. This may be because the curved water surface and water table are averaged by lumping. It is believed that further improvement may be achieved by using a more advanced approximating method for water surface and water table.

2) It can be seen that the rising slopes of the subsurface runoff discharge and intensity of the lateral flow are in excellent agreement with the results of the synthesized runoff model, but the declining slopes occur later by 3 ~ 15 min.. It is considered to be due to the same reason as the overestimation of total runoff discharge.

Even though the above conclusions are based on the simulation results of triangular rainfall, they are also true for rectangular rainfall. The simulation results for the latter case are shown in Figure 3.17.

In summary, the lumped runoff model based on the comprehensive understanding of hillslope runoff processes, even though it has a far simpler structure than the synthesized runoff model, can give results as good as the synthesized model. Its strong point is that for fully defining the model the complete specification of spatial distribution of model parameters is not necessary. This makes the lumped runoff model very suitable for a practical purpose.

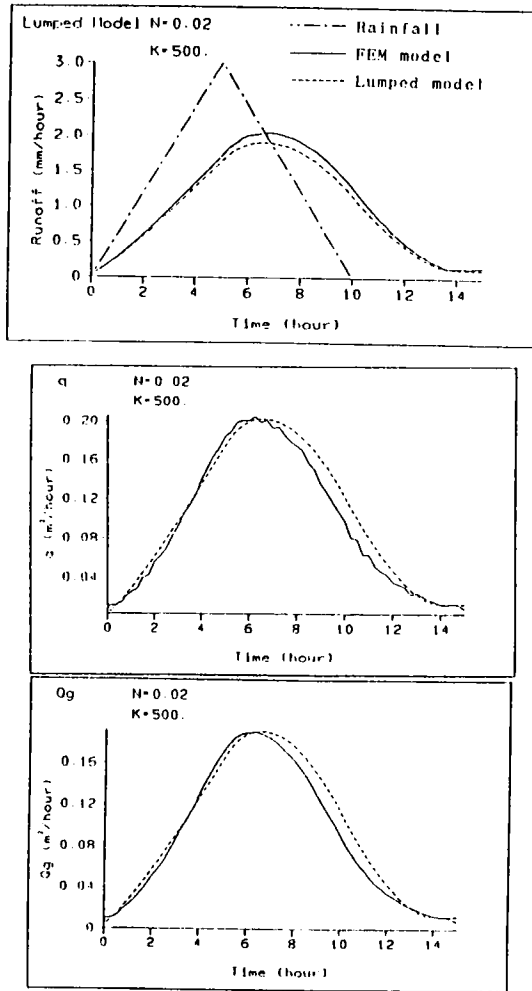


Figure 3.14 The hydrograph, subsurface runoff discharge and intensity of lateral flow.

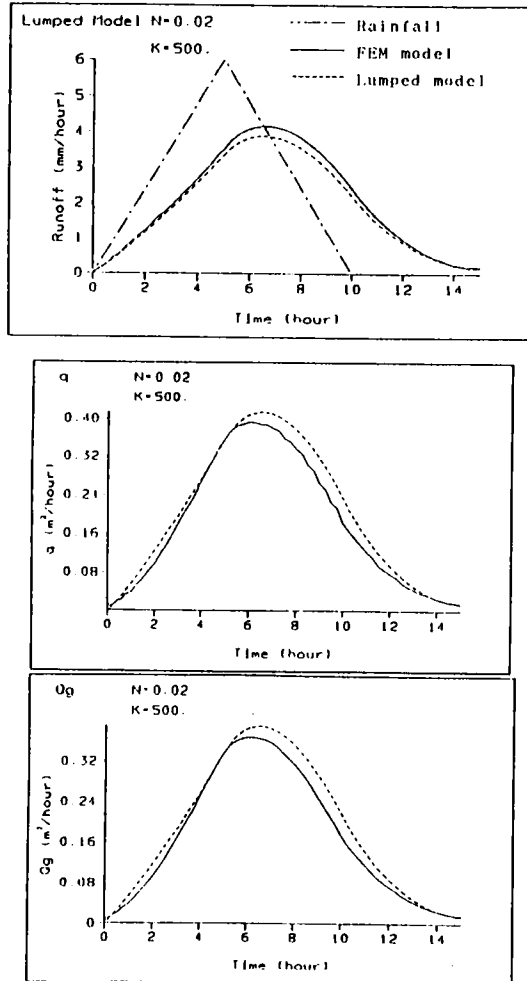


Figure 3.15 The hydrograph, subsurface runoff discharge and intensity of lateral flow.

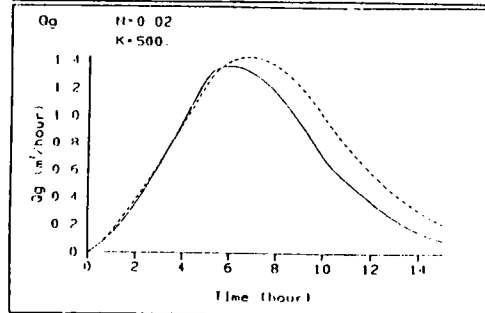
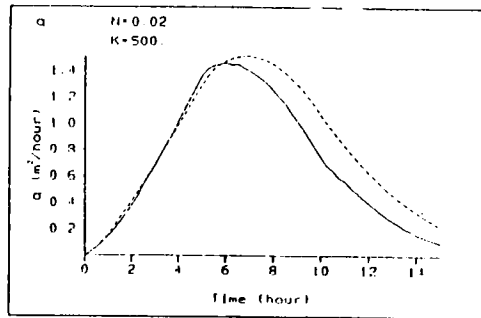
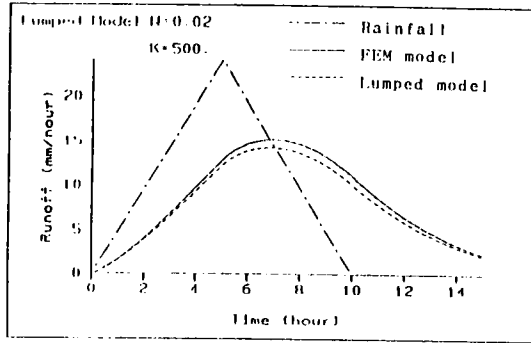


Figure 3.16 The hydrograph, subsurface runoff discharge and intensity of lateral flow.

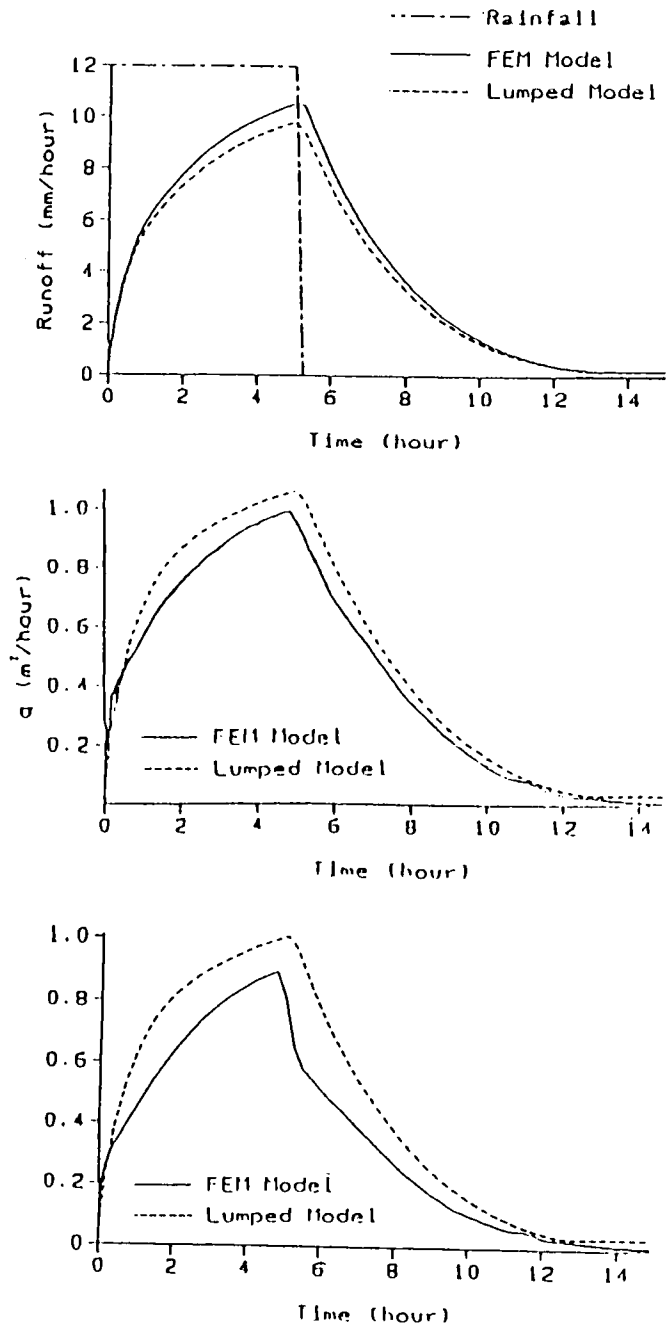


Figure 3.17 The hydrograph, subsurface runoff discharge and intensity of lateral flow in the case of rectangular rainfall.

3.5 Summary

In this chapter, based on a comprehensive understanding of hillslope runoff processes we lumped the synthesized runoff model to construct a new runoff model containing not only overland flow but also saturated-unsaturated subsurface flow. The mathematical model consists of continuity equations in three subregions, and equations of motion based on the kinematic approximation for overland flow and derived from the storage function model for subsurface flow. The model parameters have been estimated by using the simulation results of the synthesized runoff model with the regression analysis method. The mathematical model is solved by the Runge-Kutta method.

The lumped model treats overland flow, saturated subsurface flow, and unsaturated subsurface flow as a simultaneous system. The intensity of return flow can be obtained as an independent variable in the same way as in the synthesized runoff model.

The lumped runoff model does not require a complete specification of the spatial distribution of the soil's hydrologic and geohydrologic parameters such as saturated hydraulic conductivity, surface roughness characteristics. As mentioned in the beginning of this chapter, even when the distribution of these parameters is relatively even, there is seldom enough data available at field sites to provide the necessary input for the synthesized runoff model. In this meaning, we can say that the lumped runoff model is far more useful than the synthesized runoff model for a practical purpose.

Chapter 4

REAL-TIME CONTROL OF MULTIRESERVOIR SYSTEMS

4.1. Introduction and Overview

During the last 20 years, the reservoir control literature has grown impressively (Yeh(1985) and Yakowitz(1982) have reviewed the reservoir control studies in detail.). As pointed by Georgakakos and Marks(1985), this continuing research effort is not only because of the many influential, social, and environmental effects each reservoir system generates, but also because a comprehensive methodology capable of handling the problem in its general form has not yet been developed. In essence, the majority of the reservoir control models published have been developed for and perhaps adequately handle a particular reservoir system, or a particular class of systems with common predominant characteristics. However, if these characteristics were to change, the methods would no longer be adequate. The purpose of this study is to present a new method able to handle the operation problem of reservoir systems in its general form. This section will review representative stochastic reservoir control studies to identify past deficiencies and to benefit from some successful ideas.

Following Yeh(1985), the reservoir control models can be classified by the optimization philosophy adopted as follows:

- (1) Linear programming(LP) models, including chance-constrained LP, stochastic LP, and stochastic programming with recourse.

- (2) Dynamic programming(DP) models, including incremental DP(IDP), discrete differential DP(DDDP), incremental DP with successive approximation(IDPSA), stochastic DP, reliability-constrained DP, differential DP(DDP) and the progressive optimality algorithm.
- (3) Nonlinear programming models.
- (4) Simulation models.

Linear programming has been one of the most widely used techniques in water resources management. It is concerned with solving a special type of problem: one in which all relations among the variables are linear, both in constraints and in the objective function to be optimized. LP models which consider uncertainty include Chance Constraint Programming(ReVelle et al., 1969; Joeres et al., 1971; Eisel, 1972; Sobel, 1975; Sniedovich, 1980; etc.) and Reliability Programming models(Colorni and Fronza, 1976; Simonovic and Marino, 1980,1982; Marino and Mohammadi, 1983). In general, LP models cannot adequately reproduce the system's stochasticity(temporal and spatial correlation of the uncertain inputs and the induced similar probabilistic structure on the system's state variables), and a global linear approximation of the system dynamics is not likely to give accurate results. Furthermore the Linear Decision Rules(LDR) that relate releases to storage, inflow, and decision parameters are crucial assumptions in the application of chance constraint LP, but, there is a fatal limitation of the rule: the solution from an LDR model is not guaranteed to be optimal. Georgakakos and Marks(1985) have shown that the assumption of LDR is optimal for unconstrained systems with linear dynamics and quadratic performance measures, and it performs poorly in situations where the

above characteristics are absent. For these reasons, the models of this category are considered appropriate for preliminary design studies rather than for operation purposes(Loucks and Dorfman, 1975).

Nonlinear programming(NLP) has not enjoyed the popularity that LP and DP have in water resources systems analysis. This is particularly due to the fact that the optimization process is usually slow and takes up large amounts of computer storage and time when compared with other methods. The mathematics involved in the nonlinear models is much more complicated than in the linear case, and NLP unlike DP cannot easily accommodate the stochastic nature of inflows to the systems.

Simulation is a modeling technique that is used to approximate the behavior of a system on the computer, representing all the characteristics of the system largely by a mathematical or algebraic description(Ackoff, 1961; Maass et al., 1962; Yeh, 1985). It is different from a mathematical programming technique. Mathematical programming techniques find an optimum decision for system operation meeting all system constraints while maximizing or minimizing some objective. On the other hand, the simulation model provides the response of the system to certain inputs, which include decision rules, so that it enables a decision maker to examine the consequences of various scenarios of an existing system or a new system without actually building it. For these reasons, simulation models are suitable for performance evaluation rather than for optimal policy identification(Yeh, 1985; Georgakakos and Marks, 1985).

Of the four categories, the second model category, Dynamic Programming, is considered to be the most suitable for operation purposes due to the dynamic nature of a reservoir system. Little(1955) first applied DP to reservoir optimization, but the general formulation of DP was completed by Bellman(1957). DP is a procedure for optimizing a multistage decision process. The popularity and success of this technique can be attributed to the fact that the nonlinear and stochastic features which characterize a large number of water reservoir systems can be translated into a DP formulation. Applications of DP to reservoir optimization have been reported by Hall(1964), Young(1967), Takasao and Seno(1970).

However, in the application of DP models to a multireservoir system, there are two basic problems. The first problem is the phenomenon of exponentially increasing computational burden with increase in state dimension. (This problem is popularly known as the "curse of dimensionality".) The second one is the need to consider the uncertainty of a water resources system.

The curse of dimensionality is the greatest hindrance to Dynamic Programming solution of large-scale optimal control problems. To alleviate it, a number of techniques have been presented such as IDP, DDDP, IDPSA, and DDP.

The use of IDP for reservoir operation studies was reported by Hall et al.(1969). The IDP procedure starts with an assumed trial state trajectory, which is a sequence of feasible state vectors resulting in a corresponding initial policy, and an initial value of the objective function. The DP recursive equation is then used to examine the neighboring states that are just above and below the trial state trajectory. If any neighboring trajectory is found to give a

better value of the objective function, then this new trajectory replace the trial state trajectory. The procedure continues until convergence takes place.

Heidari et al.(1971) modified IDP to obtain a new state trajectory in a " corridor " centered about the trial trajectory, and referred to the algorithm as DDDP. Essentially DDDP is only the generation of IDP.

IDPSA makes use of Bellman's concept of successive approximations, which decomposes an original multi-state variable DP into a series of subproblems each with only one state variable, and solves the subproblems by IDP.

IDP, DDP, and IDPSA do provide a considerable reduction in the amount of computation, but they cannot overcome completely the dimensionality problem. Furthermore, these methods are only suitable for so-called "invertible system", they need a good initial policy(sequence of states), and the convergence of the solution to the global optimum cannot be proved. For these reasons, the DDP method proposed by Jacobsen and Mayne(1970) is considered to be the most promising. If the DP model is an LQP(Linear dynamics and Quadratic Performance criterion function) problem, and the objective function is separable and convex(for minimization problems), then it can easily be shown that the decision is a linear function of the current state, the recurrence relation is a quadratic function of the state variable for a backward solution, and that recursive formulae providing the coefficients of the linear decision can be derived. Therefore, given the initial state of the system, an analytical solution can be obtained. If the objective function is not quadratic, or the system dynamics are not linear, some approximation methods can be used to provide a quadratic approximation for the objective

function and linear expressions for the system dynamics around an initial estimate; then an iterative solution procedure can be used for the non-LQP problem. This process constitutes the so-called DDP. Murray and Yakowitz(1979) have accomplished the extension of DDP to problems with linear constraints.

From the above discussion, it can be seen that DDP does overcome the curse of dimensionality in the case of deterministic problems. However, the reservoir systems contain uncertainty. The uncertainty problem has been treated with the chance-constraint type of formulation or stochastic programming techniques.

Young(1967) introduced the Monte Carlo DP, which is an implicitly stochastic approach. Similar to this approach is the Alternate Stochastic Optimization presented by Croley(1974), Takasao, Ikebuchi and Kojiri(1976, 1980). It is apparent that if possible the approach that explicitly considers uncertainty is better than implicitly stochastic approaches. The class of typical DP models that explicitly consider uncertainty in the optimization procedure includes the models using Markov chain input process description and backward DP(Schweig and Cole 1968; Butcher, 1971; Su and Deininger, 1972, 1974; Arunkumar and Yeh, 1973; Alarcon and Marks, 1979; Buchanan and Bras 1981; etc.). In general, the models of this class perform satisfactorily in a small system(of 2 - 3 reservoirs). However, their extension to multireservoir systems is seriously limited due to dimensionality problems. The greatest disadvantage of the Markov chain DP formulation is its inability to explicitly produce policies satisfying probabilistic constraints. Such a constraint, for example, could be a reservoir storage requirement not to exceed(or fall below) a certain level with probability $\gamma(0 \leq \gamma \leq 1)$. Statements like the above are

very useful in evaluating the performance of control policies for stochastic reservoir systems. If it is not possible for the optimization program to meet such specifications, the practice is to follow a trial-and-error approach. Namely, a certain policy obtained by the optimization model is modified (certain constraints are tightened, penalty terms are introduced to or dropped from the objective function, etc.) with the hope that the new policies will give better results. Clearly, the approach is not set up in a defined manner and can be costly.

Wasimi and Kitanidis (1983) modeled the system dynamics by a set of actual and conceptual (corresponding to the river reaches) linear reservoirs and employed a quadratic penalty cost functional to force the system's state trajectory onto a prespecified track. The inputs were assumed to be Gaussian random variables and the formulation did not consider state or control constraints. Because of the characteristics of the LQG (Linear dynamics, Quadratic performance and Gaussian uncertainty) problem as mentioned earlier, the DP solution was obtained in analytical form which minimized the computational burden.

The model developed by Georgakakos (1983) and Georgakakos and Marks (1985) also employed the actual-conceptual reservoir system configuration, but it allowed for nonlinear dynamics and general performance functional. Here the objective was to identify the most rewarding state and control trajectories and the procedure consisted of an iterative optimization scheme. At each iteration a quadratic approximation of the objective function and a local linearization of the dynamics around the nominal trajectories provided by a Taylor series expansion were performed to construct a local LQG approximation of the original problem. The solution obtained in a recursive

analytical form gave rise to new state and control trajectories until convergence. The method exhibited a fast convergence rate and had a provision for probabilistic state constraints. However, since the Taylor series expansion used is a local approximation technique, the more the stochastic state variables deviate from the nominal trajectories, the less the LQG approximation of the original problem provided by Taylor series expansion is representative of the original problem (we shall discuss the nature of Taylor series expansion in the next section). The validity of the approximation is further jeopardized by the presence of system noise for, if intense, the noise causes frequent departures of the state variable away from the nominal trajectories.

Both of the previous two models allowed for updating of the current state estimates via a Kalman (or an extended Kalman) filter estimator.

The preceding survey of stochastic reservoir control studies indicated that a comprehensive model efficiently accounting for the peculiar reservoir system characteristics is still lacking. It also brought up a variety of properties which such a model should possess. Based on the many potential advantages of the previous approaches, this work will continue along these same lines. The intention is to perfect the control design so as to be efficient in handling most system idiosyncrasies. Summarily, this study will present a general reservoir system model including not only river segments and reservoirs but also hillslope systems. The solution will be obtained by a method named Statistically Approximated Linear Quadratic Gaussian (SALQG) controller, which is based on the Open-Loop Feedback Controller (OLFC). The statistical second-order approximation

technique will be applied instead of the Taylor series expansion to construct the LQG approximation of the original problem.

4.2 Statistical Second-Order Approximation

When the uncertainty of a reservoir system is considered explicitly, the state vectors are random variables, and the system dynamics, objective function and observation equations usually contain some terms that are nonlinear with respect to the state vectors. Thus, the problem of how to handle these nonlinear terms arises. The classical and widely used technique is to approximate them by means of Taylor series. However, because the Taylor series expansion is a local approximation technique, generally it cannot give a satisfactory approximation of a random nonlinear function. In this study we shall apply the theory of statistical second-order approximation developed below for handling the nonlinear function of random variable (for the details see Bierman(1977), Takasao and Shiiba(1984)).

4.2.1 Theory of Statistical Second-Order Approximation

Suppose that an $N \times 1$ random vector $X \sim N(\bar{X}, \bar{P})$, $\bar{P} > 0$, is given, for which $N(\bar{X}, \bar{P})$ denotes the Gaussian distribution with a mean vector of \bar{X} and a variance matrix of \bar{P} . In practice, often \bar{X} is merely the estimate of X , and \bar{P} is the corresponding estimation error variance matrix. Therefore, we cannot be sure that X exactly obeys the Gaussian distribution. However, even for such cases we make the simplifying assumption that $X \sim N(\bar{X}, \bar{P})$ to obtain the statistical approximation. Now, consider a nonlinear function $g(X)$. Choosing a scalar B^* , a $1 \times N$ vector H , and an $N \times N$ symmetric matrix A so that they minimize

$$E\{ |g(X) - [B^* + H(X - \bar{X}) + \frac{1}{2}(X - \bar{X})^T A (X - \bar{X})]|^2 \} \quad , \quad (4.1)$$

we approximate $g(X)$ by

$$[g(X)]_2 = B^* + H(X-\bar{X}) + \frac{1}{2}(X-\bar{X})^T A (X-\bar{X}) \quad (4.2)$$

we call this approximation the statistical second-order approximation of $g(X)$, denoting it by $[g(X)]_2$. When $g(X)$ is a vector-valued function, we take the statistical second-order approximation for each component function.

The values of B^* , H , and A can be calculated from the following equations, which are obtained by setting the partial derivatives of Eq.(4.1) with respect to B^* , H , and A equal zero.

$$B^* = E\{g(X)\} - \frac{1}{2}\text{tr}[A\bar{P}] \quad (4.3)$$

$$\bar{P}H^T = E\{(X-\bar{X})g(X)\} \quad (4.4)$$

$$\bar{P}A\bar{P}^T = E\{(X-\bar{X})(X-\bar{X})^T g(X)\} - E\{g(X)\}\bar{P} \quad (4.5)$$

in which $\text{tr}[\cdot]$ denotes the trace of the matrix in the brackets

The solutions of these equations can be easily obtained if the UDU^T factorization of the variance matrix \bar{P}

$$\bar{P} = \bar{U}\bar{D}\bar{U}^T \quad (4.6)$$

is available, in which \bar{U} is an upper triangular $N \cdot N$ matrix with unit diagonals and D is a positive diagonal $N \cdot N$ matrix. The random vector X then can be expressed as

$$X = \bar{X} + \bar{U}Z \quad (4.7)$$

in which $Z \sim N(0, D)$ is an $N \cdot 1$ random vector. The expectations in these equations can be computed from the Hermite-Gauss integration formula (Abramowitz and Stegun, 1972):

$$\int_{-\infty}^{\infty} \exp(-z^2) f(z) dz \approx \sum_{i=1}^N w_i f(z_i) \quad (4.8)$$

in which N is a positive integer, z_i is the i th zero of the Hermite polynomial $H_N(z)$ and w_i is the weight corresponding to z_i . If we set

$$\beta_i = \sqrt{2} z_i, \quad p_i = w_i/2 \quad (4.9)$$

the above formula is rewritten as

$$\int_{-\infty}^{\infty} \frac{1}{\sqrt{2\pi}} \exp(-z^2/2) f(z) dz \approx \sum_{i=1}^N p_i f(\beta_i) \quad (4.10)$$

which gives the approximation of the expectation of $f(Z)$ for $Z \sim N(0, 1)$. More generally, for $Z=(Z_1, \dots, Z_N)^T \sim N(0, \bar{D})$, we have

$$E\{f(Z)\} \approx \sum_{i_1, \dots, i_N=1}^N f(\sqrt{d_1} \beta_{i_1}, \dots, \sqrt{d_N} \beta_{i_N}) p_{i_1} \dots p_{i_N} \quad (4.11)$$

in which d_i denotes the (i,i) element of the diagonal matrix \bar{D} . For example, for $N=2$, $(\beta_i, p_i)=(-1, 0.5), (1, 0.5)$, and for $N=3$, $(\beta_i, p_i)=(-\sqrt{3}, 1/6), (0, 2/3), (\sqrt{3}, 1/6)$.

Note that the number of evaluations of function values for obtaining the expectation is N^N ; therefore, the amount of computation will become explosively large as N increases. Fortunately, however, in many cases we can reduce the amount of computation considerably due to the following properties:

- (1) The statistical second-order approximation of a first-order polynomial is equal to the original polynomial itself; i.e., for constant a_1 , a_2 , and a_3 ,

$$[a_1 X^2 + a_2 X + a_3]_2 = a_1 X^2 + a_2 X + a_3 \quad (4.12)$$

- (2) The statistical second-order approximation is a linear operation; i.e., the property

$$[g_1(X) + g_2(X)]_2 = [g_1(X)]_2 + [g_2(X)]_2 \quad (4.13)$$

holds.

- (3) If the function $g(X)$ depends only on a partial vector V of X , then $[g(X)]_2 = [g(V)]_2$ can be obtained by considering only the marginal distribution of V . Thus, denoting the dimension of V by M , the number of evaluations of function values is reduced to $N^M < N^N$.

As to the proof of these properties, we refer to Takasao and Shiiba(1984), and Takasao, Shiiba and Tomisawa(1984). From properties (1) and (2), it is clear that we need to consider only nonlinear terms that are not second-order polynomials. Such terms are often of type described in (3); therefore, considerable computation can be eliminated.

In practical applications, it is usually more convenient to rewrite Eq.(4.2) as

$$[g(X)]_2 = B + HX + \delta \tag{4.14}$$

in which

$$B = B^* + \frac{1}{2}\text{tr}[A\bar{P}] - H\bar{X} \tag{4.15}$$

$$\delta = \frac{1}{2}(X - \bar{X}) A (X - \bar{X})^T - \frac{1}{2}\text{tr}[A\bar{P}] \tag{4.16}$$

Then it can be seen that δ has a mean of zero and a variance of $R_\delta = \frac{1}{2}\text{tr}[A\bar{P}A\bar{P}]$ and is uncorrelated with X . (Note: If the covariance of two random variables is equal to zero, they are said to be uncorrelated. Even if two random variables are uncorrelated, they can be dependent. This is such a case.) We can show that when $g(X)$ is a vector-valued function, this property also holds. By denoting the dimension of $g(X)$

by m , if we take the approximations Eq(4.14) for individual component functions of $g(X)$

$$[g_1(X)]_2 = B_1 + H_1 X + \delta_1, \quad \delta_1 = \frac{1}{2}(X - \bar{X}) A_1 (X - \bar{X})^T - \frac{1}{2} \text{tr}[A_1 \bar{P}]$$

.

$$[g_m(X)]_2 = B_m + H_m X + \delta_m, \quad \delta_m = \frac{1}{2}(X - \bar{X}) A_m (X - \bar{X})^T - \frac{1}{2} \text{tr}[A_m \bar{P}]$$

and concatenate them to the same form as Eq.(4.14), then δ is uncorrelated with X and

$$E\{\delta\} = 0 \tag{4.17}$$

$$R_\delta = \{E\{\delta_i \delta_j\}\} = \left\{ \frac{1}{2} \text{tr}[A_i \bar{P} A_j \bar{P}] \right\} \tag{4.18}$$

Here the convention that $\{x_{ij}\}$ denotes a matrix with x_{ij} , an element in the i -th row and j -th column, is used.

To obtain theoretical insight into the nature of the statistical second-order approximation, denote by ε , the error in the statistical second-order approximation of $g(X)$, that is

$$g(X) = B + HX + \delta + \varepsilon \tag{4.19}$$

Then ε has a zero mean and is uncorrelated with X and δ . Based on this and the fact that the sum of the first two terms, $B + HX$, on the right-hand side of Eq(4.18) is obtained by statistical linearization (defined by omitting the second-order term from the formulation of statistical second-order approximation) it turns out that the statistical second-order approximation allows us to evaluate the lower limit of the variance of the error in the approximation by statistical linearization.

4.2.2 Relationships between the Expectation of a Stochastic Function
and the Statistical Second-Order Approximation

Suppose that an $N \times 1$ random vector $X \sim N(\bar{X}, \bar{P})$, $\bar{P} > 0$, is given. Now consider a function of the mean vector \bar{X}

$$J(\bar{X}) = E\{g(X)\} \quad (4.20)$$

where $g(X)$ is a given non-linear function and the variance matrix \bar{P} is assumed to be constant.

Differentiating $J(\bar{X})$ with respect to the i^{th} component \bar{X}_i of the mean vector \bar{X} yields

$$\begin{aligned} \frac{\partial J(\bar{X})}{\partial \bar{X}_i} &= \frac{\partial}{\partial \bar{X}_i} \int_{-\infty}^{+\infty} g(X) \exp\left\{-\frac{1}{2}(X-\bar{X})\bar{P}^{-1}(X-\bar{X})^T\right\} / \sqrt{(2\pi)^N |\bar{P}|} \, dX \\ &= (\bar{P}^{-1})_i E\{(X-\bar{X})g(X)\} \end{aligned} \quad (4.21)$$

and

$$\nabla J(\bar{X}) = \left(\frac{\partial J(\bar{X})}{\partial \bar{X}_1} \quad \dots \quad \frac{\partial J(\bar{X})}{\partial \bar{X}_N} \right)^T = \bar{P}^{-1} E\{(X-\bar{X})g(X)\} \quad (4.22)$$

where $(\bar{P}^{-1})_i$ is the i th row of the inverse matrix, \bar{P}^{-1} , of the variance matrix \bar{P} .

Differentiating $\nabla J(\bar{X})$ with respect to \bar{X}_i once again we obtain

$$\frac{\partial^2 J(\bar{X})}{\partial \bar{X}_i \partial \bar{X}_j} = (\bar{P}^{-1})_i E\{(X-\bar{X})(X-\bar{X})^T g(X)\} [(\bar{P}^{-1})_j]^T - (\bar{P}^{-1})_{ij} E\{g(X)\} \quad (4.23)$$

and

$$\nabla^2 J(\bar{X}) = \bar{P}^{-1} E\{(X-\bar{X})(X-\bar{X})^T g(X)\} [\bar{P}^{-1}]^T - \bar{P}^{-1} E\{g(X)\} \quad (4.24)$$

On the other hand, from Eqs.(4.4) and (4.5) we can obtain

$$H^T = \bar{P}^{-1} E\{(X-\bar{X})g(X)\} \quad (4.25)$$

$$A = \bar{P}^{-1} E\{(X-\bar{X})(X-\bar{X})^T g(X)\} [\bar{P}^{-1}]^T - \bar{P}^{-1} E\{g(X)\} \quad (4.26)$$

Comparing Eqs.(4.22) and (4.24) with Eqs.(4.25) and (4.26) we find that

$$\nabla J(\bar{X}) = H^T \quad (4.27)$$

$$\nabla^2 J(\bar{X}) = A \quad (4.28)$$

This means that if the variance matrix is fixed the Gradient vector and the Hessian matrix of the non-linear function with respect to the mean vector \bar{X} , $J(\bar{X}) = E\{g(X)\}$, are equal to the coefficients of the first- and second-order terms of the statistical second-order approximation of $g(X)$ respectively.

Now consider the approximation of $g(X)$ by the Taylor series expansion,

$$g(x) \approx g(\bar{X}) + N_X^T (X-\bar{X}) + \frac{1}{2} (X-\bar{X})^T N_{XX} (X-\bar{X}) \quad (4.29)$$

in which

$$N_X = \left(\frac{\partial g(\bar{X})}{\partial \bar{X}_1} \quad \dots \quad \frac{\partial g(\bar{X})}{\partial \bar{X}_N} \right)^T$$

$$N_{XX} = \begin{bmatrix} \frac{\partial^2 g(\bar{X})}{\partial \bar{X}_1 \partial \bar{X}_1} & \dots & \frac{\partial^2 g(\bar{X})}{\partial \bar{X}_1 \partial \bar{X}_N} \\ \vdots & & \vdots \\ \frac{\partial^2 g(\bar{X})}{\partial \bar{X}_N \partial \bar{X}_1} & \dots & \frac{\partial^2 g(\bar{X})}{\partial \bar{X}_N \partial \bar{X}_N} \end{bmatrix}$$

In general,

$$N_X \neq H^T \quad (4.30)$$

$$N_{XX} \neq A \quad (4.31)$$

and consequently

$$\nabla J(\bar{X}) \neq N_X \quad , \quad \nabla^2 J(\bar{X}) \neq N_{XX} \quad (4.32)$$

From the above discussion, it can be seen that the Taylor approximation cannot correctly evaluate the Gradient vector and Hessian matrix of $J(\bar{X}) = E\{g(X)\}$ while the statistical second-order approximation can evaluate them correctly. This nature of the statistical second-order approximation is expected to result in a faster convergence rate of the optimization procedure in which the statistical second-order approximation is used and make the procedure more reliable.

Figure 4.1 is an example which shows the difference between the Taylor approximation and the statistical second-order approximation, where the non-linear function $g(X)$ is

$$g(X) = (X-a)(X-3a)(X-4a)^2 \quad , \quad a = 0.9$$

Comparing #2 or #3 with #4 we find that the Taylor approximation is a local approximation around the mean. Comparing #2 with #3 it can be seen that the global approximation characteristic of the statistical second-order approximation becomes more apparent as the variance of the random variable X increases.

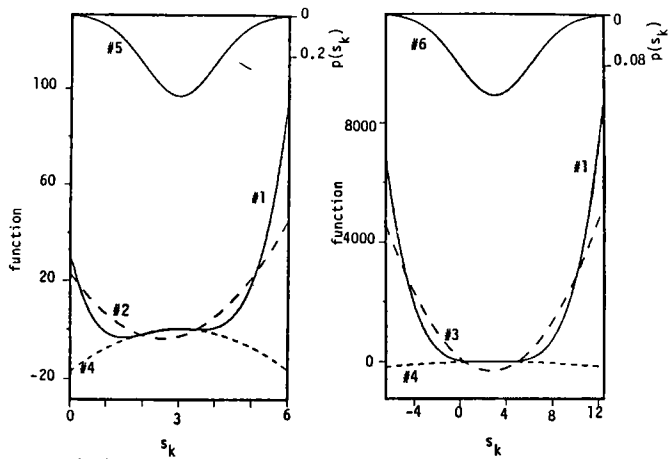


Figure 4.1 Approximation of nonlinear function of stochastic variable.

- #1: original function $l_4(s_k)$.
- #2: second-order approximation function by statistical approximation method while $s_k \sim N(3, 1)$.
- #3: second-order approximation function by statistical approximation method while $s_k \sim N(3, 10)$.
- #4: second-order approximation function by Taylor approximation method at $s_k=3$.
- #5: probability density function $p(s_k)$ while $s_k \sim N(3, 1)$.
- #6: probability density function $p(s_k)$ while $s_k \sim N(3, 10)$.

4.3 Modeling of Multireservoir Systems

The design of a controller is the second basic step of a control study. Prior to this step a credible and mathematically treatable system model must be developed. Based on physical considerations, this section will show how to represent a general reservoir system by a set of ordinary differential equations.

4.3.1 General Characteristics of a Reservoir System

A typical reservoir system consists of the following elements.

a. A set of drainage basins where the lateral flows as the outputs of the rainfall-runoff processes enter into rivers. Runoff models are used to describe this subsystem.

b. A set of reservoirs located at various river branches. Each reservoir accepts an inflow from the upstream system, contains $s(t)$ water volume, loses or gains additional water due to evaporation seepage or rainfall at a rate $e(t)$, and releases at the controllable rate $u(t)$. Each storage variable $s(t)$ is restricted to vary within a positive bounded range, $s^{\min}(t) \leq s(t) \leq s^{\max}(t)$. From physical and operational considerations, similar bounds govern each release: $u^{\min}(t) \leq u(t) \leq u^{\max}(t)$.

c. A set of river segments providing the hydrologic linkage among the existing reservoirs as well as among the reservoirs and hillslope runoff systems. Along the river segments and from the reservoirs, a number of water diversions (possible generating return flows) may supply water to municipal, agricultural, or industrial sites.

d. A set of objectives that the system is expected to serve. A general set of typically established objectives includes flood protection, water supply for municipal, agricultural, and industrial use, energy generation, recreation, navigation, water quality improvement, and wildlife enhancement.

e. A set of hydrologic inputs (as, for example, precipitation or the flows from adjacent hillslopes) which enter the system at various boundary locations.

Loosely speaking, the reservoir control problem is to identify optimal schedules of the controllable variables which will guide the system to successfully meet its objectives. This is a rather difficult task due to the following system idiosyncracies: (1) uncertainty, (2) non-linearity, (3) high dimensionality, and (4) multiplicity of conflicting objectives.

In turn, the reservoir system's uncertainty may be due to the following sources:

a. Hydrological input or natural uncertainty. Once the system is defined, the inputs are used to represent the real world lying outside its boundaries. For example, the precipitation is a stochastic process. Consequently, the uncertainty of the omitted processes (e. g. atmospheric randomness) will carry over to the inputs. while the corresponding dynamics will induce temporal and spatial correlation structure in their behavior (e. g. seasonalities, etc.).

b. Uncertainty due to imperfect knowledge concerning response of the reservoirs, of the river segments and of the drainage. This is known as model uncertainty.

c. Uncertainty due to the objectives (e. g. random demand fluctuations, or economic uncertainty).

d. Uncertainty due to observation errors

Nonlinearities in the system dynamics may be due to the reservoirs and the river segments as well as the drainage basins. The reservoir nonlinearities are caused by the evaporation and seepage processes taking place through the reservoir's irregular surfaces and also by the various constraints. The river segments and drainage basins are nonlinear elements due to many reasons: e. g. frictional effects of bottom and land surface as well as soil, fluid viscosity, turbulence, channel nonuniformity, seepage, etc.

There are many examples of large reservoir systems all over the world. For example, the Huang-He river system in China consists of at least 50 hydroprojects.

Reservoir systems are usually characterized by conflicting objectives; i. e., a certain control sequence which successfully achieves one objective may be undesirable for another. (Conflicts arise, for example, between hydroenergy generation and flood protection, or due to incompatible water use demand patterns.) Furthermore, if the system is capable of long-term river control (i. e. if the existing storage capacity gives multiyear management flexibility of the input process water volumes), then there exist multiple time scales to which the objectives pertain. Namely, the system performs successfully if it performs well from short to considerably longer time periods (e. g. a few hours to a few years)

After this preliminary introduction to the reservoir system characteristics, we next discuss the development of a representative system model.

4.3.2 System Model Development

Following Takasao and Shiiba(1984), by defining "appropriately" the state variables, most of the existing runoff models can be rewritten into the state-space runoff model with the following form:

$$\frac{dS_{ij}(t)}{dt} = f_{ij}(S_{ij}(t), r(t)) + \omega_{ij}(t) \quad (4.33)$$

$$y_{ij}(t) = g_{ij}(S_{ij}(t)) + v_{ij}(t) \quad (4.34)$$

where

ij: jth subbasin of ith basin

r(t): mean rainfall over ij subbasin

$\omega_{ij}(t)$: model noise

$f_{ij}(\cdot, \cdot)$, $g_{ij}(\cdot)$: non-linear function

$y_{ij}(t)$: observation

$v_{ij}(t)$: observation noise

t: time

For a reservoir, consider the following quantities at any time t:

ij: jth reservoir of ith river

$S_{ij}(t)$: water volume contained in the ij reservoir

$I_{ij}(t)$: inflow rate to the reservoir from the upstream system

$U_{ij}(t)$: rate of controlled releases

$L_{ij}(t)$: net water loss rate from evaporation, seepage, and rainfall, etc.

$\omega_{ij}(t)$: model noise due to the imperfect knowledge concerning the response of the reservoir

then the conservation of mass law for the ij^{th} reservoir can be expressed by

$$\frac{dS_{ij}(t)}{dt} = I_{ij}(t) - U_{ij}(t) - L_{ij}(t) + \omega_{ij}(t) \quad (4.35)$$

Consider the loss term $L_{ij}(t)$ and denote the following: (1) $e_{ij}(t)$ the net [(evaporation) - (rainfall)] rate per unit of the reservoir lake's surface area, (2) $A_{ij}(S_{ij}(t))$ the reservoir's surface area in terms of the stored volume, (3) h_{ij} a seepage coefficient per unit of water elevation, and (4) $E_{ij}(S_{ij}(t))$ the function giving water elevation in terms of the lake's volume. Then

$$L_{ij}(t) = e_{ij}(t)A_{ij}(S_{ij}(t)) + h_{ij}E_{ij}(S_{ij}(t)) \quad (4.36)$$

In reality the relationship yielding the seepage losses is much more complicated. (The coefficient h_{ij} varies spatially and the form of the seepage term depends on the general groundwater hydrology of the lake's area.) However, because of the distributed parameter nature of the underlying phenomena(spatial nonuniformity), it is most likely that they will require a lumped parameter representation(as in Eq.(4.36)) to be hypothesized and estimated from available input-output data. The inflow $I_{ij}(t)$ in Eq.(4.35) is the output from the system lying upstream of the ij^{th} reservoir(e.g., outflow rate from the upstream river segment and/or the drainage basin. The outflow from the drainage basin is expressed by Eq.(4.34). Here, the observation noise can be considered to be contained in the model noise.) If apart from the release $U_{ij}(t)$ there also exists some other constant water abstraction(say, in the form of a water supply diversion), it can be

incorporated into the inflow $I_{ij}(t)$ which should then be reduced by the corresponding abstraction rate.

Consider now the river segment i shown in Figure 4.2. It can be thought of as a number of cascaded conceptual (fictitious) reservoirs each of which stores and releases water according to the conservation of mass law:

$$\frac{dS_{ij}(t)}{dt} = I_{ij}(t) - Q_{ij}(t) - L_{ij}(t) + \omega_{ij}(t) \quad (4.37)$$

where

ij : j th conceptual reservoir of i th reach

$S_{ij}(t)$: water volume contained in the ij conceptual reservoir

$I_{ij}(t)$: inflow rate from the upstream system

$Q_{ij}(t)$: outflow rate

$L_{ij}(t)$: seepage loss rate from evaporation, seepage, and rainfall, etc.

$\omega_{ij}(t)$: model noise due to the imperfect knowledge concerning the response of the river segment

It might be that $L_{ij}(t)$ is negative, implying gains from groundwater.

$I_{ij}(t)$ may be the outflow $Q_{ij-1}(t)$ of the previous conceptual reservoir, or the previous outflow minus the rate of any existing diversion, or the outflow plus any return flow. If $j=1$, $I_{i1}(t)$ may be the outflow rate from the upstream drainage basin, or an actual reservoir's release, or the the final outflow of another branch, or some combination of the above.

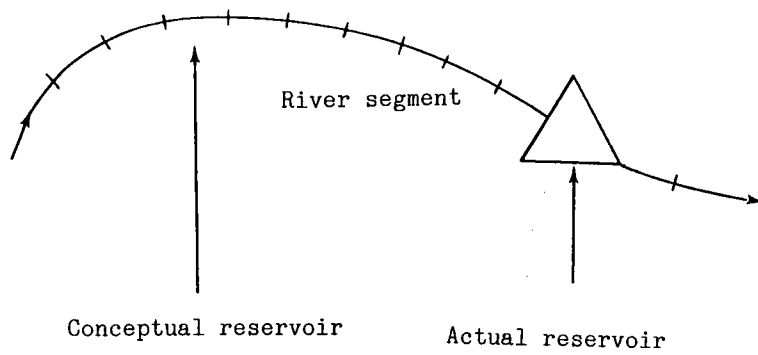


Figure 4.2 River segment and conceptual reservoir

From kinematic wave considerations one can deduce a relationship of the following form for the outflow $Q_{ij}(t)$:

$$Q_{ij}(t) = \alpha_{ij} S_{ij}^{m_{ij}}(t) \quad (4.38)$$

Under certain uniformity assumptions for the channel geometry and flow condition, one can express the coefficients α_{ij} and m_{ij} in terms of physical parameters such as bottom longitudinal slope, channel length and width, roughness coefficient, and water depth(Georgakakos and Bras, 1980). However, owing to the distributed parameter nature of the physical situation, it is suggested that these coefficients be estimated rather than obtained from the previous relationships. (In an estimation scheme the coefficients derived by physical considerations may serve as initial guesses.)

The seepage(or infiltration) losses can be represented(Burkham, 1970a,b; Granados and Bras, 1983) by a similar expression of the following form

$$L_{ij}(t) = k_{ij} S_{ij}^{\beta_{ij}}(t) \quad (4.39)$$

where β_{ij} lies approximately in the range [0.8, 1.2](Georgakakos and Marks, 1985) and k_{ij} is the infiltration coefficient. Typically, these coefficients are assumed constant over the same river segment or constant over the whole basin.

The dynamics of the entire system can then be modelled by combining the previous representations of the individual river segments with the actual reservoirs and drainage basins. To facilitate the notation let the system dynamics be expressed by the following vector differential equation

$$\frac{dS(t)}{dt} = F(S(t), r(t)) + L U(t) + \omega(t) \quad (4.40)$$

where $S(t)$ is an N_s dimensional vector including all drainage basin state variables and all actual and conceptual reservoir storage variables, $U(t)$ is an N_u dimensional vector of the controllable releases, $r(t)$ is an N_r dimensional vector of the rainfalls, $F(\cdot, \cdot)$ is an N_s dimensional time varying non-linear function, L is an $N_s \cdot N_u$ dimensional matrix associating the control vector elements with the appropriate differential equation (Obviously, the elements of this matrix are 1 or 0.) $\omega(t)$ is an N_s dimensional system noise, it is used to account for model and other error sources, and usually assumed to be a white Gaussian process with zero mean and spectral density matrix $Q_w(t)$:

$$E\{\omega(t) \cdot \omega(s)^T\} = Q_w(t) \delta(t-s) \quad (4.41)$$

in which $\delta(t-s)$ is the dirac delta function which is zero everywhere except at the origin, $t=s$, where it goes to infinity.

Under the availability of input-output data records, it is best to determine the various model parameters by a parameter estimation scheme. We shall omit the system identification since it does not affect the controller development in the subsequent sections. For the detail applications of the system identification theory, the reader is referred to Kitanidis and Bras(1978), Georgakakos and Bras(1980, 1982), and Restrepo Posada and Bras(1982).

Finally, the actual reservoir water elevation and hillslope runoff discharge as well as river discharge measurements will be grouped into a vector $y(t)$ related to the system's state vector through

$$y(t) = H(S(t)) + v(t) \quad (4.42)$$

where $v(t)$ is a white Gaussian process added to account for observation errors and has zero mean and spectral density matrix $Q_v(t)$:

$$E\{v(t) \cdot v(s)^T\} = Q_v(t) \delta(t-s) \quad (4.43)$$

4.3.3 Modeling of the System's Objectives

A major difficulty in the development of reservoir control models is to derive a suitable objective function. This is primarily due to (1) the stochastic nature of several variables present in any model, (2) the inadequacy of expected or average performance criteria to reflect the typical decision maker's aversion to poor outcome of an adopted set of release policies, (3) the multiobjective nature of reservoir operation, and (4) the antagonistic nature of the objectives.

Items (1) and (2) above are closely related. As an alternative to the expected performance criterion, a utility function can be used to reflect the risk-averting attitudes of decision makers (Dantzig, 1956, Davis, 1975, Datta and Burges, 1984, Orlovski et al., 1984, Loaiciga et al., 1986). In this study, we shall reflect the risk aversion of decision makers to poor performance of release schedules by a stringent set of constraints on the reservoir pool.

Typically, a reservoir system is expected to serve several objectives; water supply for municipal, agricultural, or industrial use, flood protection, hydropower generation, navigation, water quality control, recreation, and wildlife enhancement constitute a set of generally accepted reservoir system objectives.

What complicates the reservoir control problem even more than the multiplicity of objectives is their antagonistic nature. Take, for instance, hydropower generation and flood protection. For the purposes of the former, it is profitable to maintain reservoir storages close to capacity so that the power turbines are under the highest possible hydraulic head. At the same time for the fear of severe flooding events, one would prefer to operate the system at lower reservoir

elevations to safely attenuate the flood wave hydrograph. Similar conflicts also exist between water supply and hydropower generation, navigation and water supply, as well as among other objectives.

In multiobjective optimization one is interested in solutions which belong on the problem's Tradeoff Surface otherwise known as Transformation or Pareto Optimal Surface. A Pareto Optimal solution is noninferior with respect to any other feasible solution in the sense that it performs strictly better toward at least one objective. In deterministic problems, the Pareto Optimal Surface and methods for its reconstruction have been well studied(Haimes,1977). Stochastic multiobjective problems have not been as well explored and the Pareto Optimal Surface still needs to be defined.

Reservoir systems are usually provided by operating priorities mandated by institutional agreements. The agreements establish a specific priority ranking on the system objectives and prescribe mandatory performance levels. A commonly encountered ranking(Yeh, 1982) appoints flood protection, water supply, water quality control and navigation as the primary objectives and states that the remaining objectives be met so far as they are consistent with the primary ones. From the analyst's point of view, these specifications restrict the investigation of the problem's Tradeoff Surface to that portion which meets the set requirements. Including recreation and wildlife enhancement in the set of primary objectives or assuming that they are implicitly satisfied when water quality standards are met, the following approach for multiple objective reservoir operations can be proposed. Constrain the operation to always meet the primary objectives and maximize the hydropower production as far as possible. Conceptually, this transforms the multiobjective problem into a single objective optimization, but at the same time it allows reconstruction

of the Tradeoff Surface by varying the constraint levels or changing the optimized objective. This section will discuss how this general approach for treating multiple objectives can be quantified in relation to the system model developed in the previous section. The intention is to present a modeling framework which can be flexibly adjusted in specific applications.

Consider, for example, that a system's manager agreed to supply a user with $q(t)$ volume of water per unit of time for a specified time period $[0, T]$ at reliability not less than $[1 - \gamma_{jk}^{\min}(t)]$. Assume further that the diversion is located downstream of conceptual reservoir jk . An equivalent probabilistic statement can be written with respect to the corresponding reservoir storage variable $S_{jk}(t)$:

$$\int_{-\infty}^{S_{jk}^{\min}(t)} p(S_{jk}(t), t) dS_{jk}(t) \leq \gamma_{jk}^{\min}(t) \quad (4.44)$$

in which $S_{jk}^{\min}(t) = [q(t)/\alpha_{jk}]^{1/m_{jk}}$ (c.f. Eq.(4.38)), $p(\cdot, \cdot)$ is the probability density function(p.d.f.) of $S_{jk}(t)$ at time t , and the lower limit of the integral represents the value below which $S_{jk}(t)$ cannot lie with probabilistic significance. Thus the requirement to meet the water supply demand at $[1 - \gamma_{jk}^{\min}(t)]$ reliability level is mathematically equivalent to constraining the p.d.f. of the storage variable $S_{jk}(t)$ in a region above a certain bound. This bound is characterized by two parameters: (1) $S_{jk}^{\min}(t)$ which is specified by the demand level through Eq.(4.38) and (2) $\gamma_{jk}^{\min}(t)$ which gives the probability of failing to satisfy this demand. It is noted that as the demanded level becomes greater and /or the probability of violation

becomes smaller, constraint Eq.(4.44) increasingly confines the p.d.f.'s feasible region.

The previous example was presented to illustrate the claim that the requirement to satisfy system objectives at prespecified reliability levels implies probabilistic constraints on the system state variables.

As a second case, consider flood protection. The associated probabilistic constraints can be easily derived after specifying two characteristic parameters per storage variable: That is, the flood level $S_{jk}^{\max}(t)$ which the storage is not allowed to exceed and the probability of exceedance $\gamma_{jk}^{\max}(t)$. For an actual reservoir, $S_{jk}^{\max}(t)$ can be taken equal to reservoir's capacity(above which water flows down the spillway), while for a conceptual reservoir $S_{jk}^{\max}(t)$ can be defined by the flood discharge level $q^{\max}(t)$ and the relationship

$$S_{jk}^{\max}(t) = [q^{\max}(t)/\alpha_{jk}]^{1/m_{jk}} \quad (4.45)$$

The flood protection reliability constraint can then be stated by

$$\int_{S_{jk}^{\max}(t)}^{+\infty} p(S_{jk}(t),t)dS_{jk}(t) \leq \gamma_{jk}^{\min}(t) \quad (4.46)$$

This constraint restricts the state's p.d.f. to lie below some upper bound and becomes more restrictive for smaller $\gamma_{jk}^{\max}(t)$ and/or as less severe flood condition levels established.

The navigation objective calls for water level fluctuations within a certain range determined by the adjustability of the port structures and the navigability of the river branches. These ranges together with the reliabilities assigned to navigation by the system manager imply two more probability constraints per storage variable.

Water quality control can similarly be treated by requiring river flows to be greater than a critical level above which adequate effluent diffusion takes place.

Similar bounds on the system's storage variables can be imposed by the recreation objective after specifying the operating range of the recreational facilities along with the desirable reliability level.

Thus, it is generally valid that the system objectives can be quantified by a set of reliability constraints on each actual and conceptual storage variable. (As explained, hydropower production will not be treated by a constraint, but rather it will be maximized given that all other system objectives are satisfied at the prespecified levels.) The constraints are categorized into upper and lower types and the most severe one can be determined from each group. (Note that both the storage thresholds and the probabilities of violation determine which are the most severe constraints. Figure 4.3 illustrates a case where flood protection is more binding than water quality control.) It is evident that if the p.d.f. of a storage variable meets the most severe constraints from the upper and lower group, it also meets all others. Below these two constraints will be denoted by

$$\int_{-\infty}^{S_i^{\min}(t)} p(S_i(t), t) dS_i(t) \leq \gamma_i^{\min}(t) \quad (4.47)$$

$$\int_{S_i^{\max}(t)}^{+\infty} p(S_i(t), t) dS_i(t) \leq \gamma_i^{\min}(t) \quad (4.48)$$

where i scans the storage variables: $i=1, 2, \dots, N_s$. (For notational convenience, from here on the state variables will be referred to by one index i rather than by two jk .)

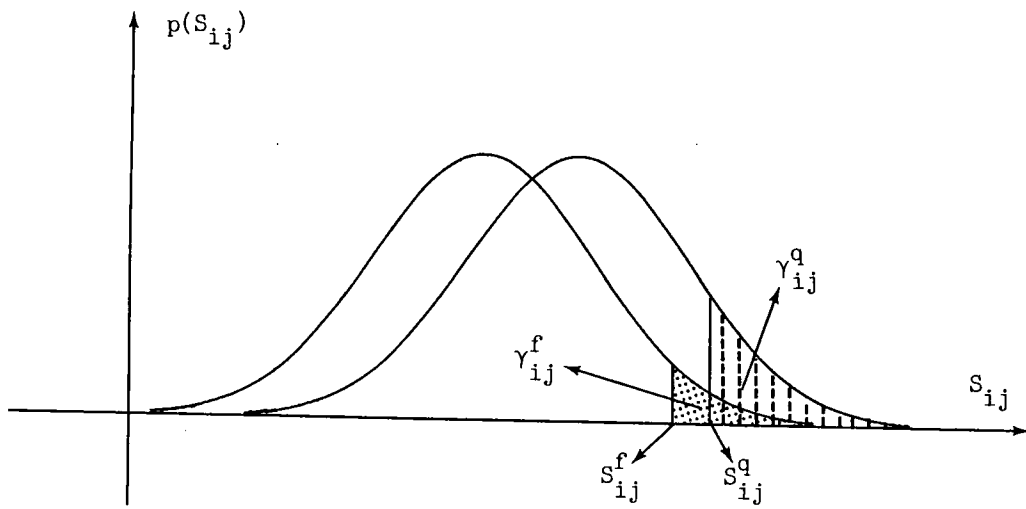


Figure 4.3 The most severe probability constraint

A Pareto optimal point corresponding to the previous reliability constraints can now be obtained by optimizing hydroelectric energy generation. This objective can be represented by the following performance index:

$$\min_{U(t)} E\left\{\int_0^T [G - \sum_j g_j(U_j(t), S_j(t))]^2 dt\right\} \quad (4.49)$$

where $E\{\cdot\}$ denotes expectation with respect to all random quantities, $U(t)$ is a vector including all $U_j(t)$, G is the total power demand assigned to hydroelectric units or the system's installed power capacity. $g_j(\cdot, \cdot)$ is the power production function for reservoir j . Performance index (4.49) maximizes energy generation by quadratically penalizing energy deficits from the total power demand of the maximal possible production.

Note that we can represent the index (4.49) by

$$\min_{U(t)} E\left\{\int_0^T g(U(t), S(t)) dt\right\} \quad (4.50)$$

where $g(U(t), S(t)) = [G - \sum_j g_j(U_j(t), S_j(t))]^2$

In order to compare the statistical second-order approximation with the Taylor approximation and make the explanation easier, in this study the following function with a special form will be used for $g(\cdot, \cdot)$:

$$g(U(t), S(t)) = l(U(t)) + m(S(t)) \quad (4.51)$$

As discussed in the beginning of this section, our objective has been to identify release(control) trajectories corresponding to points on the problem's Pareto Optimal Surface. A Pareto Optimal release trajectory $U^*(t)$ is defined here as the one which achieves the minimum value of performance index Eq.(4.50) given that it produces a probabilistic state trajectory satisfying the reliability constraints

imposed by all other system objectives. Other Pareto Optimal trajectories can be obtained by varying the probabilistic constraint levels and the entire Pareto Optimal surface can be generated and explored. Notice that the priority ranking of the system's objectives can be conveniently reflected by the allowable levels of probabilistic constraint violation. Between two objectives, the one of higher priority should have smaller $\gamma(t)$.

Having discussed the modeling of the system's dynamics and its objectives, we shall next proceed to formulate and consider the associated optimization problem.

4.4 Operation Problem of Multireservoir Systems

Based on the discussions of Section 4.3, we constructed the following mathematical system model:

a. System Dynamics:

$$\frac{dS(t)}{dt} = F(S(t), r(t)) + L U(t) + \omega(t) \quad (4.52)$$

b. Objective Function:

$$J = E\left[\int_0^T [l(U(t)) + m(S(t))] dt\right] \quad (4.53)$$

c. Constraints of Control Variables:

$$U_j^{\min}(t) \leq U_j(t) \leq U_j^{\max}(t), \quad j=1,2,\dots,N_u, \quad t \in [0, T] \quad (4.54)$$

d. Chance Constraints of State Variables

$$\int_{-\infty}^{S_j^{\min}(t)} p(S_j(t), t) dS_j(t) \leq \gamma_j^{\min}(t) \quad (4.55)$$

$$\int_{S_j^{\max}(t)}^{+\infty} p(S_j(t), t) dS_j(t) \leq \gamma_j^{\min}(t) \quad (4.56)$$

$$j=1,2,\dots,N_s, \quad t \in [0, T]$$

e. Continuing Operations After T

f. Observation Equation:

$$y(t) = H(S(t)) + v(t), \quad t \in [0, T] \quad (4.57)$$

where $S(t)$ is the N_s dimensional state vector, $S(0)$ is assumed to be a Gaussian random vector with mean S_0 and covariance P_{S0} ; $U(t)$ is the N_u dimensional control vector; $\omega(t)$ is the N_s dimensional random disturbance vector assumed to be Gaussian white noise (not autocorrelated in time) with zero mean and positive semidefinite spectral density matrix $Q_\omega(t)$, $\omega(t)$ is also assumed uncorrelated with

$S(0)$; $F(\cdot, \cdot)$ is the N_s dimensional time varying nonlinear function of the state and rainfall; $l(\cdot)$ is the nonlinear function of control vector; $r(t)$ is rainfall vector; $m(\cdot)$ is the nonlinear function of state vector; L is the $N_s \cdot N_u$ constant control coefficient matrix; $E\{\cdot\}$ denotes expectation with respect to all random quantities, namely $\{\omega(t), t \in [0, T]\}$, $\{v(t), t \in [0, T]\}$ and $S(0)$; $U_j^{\max}(t)$, $U_j^{\min}(t)$ are control thresholds, which may reflect physical or operational considerations (e.g., low flow requirements, etc.); $p(\cdot, \cdot)$ is the probabilistic density function of state variable and conditioned on all available measurements and all previously applied controls; $S_j^{\min}(t)$, $S_j^{\max}(t)$ are storage thresholds, $\gamma_j^{\min}(t)$, $\gamma_j^{\max}(t)$ are the probabilities of violation; $y(t)$ is the N_m dimensional measurements of actual reservoir elevations as well as discharge at gauged channel sections; $H(\cdot)$ is the nonlinear function of state vector and describes the relationships between reservoir elevation and storage as well as relationships between discharge and conceptual storage; $v(t)$ is the N_m dimensional random disturbance vector assumed to be Gaussian white noise (not autocorrelated in time) with zero mean and positive semidefinite spectral density matrix $Q_v(t)$, $v(t)$ is also assumed uncorrelated with $S(0)$ and $\omega(t)$.

The objective of the reservoir operation problem is to identify the release trajectory $\{U^*(t), t \in [0, T]\}$ which minimizes the objective function J subject to the constraints c.ve. given the reservoir system transits in Eq.(4.52) with which the observation Eq.(4.57) is associated. We call this problem PBO.

Clearly, it is necessary to forecast input rainfall intensity for identifying the future releases. We assume that a rainfall-forecasting system exists which provides the information of future inputs to us. Thus, if the rainfall vector at time $t=0$ is represented in a discrete time form:

$$X(0) = [X_0(0), \dots, X_{M-1}(0)]^T \quad (4.58)$$

the rainfall-forecasting system provides the forecast vector of rainfall:

$$\bar{X}(0) = [\bar{X}_0(0), \dots, \bar{X}_{M-1}(0)]^T \quad (4.59)$$

and the forecast error variance matrix:

$$V\{ X(0) - \bar{X}(0) \} = P_{X(0)} \quad (4.60)$$

where M is the number of lead time steps, $t_{m=0}=0$, $t_{m=M}=T$, T is control horizon, $X_t(0), t \in [t_m, t_{m+1}]$, are constant.

Like most interesting real world problems, the solution of the reservoir operation problem will involve a digital computer. Consequently, we find it appropriate to convert the previous formulation to the discrete time representation and work with difference rather than differential equations. This conversion is also justified because in a real application solutions of the operation problem are desired in monthly, weekly, daily, etc., time intervals.

Consider a deterministic, nominal control trajectory which is constant within each interval $[t_k, t_{k+1}]$, $k=0,1,\dots,K-1$:

$$\{ U^{\text{nom}}(t) = U^{\text{nom}}(t_k), t \in [t_k, t_{k+1}], k=0,1,\dots,K-1 \} \quad (4.61)$$

where $t_0=0$, $t_k=T$, and $\Delta t_k=t_{k+1}-t_k$. This form of the nominal control trajectory is due to the operational requirement.

Under these circumstances, we now convert the previous reservoir model in continuous time into a discrete-time, linear system in the time step $\Delta t_1=t_{1+1}-t_1$, $t_{1=0}=0$, $t_{1=L}=T$. t_1 must contain both the discrete points for rainfall forecasting, t_m , and the discrete points for nominal control trajectory, t_k . Furthermore, in order to guarantee that the difference scheme to be used is convergent, the time steps Δt_1 have to be taken very finely. Hereon, we assume:

$$\Delta t_k=t_{k+1}-t_k=t_{1+m_k}-t_1=\sum_{i=1}^{1+m_k-1} \Delta t_i \quad (4.62)$$

The rainfall in the time interval $[t_1, t_{1+1}]$, r_1 , now can be expressed by

$$r_1 = e_1^T X(0) \quad (4.63)$$

where e_1 is an M dimensional column vector and its mth element, e_{1m} , can be calculated from

$$e_{1m} = \begin{cases} 1, & t_1 \in [t_m, t_{m+1}] \\ 0, & \text{otherwise} \end{cases} \quad (4.64)$$

From Eq.(4.63) we obtain

$$\bar{r}_1 = E\{r_1\} = e_1^T \bar{X}(0), \quad \bar{r} = [\bar{r}_0, \dots, \bar{r}_{L-1}]^T \quad (4.65)$$

$$V\{r-\bar{r}\} = E P_{X(0)} E \equiv [P_{r0}, \dots, P_{rL-1}]^T \quad (4.66)$$

where $E = [e_0, \dots, e_{L-1}]^T$

We now show the discretizing procedure of the system dynamics Eq.(4.52). Suppose that the initial state vector $S(0) \sim N(\bar{S}_0, P_{s0})$ and that $r(t, t \in [t_0, t_{l+1}]) = r(0) \sim N(\bar{r}_0, P_{r0})$. We first approximate the vector function $F(S(0), r(t))$ by the statistical second-order approximation,

$$F_i(S(0), r(t)) = B_i^* + H_{s_i} [S(0) - \bar{S}(0)] + H_{r_i} [r(t) - \bar{r}_0] + \delta_i \quad (4.67)$$

where

$$\delta_i = \frac{1}{2} \begin{bmatrix} S(0) - \bar{S}(0) \\ r_0 - \bar{r}_0 \end{bmatrix}^T A_i \begin{bmatrix} S(0) - \bar{S}(0) \\ r_0 - \bar{r}_0 \end{bmatrix}$$

Then, in the interval $[t_l, t_{l+1})$, $l=0$, $F(S(t), r(t))$ can be approximately represented by

$$F_i(S(t), r(t)) = B_i^* + H_{s_i} [S(t) - \bar{S}(0)] + H_{r_i} [r_0 - \bar{r}_0] + \delta_i \quad (4.68)$$

Inserting Eq.(4.68) into Eq.(4.52) reduces the system dynamics to

$$\frac{dS(t)}{dt} = F_s S(t) + LU(t) + F_r r_0 + C' + \varepsilon'(t) \quad (4.69)$$

where

$$F_s = [H_{s1}, \dots, H_{sN_s}]^T$$

$$F_r = [H_{r1}, \dots, H_{rN_s}]^T$$

$$C' = [B_1^*, \dots, B_{N_s}^*]^T - F_s \bar{S}(0) - F_r \bar{r}_0 + E\{\delta\}$$

$$\delta = [\delta_1, \dots, \delta_{N_s}]^T$$

$$\varepsilon'(t) = \delta + \omega(t) - E\{\delta\}$$

Note that $U(t)$ is constant over the interval $[t_1, t_{1+1}]$ and equal to U_1 . In addition we assume that the random disturbance $\varepsilon'(t)$ is equal to $\varepsilon'(0) = \varepsilon'_0$. If, for example, we use the Pade difference formula, the transition equation from t_0 to t_1 of the form

$$S_1 = \Phi_0 S_0 + B_0 U_0 + G_0 r_0 + C_0 + \varepsilon_0 \quad (4.70)$$

is obtained. where

$$\begin{aligned} S_1 &= S(t=t_1), \quad \Delta t_0 = t_{1=1} - t_{1=0}, \\ \Psi_0 &= [I - \Delta t_0 F_s / 2 + \Delta t_0^2 F_s^2 / 12]^{-1} \\ \Phi_0 &= \Psi_0 [I + \Delta t_0 F_s / 2 + \Delta t_0^2 F_s^2 / 12] \\ B_0 &= \Psi_0 \Delta t_0 L \\ G_0 &= \Psi_0 \Delta t_0 F_r \\ C_0 &= \Psi_0 \Delta t_0 C' \\ \varepsilon_0 &= \Psi_0 \Delta t_0 \varepsilon'_0 \end{aligned}$$

The mean and covariance of the state vector S_1 corresponding to the nominal control trajectory then can be calculated from

$$\bar{S}^{\text{nom}}(t_1) = \Phi_0 \bar{S}_0 + B_0 U_0^{\text{nom}} + G_0 \bar{r}_0 + C_0 \quad (4.71)$$

$$P_s^{\text{nom}}(t_1) = \Phi_0^T P_s(0) \Phi_0 + G_0^T P_r G_0 + \text{cov}\{\varepsilon_0\} \quad (4.72)$$

Set $l=1+1$, and assume $S(t_1) \sim N(\bar{S}^{\text{nom}}(t_1), P_s^{\text{nom}}(t_1))$. Repetitive use of the above procedure to Eq.(4.52) results in the following discrete time system dynamics:

$$S_{1+1} = \Phi_1 S_1 + B_1 U_1 + G_1 r_1 + C_1 + \varepsilon_1 \quad (4.73)$$

However, since Eq.(4.73) has been obtained by means of time step Δt_1 , it can not be directly used for operation problem. It is necessary to reconstruct it on the basis of time step Δt_k . The following is the reconstruction procedure.

$$\begin{aligned}
 S_{1+2} &= \Phi_{1+1} S_{1+1} + B_{1+1} U_{1+1} + G_{1+1} r_{1+1} + C_{1+1} + \epsilon_{1+1} \\
 &= \Phi_{1+1} \Phi_1 S_1 + \Phi_{1+1} B_1 U_1 + \Phi_{1+1} G_1 e_1^T X(0) + \Phi_{1+1} C_1 + \Phi_{1+1} \epsilon_1 \\
 &\quad + B_{1+1} U_{1+1} + G_{1+1} e_{1+1}^T X(0) + C_{1+1} + \epsilon_{1+1} \\
 &\quad \dots\dots\dots(4.74)
 \end{aligned}$$

Notice that $U_1 = U_{1+1}$, $t_1 \in [t_k, t_{k+1}]$. We obtain

$$S_{1+2} = \Phi'_1 S_1 + B'_1 U_1 + G'_1 X(0) + C'_1 + \epsilon'_1 \quad (4.75)$$

where

$$\Phi'_1 = \Phi_{1+1} \Phi_1, \quad B'_1 = \Phi_{1+1} B_1 + B_{1+1},$$

$$G'_1 = \Phi_{1+1} G_1 e_1^T + G_{1+1} e_{1+1}^T,$$

$$C'_1 = \Phi_{1+1} C_1 + C_{1+1},$$

$$E\{\epsilon'_1\} = \bar{\epsilon}'_1 = \Phi_{1+1} \bar{\epsilon}_1 + \bar{\epsilon}_{1+1} = 0$$

$$P_{\epsilon'_1} = \Phi_{1+1}^T P_{\epsilon_1} \Phi_{1+1} + P_{\epsilon_{1+1}}$$

Repeating the above procedure m_k times we obtain the following discrete time system dynamics in time step Δt_k

$$S_{k+1} = \Phi_k S_k + B_k U_k + G_k X(0) + C_k + \epsilon_k \quad (4.76)$$

As mentioned in the beginning of this section, the information about the future rainfall, mean vector and covariance, can be obtained from the rainfall-forecasting system. In order to efficiently use this

information, we incorporate the rainfall vector into the state vector by augmenting the state vector as follows.

We first factor the covariance matrix $P_{X(0)}$ so that

$$P_{X(0)} = S_{X(0)} S_{X(0)}^T \quad (4.77)$$

in which, denoting the rank of the matrix $P_{X(0)}$ by N_X , $S_{X(0)}$ is an $M \cdot N_X$ dimensional matrix, then define a random vector d as

$$d = (S_{X(0)}^T S_{X(0)})^{-1} S_{X(0)}^T (X(0) - \bar{X}(0)) \quad (4.78)$$

where d is an N_X dimensional column vector. Because $\bar{X}(0)$ is the forecast of $X(0)$, the mean vector of d is zero, and the variance of forecast error

$$E\{dd^T\} = I \quad (4.79)$$

where I is an $N_X \cdot N_X$ dimensional identity matrix. Using d we can now represent $X(0)$ as

$$X(0) = \bar{X}(0) + S_{X(0)} d, \quad d \sim N(0, I) \quad (4.80)$$

At the stage of identifying the future releases, the time is fixed. Therefore, the random vector d can be treated as time-invariant(i.e., $d_{k+1} = d_k$). Thus, we augment the state vector S_k as

$$S'_k = \begin{Bmatrix} S_k \\ d \end{Bmatrix} \quad (4.81)$$

the mean vector of S'_k and the estimate error variance matrix are given

by

$$\bar{S}'_k = \begin{Bmatrix} \bar{S}_k \\ 0 \end{Bmatrix} \quad (4.82)$$

$$P'_{sk} = \begin{bmatrix} P_{sk} & 0 \\ 0 & I \end{bmatrix} \quad (4.83)$$

The system dynamics for the augmented state vector S'_k then can be expressed as

$$S'_{k+1} = \Phi'_k S'_k + B'_k U_k + C'_k + \epsilon'_k \quad (4.84)$$

where

$$\Phi'_k = \begin{bmatrix} \Phi_k & G_k \bar{X}(0) \\ 0 & I \end{bmatrix}$$

$$B'_k = \begin{bmatrix} B_k \\ 0 \end{bmatrix}$$

$$C'_k = \begin{bmatrix} C_k + G_k \bar{X}(0) \\ 0 \end{bmatrix}$$

$$\epsilon'_k \sim N(0, Q_{\epsilon',k}), \quad Q_{\epsilon',k} = \begin{bmatrix} Q_{\epsilon k} & 0 \\ 0 & 0 \end{bmatrix}$$

In order to simplify the notation, we remove the constant term C'_k from the system dynamics by redefining the state vector. Consider a deterministic vector \bar{S}'_k that satisfies

$$\bar{S}'_{k+1} = \Phi'_k \bar{S}'_k + C'_k, \quad \bar{S}'_0 = \bar{S}'_0 \quad (4.85)$$

Using \bar{S}'_k we define a random vector

$$S''_k = S'_k - \bar{S}'_k \quad (4.86)$$

Inserting Eqs.(4.85), (4.86) into Eq.(4.84) reduces the system dynamics to

$$S''_{k+1} = \Phi'_k S''_k + B'_k U_k + \epsilon'_k \quad (4.87)$$

On our way to the discrete time control problem, we now need to discretize the performance index and the constraints.

Integral Eq.(4.53) can be rewritten as follows:

$$J = E\left\{ \sum_{k=0}^{K-1} \int_{t_k}^{t_{k+1}} [l(U(t)) + m(S(t))] dt \right\} \quad (4.88)$$

Approximating the terms of the above summation by

$$\int_{t_k}^{t_{k+1}} [l(U(t)) + m(S(t))] dt \approx [l(U(t_k)) + m(S(t_k))] (t_{k+1} - t_k) \\ k=0, 1, \dots, K-1 \quad \dots\dots\dots(4.89)$$

one obtains

$$J \approx E\left\{ \sum_{k=0}^{K-1} [l(U(t_k)) + m(S(t_k))] (t_{k+1} - t_k) \right\} \quad (4.90)$$

The constraints will be rewritten as follows:

$$U_{jk}^{\min} \leq U_{jk} \leq U_{jk}^{\max}, \quad j=1, 2, \dots, N_u, \quad k=0, 1, \dots, K-1 \quad (4.91)$$

$$\int_{-\infty}^{S_{jk}^{\min}} p(S_{jk}, k) dS_{jk} \leq \gamma_{jk}^{\min} \quad (4.92)$$

$$\int_{S_{jk}^{\max}}^{+\infty} p(S_{jk}, k) dS_{jk} \leq \gamma_{jk}^{\min} \quad (4.93)$$

$$j=1, 2, \dots, N_s, \quad k=0, 1, \dots, K-1$$

where f_k denotes $f(t_k)$.

The influence of the continuing operation after T can be handled by introducing the terminal cost(a function of the terminal state vector) into the objective function. On the other hand, since the initial state vector(its probabilistic distribution) is known, $E\{m(S_0)\}$ is constant and then can be removed from the objective function.

In summary, the discrete time reservoir control problem which we shall refer to as PB1, is of the following form:

PB1: The Reservoir Operation Problem in Discrete Time:

$$\text{minimize } \left\{ J = \sum_{k=0}^{K-1} E \left\{ l_{k+1}(S_{k+1}) + m_k(U_k) \right\} \right\} \quad (4.94)$$

$$\{U_k\}_{k=0}^{K-1}$$

where $E(\cdot)$ denotes expectation with respect to S_0 , $\{\xi_k\}_{k=0}^{K-1}$,

$$\{v_k\}_{k=0}^K.$$

subject to

$$a. S_{k+1} = \phi_k S_k + B_k U_k + \xi_k, k=0, 1, \dots, K-1 \quad (4.95)$$

$$b. U_{jk}^{\min} \leq U_{jk} \leq U_{jk}^{\max}, j=1, 2, \dots, N_u, k=0, 1, \dots, K-1 \quad (4.96)$$

$$c. \int_{-\infty}^{S_{jk}^{\min}} p(S_{jk}, k) dS_{jk} \leq \gamma_{jk}^{\min} \quad (4.97)$$

$$\int_{S_{jk}^{\max}}^{+\infty} p(S_{jk}, k) dS_{jk} \leq \gamma_{jk}^{\min} \quad (4.98)$$

$$j=1, 2, \dots, N_s, k=0, 1, \dots, K-1$$

$$d. y_k = H(S_k) + v_k, k=0, 1, \dots, K-1 \quad (4.99)$$

This section has formulated the optimization problem associated with a multireservoir system. We shall next solve this problem to obtain the optimal control trajectories.

4.5 Solution of Optimization Problem by the Open-Loop Feedback Controller

4.5.1 Open-Loop Feedback Controller

In order to obtain the optimal control trajectories, the reservoir operation problem formulated in the previous section should be solved by a closed-loop methodology. Unfortunately, since the problem is both nonquadratic and constrained(non-linear), the optimal feedback laws are practically inaccessible. Consequently, certain suboptimal techniques are of great practical interest. Some of the widely known suboptimal control techniques are the Open-Loop Controller and the Naive Feedback or Certainty Equivalence Controller as well as the Open-Loop Feedback Controller. The first is based on the assumption of no information gathering. The second arbitrarily assumes that the problem possesses the Certainty Equivalence Property¹⁾, solves the associated deterministic problem and applies

1)If a control problem with imperfect state information takes on the same solution as the corresponding problem with perfect state information and the deterministic problem resulting when all random quantities are replaced by their expected values, we say that the problem possesses the Certainty Equivalence(C.E.) property. Thus, the C.E. property, if valid, reduces the stochastic control problem into an easier deterministic one. However, one must note that the more the characteristics of a certain problem diverge from the LQG problem, the less likely it is that the C.E. property will hold.

the resulting feedback laws on the stochastic system. In the general case, both have been found to be less reliable as compared to the Open-Loop Feedback Controller(Bertsekas, 1976).

At any time k of the control horizon, the Open-Loop Feedback Controller(OLFC) performs the following operations:

a. Estimates the conditional density $p(S_k/I_k)$ using the information set $I_k = \{ y_1, \dots, y_k, U_0, \dots, U_{k-1} \}$,

b. Assuming that no measurements will be made in the future, finds the open-loop trajectory $\{ U_k, \dots, U_{T-1} \}^{OLFC}$ which minimizes

$$\begin{aligned}
 J_k &= \mathbb{E} \left[\sum_{l=k}^{T-1} (l_{l+1}(S_{l+1}) + m_l(U_l)) \mid I_k \right] \\
 &= \mathbb{E} \left[\sum_{l=k}^{T-1} (l_{l+1}(S_{l+1}) + m_l(U_l)) \right] \quad (4.100)
 \end{aligned}$$

where $\mathbb{E}\{\cdot\}$ denotes expectation with respect to S_k and $\{\xi_l\}_{l=k}^{T-1}$. The second equality sign is because the p.d.f. of S_k is conditioned on I_k (see Step a.),

c. Applies U_k^{OLFC} ,

d. Redefines the information set at time $k+1$

$$I_{k+1} = I_k \mid \{ U_k^{OLFC}, y_{k+1} \}, I_0 \equiv \{\phi\} \text{ (empty set)} \quad (4.101)$$

e. Repeats the previous steps.

The above is an open-loop procedure because at each decision time the entire future control trajectory is determined assuming no information gathering. It is also a feedback procedure because the

applied controls U_k^{OLFC} are functions of all currently available information, The advantage of the OLFC idea is that the computations required to obtain U_k^{OLFC} are considerably simpler than those of the true optimal controls. The OLFC procedure is generally suboptimal because in the specification of the feedback OLFC controls it is not taken into account that measurement information will be gathered in the future and used.

After this subsection's introduction to the OLFC, we next begin to apply the OLFC to our reservoir operation problem. It will be completed in four main steps. In the first three steps, we shall consider the optimization problem obtained at the step b of the OLFC procedure. In the first step, a procedure capable of efficiently solving the unconstrained nonquadratic optimization problem will be developed. In the second and third steps, the basic procedure will be modified to account respectively for possible control or state constraint violations. In the fourth, the design of the OLFC will be completed for the solution of the real-time reservoir operation problem. Care is taken to maintain coherency in the presentation and for this reason lengthy mathematical derivation and background material are relegated to the appendices.

4.5.2 Solution of the Unconstrained Reservoir Optimization Problem

4.5.2.1 The Unconstrained Reservoir Optimization Problem

Neglecting all control and state constraints, the unconstrained reservoir optimization problem obtained at step b of the OLFC procedure can be stated as follows(c.f., PB1 and Section 4.5.1), For convenience, the current time k is assumed to be zero.

PB2: The Unconstrained Reservoir Optimization Problem

$$\text{minimize} \{ J = E \{ \sum_{k=0}^{T-1} [l_{k+1}(S_{k+1}) + m_k(U_k)] \} \} \quad (4.102)$$

$$\{ U_k \}_{k=0}^{T-1}$$

subject to

$$S_{k+1} = \Phi_k S_k + B_k U_k + \xi_k, \quad k=0,1,\dots,T-1 \quad (4.103)$$

where $E\{\cdot\}$ denotes the expectation with respect to S_0 and $\{\xi_k, k=0,1,\dots,T-1\}$.

The various quantities in Eq.(4.102), (4.103) have been defined in Section 4.4. The p.d.f. of the initial state S_0 has been obtained at step a of the OLFC procedure by using all available information. It is Gaussian with

$$E\{S_0\} = \bar{S}_0 \quad (4.104)$$

$$E\{(S_0 - \bar{S}_0)(S_0 - \bar{S}_0)^T\} = P_{S_0} \quad (4.105)$$

The random disturbances $\{\xi_k, k=0,1,\dots,T-1\}$ are also Gaussian independent of S_0 and have zero mean vector and covariance

$$E\{\xi_k \xi_l^T\} = \begin{cases} 0, & \text{if } k \neq l \\ Q_{\xi k}, & \text{if } k = l \end{cases} \quad (4.106)$$

Q_{ξ_k} has been defined in PB1.

This section will be concerned with developing a computationally efficient procedure to solve PB2. PB2 involves linear state dynamics, Gaussian statistics, and nonlinear performance index. Due to the nature of the performance index the solution cannot be obtained in analytical form.

Consider a nominal control trajectory $\{U_k^{nom}\}_{k=0}^{T-1}$, the corresponding nominal state trajectory is defined as

$$\bar{S}_{k+1}^{nom} = \Phi_k \bar{S}_k^{nom} + B_k U_k^{nom}, \quad \bar{S}_0^{nom} = \bar{S}_0 \quad (4.107)$$

If we define

$$\delta S_k = S_k - \bar{S}_k^{nom}, \quad k=0, 1, \dots, T \quad (4.108)$$

$$\delta U_k = U_k - U_k^{nom}, \quad k=0, 1, \dots, T-1 \quad (4.109)$$

the system dynamics then can be rewritten as the following $(\delta S_k, \delta U_k)$ based form

$$\delta S_{k+1} = \Phi_k \delta S_k + B_k \delta U_k + \xi_k, \quad k=0, 1, \dots, T-1 \quad (4.110)$$

The objective function can be rewritten as

$$\text{minimize } \{J = E\{ \sum_{k=0}^{T-1} [l_{k+1}^*(\delta S_{k+1}) + m_k^*(\delta U_k)] \} \} \quad (4.111)$$

$\{\delta U_k\}_{k=0}^{T-1}$

where

$$l_k^*(\delta S_k) = l_k(\delta S_k + \bar{S}_k^{nom}) = l_k(S_k)$$

$$m_k^*(\delta U_k) = m_k(\delta U_k + U_k^{nom}) = m_k(U_k) \quad (4.112)$$

Equivalently, we can transform the above problem into a deterministic problem by taking advantage of the assumption of no future measurements.

Since the system is linear and the uncertainties are Gaussian, it can be shown that δS_k will also be Gaussian with mean vector and covariance given by

$$\delta \bar{S}_{k+1} = \Phi_k \delta \bar{S}_k + B_k \delta U_k, \quad \delta \bar{S}_0 = 0, \quad k=0,1,\dots,T-1 \quad (4.113)$$

$$P_{\delta S_{k+1}} = P_{S_{k+1}} = \Phi_k P_{S_k} \Phi_k^T + Q_{\xi k}, \quad k=0,1,\dots,T-1 \quad (4.114)$$

if the nominal control trajectory is optimal, $\delta \bar{S}_k = 0$, $\delta S_k \sim N(0, P_{S_k})$

Consider now the reformulation of the cost functional. Since ξ_k enters in the cost functional through the state vector δS_{k+1} and does not affect the cost terms at previous time, we can write

$$J = \sum_{k=0}^{T-1} [E_{\delta S_{k+1}} \{ l_{k+1}^*(\delta S_{k+1}) \} + m_k^*(\delta U_k)] \quad (4.115)$$

The expectation in Eq.(4.105) is taken with respect to the Gaussian density. The equivalence of Eq.(4.115) and Eq.(4.102) can be seen by the fact that the randomness of each cost term $l_k^*(\delta S_k)$ is solely due to the randomness of δS_k . Since $E_{\delta S_k} \{ l_k^*(\delta S_k) \}$ is a function of $\delta \bar{S}_k$ and P_{S_k} , the reformulated problem represented by Eqs.(4.113), (4.114), and (4.115) is a deterministic problem. In general, the analytical specification of

$$\bar{l}_k^*(\delta \bar{S}_k, P_{S_k}) = E_{\delta S_k} \{ l_k^*(\delta S_k) \}$$

is not readily possible. One can expand $l_k^*(\delta S_k)$ in a power series and obtain as accurate analytical approximation of $\bar{l}_k^*(\cdot, \cdot)$ as desired by using a property of Gaussian random variables known as Gaussian moment factoring(Georgakakos and Marks, 1985). In this study we shall first approximate $l_k^*(\delta S_k)$ by a second-order function and then take the expectation with respect to δS_k .

The question now is how to efficiently solve the reformulated deterministic problem. Since this is a general nonlinear programming problem where analytical solutions are not likely to exist, one must employ some minimization procedure. The design of a suitable such procedure is taken up in the following section.

4.5.2.2 Newton's Method

There are two major concerns about a minimization method: reliability and efficiency. A method is reliable if it is guaranteed to converge to optimal (in some sense) points, and it is efficient if it exhibits a fast convergence rate. As can be seen in Luenberger(1973), Lasdon(1970), Bertsekas(1976, 1982), there exist many minimization algorithms. Perhaps the most important class of minimization algorithms is the class of the Generalized Gradient methods. When minimizing a scalar real valued function $f(x)$ with respect to the n dimensional real vector x , a method of this class at the i^{th} iteration "moves" from a point x_i to another x_{i+1} according to (Bertsekas, 1976)

$$x_{i+1} = x_i + \alpha_i d_i \quad (4.116)$$

where for all i we have $\alpha_i \geq 0$ and

$$\begin{aligned} [\nabla_x f(x_i)]^T d_i &< 0, \text{ if } \nabla_x f(x_i) \neq 0, \\ d_i &= 0, \text{ if } \nabla_x f(x_i) = 0, \end{aligned} \quad (4.117)$$

$\nabla_x f(x_i)$ denotes the Gradient vector of $f(\cdot)$ at x_i , d_i is the descent direction, and α_i is the stepsize of the iteration. The conditions in (4.117) guarantee that a reduction of the objective function value will be realized as a result of the iteration and that the method will stop at a stationary point of $f(\cdot)$ where the gradient is zero. If $f(\cdot)$ is a convex function, this point is the global minimum; otherwise, may be a local minimum or some other stationary point (e.g., an inflection point).

A method of this class is completely defined once the rules for selecting the direction d_i and the stepsize α_i are established, these rules exclusively determine whether the method is reliable and efficient.

Concerning the d_i selection rule, the best, yet not always possible, choice is to use the Newton's direction:

$$d_i = - [\nabla_{xx}^2 f(x_i)]^{-1} \nabla_x f(x_i) \quad (4.118)$$

where $\nabla_{xx}^2 f(x_i)$ is the Hessian matrix of $f(\cdot)$ evaluated at x_i . At each iteration, the Newton's direction is specified using first and second order derivative information concerning the shape of the objective function, this being both its strength and weakness. The additional information can realize a faster convergence rate, yet it also requires a heavier computational load. Our objective is to design an implementation of Newton's method which is computationally efficient. Despite our problem's large dimensionality (the vector x_i includes now all control vectors at all times: $x_i^T = [U_0^T, \dots, U_{T-1}^T]$) this will be accomplished by taking advantage of its special dynamic structure.

In general, the Newton's direction (4.118) is obtained by minimizing the second order Taylor series expansion of $f(\cdot)$ around x_i or the statistical second-order approximation of $f(\cdot)$ in the case where $f(\cdot) = E\{g(z)\}$, $z \sim N(x, P)$:

$$\bar{f}(x) = N_{x0} + N_x^T (x - x_i) + \frac{1}{2} (x - x_i)^T N_{xx} (x - x_i) \quad (4.119)$$

if $\bar{f}(x)$ is the second order Taylor series expansion of $f(\cdot)$ around x_i ,

$N_{x0} = f(x_i)$, $N_x = \nabla_x f(x_i)$, $N_{xx} = \nabla_{xx}^2 f(x_i)$, if $\bar{f}(x)$ is the statistical

second-order approximation of $f(\cdot)$, $N_{x0} = B^* + \text{tr}[AP]$, $N_x = \nabla_x f(x_i) = H$, $N_{xx} = \nabla_{xx}^2 f(x_i) = A$ (see Section 4.2). This can be easily seen by differentiating (4.119) with respect to x , setting the resulting expression equal to zero, and solving for the minimizing vector x_{i+1} . (It is assumed that the Hessian is nonsingular.) Then the Newton's direction is given by

$$d_i = x_{i+1} - x_i = - N_{xx}^{-1} N_x \quad (4.120)$$

Notice, furthermore, that the same direction would result if in place of $f(x)$ we had minimized some other quadratic function $q(x)$ such that

$$\nabla_{xx}^2 q(x_i) = \nabla_{xx}^2 f(x_i) \quad , \quad \nabla_x q(x_i) = \nabla_x f(x_i) \quad (4.121)$$

namely,

$$q(x) = q_0 + [\nabla_x q(x_i)]^T (x-x_i) + \frac{1}{2} (x-x_i)^T \nabla_{xx}^2 q(x_i) (x-x_i) \\ \dots\dots\dots (4,122)$$

This observation can be very useful in optimal control problems where the dimensionality of the vector x is very large and a direct evaluation of the Gradient and Hessian is impractical.

Returning to our problem, consider a second-order Taylor expansion of $m_k^*(\delta U_k)$ around the nominal control trajectory(i.e., around $\delta U_k = 0$) and a statistical second-order approximation of $l_k^*(\delta S_k)$ by making use of the assumption that $\delta S_k \sim N(0, P_{Sk})$ (i.e., $\delta U_k = 0$):

$$m_k^*(\delta U_k) \approx \frac{1}{2} \delta U_k^T N_{uuk} \delta U_k + N_{uk}^T \delta U_k + N_{u0k} \equiv m_k^\Delta(\delta U_k) + N_{u0k} \\ l_k^*(\delta S_k) \approx \frac{1}{2} \delta S_k^T N_{ssk} \delta S_k + N_{sk}^T \delta S_k + N_{s0k} \equiv l_k^\Delta(\delta S_k) + N \\ \dots\dots\dots (4.123)$$

where N_{uuk}, N_{ssk} are $N_U \cdot N_U, N_S \cdot N_S$ real symmetric matrices respectively, N_{uk}, N_{sk} are N_U, N_S dimensional real vectors respectively, N_{uOk}, N_{sOk} are constant.

Now consider the following problem:

$$\begin{aligned} \text{minimize } \bar{J} &= \sum_{k=0}^{T-1} \{ E_{k+1}^{\Delta} (\delta S_{k+1}) + m_k^{\Delta} (\delta U_k) - \frac{1}{2} \text{tr} [N_{ssk+1} P_{Sk+1}] \} \\ \{ \delta U_k \}_{k=0}^{T-1} & \\ &= \sum_{k=0}^{T-1} \left[\frac{1}{2} \delta \bar{S}_k^T N_{ssk} \delta \bar{S}_k + N_{sk}^T \delta \bar{S}_k + \frac{1}{2} \delta U_k^T N_{uuk} \delta U_k + N_{uk}^T \delta U_k \right] \\ & \dots\dots\dots (4.124) \end{aligned}$$

subject to the dynamical equation (4.113).

Based on the comment concerning the Newton's method, if it were true that problems (4.115) and (4.124) had equal Gradients and Hessians along the nominal sequences $\{ \delta U_k^{\text{nom}} = 0 \}_{k=0}^{T-1}, \{ \delta \bar{S}_k^{\text{nom}} = 0 \}_{k=0}^T$, then we could obtain the Newton's direction for the former by solving the latter. If this direction is denoted by $\delta U^{*(i)}$, a Newton's iteration could then be performed to identify a more rewarding nominal control trajectory $U^{(i+1)}$:

$$\begin{aligned} U^{(i+1)} &= [U_0^{(i+1)}, \dots, U_{T-1}^{(i+1)}]^T \\ &= [U_0^{(i)}, \dots, U_{T-1}^{(i)}]^T + \alpha_i [\delta U_0^{*(i)}, \dots, \delta U_{T-1}^{*(i)}]^T \quad (4.125) \end{aligned}$$

The equality of the two problems' Gradients and Hessians Has been shown by Georgakakos and Marks(1985) via direct evaluation along the nominal control and state trajectories. The final expressions do not recommend straightward implementation of the Newton's method. Comparatively, implementation through solution of problem (4.126) is

much more advantageous. The computation of the Gradient $\nabla J(\delta U_0=0, \dots, \delta U_{T-1}=0)$ and especially of the Hessian $\nabla^2 J(\delta U_0=0, \dots, \delta U_{T-1}=0)$ and its inverse is bypassed and the Newton's direction:

$$\delta U^* = -[\nabla^2 J(\delta U_0=0, \dots, \delta U_{T-1}=0)]^{-1} \nabla J(\delta U_0=0, \dots, \delta U_{T-1}=0) \quad (4.126)$$

is obtained from the solution of a deterministic optimal control problem with linear dynamics and a general quadratic cost functional. This solution is derived by Georgakakos and Marks(1985) via Dynamic Programming and is reproduced below. It has the advantage of being analytical and, therefore, computationally efficient.

Computation of the Newton's Direction for the
Unconstrained Reservoir Optimization Problem

For $k=0, 1, \dots, T-1$

$$\delta U_k^* = - D_k [L_k \delta \bar{S}_k^* + \Lambda_k] \quad (4.127)$$

$$D_k = [B_k^T K_{k+1} B_k + N_{uuk}]^{-1}$$

$$L_k = B_k^T K_{k+1} \Phi_k$$

$$\Lambda_k = B_k^T k_{k+1} + N_{uk}$$

$$\delta \bar{S}_{k+1}^* = \Phi_k \delta \bar{S}_k^* + B_k \delta U_k^* , \delta \bar{S}_0^* = 0, k=1, \dots, T-1$$

where the positive semidefinite matrices $\{K_k\}_{k=0}^T$ are obtained recursively by the following matrix Riccati equation:

$$K_T = N_{ssT}$$

$$K_k = N_{ssk} + \Phi_k^T K_{k+1} \Phi_k -$$

$$- [B_k^T K_{k+1} \phi_k]^T \cdot [B_k^T K_{k+1} B_k + N_{uuk}]^{-1} \cdot [B_k^T K_{k+1} \phi_k]$$

$$k=T-1, T-2, \dots, 0 \quad (4.128)$$

and the vectors $\{k_k\}_{k=0}^T$ result from

$$k_T = N_{sT}$$

$$k_k = N_{sk} + \phi_k^T k_{k+1} -$$

$$- [B_k^T K_{k+1} \phi_k]^T \cdot [B_k^T K_{k+1} B_k + N_{uuk}]^{-1} \cdot [B_k^T k_{k+1} + N_{uk}]$$

$$k=T-1, T-2, \dots, 0 \quad (4.129)$$

The optimal " cost to go " are given for $k=T, T-1, \dots, 1$

$$J_k(\delta \bar{S}_k) = \frac{1}{2} \delta \bar{S}_k^T K_k \delta \bar{S}_k + k_k^T \delta \bar{S}_k + C_k \quad (4.130)$$

where $C_T = 0$

$$C_k = C_{k+1} - \frac{1}{2} [B_k^T k_{k+1} + N_{uk}]^T \cdot$$

$$\cdot [B_k^T K_{k+1} B_k + N_{uuk}]^{-1} \cdot [B_k^T k_{k+1} + N_{uk}]$$

$$k=T-1, T-2, \dots, 0$$

Lastly, the optimal value of the problem is

$$J^{\min} = J_0(\delta \bar{S}_0) = \frac{1}{2} \delta \bar{S}_0^T K_0 \delta \bar{S}_0 + k_0^T \delta \bar{S}_0 + C_0 \quad (4.131)$$

Essentially, implementation of this solution is completed in two steps: (1) the matrices $\{K_k\}_{k=0}^T$ and the vectors $\{k_k\}_{k=0}^T$ are computed by a backward pass of the corresponding equations from time T to time 0 , and (2) the controls $\{\delta U_k^*\}_{k=0}^{T-1}$ are computed by the previous quantities and the sequence $\{\delta \bar{S}_k^*\}_{k=1}^{T-1}$ obtained from a forward pass of the dynamics. The computational requirements are mainly associated

with the computation of $\{K_k\}_{k=0}^T$, $\{k_k\}_{k=0}^T$ and involve multiplications and inversions of $N_S \cdot N_S$, $N_U \cdot N_U$ matrices. Compared to a straightforward implementation of Newton's method requiring the computation and inversion of a $(TN_U) \cdot (TN_U)$ Hessian, where T could be of the order of several hundreds, substantial computational savings should be realized.

The second factor influencing the success of a minimization method is the stepsize selection rule. As can be seen in Bertsekas(1982), there are many good choices available: the minimization rule, the limited minimization rule, the Goldstein rule, the Armijo rule, and many others. Here we shall present the Armijo stepsize selection rule because it is easily implemented and because it conveniently generalizes for a problem with control constraints. For the general problem of minimizing $f(x)$ with respect to x , this rule can be stated as follows:

The Armijo Stepsize Selection Rule:

Let β and σ be scalars satisfying

$$0 < \beta < 1, \quad 0 < \sigma < 1/2 \quad (4.132)$$

Given a nonstationary point x_i and a direction d_i , the stepsize α_i is obtained from

$$\alpha_i = \beta^{m_i}$$

where m_i is the first non-negative integer m for which

$$f(x_i) - f(x_i + \beta^m d_i) \geq -\sigma \beta^m [\nabla_x f(x_i)]^T d_i \quad (4.133)$$

If x_i is a stationary point of $f(x)$, we set $\alpha_i = 0$.

The logic behind this rule is to guarantee that each iteration will reduce the objective function's value by an amount proportional to the Gradient and will thus prohibit convergence to a nonstationary point.

In the case of our problem Eq.(4.133) becomes:

$$J(\delta u_0=0, \dots, \delta u_{T-1}=0) - J(\beta^m \delta U_0^*, \dots, \beta^m \delta U_{T-1}^*) \geq -\sigma \beta^m [\nabla J(\delta u_0=0, \dots, \delta u_{T-1}=0)]^T \delta U^* \quad (4.134)$$

where δU_k^* is the Newton's direction obtained from Eq.(4.129).

$$J(\delta u_0=0, \dots, \delta u_{T-1}=0) = \sum_{k=0}^{T-1} [E_{\delta S_{k+1}} \{ l_{k+1}^*(\delta S_{k+1}) \} + m_k^*(\delta U_k=0)]$$

in which $\delta S_k \sim N(0, P_{sk})$

$$J(\beta^m \delta U_0^*, \dots, \beta^m \delta U_{T-1}^*) = \sum_{k=0}^{T-1} [E_{\delta S_{k+1}} \{ l_{k+1}^*(\delta S_{k+1}) \} + m_k^*(\beta^m \delta U_k^*)]$$

in which $\delta S_k \sim N(\delta \bar{S}_k^*, P_{sk})$

$$\delta \bar{S}_{k+1}^* = \phi_k \delta \bar{S}_k^* + B_k \beta^m \delta U_k^*, \quad \delta \bar{S}_0^* = 0$$

The expectations can be computed with the Hermite-Gauss integration discussed in Section 4.2. The Gradient $\nabla J(\delta u_0=0, \dots, \delta u_{T-1}=0)$ can be efficiently computed by the following procedure(Geogakakos and Marks(1985)):

Computation of the Gradient

Consider the sequence of vectors $\{P_k\}_{k=0}^T$ obtained recursively by

$$P_T = N_{sT}$$

$$P_k = \Phi_k^T P_{k+1} + N_{sk}, \quad k=T-1, T-2, \dots, 0$$

then

$$\begin{aligned} \nabla_{\delta U_0} J(\delta U_0=0, \dots, \delta U_{T-1}=0) \\ \vdots \\ \nabla_{\delta U_{T-1}} J(\delta U_0=0, \dots, \delta U_{T-1}=0) \end{aligned} = \{ \begin{aligned} N_{u0} + B_0^T P_1 \\ \vdots \\ N_{uT-1} + B_{T-1}^T P_T \end{aligned} \}$$

Using the above results the Amijo stepsize selection rule can be stated as follows: Select the stepsize:

$$\alpha_i = \beta^{m_i} \quad (4.135)$$

where m_i is the first non-negative integer m for which

$$\begin{aligned} J(\delta u_0=0, \dots, \delta u_{T-1}=0) - J(\beta^m \delta u_0^*, \dots, \beta^m \delta u_{T-1}^*) \geq \\ -\sigma \beta^m \sum_{k=0}^{T-1} [N_{uk}^T + P_{k+1}^T B_k] \delta u_k^* \end{aligned} \quad (4.136)$$

When the problem is characterized by a convex structure (as, for example, the case of linear dynamics and convex cost terms $\{l_k(\cdot)\}_{k=0}^{T-1}$, $\{m_k(\cdot)\}_{k=1}^T$) the method will converge to the global minimum. Otherwise, the minimization process should be restarted from different initial trajectories and the global minimum should be determined by comparing the cost functional values at the indentified stationary points. In order to prohibit movements opposite to the direction of

descent, one will have to ensure that the matrices $\{K_k\}_{k=0}^T$, $\{N_{uuk}\}_{k=0}^{T-1}$ are positive (semi)definite. A procedure that enforces these properties has been proposed by Georgakakos and Marks(1985).

If the unconstrained global minimum violates no control or state constraints, it also solves the constrained problem. In the opposite event, a constrained minimization scheme should be adopted. The development of a control constrained minimization algorithm is the following section's topic. State constraints will be accounted for in Section 4.5.4.

4.5.3 Solution of the Problem with Control Constraints

4.5.3.1 The Reservoir Optimization Problem with Control Constraints

Towards reconstructing and solving the reservoir operation problem PB1, in this section we consider the following constrained formulation:

PB3. The Reservoir Optimization Problem with Control Constraints

$$\text{minimize} \{ J = \sum_{k=0}^{T-1} [E \{ l_{k+1}^* (\delta S_{k+1}) \} + m_k^* (\delta U_k)] \} \quad (4.137)$$

$\{ \delta U_k \}_{k=0}^{T-1}$ δS_{k+1}

subject to

$$\text{a. } \delta \bar{S}_{k+1} = \Phi_k \delta \bar{S}_k + B_k \delta U_k, \delta \bar{S}_0 = 0, k=0,1,\dots,T-1 \quad (4.138)$$

$$\text{b. } U_{jk}^{\min} \leq U_{jk} \leq U_{jk}^{\max}, j=1,2,\dots,N_U, k=0,1,\dots,T-1$$

or equivalently:

$$\delta U_{jk}^{\min} \leq \delta U_{jk} \leq \delta U_{jk}^{\max}, j=1,2,\dots,N_U, k=0,1,\dots,T-1 \quad (4.139)$$

$$\text{where } \delta U_{jk}^{\min} = U_{jk}^{\min} - U_{jk}^{\text{nom}}$$

$$\delta U_{jk}^{\max} = U_{jk}^{\max} - U_{jk}^{\text{nom}}$$

We wish to develop a procedure accounting for control magnitude constraints within the framework of the Open-Loop Feedback Controller. Selected classes of constrained minimization methods are now briefly reviewed to find a suitable procedure.

4.5.3.2 Constrained Minimization Methods

Three broad classes of constrained minimization methods are (1) the Feasible Direction methods, (2) the Manifold Suboptimization methods, and (3) the Projection Newton methods.

The Feasible Direction methods are natural extensions of the unconstrained Generalized Gradient methods where the descent direction d_i is such that the iteration

$$x_{i+1} = x_i + \alpha_i d_i \quad (4.140)$$

yields feasible points x_i , $i=1,2,\dots$ (α_i being the stepsize parameter).

At each iteration the feasible descent direction d_i is determined by solving a linear or a quadratic minimization problem. This requirement imposes considerable computational overhead and makes these methods unattractive for problems with many variables (such as PB3).

The Manifold Suboptimization methods are also based on (4.140) type iterations where the descent direction d_i is obtained by minimizing the objective function over the subspace defined by the active constraints. If feasibility is violated, the minimization is repeated over a new subspace defined by the currently active constraint set, and the process is repeated until a point satisfying the necessary conditions for optimality is reached. Methods of this class perform quite well for problems of relatively small dimension, but are not efficient for problems with many binding constraints. The reason is that not more than one constraint can be added to the active set at each iteration.

For the problem of minimizing $f(x)$ subject to $x > 0$, a Projected Newton method will perform the following iteration (Bertsekas, 1982):

$$x_{i+1} = [x_i + \alpha_i d_i]^+ \quad (4.141)$$

where $[\cdot]^+$ denotes the projection operator:

$$[z]^+ = [z_1, \dots, z_n]^T = [\max(0, z_1), \dots, \max(0, z_n)]^T \quad \dots\dots\dots(4.142)$$

and d_i is the descent direction given by

$$d_i = - D_i \nabla_x f(x_i) \quad (4.143)$$

D_i is a positive definite matrix of the following form.

$$D_i = \begin{bmatrix} H_i & & & & 0 \\ & h_{r_i+1} & \cdot & \cdot & \cdot & 0 \\ & \vdots & \cdot & & & \vdots \\ 0 & 0 & \cdot & \cdot & \cdot & h_n \end{bmatrix} \quad (4.144)$$

where H_i is a positive definite matrix, $\{h_l, l=r_i+1, \dots, n\}$ are positive numbers, and the set of indices

$$A^+(x_i) = \{r_i+1, \dots, n\} = \{l / 0 \leq x_{li} \leq \epsilon_i, \frac{\partial f(x_i)}{\partial x_{li}} > 0\} \quad (4.145)$$

correspond to the binding and nearly binding constraints. The specification $0 \leq x_{li} \leq \epsilon_i$ is employed rather than $x_{li} = 0$, to avert possible "zigzagging" behavior of the method. ϵ_i can be chosen from

$$\epsilon_i = \min(\epsilon, w_i), \quad w_i = |x_i - [x_i - \nabla_x f(x_i)]^+| \quad (4.146)$$

with ϵ a small positive scalar.

The stepsize α_i can be obtained by an Armijo-like stepsize selection rule as follows:

$$\alpha_i = \beta^{m_i} \quad (4.147)$$

where m_i is the first non-negative integer m for which

$$f(x_i) - f([x_i + \alpha_i d_i]^+) \geq -\sigma \left\{ \beta^m \sum_{j \notin A^+(x_i)} \frac{\partial f(x_i)}{\partial x_{ji}} d_{ji} + \sum_{j \in A^+(x_i)} \frac{\partial f(x_i)}{\partial x_{ji}} (x_{ji} - [x_{ji} + \beta^m d_{ji}]^+) \right\}$$

.....(4.148)

and $\sigma \in (0, 1/2)$, $\beta \in (0, 1)$

(Notice that if none of the constraints are binding, the previous stepsize selection rule becomes identical to the one given in Section 4.5.2)

Under assumptions which are usually valid in actual problems, an algorithm of the above type is guaranteed to identify constrained critical points in a finite number of iterations, a constrained critical point being any point x^* such that

$$\begin{aligned} \frac{\partial f(x^*)}{\partial x_j} &= 0, \text{ if } x_j^* > 0, \\ \frac{\partial f(x^*)}{\partial x_j} &\geq 0, \text{ if } x_j^* = 0, \text{ } j=1, 2, \dots, n \end{aligned} \quad (4.149)$$

If in addition $f(\cdot)$ is convex and H_i , $\{h_l, l=r_i+1, \dots, n\}$ are chosen equal to

$$H_i = \begin{bmatrix} \frac{\partial^2 f(x_i)}{\partial x_{1i} \partial x_{1i}} & \dots & \frac{\partial^2 f(x_i)}{\partial x_{1i} \partial x_{r_i i}} \\ \frac{\partial^2 f(x_i)}{\partial x_{r_i i} \partial x_{1i}} & \dots & \frac{\partial^2 f(x_i)}{\partial x_{r_i i} \partial x_{r_i i}} \end{bmatrix}^{-1} \quad (4.150)$$

$$h_l = \left[\frac{\partial^2 f(x_i)}{\partial x_{li} \partial x_{li}} \right]^{-1}, \quad l = r_i+1, \dots, n, \quad (4.151)$$

then the sequence $\{x_i\}$ converges to the global minimum x^* faster than superlinearly of an order at least two.

These convergence properties make the Projected Newton's Method quite efficient for problems with simple constraints.

The previous algorithm easily generalizes to the case where x is constrained by upper and lower bounds:

$$b_1 \leq x \leq b_2 \quad (4.152)$$

Now, the iteration takes the form

$$x_{i+1} = [x_i + \alpha_i d_i]^{++} \quad (4.153)$$

where

$$([z]^{++}) = \begin{cases} b_{j2}, & \text{if } b_{j2} \leq z_j \\ z_j, & \text{if } b_{j1} \leq z_j \leq b_{j2} \\ b_{j1}, & \text{if } z_j \geq b_{j1} \end{cases} \quad (4.154)$$

$$j = 1, \dots, n$$

and the set of active constraints is given by

$$A^{++}(x_i) = \left\{ 1 / \begin{aligned} & b_{11} \leq x_{1i} \leq b_{11} + \epsilon_i, \quad \frac{\partial f(x_i)}{\partial x_{1i}} > 0 \quad \text{or} \\ & b_{12} - \epsilon_i \leq x_{1i} \leq b_{12}, \quad \frac{\partial f(x_i)}{\partial x_{1i}} < 0 \end{aligned} \right\} \quad (4.155)$$

With these definitions replacing the ones given above, the Projected Newton method previously stated is also valid here.

It is a method of the third type that we shall employ in the solution of Problem PB3. The main difficulty is again related to the computation of the direction d_i .

4.5.3.3 A Projected Newton Method in Optimal Control

The direction d_i of a Projected Newton method consists of two parts: The first corresponds to the nonbinding constraints $j=1,2,\dots,r_i$, $j \notin A^{++}(x_i)$ and is obtained by a Newton iteration

$$d_i = [d_{1i}, \dots, d_{r_i i}]^T = -H_i \left[\frac{\partial f(x_i)}{\partial x_{1i}}, \dots, \frac{\partial f(x_i)}{\partial x_{r_i i}} \right]^T \quad (4.156)$$

assuming that the remaining variables are fixed at the respective bounds. The other is a scaled version of a Gradient method (Luenberger, 1973) where the scaling factor is equal to the inverse of the corresponding diagonal element of the Hessian at point x_i :

$$d_{li} = -\frac{\partial^2 f(x_i)}{\partial x_{li} \partial x_{li}}^{-1} \cdot \frac{\partial f(x_i)}{\partial x_{li}}, \quad l = r_i + 1, \dots, n \quad (4.157)$$

The question is how to efficiently compute these two direction parts for the control Problem PB3. Regarding the computation of the first, the approach employed for the unconstrained control problem in Section 4.5.2 is also applicable here. The difference is that now, due to the constraints, some control vectors cannot be adjusted towards the unconstrained minimum. Instead they must be fixed at their currently nominal values. Georgakakos and Marks(1985) have proposed an analytical procedure for computing the nonbinding direction part given the above requirement.

The scaled Gradient part of the direction can be conveniently obtained from the procedures derived by Georgakakos and Marks(1985). These concern the evaluation of the Gradient and the diagonal submatrices of the Hessian at the nominal sequences.

Putting all these results together, we construct the following control constrained minimization algorithm:

In a typical iteration, a Projected Newton method performs the following sequence of operations:

a. Compute the Gradient vectors $\nabla J(\delta U_0=0, \dots, \delta U_{T-1}=0)$ from

$$\nabla_{\delta U_k} J(\delta U_0=0, \dots, \delta U_{T-1}=0) = N_{uk} + B_k^T P_{k+1} \quad (4.158)$$

where

$$P_T = N_{sT}$$

$$P_k = \Phi_k^T P_{k+1} + N_{sk}, \quad k=T-1, T-2, \dots, 0$$

b. Calculate

$$w_i = |U^{(i)} - [U^{(i)} - \nabla J(\delta U_0=0, \dots, \delta U_{T-1}=0)]^{++}| \quad (4.159)$$

If $w_i \approx 0$, then stop; a stationary (or critical) control trajectory is reached. This is true because when $w_i=0$, any control element U_{jk} for all jk satisfies one of the following first order necessary conditions for optimality:

$$\begin{aligned} U_{jk}^{\min} \leq U_{jk} \leq U_{jk}^{\max} & \quad \text{and} \quad \frac{\partial J(\delta U_0=0, \dots, \delta U_{T-1}=0)}{\partial \delta U_{jk}} = 0 \\ U_{jk} = U_{jk}^{\max} & \quad \text{and} \quad \frac{\partial J(\delta U_0=0, \dots, \delta U_{T-1}=0)}{\partial \delta U_{jk}} < 0 \\ U_{jk}^{\min} = U_{jk} & \quad \text{and} \quad \frac{\partial J(\delta U_0=0, \dots, \delta U_{T-1}=0)}{\partial \delta U_{jk}} > 0 \end{aligned} \quad (4.160)$$

$j = 1, 2, \dots, N_U, \quad k = 0, 1, \dots, T-1$

(Under convexity assumptions $U^{(i)}$ is then a global minimum.)

Otherwise, determine the set $A^{++}(U^{(i)})$ of binding control constraints from

$$A^{++}(U^{(i)}) = \{jk / U_{jk}^{\min} \leq U_{jk}^{(i)} \leq U_{jk}^{\min} + \varepsilon_i \text{ and } \frac{\partial J(\delta U_0=0, \dots, \delta U_{T-1}=0)}{\partial \delta U_{jk}} > 0$$

$$\text{or } U_{jk}^{\max} - \varepsilon_i \leq U_{jk}^{(i)} \leq U_{jk}^{\max} \text{ and } \frac{\partial J(\delta U_0=0, \dots, \delta U_{T-1}=0)}{\partial \delta U_{jk}} < 0$$

$$j = 1, 2, \dots, N_U, \quad k = 0, 1, \dots, T-1 \quad (4.161)$$

where $\varepsilon_i = \min \{\varepsilon, w_i\}$,

with ε being a small positive scalar.

c. Compute the Newton direction for the nonbinding control elements as follows:

Calculate the matrices $\{K_k\}_{k=0}^T$ and the vectors $\{k_k\}_{k=0}^T$ from the following matrix Riccati equation:

$$K_T = N_{ssT},$$

$$K_k = N_{ssk} + \phi_k^T K_{k+1} \phi_k -$$

$$-[(B_{k,k+1}^T K_{k+1} \phi_k)^r]^T \cdot [(B_{k,k+1}^T K_{k+1} B_k + N_{uuk})^{rc}]^{-1} \cdot [(B_{k,k+1}^T K_{k+1} \phi_k)^r]$$

$$k=T-1, T-2, \dots, 0$$

$$k_T = N_{sT},$$

$$k_k = N_{sk} + \phi_k^T k_{k+1} -$$

$$-[(B_{k,k+1}^T K_{k+1} \phi_k)^r]^T \cdot [(B_{k,k+1}^T K_{k+1} B_k + N_{uuk})^{rc}]^{-1} \cdot [(B_{k,k+1}^T K_{k+1} + N_{uk})^r]$$

$$k=T-1, T-2, \dots, 0$$

$$(4.162)$$

where the notation $(z)^r$ or $(z)^{rc}$ implies that the rows or the rows and the columns of the matrix z corresponding to all control elements δU_{jk}

with $jk \in A^{++}(U^{(i)})$ have been deleted.

Then determine the Newton direction δU^* from

$$\delta U_k^* = - D_k [L_k \delta \bar{S}_k^* + \Lambda_k] \quad (4.163)$$

where

$$D_k = [(B_k^T K_{k+1} B_k + N_{uuk})^{rc}]^{-1}$$

$$L_k = (B_k^T K_{k+1} \phi_k)^r$$

$$\Lambda_k = (B_k^T k_{k+1} + N_{uk})^r$$

and

$$\delta \bar{S}_{k+1}^* = \phi_k \delta \bar{S}_k^* + B_k \delta U_k^* , \quad \delta \bar{S}_0^* = 0, \quad k=1, \dots, T-1 \quad (4.164)$$

In Eq.(4.164) the binding control are set equal to zero, namely,

$$\delta U_{jk}^* = 0, \quad \text{if } jk \in A^{++}(U^{(i)}) \quad (4.165)$$

d. Compute the scaled Gradient direction for the binding constraints: Having computed the Gradient in Step a, we additionally need to calculate the diagonal elements of the Hessian which can be accomplished as follows

$$\nabla_{\delta U_k \delta U_k}^2 J(\delta U_0=0, \dots, \delta U_{T-1}=0) = N_{uuk} + B_k^T G_{k+1} B_k \quad (4.166)$$

where the matrices $\{G_k\}_{k=1}^T$ are given by

$$G_T = N_{ssT},$$

$$G_k = \phi_k^T G_{k+1} \phi_k + N_{ssk}$$

$$k=T-1, T-2, \dots, 1 \quad (4.167)$$

Then the directin for the binding controls is obtained from

$$\delta U_{jk}^* = - \frac{\partial^2 J(\delta U_0=0, \dots, \delta U_{T-1}=0)}{\partial \delta U_{jk} \partial \delta U_{jk}}^{-1} \cdot \frac{\partial J(\delta U_0=0, \dots, \delta U_{T-1}=0)}{\partial \delta U_{jk}}$$

$$jk \in A^{++}(U^{(i)}) \quad (4.168)$$

Determine a stepsize α_i such that

$$\alpha_i = \beta^{m_i} \quad (4.169)$$

where m_i is the first non-negative integer m for which

$$\begin{aligned} & J(\delta U_0=0, \dots, \delta U_{T-1}=0) - J([\beta^m \delta U_0^*]^{++}, \dots, [\beta^m \delta U_{T-1}^*]^{++}) \geq -\sigma [\\ & \beta^m \sum_{jk \notin A^{++}(U^{(i)})} \frac{\partial J(\delta U_0=0, \dots, \delta U_{T-1}=0)}{\partial \delta U_{jk}} \delta U_{jk}^* + \\ & + \sum_{jk \in A^{++}(U^{(i)})} \frac{\partial J(\delta U_0=0, \dots, \delta U_{T-1}=0)}{\partial \delta U_{jk}} [\beta^m \delta U_{jk}^*]^{++}] \end{aligned} \quad (4.170)$$

where $\beta \in (0,1)$, $\sigma \in (0,1/2)$

and

$$[\beta^m \delta U_{jk}^*]^{++} = \begin{cases} U_{jk}^{\min} - U_{jk}^{(i)}, & \text{if } U_{jk}^{(i)} + \beta^m \delta U_{jk}^* \leq U_{jk}^{\min} \\ \beta^m \delta U_{jk}^*, & \text{if } U_{jk}^{\min} \leq U_{jk}^{(i)} + \beta^m \delta U_{jk}^* \leq U_{jk}^{\max} \\ U_{jk}^{\max} - U_{jk}^{(i)}, & \text{if } U_{jk}^{(i)} + \beta^m \delta U_{jk}^* \geq U_{jk}^{\max} \end{cases} \quad (4.171)$$

f. Perform the iteration

$$U^{(i+1)} = U^{(i)} + [\alpha_i \delta U^*]^{++} \quad (4.172)$$

obtain the new nominal control trajectory $U^{(i+1)}$ and continue the iterations until a stationary control trajectory U^* is found with respect to Problem PB3.

The above algorithm is the core of the control design. As will be seen in the next section, the modification which is needed to account for the probabilistic state constraints only involves addition of some more quadratic terms in the present performance index. Now we note the following comments:

1. In Step d, the computation of diagonal Hessian submatrices can be avoided by using an ordinary Gradient direction where the scaling factor is unit or some other positive number. The resulting method is still reliable, yet it may take more iterations to converge.

2. In the absence of convexity assumptions, one must assure that a descending direction is obtained. This can be accomplished by enforcing positive definiteness properties on the matrices $\{K_k\}_{k=0}^T$, $\{N_{uuk}\}_{k=0}^{T-1}$.

3. If no control constraints are found binding (i.e., if the set $A^{++}(U^{(i)})$ is empty), then the algorithm conveniently becomes the Newton method for unconstrained minimization presented in Section 4.5.2.2.

4. Under convexity assumptions, every point of the sequence $\{U^{(i)}\}$ generated by this algorithm is a stationary control trajectory. If the method converges to a local minimum U^* , it identifies the set of active constraints at U^* in a finite number of iterations. Then it becomes the unconstrained Newton method.

5. After a new nominal control sequence $U^{(i+1)}$ has been obtained, one can continue the iterations by reconstructing the corresponding Problem PB3 from PBO as has been presented in Sections 4.3, 4.4, and 4.5. Concerning the continuous time nonlinear dynamics, this iteration is an ordinary Gradient method iteration. However, the milder the nonlinearity of the dynamics, the more Newtonlike the procedure becomes. With respect to the reservoir system, if the releases cannot effect drastic storage changes, then linearization of

the dynamics is a good approximation for a wide release range and the procedure will exhibit a fast convergence rate.

The above algorithm is a well defined minimization procedure capable of efficiently handling large numbers of control constraints. Next we shall modify it to account for the probabilistic state constraints.

4.5.4 Solution of the Operation Problem with Both Control
and State Constraints

4.5.4.1 The Reservoir Optimization Problem with Both
Control and State Constraints

In this section, all state constraints are restored and the following control problem is considered:

PB4. The Reservoir Operation Problem With
Control and State Constraints

$$\text{minimize } J = \sum_{k=0}^{T-1} [E \{ l_{k+1}^* (\delta S_{k+1}) \} + m_k^* (\delta U_k)] \quad (4.173)$$

$$\{ \delta U_k \}_{k=0}^{T-1}$$

subject to

$$a. \delta \bar{S}_{k+1} = \Phi_k \delta \bar{S}_k + B_k \delta U_k, \delta \bar{S}_0 = 0, k=0,1,\dots,T-1 \quad (4.174)$$

$$b. \delta U_{jk}^{\min} \leq \delta U_{jk} \leq \delta U_{jk}^{\max}, j=1,2,\dots,N_U, k=0,1,\dots,T-1 \quad (4.175)$$

$$c. \int_{-\infty}^{S_{jk}^{\min}} p(S_{jk}) dS_{jk} \leq \gamma_{jk}^{\min}, j=1,2,\dots,N_S, k=0,1,\dots,T-1$$

$$\int_{S_{jk}^{\max}}^{+\infty} p(S_{jk}) dS_{jk} \leq \gamma_{jk}^{\max}, j=1,2,\dots,N_S, k=0,1,\dots,T-1$$

or equivalently:

$$\int_{-\infty}^{S_{jk}^{\min}} p(\delta S_{jk}) d\delta S_{jk} \leq \gamma_{jk}^{\min}, j=1,2,\dots,N_S, k=0,1,\dots,T-1 \quad (4.176)$$

$$\int_{S_{jk}^{\max}}^{+\infty} p(\delta S_{jk}) d\delta S_{jk} \leq \gamma_{jk}^{\max}, j=1,2,\dots,N_S, k=0,1,\dots,T-1$$

.....(4.177)

For consistency with the Open Loop Feedback control philosophy, the probability densities of the states at all times $k=0, \dots, T$ are conditioned on all information available at time k . Namely, the possibility of future information gathering is ignored. Under this assumption, in Section 4.5.2 it was shown that all probability densities are Gaussian with mean vectors obtained by Eq.(4,174) and covariance matrices resulting from (c.f., Eq.(4.114))

$$P_{sk+1} = \Phi_k P_{sk} \Phi_k^T + Q_{\xi k}, \quad P_{s0} = P_0, \quad k=0,1,\dots,T-1 \quad (4.178)$$

It follows that $p(\delta S_{jk})$ is given by

$$p(\delta S_{jk}) = \frac{1}{\sqrt{2\pi}(P_{sk})_{jj}} \exp\left(-\frac{1}{2} \frac{(\delta S_{jk} - \bar{\delta S}_{jk})^2}{(P_{sk})_{jj}}\right) \quad (4.179)$$

where $(P_{sk})_{jj}$ denotes the j^{th} diagonal element of P_{sk} . It is now possible to substitute the probabilistic constraints (4.176) (4.177) by equivalent deterministic constraints on the mean value of the state. This is facilitated by the following two facts: First, the density (4.179) is completely characterized by its mean and variance. Second, the covariance Eq.(4.178) does not depend on the controls δU_k , $k=0, \dots, T-1$. As a result, we can change the position of $p(\delta S_{jk})$ along the δS_{jk} axis but we cannot alter its shape. The equivalent constraints on the mean value can be easily derived as follows: Consider the constraint

$$\int_{-\infty}^{\delta S_{jk}^{\min}} p(\delta S_{jk}) d\delta S_{jk} \leq \gamma_{jk}^{\min} \quad (4.180)$$

and the standard Gaussian variate $z \sim N(0,1)$. The level Z_{jk}^{\min} can be found (from standard normal variate tables) for which

$$\int_{-\infty}^{z_{jk}^{\min}} \frac{1}{\sqrt{2\pi}} \exp(-z^2/2) dz = \gamma_{jk}^{\min} \quad (4.181)$$

Then, as long as

$$z_{jk}^{\min} \sqrt{(\overline{P}_{sk})_{jj}} + \delta \overline{S}_{jk} \geq \delta S_{jk}^{\min}$$

or $\delta \overline{S}_{jk} \geq \delta S_{jk}^{\min} - z_{jk}^{\min} \sqrt{(\overline{P}_{sk})_{jj}}$ (4.182)

holds true, the probabilistic constraint (4.176) is also satisfied and vice versa. Now we can call

$$\delta \overline{S}_{jk}^{\min} = \delta S_{jk}^{\min} - z_{jk}^{\min} \sqrt{(\overline{P}_{sk})_{jj}} \quad (4.183)$$

and in place of (4.180) consider the inequality

$$\delta \overline{S}_{jk}^{\min} \leq \delta \overline{S}_{jk} \quad (4.184)$$

For example, if the reliability parameter γ_{jk}^{\min} is equal to 0.025 (i.e., if the state δS_{jk} is allowed to violate its lower bound δS_{jk}^{\min} at most 2.5% of the time), the level z_{jk}^{\min} equals -1.96. Then the constraint (4.184) implies that the mean value $\delta \overline{S}_{jk}$ should be kept a distance of 1.96 standard deviations above δS_{jk}^{\min} .

Similarly the upper probability constraints can be transformed to constraints of the following type

$$\delta \overline{S}_{jk} \leq \delta \overline{S}_{jk}^{\max} \quad (4.185)$$

$$\text{where } \delta \overline{S}_{jk}^{\max} = \delta S_{jk}^{\max} - z_{jk}^{\max} \sqrt{(\overline{P}_{sk})_{jj}} \quad (4.186)$$

with z_{jk}^{\max} such that

$$\int_{S_{jk}^{\max}}^{+\infty} \frac{1}{\sqrt{2\pi}} \exp(-z^2/2) dz = \gamma_{jk}^{\min}, j=1, \dots, N_S, k=1, \dots, T \quad (4.187)$$

Thus, we have shown how to convert the probabilistic constraints (4.176) (4.177) into equivalent constraints on the state's mean:

$$\delta \bar{S}_{jk}^{\min} \leq \delta \bar{S}_{jk} \leq \delta \bar{S}_{jk}^{\max}, j=1, \dots, N_S, k=1, \dots, T \quad (4.188)$$

or
$$\delta \bar{S}_k^{\min} \leq \delta \bar{S}_k \leq \delta \bar{S}_k^{\max}, k=1, \dots, T \quad (4.189)$$

in vector notation.

Although these constraints are similar to the ones imposed on the controls, they cannot be handled by the Projected Newton developed in the previous section. The reason is that the states are functionally related to the controls through the system dynamics, and is either the controls or the states that serve as an independent set of variables for the minimization of J . Optimal control problems with state constraints are best handled by Penalty Function of Multiplier methods a discussion of which will be offered in the following section.

A last comment refers to the proposed treatment of the probabilistic constraints in relation to the Open Loop Feedback control procedure. According to the discussion in Section 4.5.1 at each time k the OLF controller determines the entire control trajectory $\{U_k^*\}_{k=0}^{T-1}$ assuming that no other decision specifications take place over the period $[k, T-1]$. In reality only the first member from each optimal trajectory is used and the process is repeated at the next decision time. Thus, owing to this sequential set-up, the applied controls are of a feedback nature $U_k^* = u_k^*(\bar{S}_k)$, $k=0, 1, \dots$, although Open Loop controls are being determined. The OLF control structure relates to this section's developments through the covariance propagation Eq.(4.178). The covariance is propagated under the

assumption of Open Loop control sequences. For a certain class of systems this may result in covariance matrices with diagonal elements growing unbounded over time. On the other hand, if the feedback laws were taken into account, the above elements be either stabilized at a finite level or they would grow at a lower rate. It is evident that the Open Loop approach could result in suboptimal control policies in the sense that the applied controls would meet the probabilistic constraints at greater percentages of time than the one required. However, the feedback control functions cannot be obtained explicitly and therefore cannot be used in the covariance calculations.

4.5.4.2 A Penalty Function Method

The idea of the Penalty Function method is to obtain the solution of a constrained problem by solving a sequence of unconstrained ones. Its validity is based on the fact that for well-posed problems the sequence of the unconstrained solutions converges to the solution of the constrained problem.

For Problem PB4 a Penalty Function method can be derived as follows:

Each two-sided state inequality constraint (4.188) can be broken up into two one-sided constraints:

$$\delta \bar{S}_{jk}^{\min} - \delta \bar{S}_{jk} \leq 0 \quad , j=1, \dots, N_S, k=1, \dots, T \quad (4.190)$$

$$\delta \bar{S}_{jk} - \delta \bar{S}_{jk}^{\max} \leq 0 \quad , j=1, \dots, N_S, k=1, \dots, T \quad (4.191)$$

and these can be converted into equality constraints by introducing the non-negative variables y_{jk}^{\min} , y_{jk}^{\max}

$$\delta \bar{S}_{jk}^{\min} - \delta \bar{S}_{jk} + y_{jk}^{\min} = 0, \quad y_{jk}^{\min} \geq 0, \\ , j=1, \dots, N_S, k=1, \dots, T \quad (4.192)$$

$$\delta \bar{S}_{jk} - \delta \bar{S}_{jk}^{\max} + y_{jk}^{\max} = 0, \quad y_{jk}^{\max} \geq 0, \\ , j=1, \dots, N_S, k=1, \dots, T \quad (4.193)$$

Now define the Lagrangian function

$$L_{C_i}(\delta U_0, \dots, \delta U_{T-1}, y_1^{\min}, \dots, y_T^{\min}, y_1^{\max}, \dots, y_T^{\max}) = \\ = J(\delta U_0, \dots, \delta U_{T-1}) + \sum_{jk} \frac{1}{2} C_i (\delta \bar{S}_{jk}^{\min} - \delta \bar{S}_{jk} + y_{jk}^{\min})^2 + \\ \sum_{jk} \frac{1}{2} C_i (\delta \bar{S}_{jk} - \delta \bar{S}_{jk}^{\max} + y_{jk}^{\max})^2$$

.....(4.194)

where C_i is a positive penalty parameter and consider the following sequence of problems:

$$\begin{aligned} &\text{Minimize } L_{C_i}(\delta U_0, \dots, \delta U_{T-1}, y_1^{\min}, \dots, y_T^{\min}, y_1^{\max}, \dots, y_T^{\max}) \\ &\{\delta U\} \\ &\{y^{\min}, y^{\max}\} \end{aligned} \quad (4.195)$$

subject to

$$a. \delta \bar{S}_{k+1} = \Phi_k \delta \bar{S}_k + B_k \delta U_k, \delta \bar{S}_0 = 0, k=0, 1, \dots, T-1 \quad (4.196)$$

$$b. \delta U_{jk}^{\min} \leq \delta U_{jk} \leq \delta U_{jk}^{\max}, j=1, 2, \dots, N_U, k=0, 1, \dots, T-1 \quad (4.197)$$

$$c. y_{jk}^{\min} \geq 0,$$

$$y_{jk}^{\max} \geq 0, \quad (4.198)$$

where $i=0, 1, \dots, C_{i+1} > C_i > 0$, and $C_i \rightarrow \infty$,

If $(\delta U^*, y^*)_i$ is a global minimum of the above problem, then it can be

shown that every limit point of the sequence $\{\delta U^*\}_i$ is a global

minimum of problem PB4. (For a proof in a general nonlinear programming context, see Luenberger, 1973, or Bertsekas, 1982,)

Intuitively, this result is expected to hold because for large C_i

values the penalty terms $C_i(\delta \bar{S}_{jk} - \delta \bar{S}_{jk}^{\max} + y_{jk}^{\max})^2$ are minimized when

$(\delta \bar{S}_{jk} - \delta \bar{S}_{jk}^{\max} + y_{jk}^{\max})$ approaches zero or equivalently when the

constraint $\delta \bar{S}_{jk} - \delta \bar{S}_{jk}^{\max} \leq 0$ is satisfied. (Similar argument holds for

the lower bound penalties as well.)

It is still questionable why one should choose to solve the sequence of the above problems rather than the original one. Notice,

however, that for a particular state and control trajectory the minimization with respect to y^{\min} and y^{\max} can be explicitly performed. Consider for instance, minimizing the Lagrangian in Eq.(4.194) with respect to y_{jk}^{\min} subject to $y_{jk}^{\min} \geq 0$. This is equivalent to

$$\underset{y_{jk}^{\min}}{\text{minimize}} \left\{ \frac{1}{2} C_i (\delta \bar{S}_{jk}^{\min} - \delta \bar{S}_{jk} + y_{jk}^{\min})^2 \right\} \quad (4.199)$$

subject to $y_{jk}^{\min} \geq 0$. Since (4.199) is a convex quadratic function with respect to y_{jk}^{\min} the solution is

$$(y_{jk}^{\min})^* = \begin{cases} -(\delta \bar{S}_{jk}^{\min} - \delta \bar{S}_{jk}) & , \text{ if } \delta \bar{S}_{jk}^{\min} < \delta \bar{S}_{jk} \\ 0 & , \text{ if } \delta \bar{S}_{jk}^{\min} > \delta \bar{S}_{jk} \end{cases} \quad (4.200)$$

Similarly the optimal value of any y_{jk}^{\max} variable can be seen to be

$$(y_{jk}^{\max})^* = \begin{cases} -(\delta \bar{S}_{jk} - \delta \bar{S}_{jk}^{\max}) & , \text{ if } \delta \bar{S}_{jk}^{\max} > \delta \bar{S}_{jk} \\ 0 & , \text{ if } \delta \bar{S}_{jk}^{\max} < \delta \bar{S}_{jk} \end{cases} \quad (4.201)$$

Substituting these results into the Lagrangian function we find

$$\begin{aligned} L_{C_i}(\delta U_0, \dots, \delta U_{T-1}) &= J(\delta U_0, \dots, \delta U_{T-1}) + \\ &+ \sum_{jk} \frac{1}{2} C_i [\max\{0, (\delta \bar{S}_{jk}^{\min} - \delta \bar{S}_{jk})\}]^2 + \\ &+ \sum_{jk} \frac{1}{2} C_i [\max\{0, (\delta \bar{S}_{jk} - \delta \bar{S}_{jk}^{\max})\}]^2 \end{aligned} \quad (4.202)$$

and our problem becomes one of minimizing (4.202) with respect to $\{\delta U_k\}_{k=0}^{T-1}$ subject to the dynamics (4.196) and the control magnitude constraints (4.197). The penalty terms in (4.202) are zero when the

corresponding constraints are not violated while they prescribe quadratic costs whenever there is a violation. Notice, however, that this problem can be solved by the Projected Newton Algorithm presented in Section 4.5.3. The only adjustment needed at each iteration is to determine which of the state constraints (4.190) or (4.191) are currently violated and include in the objective function $J(\delta U_0, \dots, \delta U_{T-1})$ the corresponding quadratic and linear penalty terms. The procedure involves the following sequence of operations: For a level C_i of the penalty parameter use the Projected Newton Method to find the minimizing control trajectory $U^*(C_i)$; then increase C_i to $C_{i+1} > C_i$ and repeat the previous step until the sequence $\{u^*(C_i)\}_i$ converges to the solution U^* . For convex problems the method can also be operated by increasing C_i at each Projected Newton iteration, but in the general case this may cause failures.

The rate at which C_i should be increased can be determined by preliminary experimentation. Slow increment will result in slow convergence while an extremely fast rate will render the problem ill-conditioned. In the latter case a solution at some iteration may not exist or it may become increasingly difficult to obtain. However, our computational experience with the Penalty Function method in relation to reservoir operation problems shows that the method is quite reliable and that a penalty increment formula (see also Bertsekas, 1982, Chapter 2)

$$C_{i+1} = \beta C_i, \beta \in [4, 10] \quad (4.203)$$

performs well.

4.5.5 Completing the OLFC Procedure

4.5.5.1 Observation Information

According to the OLFC procedure, after the optimal control trajectory $\{U_k^{OLFC}\}_{k=k_0}^{T-1}$ have been obtained, we need to apply the control $U_{k_0}^{OLFC}$ at the current time k_0 to the reservoir system, and make the measurements of observation vector y_{k_0+1} . The information set will then be updated as follows:

$$I_{k_0+1} = I_{k_0} U \{U_{k_0}^{OLFC}, y_{k_0+1}\} \quad (4.204)$$

$$\text{where } y_{k_0+1} = H(S_{k_0+1}) + v_{k_0+1} \quad (4.205)$$

On the other hand, the input rainfall vector $X(k_0+1)$ is provided by the rainfall-forecasting system, we have no need to augment the state vector. After the control $U_{k_0}^{OLFC}$ have been applied, the system dynamics become:

$$S_{k_0+1} = \Phi_{k_0} S_{k_0} + B_{k_0} U_{k_0}^{OLFC} + G_{k_0} \bar{X}(k_0+1) + \xi_{k_0} \quad (4.206)$$

4.5.5.2 Statistically Approximated Second-Order Filter

The question is how to obtain the conditional contribution density functions $p(S_{k_0+1} / I_{k_0+1})$. These conditional statisticals are provided by the following procedures which constitute the Statistically Approximated Second-Order Filter(SASOF)(Takasao and Shiiba, 1984).

a. Initialization:

$$\bar{S}_{0/I_0} = \bar{S}_0, P_{s0/I_0} = P_{s0},$$

$$S_{0/I_0} = S_0 \sim N(\bar{S}_0, P_{s0}) \quad (4.207)$$

b. Propagation Step:

$$\begin{aligned} \bar{S}_{k_0+1/I_{k_0}} &= E\{S_{k_0+1} / I_{k_0}\} \\ &= \phi_{k_0} \bar{S}_{k_0/I_{k_0}} + B_{k_0} U_{k_0}^{OLFC} + G_{k_0} X(k_0+1) + C_{k_0} \\ P_{sk_0+1/I_{k_0}} &= E\{(S_{k_0+1} - \bar{S}_{k_0+1} / I_{k_0})(S_{k_0+1} - \bar{S}_{k_0+1} / I_{k_0})^T / I_{k_0}\} \\ &= \phi_{k_0} P_{sk_0/I_{k_0}} \phi_{k_0}^T + Q_{\xi k_0} \end{aligned} \quad (4.208)$$

Since the system is linear,

$$S_{k_0+1/I_{k_0}} \sim N(\bar{S}_{k_0+1/I_{k_0}}, P_{sk_0+1/I_{k_0}})$$

c. Update Step:

Approximate first $H(S_{k_0+1})$ with the Statistical Second-order

Approximation:

$$H_i(S_{k_0+1}) \approx B_i^* + H_{si}(S_{k_0+1} - \bar{S}_{k_0+1/I_{k_0}}) + \delta_i \quad (4.209)$$

$$\text{where } \delta_i = \frac{1}{2} (S_{k_0+1} - \bar{S}_{k_0+1/I_{k_0}})^T A_i (S_{k_0+1} - \bar{S}_{k_0+1/I_{k_0}})$$

Calculating the mean vector $E\{\delta\}$ and variance $V\{\delta\}$, and replacing $H(S_{k_0+1})$ by its statistical second-order approximation we can rewrite the observation equation as

$$y_{k_0+1} - \{ B^* - H_s \bar{S}_{k_0+1/I_{k_0}} + E\{\delta\} \} = H_s S_{k_0+1} + v_{\text{new}} \quad (4.210)$$

where

$$B^* = [B_1^*, \dots, B_M^*]^T$$

$$H_s = [H_{s1}^T, \dots, H_{sM}^T]^T$$

$$v_{\text{new}} = \delta + v_{k_0+1} - E\{\delta\}$$

$$E\{v_{\text{new}}\} = 0, \quad V\{v_{\text{new}}\} = V\{\delta\} + Q_{v_{k_0+1}}$$

M: dimension of y_{k_0+1}

Noting that v_{new} is uncorrelated with S_{k_0+1} and using the conventional Kalman filtering algorithm, we obtain the posteriori estimate of S_{k_0+1} and the corresponding estimate error variance matrix by

$$\begin{aligned} \bar{S}_{k_0+1/I_{k_0+1}} &= \bar{S}_{k_0+1/I_{k_0}} + \kappa(y_{k_0+1} - B^* - \frac{1}{2} \text{tr}[A P_{sk_0+1/I_{k_0}}]) \\ P_{sk_0+1/I_{k_0+1}} &= P_{sk_0+1/I_{k_0}} - \kappa H_s^T P_{sk_0+1/I_{k_0}} \end{aligned} \quad (4.211)$$

$$\kappa = P_{sk_0+1/I_{k_0}} H_s^T (H_s P_{sk_0+1/I_{k_0}} H_s^T + Q_{vk_0+1} + \frac{1}{2} \text{tr}[A P_{sk_0+1/I_{k_0}} A P_{sk_0+1/I_{k_0}}])^{-1} \quad (4.212)$$

If the observation is missing we set:

$$\bar{S}_{k_0+1/I_{k_0+1}} = \bar{S}_{k_0+1/I_{k_0}} \quad (4.213)$$

$$P_{sk_0+1/I_{k_0+1}} = P_{sk_0+1/I_{k_0}} \quad (4.214)$$

As mentioned in Section 4.2, the statistical second-order approximation is performed with ease when the UDU^T factorization of the variance matrix $P_{sk_0+1/I_{k_0}}$ is available. By the Bierman's U-D filter(1977), the UDU^T of $P_{sk_0+1/I_{k_0+1}}$ can be obtained directly.

The previous discussion completes the design of the Open-Loop Feedback Controller for the solution of the reservoir operation problem. The method developed here can be employed to non-linear, constrained, and unquadratic problems. The method developed here will be called Statistically Approximated Linear Quadratic Gaussian control (SALQG). The following chapter will apply this method to reservoir systems and verify the method's reliability and computational efficiency as well as potential in real-time decision making.

Chapter 5

SIMULATION ANALYSIS ON REAL-TIME CONTROL OF MULTIRESERVOIR SYSTEMS

5.1 Introduction

The control method developed in Chapter 4 was theoretically designed to exhibit reliability and computational efficiency for handling dimensionally large reservoir system control problems in their general form. The simulations presented in this chapter will be a verification and test of the method's potential in real-time decision making.

In Section 2, an example of an optimization problem (e.i. off-line control problem) is presented for comparison of the statistical approximation second-order method with the Taylor approximation. The efficiency of the statistical approximation for updating system state vectors has been shown by Takasao and Shiiba(1984) with an on-line runoff forecasting model. Therefore, if the statistical approximation is proven to be efficient in the optimization process of an uncertainty problem, we can say it is also efficient for a real-time control problem.

In Section 3, the control method discussed in Chapter 4 is applied to a two-reservoir system. According to the Open-Loop Feedback controller, the method will first be applied to an off-line control problem, and then to a real-time control problem.

5.2 Efficiency of the Statistical Second-Order Approximation

Consider a function

$$J(\bar{x}) = E\{g(x)\}$$

in which x is an $N * 1$ dimensional random vector, $x \sim N(\bar{x}, \bar{P})$, and $\bar{P} > 0$ is given. In Section 4.2, we have shown that when $g(x)$ is approximated by the statistical second-order approximation, the Gradient vector and the Hessian matrix of $J(\bar{x})$ can be evaluated correctly, and that if the Taylor approximation is applied to $g(x)$ the Gradient vector and Hessian matrix generally cannot be evaluated correctly. This means that the statistical second-order approximation may result in a faster convergence rate of optimization process. In this section we shall verify it with an practical example.

The example problem is shown in Figure 5.1. The biquadratic function used in section 4.2 for showing the difference between the statistical second-order and Taylor approximations is employed for $l_K(S_K)$. The problem has been selected in such a way so that

- 1) the expectation $E\{l_K(S_K)\}$ exists, and the problem can be solved analytically(to compare the numerical results with the correct results and thus check the accuracy of the numerical results),
- 2) the objective function has a global minimum and has no local minimum,
- 3) it is a non-linear function and has at least a local minimum,
- 4) it is two times continuously differentiable and its statistical second-order approximation and Taylor approximation are different.

Dimension of state vector $n_s = 1$
 Dimension of control vector $n_u = 1$
 Control horizon $T = 2$
 System dynamics
 $s_{k+1} = s_k - u_k + 5.0 + \xi_k \quad k=0, \dots, T-1$
 $s_0 \sim N(\bar{s}_0, p_{s0}), \quad \bar{s}_0 = 3.0, \quad p_{s0} = 1.0$
 $\xi_k \sim N(0, Q_{\xi k}), \quad Q_{\xi k} = 1.0$
 Objective function
 $J = E\{\sum_{k=0}^{T-1} (l_{k+1}(s_{k+1}) + m_k(u_k))\}$
 $l_{k+1}(s_{k+1}) = (s_{k+1} - a_{k+1})(s_{k+1} - 3a_{k+1}(s_{k+1} - 4a_{k+1}))^2$
 $a_1 = 0.9 \quad a_2 = 0.9$
 $m_k(u_k) = 1/10 \cdot (u_k - b_k)^2$
 $b_0 = 1.0 \quad b_1 = 1.0$
 Constraints of control variables
 $4.0 \leq u_k \leq 7.0, \quad k=0, \dots, T-1$

Figure 5.1 Problem 1 for comparing the Taylor Approximation with the Statistical Second-Order Approximation.

The simulation results are shown in Table 5.1, and the value of the objective function at each iteration is given in Figure 5.2. It can be seen that the numerical results using the statistical second-order approximation are in excellent agreement with the analytical(correct) results without reference to the nominal control trajectory. However, when the Taylor approximation is used, the numerical results varied following the numerical control and did not converge to the correct results.

Table 5.1 Computational result of problem 1
—value of objective function and control series

| | St. A. 1 ^{#1} | Ta. E. 1 ^{#2} | St. A. 2 ^{#3} | Ta. E. 2 ^{#4} | An. So. ^{#5} |
|---------------|------------------------|------------------------|------------------------|------------------------|-----------------------|
| value of J | 30.242 | 57.722 | 30.242 | 66.998 | 30.242 |
| control u_0 | 5.372 | 4.419 | 5.372 | 6.506 | 5.372 |
| control u_1 | 4.950 | 4.858 | 4.950 | 4.960 | 4.950 |

- #1: $I_4(s_k)$ is approximated by statistical second-order method and the initial nominal control is the upper constraints of control.
 #2: $I_4(s_k)$ is approximated by Taylor second-order approximation method and the initial nominal control is the upper constraints of control.
 #3: $I_4(s_k)$ is approximated by statistical second-order method and the initial nominal control is the lower constraints of control.
 #4: $I_4(s_k)$ is approximated by Taylor second-order approximation method and the initial nominal control is the lower constraints of control.
 #5: analytical solution.

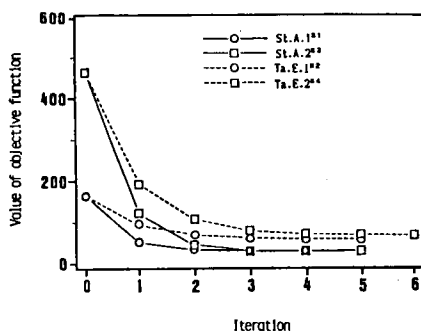


Figure 5.2 Computational result of problem 1.
—decreasing value of objective function with iteration.

5.3 A Two-Reservoir Case Study

The configuration of a two-reservoir system is shown in Figure 5.3. We have assumed that the time in which the released water from the upstream reservoir reaches to the downstream reservoir is too short to be ignored as compared with the control time step.

We first consider an off-line control problem, which is shown in Figure 5.4. When the chance constraints of state vectors are removed, the problem can be solved analytically. The numerical results and analytical results have been shown in Table 5.2 and Figure 5.5. It can be seen that the numerical results converged quickly to the correct results of the problem.

The results of the problem with chance constraints of state vectors are shown in Table 5.3. The value of the penalty function corresponding to the optimal control trajectory at each iteration has been calculated; the results are shown in Figure 5.6. The values of the objective function and the extended objective function are shown in Figure 5.7. It can be seen that the value of the penalty function converged to zero within very few iterations and the chance constraints are satisfied.

Figure 5.8 shows a real-time control problem. The observations are given by

$$y_{iK} = S_{iK}^3 + R(\omega_{iK}) \quad , \quad i=1,2,\dots,N_s; \quad K=1,2,\dots,T-1$$

where $R(\omega_{iK})$ is a random number of ω_{iK} , which has been generated in the following way. Suppose $x \sim N(m,P)$,

- 1) factor the variance matrix P as

$$P = UDU^T$$

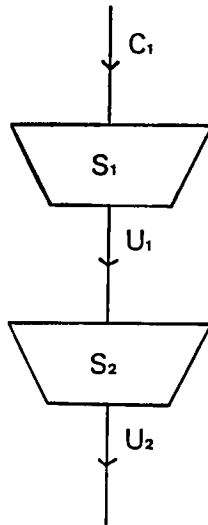


Figure 5.3 Two-reservoir problem configuration.

Dimension of state vector $n_s=2$
 Dimension of control vector $n_u=2$
 Control horizon $T=6$

System dynamics

$$s_{k+1} = \phi_k s_k + B_k u_k + C_k + \xi_k, \quad k=0, \dots, T-1$$

$$\phi_k = \begin{bmatrix} 1 & 0 \\ 0 & 1 \end{bmatrix}, \quad B_k = \begin{bmatrix} -1 & 0 \\ 1 & -1 \end{bmatrix}, \quad C_k = \begin{bmatrix} 0.3 \\ 0.0 \end{bmatrix}$$

$$\xi_k \sim N(0, Q_{\xi k}), \quad Q_{\xi k} = \begin{bmatrix} 0.3 & 0.0 \\ 0.0 & 0.3 \end{bmatrix}, \quad k=0, \dots, T-1$$

$$s_0 \sim N(\bar{s}_0, P_{s0}), \quad \bar{s}_0 = \begin{bmatrix} 0.7 \\ 0.7 \end{bmatrix}$$

$$P_{s0} = \begin{bmatrix} 0.3 & 0.0 \\ 0.0 & 0.3 \end{bmatrix}$$

Objective function

$$J = E \left\{ \sum_{k=0}^{T-1} (l_{k+1}(s_{k+1}) + m_k(u_k)) \right\}$$

$$l_{k+1}(s_{k+1}) = \cosh(s_{1,k+1} - a_{1,k+1}) + \cosh(s_{2,k+1} - a_{2,k+1})$$

$$m_k(u_k) = \cosh(u_{1,k} - b_{1,k}) + \cosh(u_{2,k} - b_{2,k})$$

$$\begin{bmatrix} a_{11} & a_{12} & a_{13} & a_{14} & a_{15} & a_{16} \\ a_{21} & a_{22} & a_{23} & a_{24} & a_{25} & a_{26} \end{bmatrix} = \begin{bmatrix} 0.8 & 0.85 & 0.9 & 0.95 & 1.0 & 1.05 \\ 0.6 & 0.7 & 0.8 & 0.9 & 1.0 & 1.1 \end{bmatrix}$$

$$\begin{bmatrix} b_{10} & b_{11} & b_{12} & b_{13} & b_{14} & b_{15} \\ b_{20} & b_{21} & b_{22} & b_{23} & b_{24} & b_{25} \end{bmatrix} = \begin{bmatrix} 0.5 & 0.55 & 0.6 & 0.65 & 0.7 & 0.75 \\ 0.3 & 0.4 & 0.5 & 0.6 & 0.7 & 0.8 \end{bmatrix}$$

Constraints of control variables

$$0.0 \leq u_{i,k} \leq 3.0 \quad i=1, \dots, n_u \quad k=0, \dots, T-1$$

Chance constraints of state variables

$$s_{j_k}^{m_k} = 0.0, \quad s_{j_k}^{M_k} = 3.0, \quad j=1, \dots, n_s, \quad k=1, \dots, T$$

$$\gamma_{j_k}^{m_k} = 0.2, \quad \gamma_{j_k}^{M_k} = 0.2, \quad j=1, \dots, n_s, \quad k=1, \dots, T$$

Figure 5.4 Problem 2 for testing the optimization method.

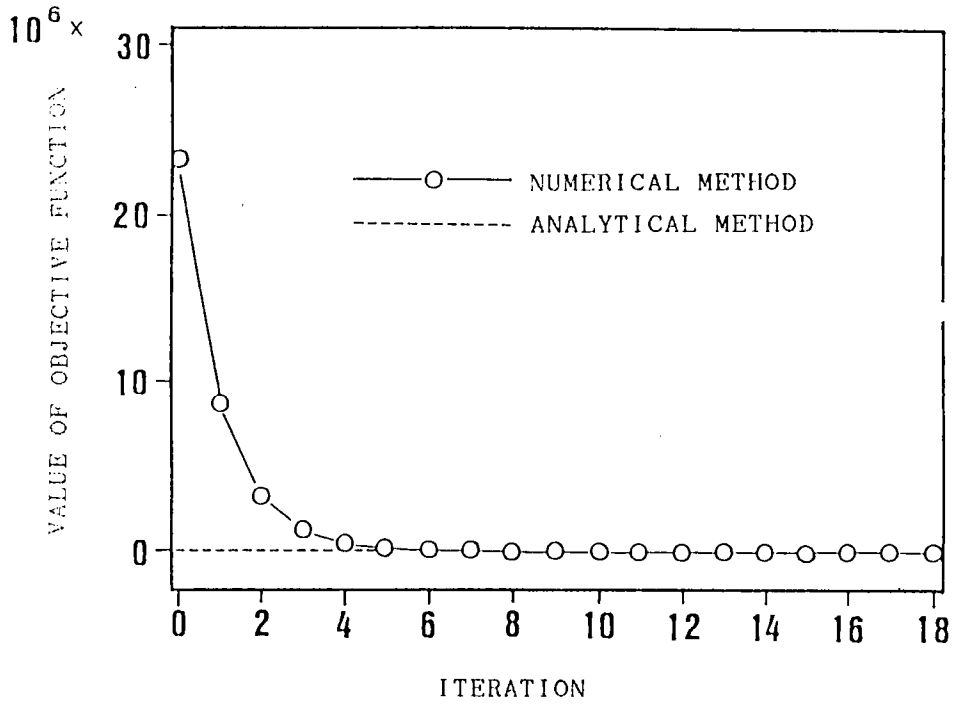


Figure 5.5 The results of problem 2 without the probabilistic constraints

Table 5.2 The resulting control trajectories of problem 2 without the probabilistic constraints.

| | NUMERICAL METHOD | | ANALYTICAL METHOD | |
|---------|------------------|----------|-------------------|----------|
| J | 37.165 | | 37.165 | |
| control | u_{1k} | u_{2k} | u_{1k} | u_{2k} |
| k = 0 | 0.147 | 0.167 | 0.147 | 0.167 |
| k = 1 | 0.234 | 0.159 | 0.234 | 0.159 |
| k = 2 | 0.262 | 0.177 | 0.262 | 0.177 |
| k = 3 | 0.285 | 0.207 | 0.285 | 0.207 |
| k = 4 | 0.326 | 0.272 | 0.326 | 0.272 |
| k = 5 | 0.436 | 0.437 | 0.436 | 0.437 |

Table 5.3 Computational result of problem 2
 —value of objective function, control and state series

| | | | | |
|---------------------------------|----------|----------|---|---|
| value of objective function (J) | | | 37.705 | |
| value of penalty function (h) | | | 0.000 | |
| J+h | | | 37.705 | |
| | control | | state | |
| time | u_{1k} | u_{2k} | $\bar{s}_{1,k+1}(\bar{s}_{1,k+1}^{min}, \bar{s}_{1,k+1}^{max})$ | $(\bar{s}_{2,k+1}(\bar{s}_{2,k+1}^{min}, \bar{s}_{2,k+1}^{max}))$ |
| $k=0$ | 0.138 | 0.145 | 0.862 (0.652, 2.348) | 0.693 (0.652, 2.202) |
| $k=1$ | 0.227 | 0.122 | 0.936 (0.798, 2.202) | 0.798 (0.798, 2.202) |
| $k=2$ | 0.247 | 0.124 | 0.988 (0.922, 2.078) | 0.922 (0.922, 2.078) |
| $k=3$ | 0.241 | 0.132 | 1.048 (1.031, 1.969) | 1.031 (1.031, 1.969) |
| $k=4$ | 0.219 | 0.120 | 1.129 (1.129, 1.871) | 1.129 (1.129, 1.871) |
| $k=5$ | 0.210 | 0.119 | 1.220 (1.220, 1.780) | 1.220 (1.220, 1.780) |

Gothic: chance constraint of state variable is active

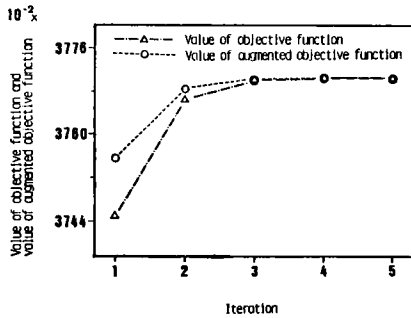


Figure 5.7 Computational result of problem 2.
 —converging value of objective function with iteration.

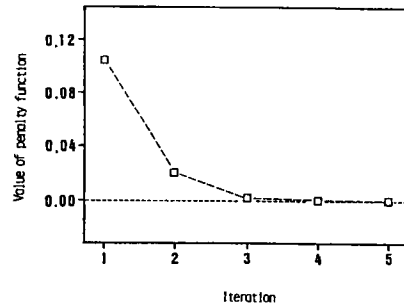


Figure 5.6 Computational result of problem 2.
 —decreasing value of penalty function with iteration.

Dimension of state vector $n_s=2$

Dimension of control vector $n_u=2$

Control horizon $T=6$

System dynamics

$$s_{k+1} = \phi_k s_k + B_k u_k + C_k + \xi_k \quad k=0, \dots, T-1$$

$$\phi_k = \begin{bmatrix} 1 & 0 \\ 0 & 1 \end{bmatrix} \quad B_k = \begin{bmatrix} -1 & 0 \\ 1 & -1 \end{bmatrix} \quad C_k = \begin{bmatrix} 5.0 \\ 0.0 \end{bmatrix}$$

$$\xi_k \sim N(0, Q_{\xi k}), \quad Q_{\xi k} = \begin{bmatrix} 4.0 & 0.0 \\ 0.0 & 4.0 \end{bmatrix}, \quad k=0, \dots, T-1$$

$$s_0 \sim N(\bar{s}_0, P_{s0}), \quad \bar{s}_0 = \begin{bmatrix} 10.0 \\ 80.0 \end{bmatrix}$$

$$P_{s0} = \begin{bmatrix} 1.0 & 0.0 \\ 0.0 & 1.0 \end{bmatrix}$$

Objective function

$$J = E \{ \sum_{k=0}^{T-1} (1_{k+1}(s_{k+1}) + m_k(u_k)) \}$$

$$1_{k+1}(s_{k+1}) = \cosh \{ 0.01 (s_{1,k+1} - a_{1,k+1}) \} + \cosh \{ 0.01 (s_{2,k+1} - a_{2,k+1}) \}$$

$$m_k(u_k) = \cosh \{ 0.01 (u_{1,k} - b_{1,k}) \} + \cosh \{ 0.01 (u_{2,k} - b_{2,k}) \}$$

$$a_{i,k} = 20.0, \quad i=1, \dots, n_s, \quad k=1, \dots, T$$

$$b_{i,k} = 10.0, \quad i=1, \dots, n_u, \quad k=0, \dots, T-1$$

Constraints of control variables

$$0.0 \leq u_{i,k} \leq 50.0 \quad i=1, \dots, n_u \quad k=0, \dots, T-1$$

Chance constraints of state variables

$$s_{j,k}^{max} = 5.0, \quad s_{j,k}^{min} = 95.0, \quad j=1, \dots, n_s, \quad k=1, \dots, T$$

$$\gamma_{j,k}^{max} = 0.05, \quad \gamma_{j,k}^{min} = 0.05, \quad j=1, \dots, n_s, \quad k=1, \dots, T$$

Observation equations

$$y_{i,k} = s_{i,k}^3 + w_{i,k}, \quad i=1, \dots, n_s, \quad k=0, \dots, T-1$$

$$w_{i,k} \sim N(0, Q_{w,k}), \quad Q_{w,k} = \begin{bmatrix} 1.0 & 0.01 \\ 0.01 & 1.0 \end{bmatrix}$$

Figure 5.8 Problem 3 for testing the real-time operation algorithm.

where U is an upper triangular matrix with unit diagonals and D is a positive diagonal matrix. It can be shown that random vector $x = Uz$, where $z \sim N(m,D)$.

2) generate the random numbers of the independent random vector $z \sim N(m,D)$.

The value of state variable S_{iK} is calculated from the system dynamics and the random number of system noise are obtained in the same way as above.

The control trajectories obtained from the real-time control model are shown in Figure 5.9 and the corresponding state trajectories in Figure 5.10. Since the influence of initial conditions becomes less as time passes, the control vector and state vector should asymptotically approach some equilibrium values if the inflows into the system are stable. Notice that the value of the objective function is minimum when the control vectors are $[10 \ 10]^T$ and the state vectors are $[20 \ 20]^T$. Since the inflow from the upstream is only 5 (less than 10), the equilibrium values of the control vector and the state vector are less than $[10 \ 10]^T$ and $[20 \ 20]^T$, respectively. Since S_{11} is only 9.6, much less than 20, no water is released from the upstream reservoir at time steps 0 and 1. On the other hand, the releases from the downstream reservoir at time steps 0 and 1 are very large due to the large initial storage(78.5) in the downstream reservoir.

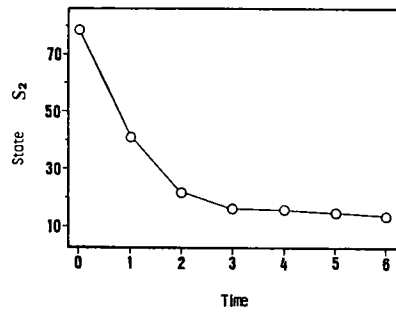
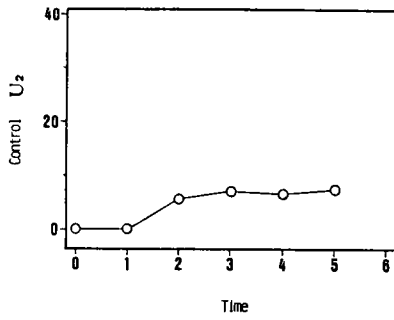
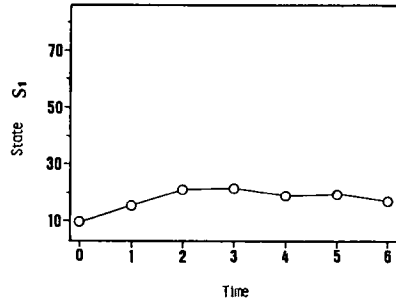
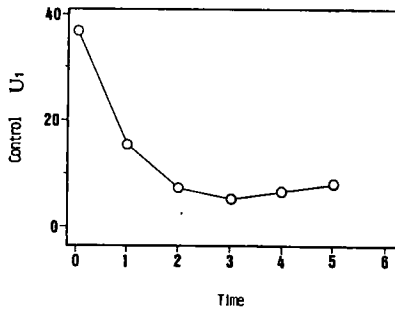


Figure 5.9 Computational result of problem 3
—control series.

Figure 5.10 Computational result of problem 3
—changing state value.

5.4 Summary

In this chapter we applied the control model developed in Chapter 4 to reservoir systems and verified that the control model is very powerful for real-time decision making. From the simulation results we come to the following conclusions.

1) The statistical second-order approximation is more efficient and reliable than the Taylor approximation for a real-time control problem in which the uncertainties of a reservoir system are explicitly taken into consideration. This is because the Taylor approximation is a local approximation technique while the statistical second-order approximation is a global approximation technique.

2) The control method is very stable and has quite a fast convergence rate.

3) The "curse of dimensionality" has been completely overcome.

4) The control model can be employed for all non-linear, constrained and non-quadratic problems.

Chapter 6

SUMMARY OF RESULTS AND FUTURE WORK

6.1 Summary of Results

This work is composed of two parts: a hillslope hydrological model and real-time control of multireservoir systems.

A physically-based, synthesized hillslope runoff model of overland flow and saturated-unsaturated subsurface flow was developed in Chapter 2. The mathematical model consisted of the simultaneous solution of the kinematic equations of overland flow and the two-dimensional form of the saturated-unsaturated subsurface flow. The only input to the flow system was rainfall. The intensity of return flow(or seepage), which conventionally has been treated as an input to the flow system, was treated as another independent variable in addition to pressure head. This was made possible by the governing equations, which were derived by consideration of both the conservation of mass and the balance of momentum along land surface. The model was solved by the Galerkin Finite Element Method. The straight line approximation of land surface was proven to be possible, which means that it is very easy to extend the model to a three-dimensional system.

The synthesized runoff model was applied to hillslope systems under various flow conditions and performed impressively even for the

case with extremely heterogeneous and anisotropic soil. From the spatial distribution of pressure head, the hydrograph, moisture profile, water table level, elevation of seepage point, depth of overland flow and distribution of flow velocity were calculated. Based on the simulation results, we tried to examine the influences of the hydrological and geohydrological parameters on runoff. It was found that the characteristics of hillslope runoff are mainly determined by the combination of saturated hydraulic conductivity, land surface roughness and moisture characteristic curve. Analysis of internal variables such as moisture profile, distribution of velocity and interaction of overland flow and subsurface flow, has shown that on the hillslope where the A-layer of soil profile develops(Ishihara and Takasao(1963) have pointed out that this is the case for almost all natural hillslopes) rainfall intensities generally do not exceed infiltration capacities and Horton overland flow does not occur. Further, it has been shown that return flow usually plays a very important part in the interaction of overland flow with subsurface flow.

In Chapter 3, the synthesized hillslope runoff model was lumped to form a simpler empirical runoff model. The lumped model consisted of three ordinary differential equations corresponding to overland flow, saturated subsurface flow and unsaturated subsurface flow. The storage function model was used for the subsurface runoff discharge and the intensity of lateral flow from an unsaturated zone into a saturated zone across the water table. The model parameters were derived from simulation results with the synthesized runoff model (when the model is applied to an actual hillslope they must be identified by the input-output record data). In the lumped model, the water table of subsurface flow and the free water surface of overland

flow were both assumed to be linear. The resulting mathematical model was solved by the Runge-Kutta method. The simulation results shown that the lumped model can reproduce very well the hydrograph obtained by the synthesized runoff model. Since there is seldom enough data available at field sites to provide the necessary input to the synthesized runoff model, we can say that the lumped model is more useful for practical purposes. However, the lumped model cannot be employed to analyze hillslope runoff processes instead of the synthesized model.

Based on the comprehensive understanding of hillslope runoff processes obtained in the previous chapters, in Chapter 4 we used stochastic control theory to design a method for the operational management of existing multireservoir systems. The actual reservoir, river segment and hillslope response was modelled by a set of coupled non-linear ordinary differential equations in continuous time. It was assumed that a rainfall forecasting system exists which provides the information of future inputs to the reservoir system. The system model was linearized around nominal control and state trajectories by means of the statistical second-order approximation method and subsequently converted into a discrete time linear perturbation model where the discretization interval can be selected arbitrarily according to user's purpose. The various system objectives and operational characteristics were formulated as control and probabilistic state constraints. The goal assigned to the control procedure was to generate points on the properly defined tradeoff surface.

According to the Open-Loop Feedback Control philosophy, the stochastic control problem was seen to be equivalent to a deterministic problem in the space of the state's probability density.

Since the system was linearized, this function was approximated by a Gaussian density. It was updated by the statistically approximated second-order filter. The algorithm to solve this problem was designed on the basis of the Linear Quadratic Gaussian(LQG) controller, which is of the trajectory iteration type. It successively treats the unconstrained problem, the problem with control constraints and the problem with both control and probabilistic state constraints. For these operations, it uses a Newton, a Projected Newton and a Penalty Function method, respectively. The algorithm is repeated along directions obtained via analytical considerations to account for the non-linear nature of the system model. When the problem is characterized by a convex structure, it will converge to the global optimum, Otherwise, it only identifies local optimal trajectories. In this case, the method should be restarted from different initial trajectories and the global optimum should be determined by comparing the objective functional values at the identified stationary points. By its analytical structure, the method does not suffer from dimensionality limitation and it is expected to display reliability and a fast convergence rate.

The method was tested in two cases. The first case concerned the comparison between the statistical second-order approximation and the Taylor approximation. It was shown that the statistical second-order approximation is more efficient and reliable than the Taylor approximation. The control method using the statistical second-order approximation can give the optimal trajectories regardless of the nominal control trajectories. The second case concerned the control of a two-reservoir system. It was shown that both the control and the probabilistic state constraints were satisfactorily accounted for within very few iterations(5 or 6). For a simple problem that can be

solved analytically, the results obtained via the method were in excellent agreement with the correct results.

6.2 Areas for Future Work

Future research work can be outlined as follows.

1) The synthesized runoff model is two-dimensional in vertical plane, the possibility of extending it to a three-dimensional model can be investigated to account for detailed spatial variations.

2) Both the synthesized and the lumped runoff models are deterministic. However, runoff processes generally characterized by uncertainty. Thus, the incorporation of uncertainty into the models is a very meaningful problem.

3) The parameters of both the runoff models and the reservoir system model should be identified by the input-output data records, parameter estimation techniques should be studied.

4) When the control method developed here is applied to a real reservoir system, the problems such as how to decide the control horizon, how to divide the river segments, etc. should be studied.

5) According to the optimal control theory, the Open-Loop Feedback controller applied in this study belongs to the class of suboptimal techniques. The application of a optimal technique to reservoir systems remains to be studied.

REFERENCES

- Abramowitz, M. and Stegun, I. A., 1972, Handbook of Mathematical Functions, Dover Publications, p. 890.
- Ackoff, R. L., 1961, Progress in Operations Research, Vol. 1, John Wiley, New York.
- Akai, K., Ohnishi, Y. and Nishigaki, M., 1977, Finite Element Analysis of Saturated-Unsaturated Seepage in Soil, Trans. JSCE, No. 264, pp. 87-96, (in Japanese).
- Alarcon, L. and Marks, D., 1979, A Stochastic Dynamic Programming Model for the Operation of the High Aswan Dam, Ralph M. Parsons Lab. for Water Resources and Hydrodynamics, Dept. of Civil Engineering, M.I.T., TR No. 246.
- Arunkumar, S. and Yeh, W. W-G., 1973, Probabilistic Models in the Design and Operation of a Multi-Purpose Reservoir System, Contrib. 144, Calif. Water Resour. Cent., Univ. of Calif., Davis.
- Bellman, R., 1957, Dynamic Programming, Princeton Univ. Press, Princeton, New Jersey.
- Bertsekas, D., 1976, Dynamic Programming and Stochastic Control, Academic Press, New York.
- Bertsekas, D., 1982, Constrained Optimization and Lagrange Multiplier Methods, Academic Press, New York.
- Bierman, G. J., 1977, Factorization Methods for Discrete Sequential Estimation, Academic Press, New York.
- Buchanan, R. and Bras, R., 1981, Study of Real-Time Adaptive Closed-Loop Control for Reservoir Operation, Ralph M. Parsons Lab. for Water Resources and Hydrodynamics, Dept. of Civil Engineering, M.I.T., TR No. 265.
- Butcher, W. S., 1971, Stochastic Dynamic Programming for Optimum Reservoir Operation, Water Res. Bull., Vol. 7, No. 1, pp. 115-123.
- Chen, C. L. and Chow, V. T., 1968, Hydrodynamics of Mathematically-Simulated Surface Runoff, Hydraul., Eng., Ser. 18, Univ. Illinois, Urbana, 132 pp.
- Chow, V. T., 1959, Open-Channel Hydraulics, McGraw-Hill, New York.
- Clarke, R. T., 1973, A Review of Some Mathematical Models Used in Hydrology, with Observations on Their Calibration and Use, J. Hydrology, No. 19, pp. 1-20.
- Colorni, A. and Fronza, G., 1976, Reservoir Management via Reliability Programming, Water Res. Res., Vol. 12, No. 1, pp. 85-88.
- Croley, T. E., 1974, Sequential Stochastic Optimization for Reservoir System, J. Hydraul. Div. Am. Soc. Civ. Eng., 100HY1, pp. 201-219.

- Dantzig, D. van, 1956, Economic Decision Problems for Flood Protection, *Econometrica*, No. 24, pp. 276-287.
- Datta, B. and Burges, S. J., 1984, Short-Term, Single, Multipurpose Reservoir Operation: Importance of Loss Functions and Forecast Errors, *Water Res. Res.*, Vol. 20, No. 9, pp. 1167-1176.
- Davis, D. W., 1975, Optimal Sizing of Urban Flood-Control Systems, *J. Hydraul. Div. Am. Soc. Cil. Eng.*, 101HY8, pp. 1077-1092.
- Eisel, L. M., Chance Constrained Reservoir Model, *Water Res. Res.*, Vol. 8, No. 2, pp. 339-347.
- Freeze, R. A., 1971, Three-dimensional, Transient, Saturated-Unsaturated Flow in a Groundwater basin, *Water Res. Res.*, Vol. 7, No. 3, pp. 347-366.
- Freeze, R. A., 1972a, Role of Subsurface Flow in Generating Surface Runoff. 1. Base Flow Contributions to Channel Flow, *Water Res. Res.*, Vol. 8, No. 3, pp. 609-623.
- Freeze, R. A., 1972b, Role of Subsurface Flow in Generating Surface Runoff. 1. Upstream Source Areas, *Water Res. Res.*, Vol. 8, No. 5, pp. 1272-1283.
- Georgakakos, A., 1983, Optimal Operation Planning of Uncertain Multi-reservoir Systems, Ralph M. Parsons Lab. for Hydrology and Water Resource Systems, Dept. of Civil Engineering, Cambridge, Mass.
- Georgakakos, K. and Bras, R., 1980, A Precipitation Model and Its Use in Real-Time River Flow Forecasting, Ralph M. Parsons Lab. for Water Resources and Hydrodynamics, Dept. of Civil Engineering, M.I.T., TR No. 256, Cambridge, Mass.
- Georgakakos, A. P. and Marks, D. H., 1985, Real Time Control of Reservoir Systems, Ralph M. Parsons Lab. for Hydrology and Water Resource Systems, Dept. of Civil Engineering, M.I.T., TR No. 301, Cambridge, Mass.
- Haimes, Y., 1977, Hierarchical Analyses of Water Resources Systems, McGraw-Hill, New York.
- Hall, W. A., 1964, Optimal Design of a Multiple-Purpose Reservoir, *J. Hydraulic Division, HY4*, Vol. 90, pp. 141-150.
- Hall, W. A., Tauke, G. W., and Yeh, W. W-G., 1969, An Alternative Procedure for the Optimization of Operations for Planning with Multiple River, Multiple Purpose Systems, *Water Res. Res.*, Vol. 5, No. 6, pp. 1367-1372.
- Harbaugh, T. E. and Chow, V. T., 1967, A Study of Roughness of Conceptual River Systems or Watersheds, Twelfth Congress of the International Association for Hydraulic Research, Fort Collins, Colorado, I, pp. 9-17.
- Heidari, M., Chow, V. T., Kokotovic, P. V., and Meredith, D. D., Discrete Differential Dynamic Programming Approach to Water

- Resources System Optimization, Water Res. Res., Vol. 7, No. 2, pp. 273-283.
- Hewlett, J. D. and Hibbert, A. R., 1963, Moisture and Energy Conditions within a Sloping Soil Mass During Drainage, J. Geophys. Res., No. 68, pp. 1081-1087.
- Hillel, D., 1971, Soil and Water: Physical Principles and Processes, Academic Press, New York.
- Horton, R. E., 1933, The Role of Infiltration in the Hydrologic Cycle, Transactions of the American Geophysical Union, No. 14, pp. 446-460.
- Ishihara, T. and Takasao, T., 1959, Fundamental Reserches on the Unit Hydrograph Method and Its Application, Trans. JSCE, No. 60 Extra papers, (in Japanese).
- Ishihara, T. and Takasao, T., 1963, A Study on Runoff Pattern and Its Characteristics, Bull. DPRI, No.65.
- Ishihara, T. and Takasao, T., 1962, A Study on the Subsurface Runoff and Its Effects on Runoff Process, Trans. JSCE, No. 79, pp. 15-21, (in Japanese).
- Jacobsen, D. and Mayne, D., 1970, Differential Dynamic Programming, Elsevier, New York.
- Joeres, E. F., Liegman, G. J., and ReVelle, C. S., 1971, Operating Rules for a Joint Operation of Raw Water Sources, Water Res. Res., Vol. 7, No. 2, pp. 25-235.
- Kibler, D. F. and Woolhiser, D. A., 1970, The Kinematic Cascade as a Hydrologic Model, Colorado State University Hydrology Paper, No. 39.
- Kimura, T., 1961, Flood Runoff Routing Using Storage Function Method, Public Work Research Inst., Ministry of Construction of Japan, (in Japanese).
- Kitanidis, P. and Bras, R., 1978, Real Time Forecasting of River Flows, Ralph M. Parsons Lab. for Water Resources and Hydrodynamics, Dept. of Civil Engineering, M.I.T., TR No. 235, Cambridge, Mass.
- Lasdon, L. S., 1970, Optimization Theory for Large Scale Systems, MacMillan Co., New York.
- Liakopoulos, A. C., 1965, Retention and Distribution of Moisture in Soils after Infiltration Has Ceased, Bull. Internat. Assoc. Sci. Hydrology, No. 10, pp. 58-69.
- Little, J. D. C., 1955, The Use of Storage Water in a Hydroelectric System, Oper. Res., Vol. 3, No. 3, pp. 187-197.
- Loaiciga, H. A. and Marino, M. A., 1986, Risk Analysis for Reservoir Operation, Water Res. Res., Vol. 22, No. 4, pp. 483-488.

- Loucks, D. and Dorfman, P., 1975, An Evaluation of Some Linear Decision Rules in Chance-Constrained Models for Reservoir Planning and Operation, *Water Res. Res.*, Vol. 11, No. 6.
- Luenberger, D., 1973, *Introduction to Linear and Nonlinear Programming*, Addison-Welsley Publishing Co., Reading, Mass.
- Maass, A., et al.(Eds.), 1962, *Design of Water-Resource Systems*, Harvard University Press, Cambridge, Mass.
- Marino, M. and Mohammadi, B., 1983, Reservoir Management: A Reliability Programming Approach, *Water Res. Res.*, Vol. 19, No. 3, pp. 613-620.
- Murray, D. M. and Yakowitz, S. J., 1979, Constrained Differential Dynamic Programming and Its Application to Multireservoir Control, *Water Res. Res.*, Vol. 15, No. 5, pp. 1017-1027.
- Neuman, S. P., 1973, Saturated-Unsaturated seepage by Finite Elements, *Proc. ASCE*, Vol. 99, HY12, pp. 2233-2250.
- Orlovski, S., Rinaldi, S., and Soncini-Sessa, R., 1984, A Min-Max Approach to Reservoir Management, *Water Res. Res.*, Vol. 20, No. 11, pp. 1506-1514.
- Ragan, R., 1966, Laboratory Evaluation of a Numerical Flood Routing Technique for Channels Subject to Later Inflows, *Water Res. Res.*, Vol. 2, No. 1, pp. 111-121.
- Restrepo-Posada, P. and Bras, R., 1982, Automatic Parameter Estimation of a Large Conceptual Rainfall-Runoff Model: A Maximum Likelihood Approach, Ralph M. Parsons Lab. for Water Resources and Hydrodynamics, Dept. of Civil Engineering, M.I.T., TR No. 267.
- ReVelle, C., Joeres, E., and Kirby, W., 1969, The Linear Decision Rule in Reservoir Management and Design 1: Development of the Stochastic Model, *Water Res. Res.*, Vol. 5, No. 4, pp. 767-777.
- Richards, L. A., 1931, Capillary Conduction of Liquids in Porous Mediums, *Physics*, No. 1, pp. 318-333.
- Schweig, Z. and Cole, J. A., 1968, Optimal Control of Linked Reservoir, *Water Res. Res.*, Vol. 4, No. 3, pp. 479-497.
- Sherman, L. K., 1932, Streamflow from Rainfall by Unit-Graph Method, *Eng. News Record*, No. 108, pp. 501-505.
- Simonovic, S. P. and Marino, M. A., 1980, Reliability Programming in Reservoir Management, 1: Single Multipurpose Reservoirs, *Water Res. Res.*, Vol. 16, No. 5, pp. 844-848.
- Simonovic, S. P. and Marino, M. A., 1982, Reliability Programming in Reservoir Management, 1: Single Multipurpose Reservoirs, *Water Res. Res.*, Vol. 18, No. 4, pp. 735-743.
- Sloan, P. G. and Moore, I. D., 1984, Modeling Subsurface Stormflow on Steeply Sloping Forested Watersheds, *Water Res. Res.*, Vol. 20, No. 12, pp. 1815-1822.

- Smith, R. E. and Woolhiser, D. A., 1971a, Mathematical Simulation of Infiltrating Watersheds, Colorado State University Hydrology Paper, No. 47.
- Smith, R. E. and Woolhiser, D. A., 1971b, Overland Flow on an Infiltrating Surface, Water Res. Res., Vol. 7, No. 4, pp. 899-913.
- Sniedovich, M., 1980, Analysis of a Chance-Constrained Reservoir Control Model, Water Res. Res., Vol. 16, No. 5, pp. 849-853.
- Sobel, M., 1975, Reservoir Management Models, Water Res. Res., Vol. 11, No. 6, pp. 767-777.
- Strelkoff, t., 1969, One-dimensional Equations of Open-Channel Flow, J. Hydraul. Div. Am. Soc. Civil Eng., 94HY3, pp. 861-876.
- Su, S. Y. and Deininger, 1972, Generalization of White's Method of Successive Approximations to Periodic Markovian Decision Process, Oper. Res., Vol. 20, No. 2, pp. 318-326.
- Su, S. Y. and Deininger, R. A., 1974, Modling the Regulation of Lake Superior under Uncertainty of Future Water Supplies, Water Res. Res., Vol. 10, No. 1, pp. 11-25.
- Sueishi, T., 1955, On the Run-off Analysis by the Method of Characteristics: Hydraulic studies on the Run-off Phenomena of Rain Water, Trans. JSCE, No. 29, pp. 74-87, (in Japanese).
- Takasao, T., Ikebuchi, s., and Kojiri, M., 1977, A Study for the Optimal Control of Multi-Reservoir and Multi-Defence Point System, Disaster Prevention Res. Inst. Annuals, Kyoto Univ., No. 21-B-2, pp. 193-206, (in Japanese).
- Takasao, T., Ikebuchi, s., and Kojiri, M., A Study for Optimal Reservoir Operation Including Flood, Low Flow and Turbidity Controls, Disaster Prevention Res. Inst. Annuals, Kyoto Univ., No. 23-B-2, pp. 279-291, (in Japanese).
- Takasao, T., Ikebuchi, s., and Shiiba, M., 1977, A Study on the Flood Runoff Analysis in a River Basin to Consider the Effect of the Stream Network Structure, Disaster Prevention Res. Inst. Annuals, Kyoto Univ., No. 20-B-2, pp. 185-199, (in Japanese).
- Takasao, T. and Kishimoto, S., 1961, An Experimental Study on the Runoff Process of Rainfall, Disaster Prevention Res. Inst. Annuals, Kyoto Univ., No. 4, pp. 132-153, (in Japanese).
- Takasao, T. and Seno, K., 1970, A Study on Flood Control by Group of Dam Reservoirs(I): Utilization of DP and Some Incidental Problems, Disaster Prevention Res. Inst. Annuals, Kyoto Univ., No. 13-B, pp. 83-103, (in Japanese).
- Takasao, T. and Shiiba, M.; 1979, Identification and Validation of the Runoff Model Based on the Kinematic Wave Theory, Disaster Prevention Res. Inst. Annuals, Kyoto Univ., No. 22-B-2, pp. 225-236, (in Japanese).

- Takasao, T. and Shiiba, M., 1981, Incorporation of the Effect of Concentration of Flow into the Kinematic Wave Equations, Disaster Prevention Res. Inst. Annuals, Kyoto Univ., No. 24-B-2, pp. 159-170, (in Japanese).
- Takasao, T. and Shiiba, M., 1984, Development of Techniques for On-Line Forecasting of Rainfall and Flood Runoff, Natural Disaster Science, Vol. 6, No. 2, pp. 83-112.
- Takasao, T., Shiiba, M., and Tomisawa, N., 1984, Building of a Runoff Prediction System on the Basis of the Statistical Second-Order Approximation Theory, Disaster Prevention Res. Inst. Annuals, Kyoto Univ., No. 27-B-2, pp. 255-273, (in Japanese).
- Tani, M., 1982, The Properties of a Water-Table Rise Produced by a One-Dimensional, Vertical, Unsaturated Flow, J. Jap. For. Soc., Vol. 64, No. 11, pp. 409-418, (in Japanese).
- Wasimi, S. and Kitanidis, Real-Time Forecasting and Daily Operation of a Multireservoir System During Floods by Linear Quadratic Gaussian Control, Water Res. Res., Vol. 19, No. 6, pp. 1511-1522.
- Wooding, R. A., 1965a, A Hydraulic Model for the Catchment-Stream Problem, 1, Kinematic Wave Theory, J. Hydrology, No. 3, pp. 254-267.
- Wooding, R. A., 1965a, A Hydraulic Model for the Catchment-Stream Problem, 2, Numerical Solutions, J. Hydrology, No. 3, pp. 268-282.
- Wooding, R. A., 1966, A Hydraulic Model for the Catchment-Stream Problem, 3, Comparison with Runoff Observations, J. Hydrology, No. 4, pp. 21-37.
- Woolhiser, D. A. and Liggett, J. A., 1967, Unsteady, One-dimensional Flow over a Plane- The Rising Hydrograph, Water Res. Res., Vol. 3, No. 3, pp. 753-771.
- Yakowitz, S., 1982, Dynamic Programming Applications in Water Resources, Water Res. Res., Vol. 18, No. 4, pp. 673-696.
- Yeh, W. W-G., 1982, State of the Art Review: Theories and Applications of Systems Analysis Techniques to the Optimal Management and Operation of a Reservoir System, NCLA-ENG-85-52.
- Yeh, W. W-G., 1985, Reservoir Management and Operations Models: A State-of-the-Art Review, Water Res. Res., Vol. 21, No. 12, pp. 1797-1818.
- Young, G. K., 1967, Finding Reservoir Operation Rules, J. Hydraul. Div. Am. Soc. Civ. Eng., 93HY6, pp. 297-321.

Appendix A

EQUATION OF MOTION FOR SATURATED-UNSATURATED FLOW

When the physical properties of a medium are dependent on direction, the medium is said to be anisotropic. Darcy's law was given in Eq.(2.7) for the case of an isotropic medium. In this appendix Darcy's law is generalized to a two-dimensional anisotropic medium.

In a coordinate system the off-diagonal components of the hydraulic conductivity tensor are zero, the coordinate axes direction are called the principal directions. In Figure A.1, ξ and η are the principal directions; x axis is horizontal and z axis is vertical. Suppose that the hydraulic conductivity components in the principal directions are K_ξ and K_η , then in the coordinate system (ξ, η) , the generalized form of Darcy's law is

$$\mathbf{V} = V_\xi \mathbf{f} + V_\eta \mathbf{h} = -K_\xi \partial H / \partial \xi \mathbf{f} - K_\eta \partial H / \partial \eta \mathbf{h} \quad (\text{A.1})$$

where \mathbf{V} denotes the Darcy velocity, V_ξ and V_η are the components of Darcy velocity in the coordinate system (ξ, η) , \mathbf{f} and \mathbf{h} are the unit vectors in ξ -direction and η -direction, respectively, H is the hydraulic head.

Let α be the counterclockwise rotation angle of the coordinate system (ξ, η) relative to the coordinate system (x, z) . The following relation exists between the two coordinate systems:

$$\begin{aligned} \mathbf{f} &= \cos\alpha \mathbf{i} + \sin\alpha \mathbf{j} \\ \mathbf{h} &= -\sin\alpha \mathbf{i} + \cos\alpha \mathbf{j} \end{aligned} \quad (\text{A.2})$$

where i and j are the unit vectors in x-direction and z-direction, respectively.

Substituting Eq.(A.2) into Eq.(A.1) gives

$$\mathbf{V} = - [K_{\xi} \frac{\partial H}{\partial \xi} \cos \alpha - K_{\eta} \frac{\partial H}{\partial \eta} \sin \alpha] i - [K_{\xi} \frac{\partial H}{\partial \xi} \sin \alpha + K_{\eta} \frac{\partial H}{\partial \eta} \cos \alpha] j \quad (\text{A.3})$$

From the rotation relation Eq.(A.2) we can obtain

$$\begin{aligned} \xi &= \cos \alpha x + \sin \alpha z \\ \eta &= -\sin \alpha x + \cos \alpha z \end{aligned} \quad (\text{A.4})$$

and consequently

$$\begin{aligned} \frac{\partial}{\partial \xi} &= \cos \alpha \frac{\partial}{\partial x} + \sin \alpha \frac{\partial}{\partial z} \\ \frac{\partial}{\partial \eta} &= -\sin \alpha \frac{\partial}{\partial x} + \cos \alpha \frac{\partial}{\partial z} \end{aligned} \quad (\text{A.5})$$

Substituting Eq.(A.5) into Eq.(A.3) yields

$$\begin{aligned} \mathbf{V} &= -(i \ j) \begin{bmatrix} \cos \alpha & -\sin \alpha \\ \sin \alpha & \cos \alpha \end{bmatrix} \begin{bmatrix} K_{\xi} & 0 \\ 0 & K_{\eta} \end{bmatrix} \begin{bmatrix} \frac{\partial H}{\partial \xi} \\ \frac{\partial H}{\partial \eta} \end{bmatrix} \\ &= -(i \ j) \begin{bmatrix} \cos \alpha & -\sin \alpha \\ \sin \alpha & \cos \alpha \end{bmatrix} \begin{bmatrix} K_{\xi} & 0 \\ 0 & K_{\eta} \end{bmatrix} \begin{bmatrix} \cos \alpha & \sin \alpha \\ -\sin \alpha & \cos \alpha \end{bmatrix} \begin{bmatrix} \frac{\partial H}{\partial x} \\ \frac{\partial H}{\partial z} \end{bmatrix} \end{aligned} \quad (\text{A.6})$$

or

$$\mathbf{V} = -(i \ j) \begin{bmatrix} K_{xx} & K_{xz} \\ K_{zx} & K_{zz} \end{bmatrix} \begin{bmatrix} \frac{\partial H}{\partial x} \\ \frac{\partial H}{\partial z} \end{bmatrix} \quad (\text{A.7})$$

where

$$\begin{aligned} K_{xx} &= K_{\xi} \cos^2 \alpha + K_{\eta} \sin^2 \alpha \\ K_{zz} &= K_{\xi} \sin^2 \alpha + K_{\eta} \cos^2 \alpha \\ K_{xz} &= K_{zx} = (K_{\xi} - K_{\eta}) \cos \alpha \sin \alpha \end{aligned}$$

In general, the Darcy velocity in direction $\mathbf{n} = (n_x, n_z)$, V_n , can be expressed as

$$\begin{aligned}
 V_n &= \mathbf{V} \cdot \mathbf{n} \\
 &= - (n_x \ n_z) \begin{bmatrix} K_{xx} & K_{xz} \\ K_{zx} & K_{zz} \end{bmatrix} \begin{bmatrix} \partial H / \partial x \\ \partial H / \partial z \end{bmatrix}
 \end{aligned} \tag{A.8}$$

The velocity in a triangular element can be calculated as follows:

If the pressure head $h = H - z$ is represented by

$$h = \sum_{k=1}^3 h_k \alpha_k \tag{A.9}$$

in which α_k are basis functions, then

$$\begin{aligned}
 \partial H / \partial x &= \sum_{i=1}^3 h_i \partial \alpha_i / \partial x \\
 \partial H / \partial z &= \sum_{i=1}^3 h_i \partial \alpha_i / \partial z + 1
 \end{aligned} \tag{A.10}$$

Substituting Eq.(A.10) into Eq.(A.8) yields:

$$V_n = - (n_x \ n_z) \begin{bmatrix} K_{xx} & K_{xz} \\ K_{zx} & K_{zz} \end{bmatrix} \begin{bmatrix} \partial \alpha_1 / \partial x & \partial \alpha_2 / \partial x & \partial \alpha_3 / \partial x & 0 \\ \partial \alpha_1 / \partial z & \partial \alpha_2 / \partial z & \partial \alpha_3 / \partial z & 1 \end{bmatrix} \begin{bmatrix} h_1 \\ h_2 \\ h_3 \\ 1 \end{bmatrix} \tag{A.8}$$

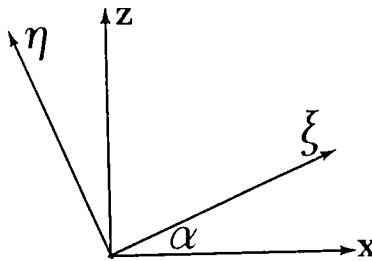


Figure A.1 Coordinate System Rotation

Appendix B

THE TRANSFORMATION OF CARTESIAN COORDINATE SYSTEM TO A NATURAL COORDINATE SYSTEM

As shown in Figure B.1, by dividing the region of subsurface flow, land surface becomes a series of curves defined over the discrete intervals

$$L_2 = x_1 > x_2 > \dots > x_{M-1} > x_M = L_1 \quad (B.1)$$

where M is the number of the nodes on the saturated surface. Because S is a axis of the curvilinear coordinate system, C^1 -continuity is required, therefore we approximate it by

$$z_i(x) = z_i(x_i) + \alpha_i(x-x_i) + \beta_i(x-x_i)^2, \quad x_i \leq x \leq x_{i+1}$$

$$i = 1, 2, \dots, M-1 \quad (B.2)$$

where α_i and β_i are constants, these constants are determined by such a way that the following conditions are satisfied

$$z_i(x_{i+1}) = z_{i+1}(x_{i+1})$$

$$z'_i(x_{i+1}) = z'_{i+1}(x_{i+1})$$

$$i = 1, 2, \dots, M-1 \quad (B.3)$$

The length of the curved side of the surface element can be calculated by

$$S_i(x) = \int_{x_i}^{x_{i+1}} \sqrt{1 + [dz_i(x)/dx]^2} dx$$

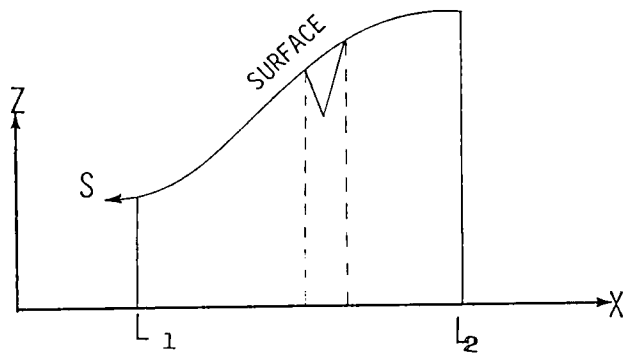


Figure B.1 The division of land surface.

$$= \frac{1}{4\beta_i} [r_i(x) \sqrt{1+r_i^2(x)} + \ln | r_i(x) + \sqrt{1+r_i^2(x)} |] \Big|_{x=x}^{x=x_i}$$

$$x_i \leq x \leq x_{i+1} \quad (B.4)$$

where $r_i(x) = \alpha_i + 2\beta_i(x-x_i)$

Referring to Figure B.2, The Cartesian coordinate system (x, z) can be transformed into a natural coordinate system (ξ, η) by

$$\xi = PQ/L, \quad \eta = QS/OS \quad (B.5)$$

or equivalently

$$\xi = S_i(x_s)(1-\eta)/L \quad (B.6)$$

$$\eta = (x-x_s)/(x_3-x_s) \quad (B.7)$$

$$\eta = (z-z_s)/(z_3-z_s) \quad (B.8)$$

Eqs.(B.6) ~ (B.8) can be rewritten as

$$\xi = S_i(x_s)(1-\eta)/L \quad (B.9)$$

$$x = (1-\eta)x_s + \eta x_3 \quad (B.10)$$

$$z = (1-\eta)z_s + \eta z_3 \quad (B.11)$$

On the other hand, for the element i Eq.(B.2) becomes

$$z_s = z_1 + \alpha_i(x_s-x_1) + \beta_i(x_s-x_1)^2 \quad (B.12)$$

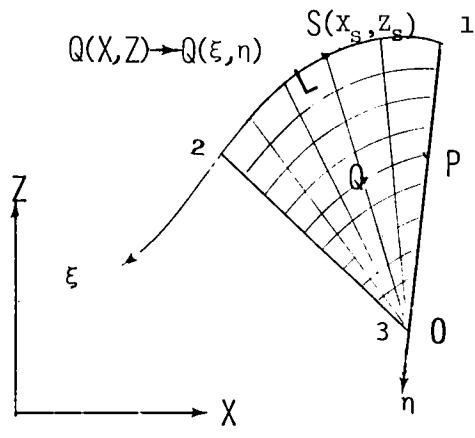
Eqs.(B.9) ~ (B.12) are the relationship between the natural and Cartesian coordinate systems.

The Jacobian matrix can be obtained as follows:

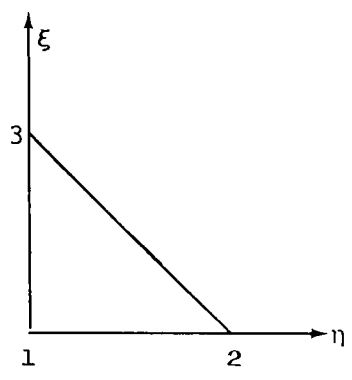
Differentiating Eq.(B.9) with respect to ξ and η gives

$$1 = S_i'(x_s) \partial x_s / \partial \xi (1-\eta)/L$$

$$0 = S_i'(x_s) \partial x_s / \partial \eta (1-\eta)/L - S_i(x_s)/L \quad (B.13)$$



(a)



(b)

Figure B.2 The natural coordinate system for sureface curved-sided elements.

where $S'_i(x_s) = -\sqrt{1+r_i^2(x_s)}$

$$r_i(x_s) = \alpha_i + 2\beta_i(x_s - x_1)$$

On the other hand, differentiating Eq.(B.12) with respect to ξ and η gives

$$\begin{aligned}\partial z_s / \partial \xi &= dz_s / dx_s \cdot \partial x_s / \partial \xi \\ \partial z_s / \partial \eta &= dz_s / dx_s \cdot \partial x_s / \partial \eta\end{aligned}\tag{B.14}$$

where $dz_s / dx_s = r_i(x_s)$

Similarly, from Eqs.(B.10), (B.11) we can obtain

$$\begin{aligned}\partial x / \partial \xi &= (1-\eta) \partial x_s / \partial \xi \\ \partial z / \partial \xi &= (1-\eta) \partial z_s / \partial \xi \\ \partial x / \partial \eta &= -x_s + (1-\eta) \partial x_s / \partial \eta + x_3 \\ \partial z / \partial \eta &= -z_s + (1-\eta) \partial z_s / \partial \eta + z_3\end{aligned}\tag{B.15}$$

Substituting Eqs.(B.13), (B.14) into Eq.(B.15) yields

$$\begin{aligned}\partial x / \partial \xi &= L / S'_i(x_s) \\ \partial z / \partial \xi &= L r_i(x_s) / S'_i(x_s) \\ \partial x / \partial \eta &= x_3 - x_s + S_i(x_s) / S'_i(x_s) \\ \partial z / \partial \eta &= z_3 - z_s + r_i(x_s) S_i(x_s) / S'_i(x_s)\end{aligned}\tag{B.16}$$

From the above equations we can compute the Jacobian matrix by

$$J = \frac{\partial(x, z)}{\partial(\xi, \eta)} = \begin{vmatrix} \partial x / \partial \xi & \partial x / \partial \eta \\ \partial z / \partial \xi & \partial z / \partial \eta \end{vmatrix}\tag{B.17}$$

and then we have

$$dx dz = |J| d\xi d\eta\tag{B.18}$$

The derivatives of the basis functions then can be calculated easily as follows:

Differentiating the basis functions with respect to ξ and η yields:

$$\begin{aligned}\partial\phi_i^e/\partial\xi &= \partial\phi_i^e/\partial x \cdot \partial x/\partial\xi + \partial\phi_i^e/\partial z \cdot \partial z/\partial\xi \\ \partial\phi_i^e/\partial\eta &= \partial\phi_i^e/\partial x \cdot \partial x/\partial\eta + \partial\phi_i^e/\partial z \cdot \partial z/\partial\eta, i=1,2,3.\end{aligned}\quad (\text{B.19})$$

Solving the above equations for $\partial\phi_i^e/\partial x$ and $\partial\phi_i^e/\partial z$ we obtain

$$\begin{aligned}\partial\phi_i^e/\partial x &= \begin{vmatrix} \partial\phi_i^e/\partial\xi & \partial z/\partial\xi \\ \partial\phi_i^e/\partial\eta & \partial z/\partial\eta \end{vmatrix} / |J| \\ \partial\phi_i^e/\partial z &= \begin{vmatrix} \partial x/\partial\xi & \partial\phi_i^e/\partial\xi \\ \partial x/\partial\eta & \partial\phi_i^e/\partial\eta \end{vmatrix} / |J|, i=1,2,3.\end{aligned}\quad (\text{B.20})$$

Finally, we shall show the computation procedure of x_s and z_s from Eq.(B.9). For convenience' sake, we rewrite Eq.(B.9) as

$$F(M) = 0 \quad (\text{B.20})$$

where

$$F(M) = S_i(M) - L\xi/(1-\eta)$$

$$S_i(M) = \frac{1}{4\beta_i} \left[W \sqrt{1+W^2} + \ln |W + \sqrt{1+W^2}| \right] \begin{vmatrix} W=\alpha_i \\ W=M \end{vmatrix}$$

$$M = \alpha_i + 2\beta_i(x_s - x_1)$$

According to the Newton method, we have

$$M_n = M_{n-1} - F(M_{n-1}) / F'(M_{n-1}) \quad (\text{B.21})$$

where

$$F'(M) = S_i'(M) = \frac{1}{2\beta_i} \sqrt{1+M^2}$$

In order to guarantee that the following conditions of convergence are satisfied

$$F(M_0)F''(M_0) > 0$$

$$F(M)F'(M)/F''(M) \leq k < 1 \quad (\text{B.22})$$

we take

$$M_0 = \alpha_i + 2\beta_i(x_2 - x_1) \xi / (1 - \eta) \quad (\text{B.23})$$

The iteration procedure is repeated until the difference between successive iterations is within a specified error α , i. e.

$$|M_n - M_{n-1}| < \alpha \quad (\text{B.24})$$

then x_s can be obtained by

$$x_s = (M_n - \alpha_i) / 2\beta_i + x_1 \quad (\text{B.25})$$

Appendix C

NUMERICAL INTEGRATION

In our problem the integrals of the following two types are encountered

$$I_1 = \int_0^1 \int_0^{1-\eta} G(\xi, \eta) d\xi d\eta \quad (C.1)$$

$$I_2 = \int_{\xi(2)}^{\xi(1)} G(\xi) d\xi \quad (C.2)$$

With the transformation

$$\begin{aligned} \xi &= [1 - (1 + \bar{\eta})/2](1 + \bar{\xi})/2 \\ \eta &= (1 + \bar{\eta})/2 \end{aligned} \quad (C.3)$$

we can rewrite the integral (C.1) as

$$I_1 = \int_{-1}^1 d\bar{\eta} \int_{-1}^1 G(\xi, \eta) \frac{1}{4} [1 - (1 + \bar{\eta})/2] d\bar{\xi} \quad (C.4)$$

Similarly, with the transformation

$$\xi = \xi(1) + [\xi(2) - \xi(1)](1 + \bar{\xi})/2 \quad (C.5)$$

we can rewrite the integral (C.2) as

$$I_2 = \int_{-1}^1 G(\xi) \frac{1}{2} [\xi(2) - \xi(1)] d\bar{\xi} \quad (C.6)$$

Now the integrals can be evaluated in conjunction with the tabulated Gauss point locations and weighting factors in Table C.1.

Table C.1 One-Dimensional Gauss-Legendre
Points and Weights.

$$\int_{-1}^1 f(x) dx = \sum_{i=1}^m W_i f(x_i)$$

| $\pm x_i$ | m | W_i |
|-----------------|-----|------------------|
| 0.5773502691896 | 2 | 1.0 |
| 0.7745966692415 | 3 | 0.55555555555556 |
| 0.0000000000000 | | 0.88888888888889 |

Appendix D

COEFFICIENTS OF THE LUMPING RUNOFF MODEL

All of the coefficients of the lumping runoff model are as follows:

$$a_{11} = H/(tg\theta - tg\beta) \quad (D.1)$$

$$a_{12} = 0.5 H^2 / [(tg\theta - tg\beta)^2 \cos^2 \beta] \quad (D.2)$$

$$a_{13} = 0 \quad (D.3)$$

$$a_{21} = C_s D [1/(tg\theta - tg\beta) - 1/(tg\theta - tg\gamma) - 1/[(tg\theta - tg\beta) \cos^2 \gamma]] \quad (D.4)$$

$$a_{22} = C_s H D (\cos \gamma \cos^2 \beta - 1) / [(tg\theta - tg\beta)^2 \cos^3 \gamma \cos^2 \beta] \quad (D.5)$$

$$a_{23} = 0.5 C_s D^2 / [(tg\theta - tg\gamma)^2 \cos^2 \gamma] - (C_s / 2 - \omega_0) D / [(tg\theta - tg\gamma) \cos \gamma] \quad (D.6)$$

$$a_{31} = \partial S_u / \partial h_1 \cdot \partial h_1 / \partial l_1 \cdot \partial l_1 / \partial H + C_s \cdot D [1/(tg\theta - tg\gamma) - 1/[(tg\theta - tg\beta) \cos^2 \gamma]] \quad (D.7)$$

$$a_{32} = \partial S_u / \partial h_1 \cdot \partial h_1 / \partial l_1 \cdot \partial l_1 / \partial \beta + C_s \cdot H \cdot D / [(tg\theta - tg\beta)^2 \cos^3 \gamma \cos^2 \beta] \quad (D.8)$$

$$a_{33} = \partial S_u / \partial h_1 [\partial h_1 / \partial l_2 \cdot \partial l_2 / \partial \gamma + \partial h_1 / \partial \gamma] + \partial S_u / \partial l_2 \cdot \partial l_2 / \partial \gamma + \partial S_u / \partial \gamma^* + \partial S_u / \partial \gamma^{**} +$$

$$+ C_s \cdot H \cdot D / [(tg\theta - tg\beta)^2 \cos^3 \gamma \cos^2 \beta] \quad (D.9)$$

where

$$\begin{aligned} \partial S_u / \partial h_1 &= \partial S_u / \partial ph_2 \cdot \partial ph_2 / \partial h_2 \cdot \partial h_2 / \partial h_1 + \\ &\quad \partial S_u / \partial ph_1 \cdot \partial ph_1 / \partial h_1 + \\ &\quad \partial S_u / \partial h_1^* + \partial S_u / \partial h_2 \cdot \partial h_2 / \partial h_1 \end{aligned}$$

in which h_1^* stands for the h_1 that occurred explicitly in the expression of S_u .

$$\begin{aligned} \partial S_u / \partial ph_2 \cdot \partial ph_2 / \partial h_2 \cdot \partial h_2 / \partial h_1 &= \\ &= -D(C_s - \omega_0) [(ph_2 - 1) \exp(ph_2) + \\ &\quad + (h_1 + h_0 \cdot ph_2)(ph_2 - 1) \exp(ph_2) / (D \cos \gamma)] / \\ &\quad / [(tg\theta - tg\gamma) \cos \gamma] \\ \partial S_u / \partial ph_1 \cdot \partial ph_1 / \partial h_1 &= \\ &= (C_s - \omega_0)(h_1 + h_0 \cdot ph_2)(ph_2 - 1) \exp(ph_2) / \\ &\quad / [(tg\theta - tg\gamma) \cos^2 \gamma] \\ \partial S_u / \partial h_1^* &= h_0(C_s - \omega_0) [(ph_2 - 2) \exp(ph_2) - (ph_2 - 2) \exp(ph_1)] / \\ &\quad / [(tg\theta - tg\gamma) \cos^2 \gamma] + 0.5 D \omega_0 / [(tg\theta - tg\gamma) \cos \gamma] \\ \partial S_u / \partial h_2 \cdot \partial h_2 / \partial h_1 &= 0.5 \omega_0 / [(tg\theta - tg\gamma) \cos \gamma] \\ h_1 &= \cos \gamma (tg\theta - tg\gamma) [L - H / (tg\theta - tg\beta) - D / (tg\theta - tg\gamma)] \\ ph_1 &= -h_1 / h_0 \\ ph_2 &= - (D \cos \gamma + h_1) / h_0 \\ \partial h_1 / \partial l_1 &= -\cos \gamma (tg\theta - tg\gamma) \\ \partial l_1 / \partial H &= 1 / (tg\theta - tg\beta) \end{aligned}$$

$$\partial l_1 / \partial \beta = H / [(\operatorname{tg} \theta - \operatorname{tg} \beta)^2 \cos^2 \beta]$$

$$\partial h_1 / \partial l_2 = -(\operatorname{tg} \theta - \operatorname{tg} \gamma) \cos \gamma$$

$$\partial l_2 / \partial \gamma = -(\operatorname{tg} \theta \sin \gamma + \cos \gamma) [L - H / (\operatorname{tg} \theta - \operatorname{tg} \beta) - D / (\operatorname{tg} \theta - \operatorname{tg} \gamma)]$$

$$\partial h_1 / \partial \gamma = (\operatorname{tg} \theta - \operatorname{tg} \gamma) S_u / D$$

$$\partial S_u / \partial l_2 = D / [(\operatorname{tg} \theta - \operatorname{tg} \gamma)^2 \cos^2 \gamma]$$

$$\partial S_u / \partial \gamma^* = \operatorname{tg} \gamma \cdot S_u$$

$$\begin{aligned} \partial S_u / \partial \gamma^{**} = h_0 (C_s - \omega_0) \{ & h_1 [(x-2) \exp(x)] \Big|_{\text{ph}_1}^{\text{ph}_2} + \\ & + h_0 [(x^2 - 3x + 3) \exp(x)] \Big|_{\text{ph}_1}^{\text{ph}_2} \} / [(\operatorname{tg} \theta - \operatorname{tg} \gamma) \cos^2 \gamma] \end{aligned}$$

$$\begin{aligned} S_u = D \{ & 0.5 \omega_0 (h_1 + h_2) + h_0 (C_s - \omega_0) \{ [(x-2) \exp(x)] \Big|_0^{\text{ph}_2} + \\ & + [h_1 [(x-2) \exp(x)] \Big|_{\text{ph}_1}^{\text{ph}_2} + h_0 [(x^2 - 3x + 3) \exp(x)] \Big|_{\text{ph}_1}^{\text{ph}_2} \} / \\ & / (D \cos \gamma) \} \} \end{aligned}$$

$$[f(x)] \Big|_{x(1)}^{x(2)} = f(x(2)) - f(x(1))$$